Bench-Scale Silicone Process for Low-Cost CO_2 Capture

Final Scientific/Technical Report

Reporting Period Start Date: 10/1/2011

Reporting Period End Date: 12/31/2013

Benjamin Wood, Sarah Genovese, Robert Perry, Irina Spiry, Rachael Farnum, Surinder Singh, Paul Wilson, Paul Buckley, Harish Acharya, Wei Chen, John McDermott

GE Global Research

1 Research Circle, Niskayuna, NY

Ravikumar Vipperla, Michael Yee, Ray Steele

GE Power and Water

300 Garlington Road, Greenville, SC

Megan J. Fresia, Kirk Vogt

Milliken & Company

920 Milliken Rd, Spartanburg, SC

Date Report Issued: April 2014

DE-FE0007502

Disclaimer:

Abstract:

A bench-scale system was designed and built to test an aminosilicone-based solvent. A model was built of the bench-scale system and this model was scaled up to model the performance of a carbon capture unit, using aminosilicones, for CO_2 capture and sequestration (CCS) for a pulverized coal (PC) boiler at 550 MW. System and economic analysis for the carbon capture unit demonstrates that the aminosilicone solvent has significant advantages relative to a monoethanol amine (MEA)-based system. The CCS energy penalty for MEA is 35.9% and the energy penalty for aminosilicone solvent is 30.4% using a steam temperature of 395 °C (743 °F). If the steam temperature is lowered to 204 °C (400 °F), the energy penalty for the aminosilicone solvent is reduced to 29%. The increase in cost of electricity (COE) over the non-capture case for MEA is ~109% and increase in COE for aminosilicone solvent is ~98 to 103% depending on the solvent cost at a steam temperature of 395 °C (743 °F). If the steam temperature is lowered to 204 °C (400 °F), the increase in COE for the aminosilicone solvent is reduced to ~95-100%.

Table of Contents

Executive Summary:

This report details the results of a project to test aminosilicone-based solvents for CO_2 capture at the bench scale. The aminosilicone-based solvent was a 60/40 (wt/wt) mixture of 3-aminopropyl end-capped polydimethylsiloxane (GAP-1m) and triethylene glycol (TEG). A continuous bench-scale system was designed and built to study the performance of this material for CO_2 capture.

The bench-scale system consists of a gasoline generator that produces exhaust gas as a proxy for the flue gas from a coal-fired power plant. The exhaust from this generator is chilled in a heat exchanger to lower the water content to that typical of the flue gas from a coal-fired power plant. The exhaust can then be mixed with a variety of gases, such as SO_2, supplied from a gas manifold, to adjust the composition to match the flue gas from coal. The mixture is then heated to 40 to 60 °C. The exhaust, with a flow rate of 50-200 standard liters per minute (SLPM), is sent to the bottom of a column, where it flows up, countercurrent to the aminosilicone solution at a flow rate of 1-2 liter per minute (LPM) which captures CO_2. The column is designed in a modular fashion, so that the height of the column can be adjusted, and a variety of different packing materials can be tested. The stripped exhaust exits the top of the column and is sent to a mass spec and CO_2 analyzer for compositional analysis. The rich solvent leaves the bottom of the column, and is pumped to the high pressure desorber.

The desorber is a jacketed, high-pressure, continuous, stirred-tank reactor. It has a recirculation loop, with a heat exchanger. The recirculation loop is designed to provide additional heat input to that provided by the jacketing on the tank. In addition, the recirculation is used to increase mass transfer in the reactor. The lean sorbent leaves the bottom of the desorber and is cooled, dropped in pressure, and sent to a storage tank, before being sent back to the top of the column. The CO_2 produced in the desorber is throttled down in pressure and sent to gas analysis. The system is fully automated, with detailed measurements of all important process variables, including temperatures and pressures.

The system was operated under a variety of process conditions, to determine the impact of various process variables on system performance. Solvent degradation was studied, due to both thermal effects and exposure to flue-gas impurities. Corrosion studies were performed to determine suitable materials of construction for process equipment. The resulting data from the bench-scale tests were used to develop an Aspen Plus™ process model of the bench-scale process. This model was scaled up to capture 90% of the CO_2 from a 550 MW pulverized coal (PC) boiler.

System and economic analyses were performed for the aminosilicone-based process for CO_2 capture and sequestration (CCS). For comparison purposes, the report also shows results for a CCS unit based on a conventional approach using monoethanol amine (MEA).

Aspen Plus™ models developed for both the MEA and aminosilicone solvent-based CO_2 separation units were used to calculate the mass and energy balances and system performance. The models account for steam load for the CO_2 separation units and parasitic loads for solvent pumps, CO_2 compressors, and cooling water pumps.

Capital costs were estimated by the Aspen™ Cost Estimator program and a relative cost comparison between the two configurations is presented. The energy penalty for the plant and cost of electricity (COE) were calculated using the assumptions specified by the Department of Energy (DOE) in the cooperative agreement for this project (Award #DE-FE0007502).

At a steam temperature of 395 °C (743 °F), the CCS energy penalty for aminosilicone solvent is only 30.4% which compares to a 35.9% energy penalty for MEA. At a lower steam temperature of 204 °C (400 °F), the energy penalty for the aminosilicone solvent is 29.0%.

At a steam temperature of 395 °C (743 °F), the increase in COE for aminosilicone solvent relative to the non-capture case is between 98% and 103% (depending on the solvent cost) which compares to an ~109% COE cost increase for MEA. At a lower steam temperature of 204 °C (400 °F), the increase in COE for the aminosilicone solvent is between 95% and 100%. In summary, the aminosilicone solvent has a significant advantage over conventional systems using MEA.

Results and Discussion

The major goal of the project was to design and optimize a bench-scale process for novel silicone CO_2-capture solvents and establish scalability and potential for commercialization of post-combustion capture of CO_2 from coal-fired power plants. Work and accomplishments for the project are detailed by task below.

Task 1: Project Management and Planning

The milestones for this project are listed in Table 1. These milestones are complete.

Table 1. Project milestones.

Milestone Title/Description	Planned Completion Date	Actual Completion Date	Verification Method	Comments (progress toward achieving milestone, explanation of deviation from plan, etc.)
Update of Project Management Plan	12/1/2011	12/12/2011	Confirmation from DOE/NETL	None
Kick-off meeting	12/31/2011	11/22/2011	N/A	None
Determination of Energy required for CO_2 separation sub-system	6/30/2012	6/30/2012	Report to DOE/NETL	100% complete
Design of continuous bench-scale absorption /desorption unit	6/30/2012	6/30/2012	Report to DOE/NETL	100% complete
Manufacturability analysis of aminosilicone-based solvent for bench-scale testing	6/30/2012	6/30/2012	Report to DOE/NETL	100% complete
Establish capital requirements for material manufacturing and material price model	9/30/2012	9/30/2012	Report to DOE/NETL	100% complete
Delivery of synthesized aminosilicone-based solvent	9/30/2012	9/30/2012	Report to DOE/NETL	100% complete
Preliminary technical and economic feasibility study	10/31/2012	10/31/2012	Topical Report to DOE/NETL	100% complete
Assembly of operational bench-scale system	12/31/2012	11/30/2012	Report to DOE/NETL	100% complete
Bench-scale test plan	12/31/2012	12/31/2012	Written Report to DOE/NETL	100% complete
Plan for large-scale raw material supply and manufacturing and material price model	12/31/2012	2/12/2013	Topical Report to DOE/NETL	100% complete
Absorption material for bench-scale testing delivered from SiVance to GE Global Research	3/31/2013	2/4/2013	Reciept of materials	100% complete
Bench-scale process model	6/30/2013	6/30/2013	Report to DOE/NETL	100% complete
Updated state-point table	9/30/2013	10/10/2013	Report to DOE/NETL	100% complete
Technology EH&S risk assessment	12/31/2013	12/31/2013	Topical Report to DOE/NETL	100% complete
Design parameters identified and reported	12/31/2013	12/31/2013	Report to DOE/NETL	100% complete
Scale-up strategy	12/31/2013	12/31/2013	Report to DOE/NETL	100% complete
Final Technical and Economic Feasibility Study	12/31/2013	12/31/2013	Topical Report to DOE/NETL	100% complete

Task 2: Conduct Preliminary Technical and Economic Feasibility Study

Task 2.1: Develop Preliminary Process Models

Preliminary process models were developed in 2012 based on the data collected in previous work as part of the DOE award # DE-NT0005310. These process models were used to perform the Preliminary Technical and Economic Feasibility Study. However, in 2013, the bench-scale process was tested with aminosilicone-based solvent, and the process models were updated

based on information obtained from the bench-scale tests. The discussion of these updated models is given in Task 8 of this document.

Task 2.2: Perform Preliminary Technical and Economic Feasibility Study

A Preliminary Technical and Economic Feasibility Study was performed in 2012 based on the process models developed in Task 2.1. This study was updated in 2013, in Task 8.2, in the Final Technical and Economic Feasibility Study. The Final Technical and Economic Feasibility Study results are discussed in section 8.2 of this document.

Task 3: Design and Build Bench-Scale System

Task 3.1: Design Bench-Scale System

During the first two quarters of 2012, the conceptual design of a bench-scale system to utilize aminosilicones for CO_2 capture was developed. The detailed design of this system was then conducted by GE Global Research working with Techniserv, Inc., who built the bench-scale system. In order to complete the detailed design, experiments were conducted to obtain information, such as kinetic rates and heats of reaction, necessary for the sizing of the main unit operations. The design of the main unit operations were completed, and the auxiliary equipment, such as control valves, tubing size and type, and process monitoring equipment were specified. The following discussion provides additional detail about thos e design activities.

Gas Delivery System Design

The continuous bench-scale system includes a flue gas generation unit, which delivers flue gas flow with a specified concentration of CO_2 at a specified temperature to the absorption column. In the initial stages of the project several options were considered, and a gasoline generator was decided to be an optimal option for the bench-scale process. The design includes a home-use gasoline 6000 W generator. Small generator engines use pre-mix combustion of the fuel, and air and fuel are mixed at a fixed ratio in a carburetor. When load on the generator is increased, the amounts of air and fuel are increased respectively, but the ratio stays the same. Due to a constant value of the air to fuel ratio, the composition of the flue gas stays relatively constant at different loads. The theoretical composition of the exhaust gas was determined, and it is shown in Table 2.

The following combustion equation for a hydrocarbon fuel of average molar H/C ratio (y) needs to be considered:

$$\varepsilon\phi C + 2(1-\varepsilon)\phi H_2 + O_2 + \psi N_2 \rightarrow n_{CO2} + n_{H2O} + n_{CO} + n_{H2} + n_{O2} + n_{N2}$$

where

C, H_2, O_2, and N_2 are the moles of carbon, H_2, O_2, and N_2 in the inlet

ψ- the molar N/O ratio (3.773 for air)

$\varepsilon = \frac{4}{4+y}$

y – the molar H/C ratio of fuel

ϕ = fuel/air equivalence ratio

n_i = moles of species i in exhaust per mole O_2 reactant[1]

Table 2. Theoretical composition of exhaust gas from a gasoline engine.

Table 4.3 Burned gas composition under 1700K			**Gasoline engine exhaust**	
	n_i, moles/mole O2 reactant		*Moles*	*%mol*
Species	ϕ ≤ 1	ϕ > 1	ϕ = 1	*Theoretical*
CO_2	εϕ	εϕ-c	0.681	13.38%
H_2O	2*(1-ε)*ϕ	2*(1-εϕ) + c	0.637	12.51%
CO	0	c	0.000	0.00%
H_2	0	2*(ϕ-1) - c	0.000	0.00%
O_2	1-ϕ	0	0.000	0.00%
N_2	ψ	ψ	3.773	74.10%
SOx	0	0	0.000	0.00%
NOx	0	0	0.000	0.00%

Experiments were conducted at GE's Global Research Center to verify the composition, temperature, and approximate level of CO and unburned hydrocarbons for the exhaust gas from a home-use gasoline 6000 W generator.

The above mentioned parameters were tested for different loadings on the generator: ~25%, ~50%, ~75%, and ~100%. Load on the gasoline generator was applied with heaters rated for 1500 W. The composition of the exhaust gas is presented in Table 3.

[1] "Internal Combustion Engine Fundamentals", John B. Heywood, McGraw Hill, Inc.

Table 3. Experimental results for a home-use gasoline 6000 W generator.

Load	Total Amp	Total Load, W	% of Rated Load	Exhaust Gas Temperature, ^{0}C	CO2, % on wet basis	O2, %
1 Heater	12.45	1487.775	24.80%	406.5	10.2	2
2 Heaters	23.15	2766.425	46.11%	462.5	10.9	1.96
3 Heaters	34.65	4140.675	69.01%	510	11.3	1.13
4 Heaters	44.45	5311.775	88.53%	556.5	11.4	0.43
5 Heaters	49.85	5957.075	99.28%	*565*	11.3	0.37

It can be seen that composition of the flue gas stays relatively constant over a range of loadings, which was critical for the continuous bench-scale CO_2 absorption experiments. When the load on the generator is sufficiently high, the engine operation is more efficient, which can be noticed with decreasing amounts of oxygen in the exhaust gas.

Absorber Design

Design of the absorption column requires the system to be well characterized. Properties such as viscosity, equilibrium loading, and heat of reaction must be measured.

Solvent Viscosity

It was critical to know the dependence of viscosity on temperature and CO_2 loading, because it influences the operation of the packed absorber column. Additionally, viscosity has an impact on sizing of tubing, pumps, and valves. The viscosity of the aminosilicone solution, 60/40 wt/wt 3-aminopropyl end-capped polydimethylsiloxane (GAP-1m)/triethylene glycol (TEG) was measured with a TA Instruments AR 62 viscometer for different temperatures and CO_2 loadings. Results are presented on Figure 1. As shown on this plot, viscosity of the solution increases significantly with loading increase. Also, the viscosity decreases with the temperature increase, as expected.

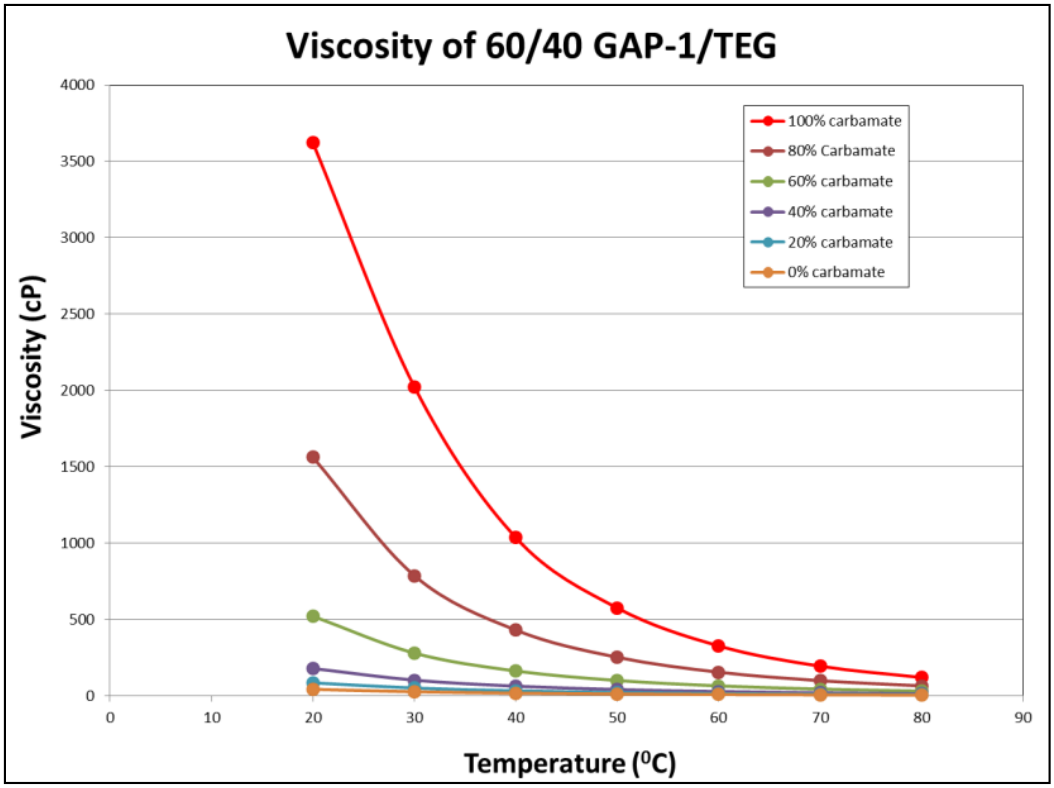

Figure 1. The viscosity of 60/40 GAP-1m/TEG as a function of carbamate loading and temperature.

Fourier Transform Infrared Spectroscopy

Fourier Transform Infrared Spectroscopy (FT-IR) was investigated as a method for determining the loading of carbamate in liquid samples. FT-IR analysis was conducted for samples with various carbamate loadings in 60/40 GAP-1m/TEG. The spectra results are presented in Figure 2 and Figure 3 (finger region).

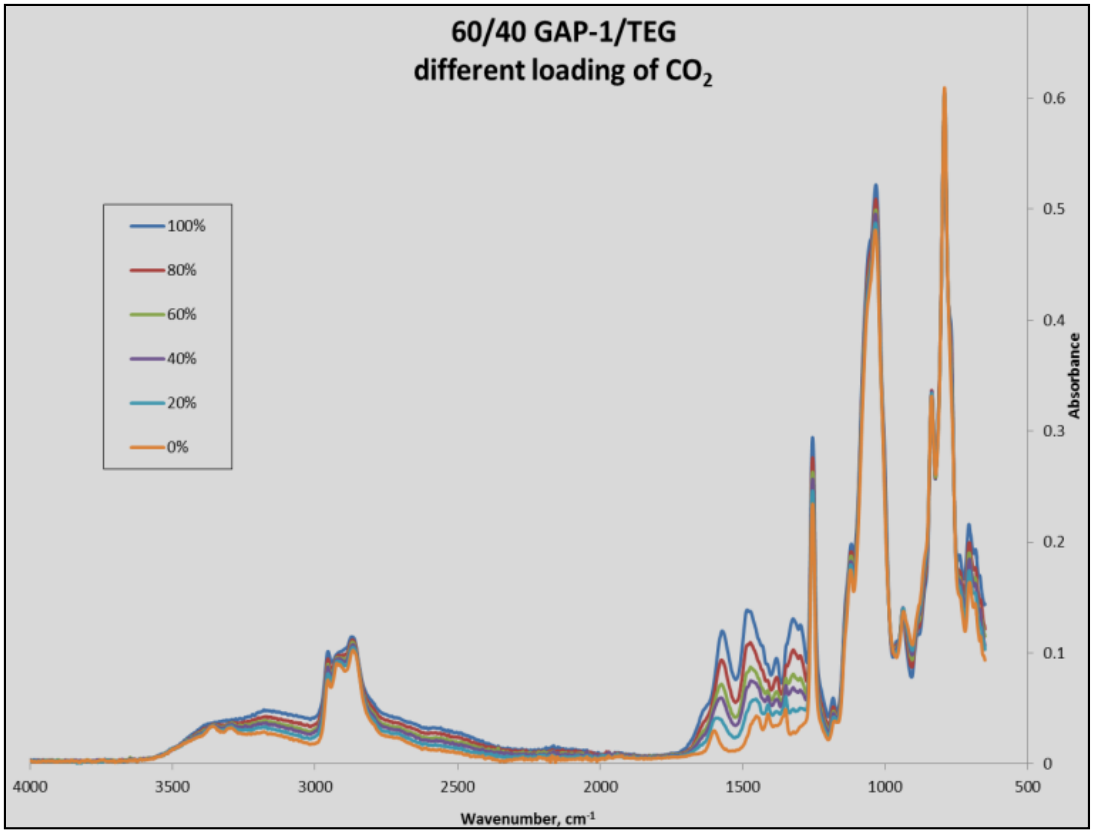

Figure 2. Spectra results for 60/40 GAP-1m/TEG mixture with various carbamate loadings.

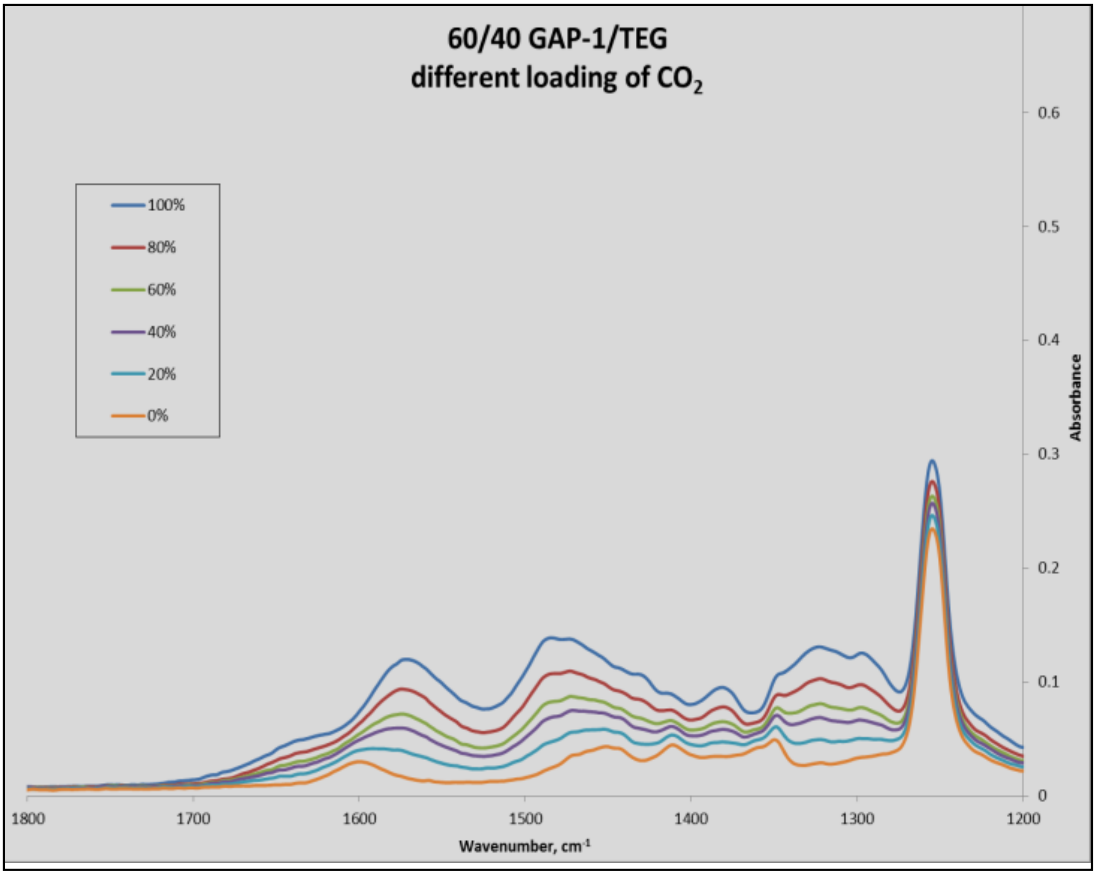

Figure 3. FTIR spectra for 60/40 GAP-1m/TEG mixture with various carbamate loadings – finger region.

From these spectra it can be seen that there is a significant difference in absorbance at 1572 cm^{-1} for samples with different carbamate loadings. Normalized absorbance has been determined for the band at 1572 cm^{-1}, and a corresponding calibration curve was constructed and presented on Figure 4.

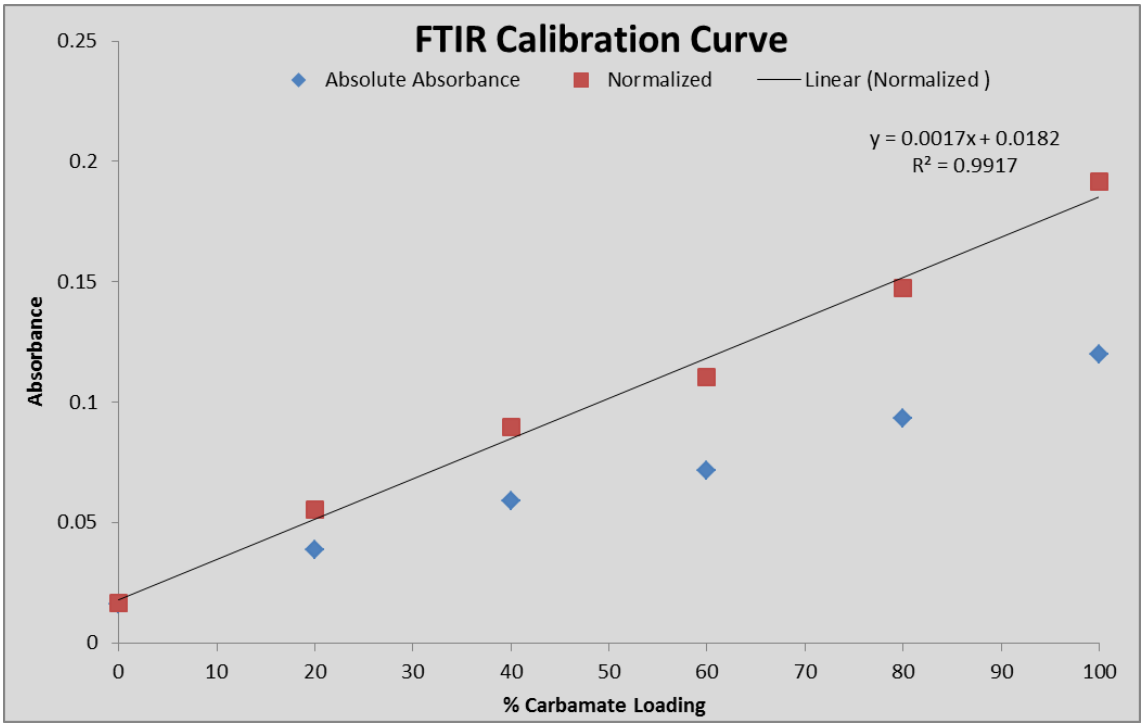

Figure 4. Calibration curve for FTIR spectra for samples with various loadings of carbamate.

From this analysis it can be concluded that FTIR can be used to determine carbamate loading.

Equilibrium CO_2 Loading

The equilibrium loading measurements of CO_2 in a 60/40 (wt/wt) GAP-1m/TEG solution were completed as a function of temperature and partial pressure of CO_2. These data were required for sizing the bench-scale absorption column. The temperatures studied ranged from 30 °C to 75 °C and the CO_2 partial pressures ranged from 0.27 psi to 2.41 psi. These temperatures and pressures were chosen to span the range of conditions expected in the absorption column. To achieve sub-atmospheric partial pressures of CO_2, the 16.44 vol% CO_2 in N_2 was mixed with 100% N_2. The results are shown in Figure 5. The error bars shown are 95% confidence intervals. Figure 5 shows that under these conditions, equilibrium loading is a strong function of both temperature and CO_2 partial pressure. At low temperatures, the CO_2 partial pressure does not significantly impact the equilibrium loading. However, at higher temperatures, the equilibrium loading in the liquid drops significantly at lower CO_2 partial pressures.

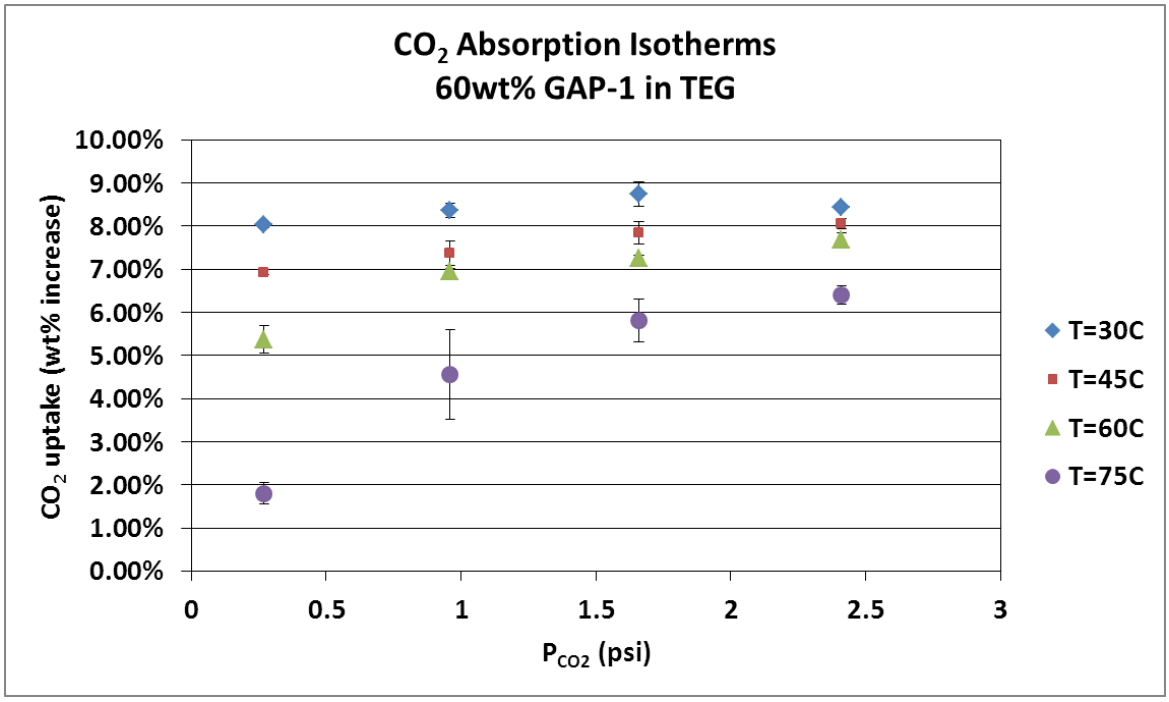

Figure 5. Equilibrium loading of CO_2 in 60/40 (wt/wt) GAP-1m/TEG mixture (error bars shown are 95% confidence intervals).

For the equilibrium loading experiments a 25 mL 3-neck round bottom flask was loaded with approximately 2 g of a 60/40 (wt/wt) GAP-1m/TEG. The flask was fitted in one neck with a glass stirrer bearing, a ground glass stir shaft, and a Teflon stirrer paddle. In the other two necks were a gas inlet port and a gas outlet port. The gas outlet port was then connected with Tygon tubing to a silicone bubbler containing less than 1" of silicone oil. The gas inlet port was connected to two mass flow controllers, one of which was connected to a bottle of 16.44 vol% CO_2 in N_2 and the other of which was connected to a bottle of 100% N_2. The set points for the mass flow controllers were varied for each experiment to adjust the partial pressure of CO_2 to the desired value. The total flow sent to the round bottom flask was fixed at 45 standard cubic centimeters (SCC). The flask loaded with the GAP-1m/TEG mixture was immersed in a silicone oil bath set at the desired temperature. The overhead stirrer was set at a fixed stir rate. A schematic of the experimental setup is shown in Figure 6. The gas outlet and gas inlet were connected to the flask and the gas flow was started. The gas flow was stopped and the flask was removed from the oil bath and weighed every 5-10 minutes to track the uptake of CO_2 in the liquid. The experiment was stopped when the reaction was determined to have reached equilibrium (the weight did not change significantly for at least 3 measurements).

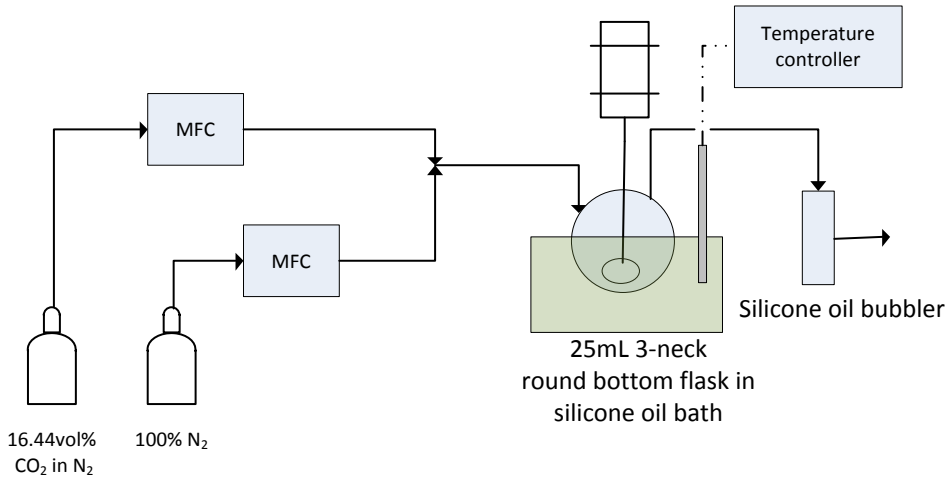

Figure 6. Schematic of equilibrium absorption test apparatus.

Mass Transfer Coefficient

To determine the size the bench scale absorption column required to achieve 90% CO_2 capture using 60/40 (wt/wt) GAP-1m/TEG, the overall gas-phase mass transfer coefficient ($K_G a$) for the system needed to be estimated. To estimate the $K_G a$ for the bench-scale system, the $K_G a$ for a laboratory-scale column was determined at room temperature for 60/40 (wt/wt) GAP-1m/TEG, 16.44 vol% CO_2 in N_2, and a liquid flowrate of 10 mL/min. A series of experiments were performed for four packing heights and five molar gas to liquid ratios (Gm/Lm) spanning from 0.4-1.2. At each condition, $K_G a$ was calculated using Equation 1 and Equation 2. These results are shown in Figure 7. As expected, as the gas flow rate increases, so does $K_G a$. While this $K_G a$ is specific to this column size, packing, and temperature, and this value will change with varying operating conditions and packing, this value was used to estimate the size of the bench-scale column.

$Z = H_{OG} N_{OG}$, where Z = packing height and N_{OG} was determined numerically (1)

$H_{OG} = \frac{G_m}{K_G a P}$, where P = column pressure (2)

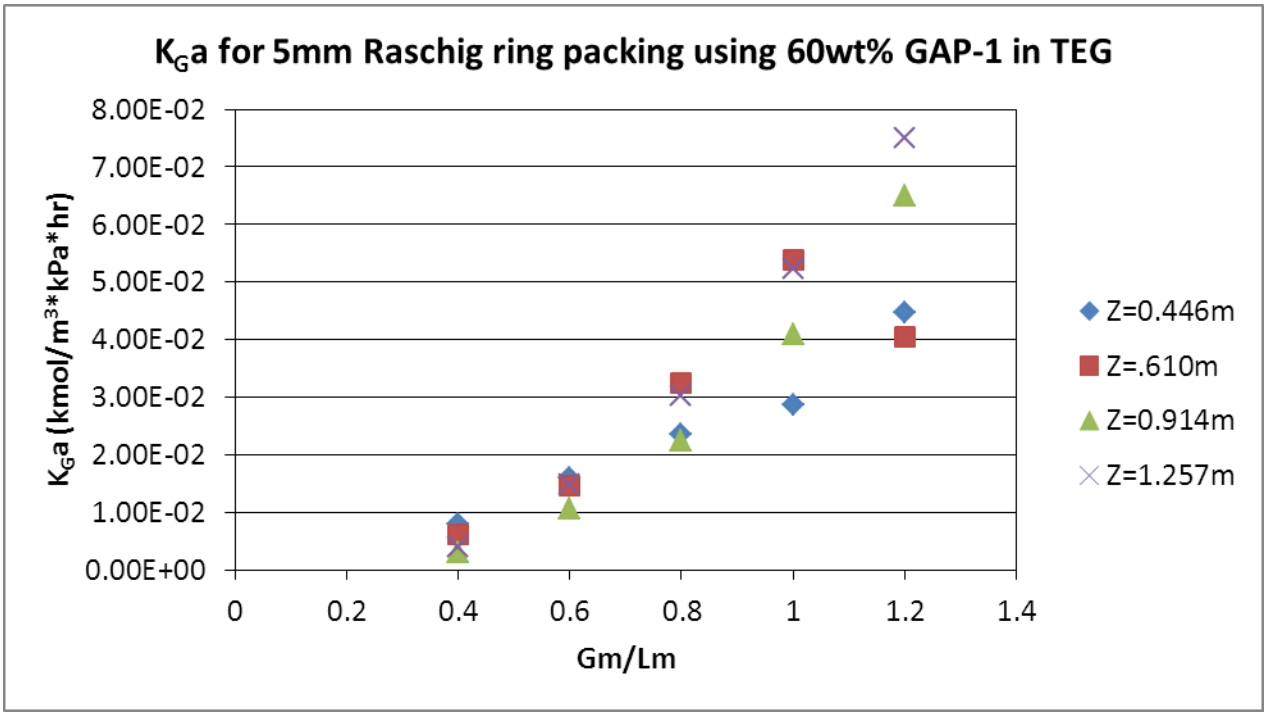

Figure 7. K_Ga for 50mm laboratory-scale absorption column and 5mm Raschig rings, T = 20 °C.

The temperature of the column was monitored to determine the temperature rise as a function of column height. Table 4 gives the temperature rise from the top to the bottom of the column as recorded at the highest Gm/Lm for each packing height. As expected, a temperature rise was observed in the column. The temperature rise was small, despite the large heat of absorption measured for this reaction, due to the non-adiabatic nature of the column.

Table 4. Temperature rise in 50mm laboratory scale absorption column.

Packing Height (m)	T Rise (°C)
0.446	3.3
0.610	4.0
1.257	3.5

For the mass transfer experiments a laboratory-scale column 50 mm in diameter and approximately 1.3 m tall was packed with Raschig rings having a length of 5.3 ± 0.5 mm, an outer diameter of 5.02 ± 0.04 mm, and an inner diameter of 3.4 ± 0.4 mm. The bulk density was

measured to be 807 kg/m^3 and the surface area per unit volume (a_v) was calculated to be 921 m^2/m^3. The column was supplied with a 16.44% (by volume) CO_2 in N_2 mixture from a cylinder purchased from AirGas. The composition of the gas entering the column was measured using a MKS Cirrus mass spectrometer and the composition of the gas exiting the column was monitored throughout the experiments. The column was filled with 0.446 m of packing. The liquid flow rate was set to 10 mL/min and the gas flow rate was set to 0.464 standard liters per minute (SLPM) (Gm/Lm = 0.4). The system was allowed to come to steady-state and the system pressures, temperatures, and gas compositions were recorded. The gas flow rate was increased and the procedure was repeated for Gm/Lm = 0.4, 0.6, 0.8, 1.0, and 1.2 and for packing heights of 0.446 m, 0.610 m, 0.914 m, and 1.257 m.

Column Pressure Drop

The expected pressure drop in the column was calculated for a column diameter of 12 inches, a liquid flow rate of 1 liter per minute (LPM), gas flow rates of 19-135 SLPM (Gm/Lm = 0.2-1.2), and packing factors (F_p) of 200-1200m^{-1} using the generalized pressure drop correlation found in Perry's Chemical Engineers' Handbook.[2] The packing factors studied span the range found for conventional random packing. The maximum pressure drop calculated was 8 mm H_2O/m packing at Fp = 1200 m^{-1} and Gm/Lm = 1.2. The recommended design values for the pressure drop in random packed column absorbers is 15-50 mm H_2O/m packing.[3] For a column 3 m high, a pressure drop of 8 mm H_2O/m packing equals a total pressure drop across the column of 0.03 psi and a pressure drop of 50 mm H_2O/m packing equals a total pressure drop across the column of 0.21 psi. Pressure drop of 0.21psi or less across the column is acceptable. This number was used for the design of the continuous system to determine the required delivery pressure of the rich gas to the column.

Column Packing Height

The packing height required to achieve 90% capture was calculated based on the K_Ga determined from the laboratory scale column and assuming a column diameter of 12 inches. The column height was calculated from Equation 1 and Equation 2 using P = 17 psia and an N_{OG} calculated numerically. To calculate N_{OG}, a straight operating line was assumed such that 90% CO_2 capture was achieved with a liquid working capacity that is 50% of the total CO_2 capacity of the liquid based on stoichiometry. Figure 8 shows the packing height for three different scenarios. Scenario 1 is calculated using a liquid flow rate of 1 LPM and the K_Ga calculated from the laboratory scale column for the 0.914 m packing height. Scenario 2 is calculated using a

[2] Green, Don W.; Perry, Robert H. (2008). Perry's Chemical Engineers' Handbook (8th Edition). McGraw-Hill.
[3] Sinnott, R.K. (2005). Coulson and Richardson's Chemical Engineering Volume 6 - Chemical Engineering Design (4th Edition). Elsevier.

liquid flow rate of 0.75 LPM and the K_Ga calculated from the laboratory scale column for the 0.914 m packing height. Scenario 3 is calculated using a liquid flow rate of 1 LPM and a K_Ga an order of magnitude smaller than the value calculated from the laboratory scale column for the 0.914 m packing height.

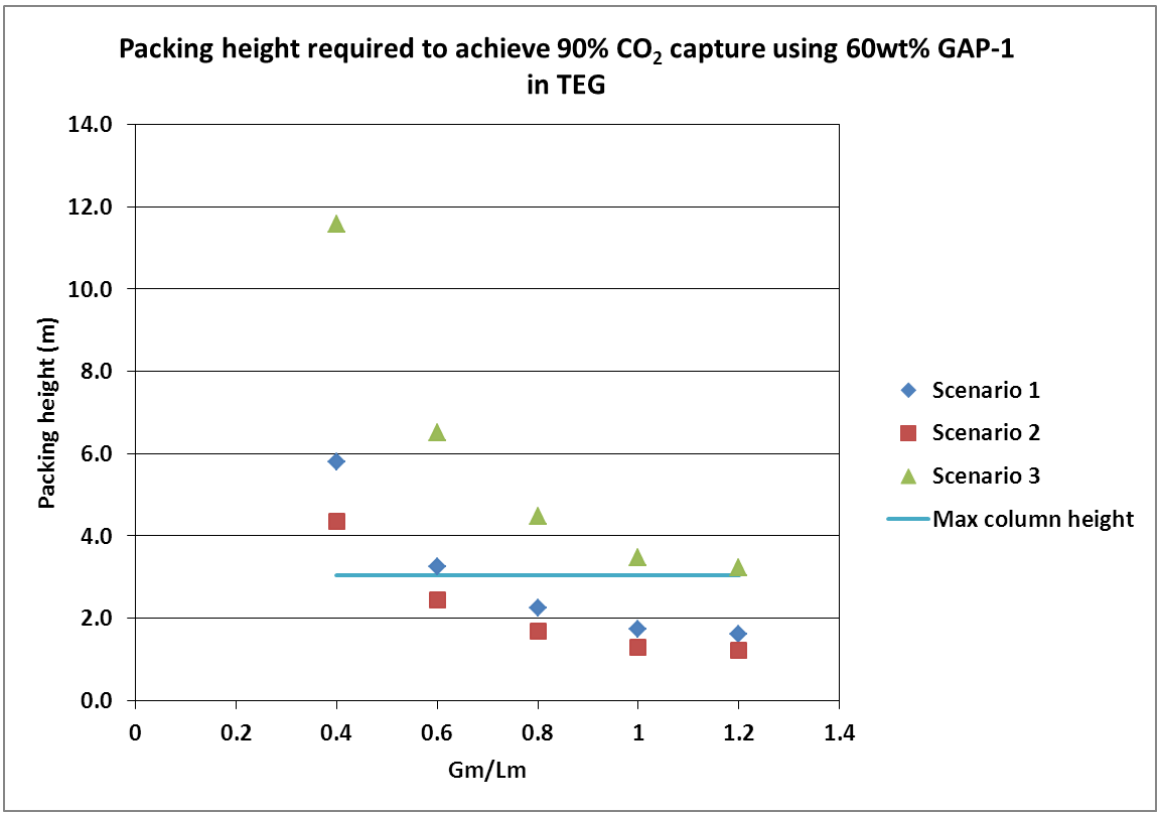

Figure 8. Packing height required for 90% CO_2 capture for a 12 inch diameter column using 60/40 (wt/wt) GAP-1m/TEG.

Figure 8 shows that 90% CO_2 capture can be achieved with a column diameter of 12 inches and a packing height of 3 m. It is important, however, that the liquid and gas flow rates in the bench-scale system can be varied over a fairly wide range so that the capture efficiency can be varied and the effect of the Gm/Lm ratio can be studied.

Figure 8 uses the K_Ga value calculated from the lab scale column using 5mm Raschig ring packing with an $a_v = 921 m^2/m^3$. On a larger scale column, the K_Ga value will change as a function of the packing type and size, as the a_v changes with packing type. To estimate the impact of changing the packing type, the packing height required to achieve 90% CO_2 capture in a random packed column having a diameter of 12 inches at a liquid flow rate of 1 LPM was

calculated as a function of a_v. The column height was determined by first calculating the surface area of 5mm Rasching ring packing that would be required to achieve 90% capture at the bench-scale conditions, then dividing that number by the new a_v to get the volume of the new packing required. That value was then divided by the cross-sectional area of the column to get the height of the packing. These results are shown in Figure 9. This figure also shows that for a packing height of 3 m and a column diameter of 12 inches, 90% CO_2 capture can be achieved using 60/40 (wt/wt) GAP-1m/TEG.

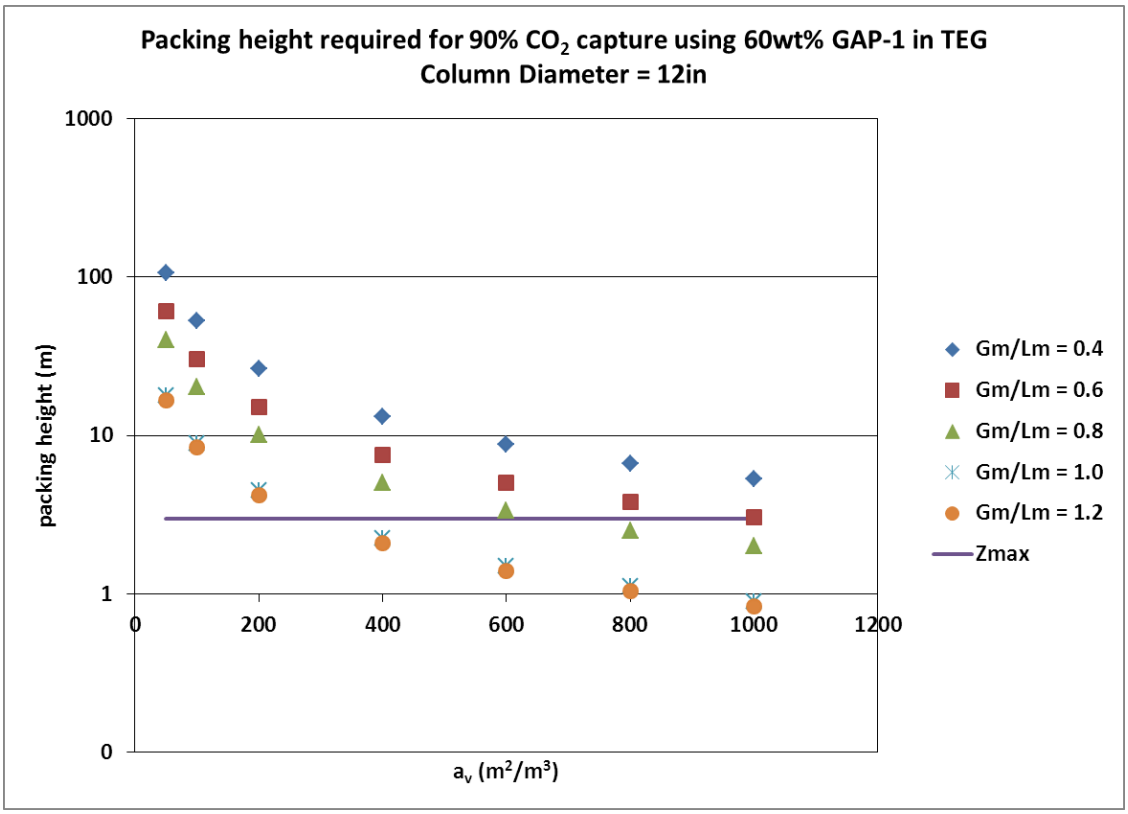

Figure 9. Packing height required for 90% CO_2 capture for a 12 inch diameter column using 60/40 (wt/wt) GAP-1m/TEG for varying a_v values.

Heat of Absorption

The heat of absorption of CO_2 in 60/40 (wt/wt) GAP-1m/TEG was required to determine the energy requirements for the absorber and desorber. The heat of absorption of 60/40 (wt/wt) GAP-1m/TEG was measured to be 2265 ± 75 kJ/kg CO_2 at 40 °C. Figure 10 shows a comparison

of the heat of absorption of 60/40 (wt/wt) GAP-1m/TEG with 30 wt% monoethanol amine (MEA) in water measured on the same reaction calorimeter.

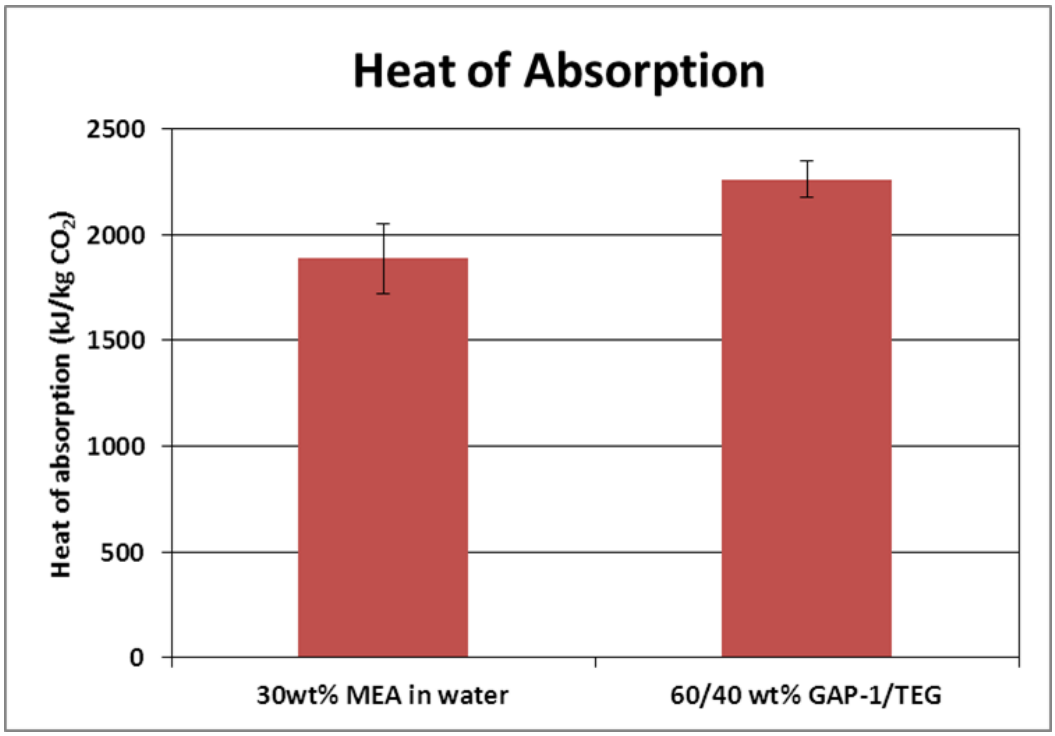

Figure 10. Heat of absorption of CO_2 at 40 °C for 30 wt% MEA in water and 60/40 (wt/wt) GAP-1/TEG (error bars shown are 95% confidence intervals).

The heats of absorption of CO_2 with 60/40 (wt/wt) GAP-1m/TEG were measured using an OmniCal ReactMax–Z3-UL Reaction Calorimeter. Hasteloy-C reactor vessels (25mL) supplied by the calorimeter manufacturer were used that can withstand pressures up to 34.5 bar. An additional stainless steel vessel was added adjacent to the calorimeter in order to supply heated CO_2 to the reactor vessel. This additional vessel was placed in a heated box fitted with a circulating fan. A Sierra Instruments Smart-Trak®2 Model# C100L mass flow controller was installed in-between the reactor vessel and the additional stainless steel CO_2 storage vessel to measure the amount of CO_2 added to the reactor. This mass flow controller has an integrated totalizer to measure the total flow of a gas over a user-defined time.

The reactor vessel was filled with ~2.5 g of sample and a magnetic stir bar was added. The exact volume of the sample was calculated using the density of each sample. The reactor was sealed,

placed inside the calorimeter, stirring set to between 600 and 780 RPM and the temperatures of the calorimeter and the CO_2 storage vessel were set to 40 °C. The CO_2 storage vessel was filled with CO_2 from the supply tank. The system was then allowed to come to equilibrium for 1-2 hours. When both the heat flow and the calorimeter temperature achieved steady-state, the system was considered to be at equilibrium.

The totalizer on the mass flow controller was reset to zero and the reactor was filled with ~20 SCC of CO_2. The value on the mass flow controller totalizer was recorded and the reaction was allowed to proceed for 2 hours. This procedure was repeated 13 more times, for a total CO_2 addition of ~280 SCC of CO_2. For each addition of CO_2, the baseline value for the heat flow was established and subtracted from the raw data. The baseline-subtracted heat flow was then integrated over the reaction time to determine the total reaction heat. The total amount of CO_2 remaining in the headspace of the reactor was calculated from the pressure, temperature, and headspace volume. The total amount of CO_2 absorbed by the sample was calculated by subtracting the CO_2 remaining in the headspace at the end of the reaction from the total CO_2 that was added plus the CO_2 remaining in the headspace after the previous reaction step. The heat of reaction for each step was then calculated by dividing the total reaction heat by the amount of CO_2 absorbed by the sample.

Desorber Design

In order to design the CO_2 desorption system, the CO_2 loading as a function of temperature and pressure was needed. Kinetic information was also required to size the system. Note that solvent thermal stability discussions will be in the Task 4.2 section.

<u>Desorption Isotherms</u>

Equilibrium isotherms of the carbamate in 60/40 (wt/wt) GAP-1m/TEG at the temperatures and pressures of the desorber were determined. The experimental system is presented below on Figure 11.

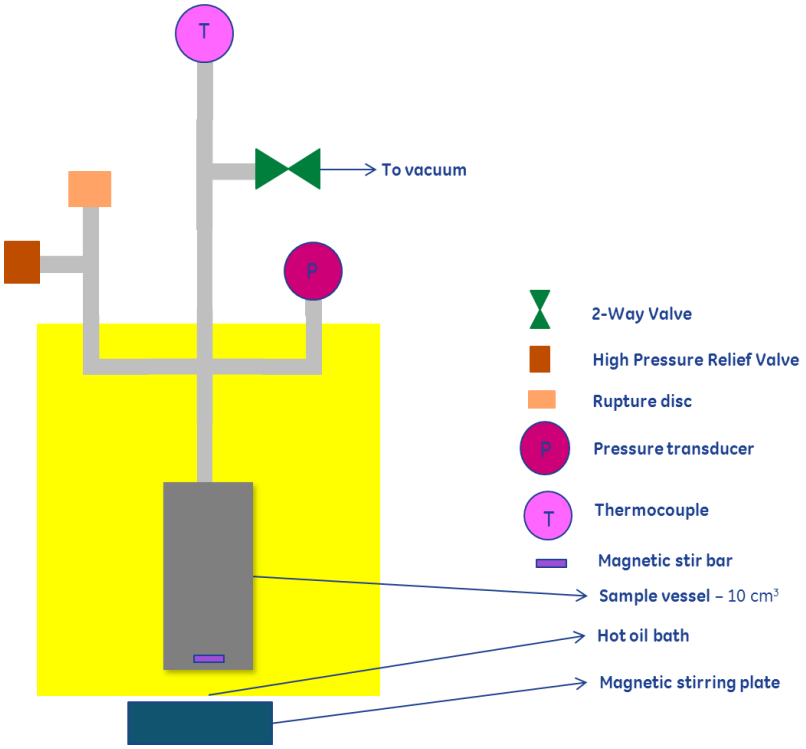

Figure 11. Desorption isotherm experimental setup.

At the beginning of each experiment, the system was cleaned with methanol and dried in a vacuum oven. The magnetic stirrer was placed into the reactor, and then ~2 g of sample were added. After the sample vessel was connected to the system, evacuation of the system was performed to remove any air from the head space. Afterwards, the system was placed into a hot-oil bath, and a temperature ramp was performed to heat up the solution to 100 °C, 120 °C, 140 °C, 160 °C, and 180 °C. The system was held at each temperature for 3 to 5 hours, in order to provide a sufficient time to reach equilibrium. Pressure readings were continuously collected and the amount of CO_2 in the gas phase and equilibrium carbamate loading in the liquid phase were determined. The experiment was run with samples with carbamate loadings of 20%, 40%, 60%, 80%, and 100%. Resulting equilibrium isotherms and 95% confidence intervals are presented in Figure 12.

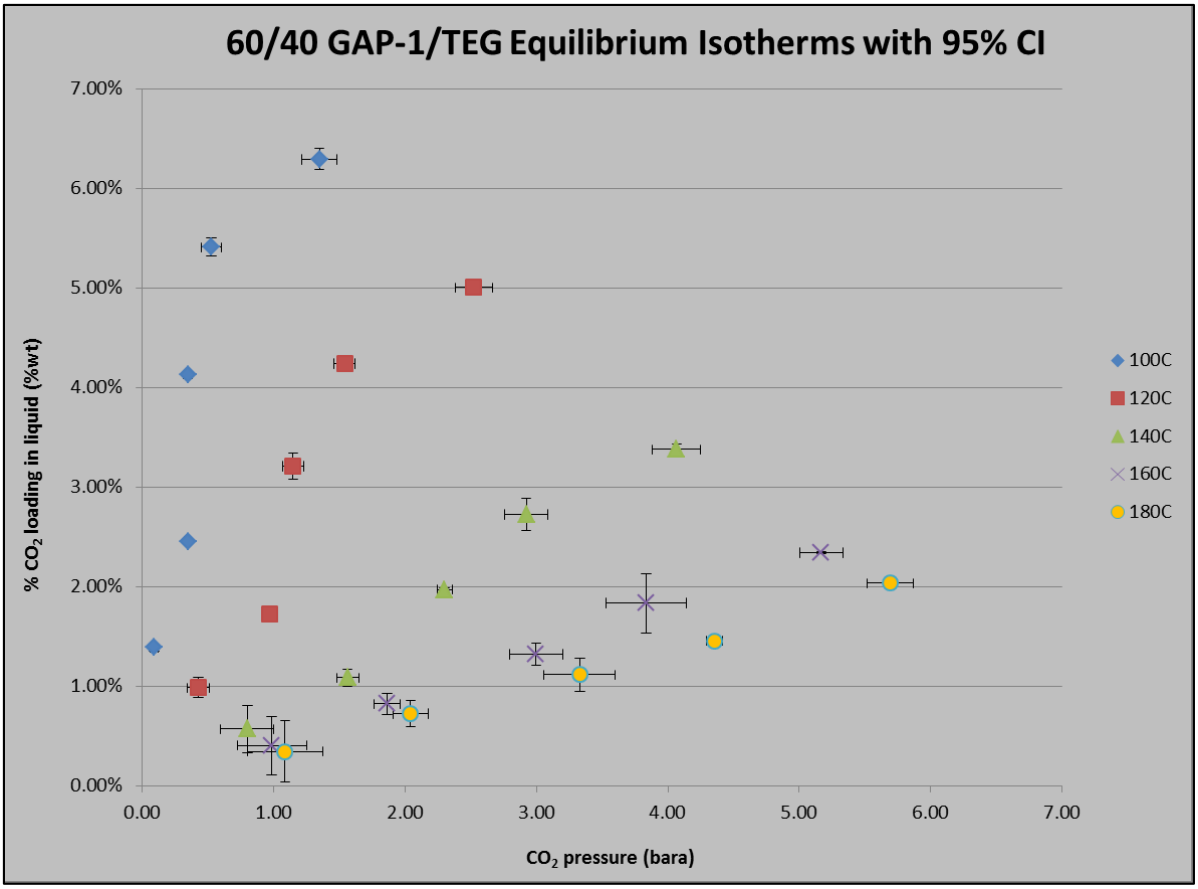

Figure 12. Equilibrium isotherms for 60/40 (wt/wt) GAP-1m/TEG solution.

Desorption Kinetics

To determine the kinetic rate of desorption of CO_2 from the 60/40 (wt/wt) GAP-1m/TEG mixture Thermogravimetric Analysis (TGA) was performed for samples with various carbamate loadings. For consistency, sample sizes were ~8-8.5mg, and the heating rate was set to 5 °C/min. Pure 60/40 (wt/wt) GAP-1m/TEG mixture was used as a background curve for the analysis, and each sample was run three times for repeatability purposes. In Figure 13 it can be observed that there is a peak which corresponds to desorption of CO_2 from the 60/40 (wt/wt) GAP-1m/TEG carbamate mixture loaded to 100%. The background of GAP-1m/TEG evaporation was subtracted from the carbamate sample run and the resulting CO_2 peak is presented on Figure 14.

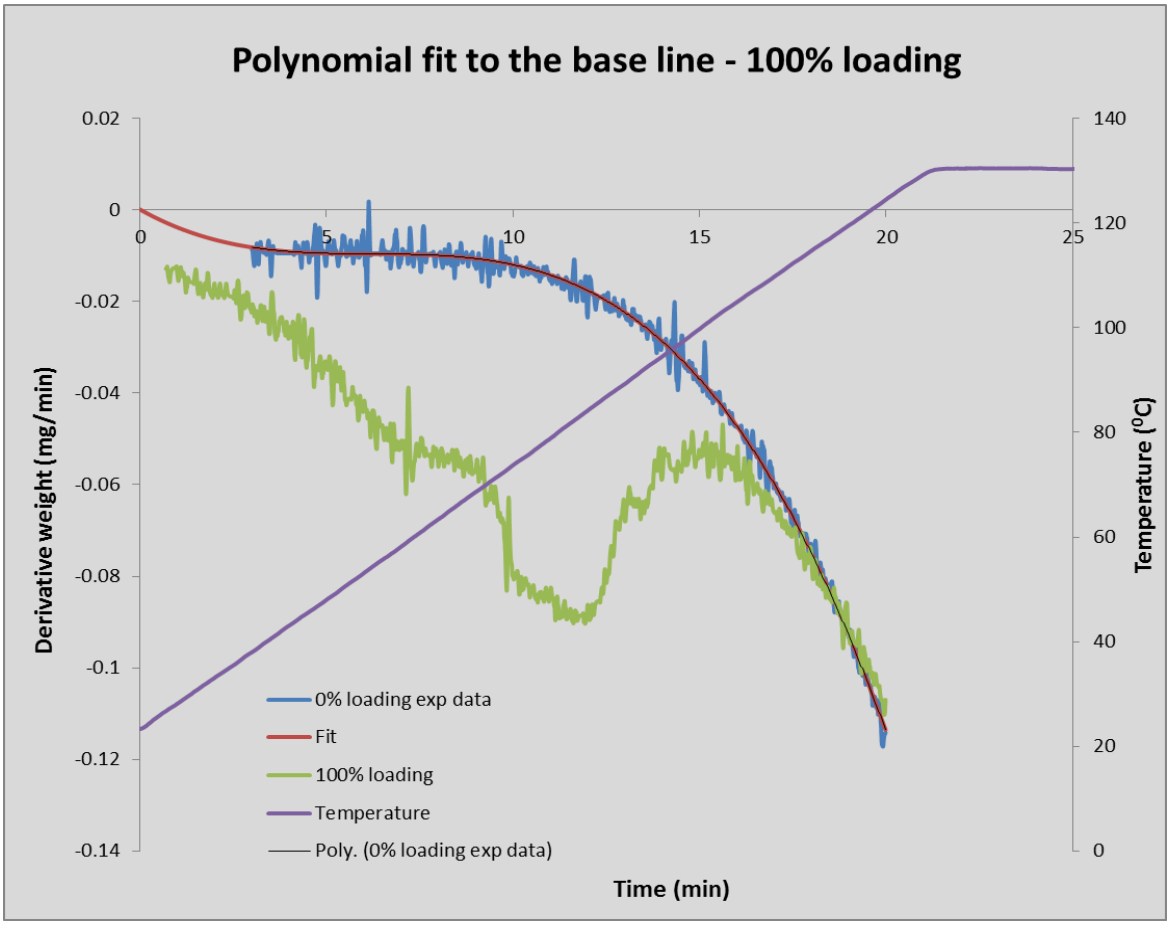

Figure 13. TGA run results for 60/40 (wt/wt) GAP-1m/TEG and 100% loaded carbamate in 60/40 (wt/wt) GAP-1m/TEG.

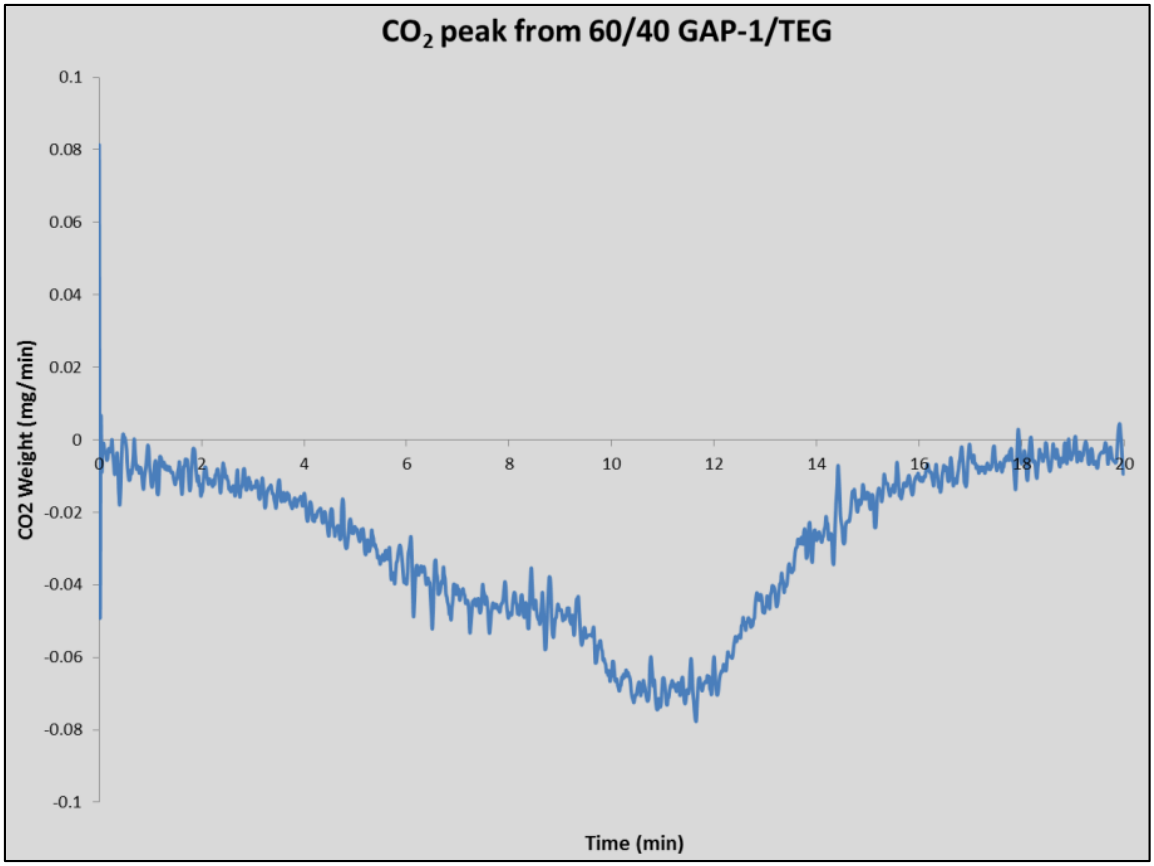

Figure 14. TGA peak corresponding to CO_2 desorption from 60/40 (wt/wt) GAP-1m/TEG carbamate mixture.

To determine the area under the CO_2 peak, it was fitted to a Gaussian curve. The Gaussian was then fitted with five Lorentzian peaks using Peak Fit Software as shown in Figure 15.

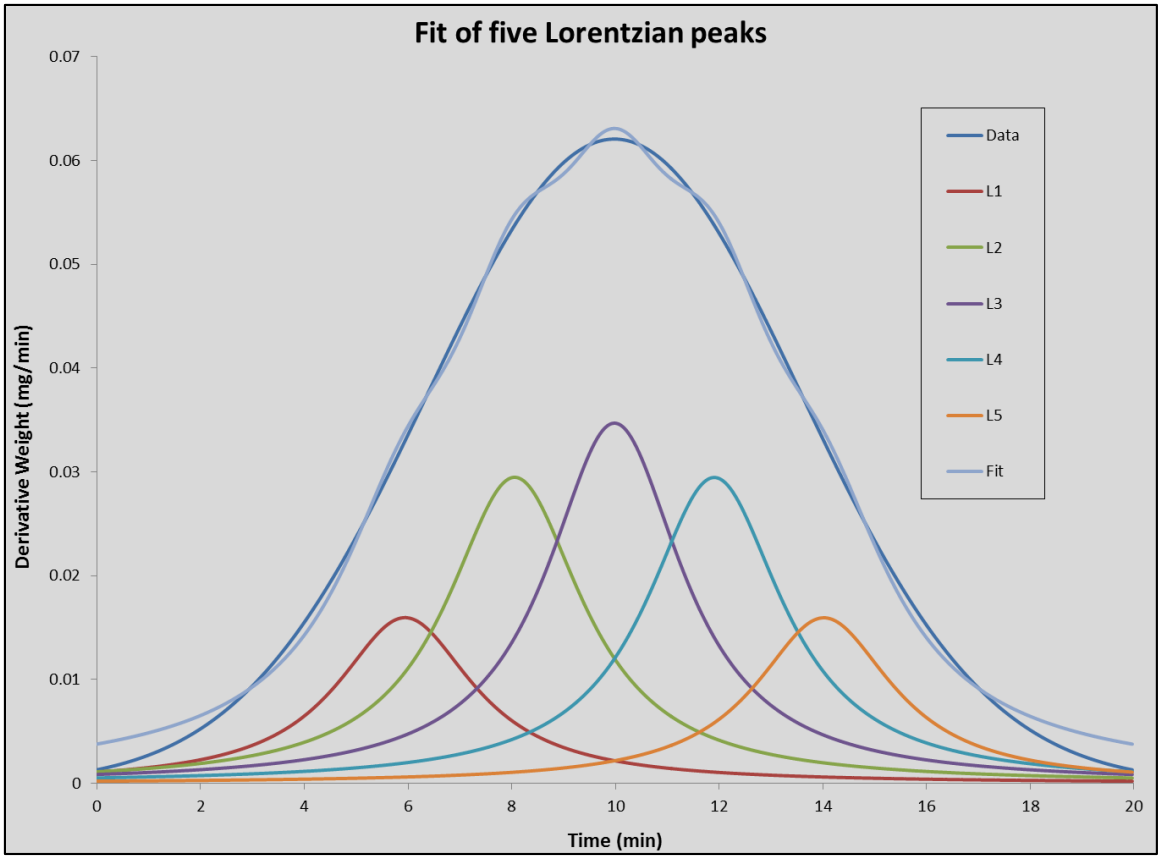

Figure 15. CO_2 peak fitted with five Lorentzian peaks.

The Lorentzian peak fitting parameters allow the integration of the area under the CO_2 desorption curve and the determination of the amount of CO_2 desorbed. Desorption reaction order was assumed to be 1, and from the available data it was possible to plot $\ln(k_2)$ vs 1/T, where k_2 = desorption constant and T = temperature. This plot is shown in Figure 16.

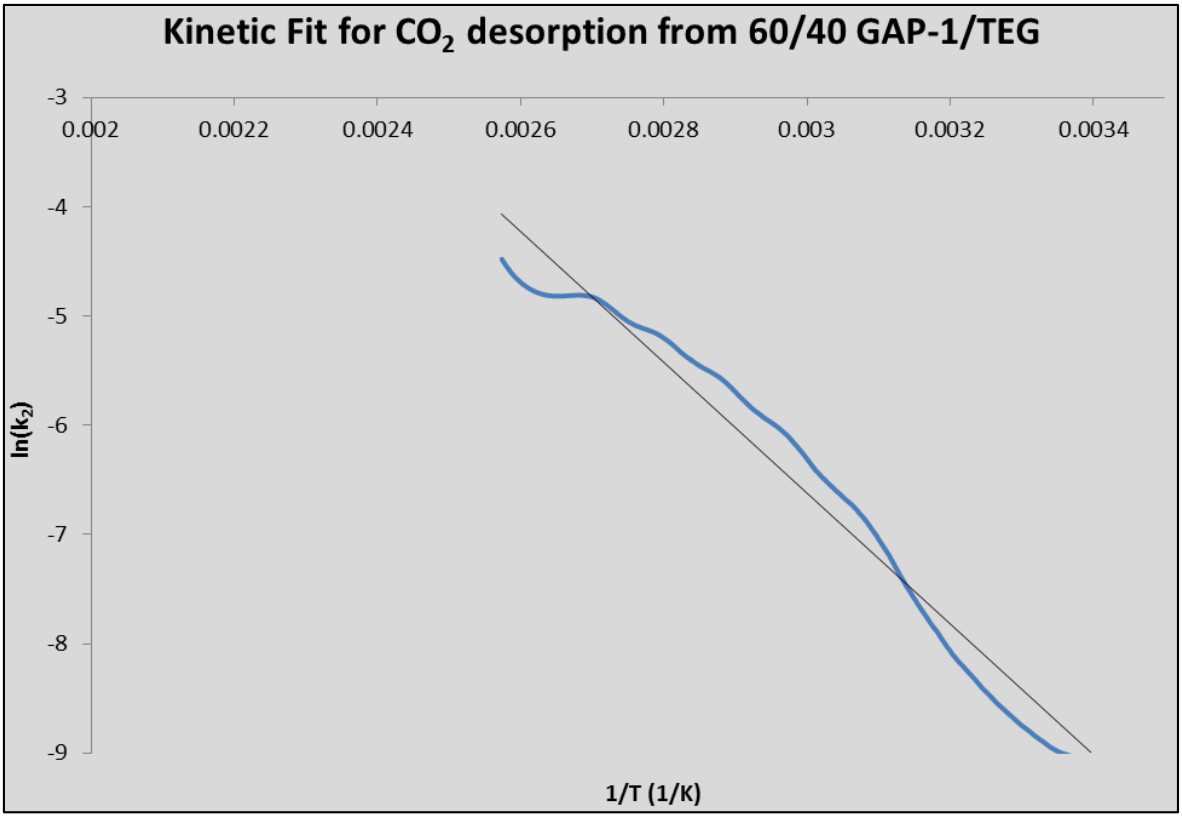

Figure 16. Dependence of desorption rate constant on temperature.

According to the Arrhenius equation:

$$lnk = -\frac{E_a}{R} * \frac{1}{T} + lnA_0$$

Where T = Temperature (K)

R = gas constant = 8.314 (kJ/kmol*K)

E_a = activation energy (kJ/kmol)

A_0 = frequency factor

Therefore, using the plot from Figure 16, the activation energy and frequency factor can be determined, and their values were estimated to be E_a = 7.69 kcal/mol and A_0 = 568. These reaction parameters were used to determine the residence time required for the desired

desorption in a continuous stirred-tank reactor (CSTR). Figure 17 shows that small residence times are required to desorb most of the CO_2 from the solution.

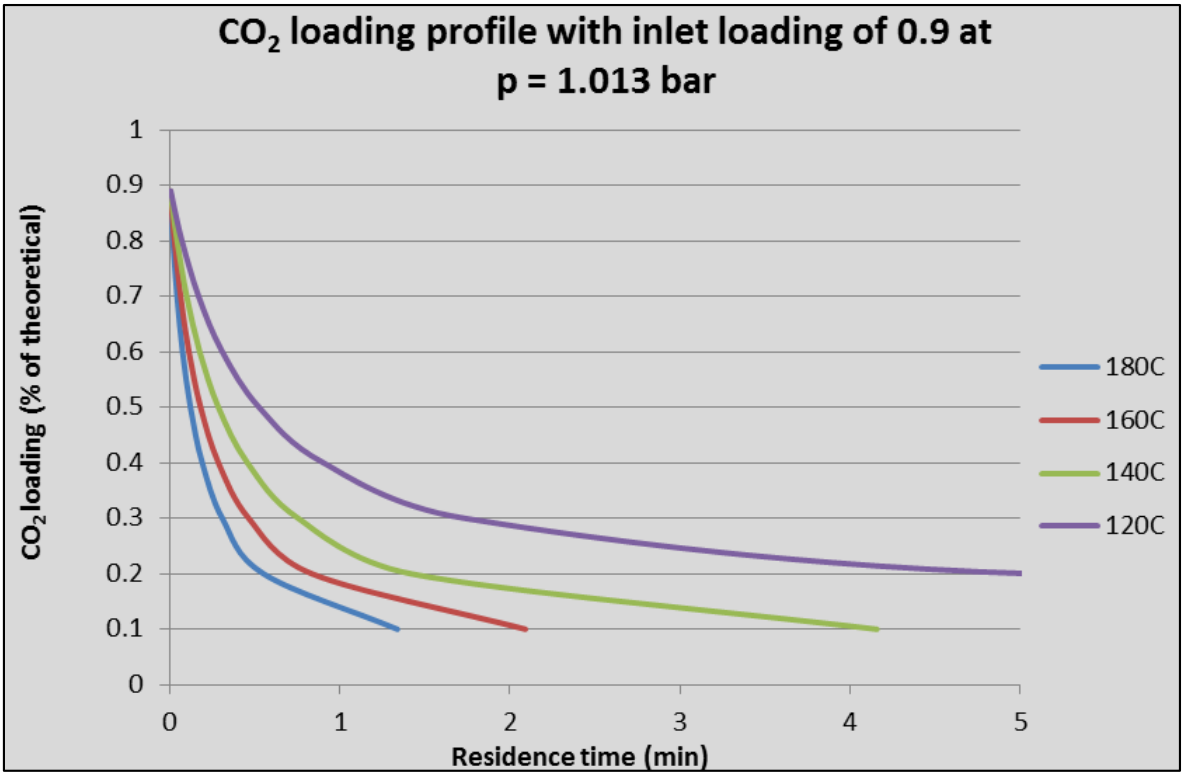

Figure 17. CO_2 loading profile with inlet loading of 0.9 at p = 1.013 bar for a CSTR.

Bench-Scale Desorber Design Details

The bench-scale desorber size was determined using the kinetic parameters determined for desorption. The bench-scale desorber is a CSTR with a working volume of 15 liters, which provides a residence time of up to 15 minutes, and total volume of ~30 liters. The reactor is designed to withstand 300 psig and 300 °C. A reactor jacket was provided, and a hot oil system was connected for heating. An impeller and three baffles were added to provide sufficient mixing to improve mass and heat transfer. Also, the recirculation loop with a high pressure gear pump and heat exchanger were added to the desorber to ensure required heating and to increase the mass transfer through sparging of the liquid back to the reactor. The level of the liquid in the desorber, temperature, and pressure were controlled by the instrumentation and the control system.

The desorber construction was completed. The construction drawing for the desorber is presented in Figure 18.

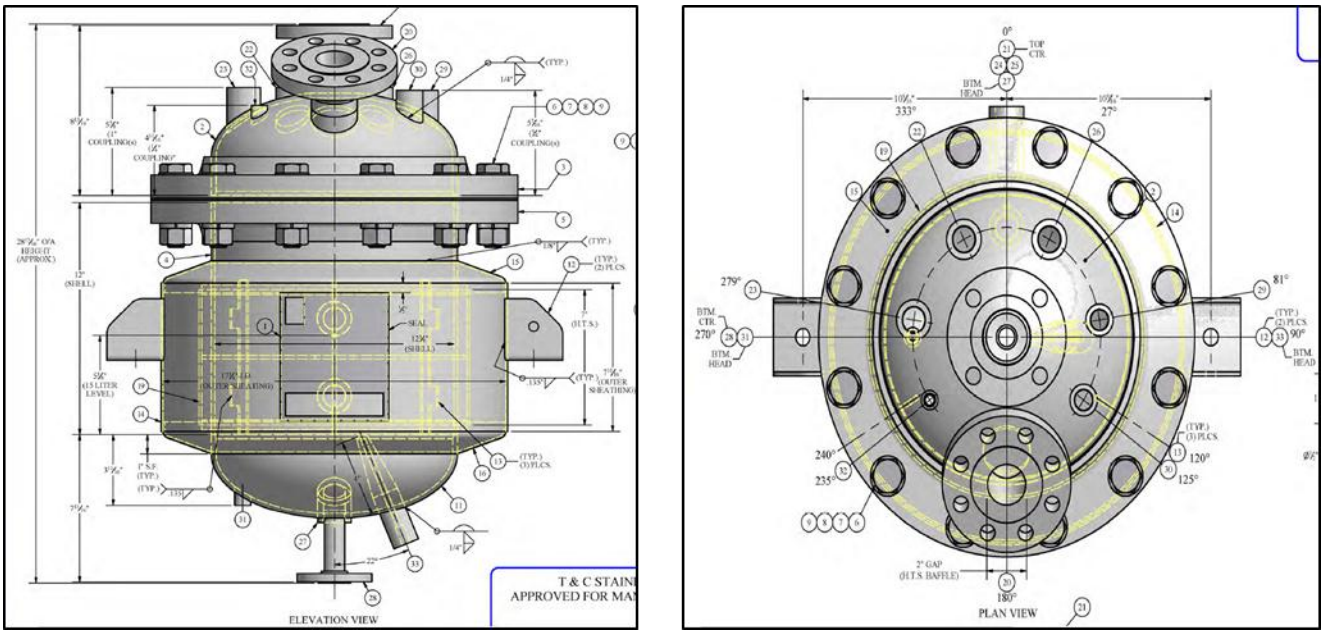

Figure 18. Desorber drawing.

The desorber has a removable lid for accessibility to the agitator. The agitator is located at the top of the desorber, and there are a sufficient number of inlets on the top of the reactor for the required streams and instrumentation.

In order to determine how much heat can be delivered through the reactor jacket, the overall heat transfer coefficient, U, was calculated, and the following expression was used:

$$\frac{hD_j}{k} = a\left(\frac{L_p^2 N_r \rho}{\mu}\right)^b \left(\frac{c\mu}{k}\right)^{1/3} \left(\frac{\mu_b}{\mu_w}\right)^m$$

where h – film coefficient for the inner wall, D_f is the inside diameter of the mixing vessel, L_p – agitator diameter, N_r – speed of agitator; a, b, m – are constant values specific to the impeller type. Several assumptions were made to estimate the value of film and overall coefficients:

- Impeller speed is 400 rpm
- Paddle agitator (45-degree pitch blade information was not available)
- Ratio of bulk viscosity to wall viscosity is 10. It was determined that this value has no significant impact, and therefore a conservative value of 10 was assumed.

The final overall value of the heat transfer coefficient for the jacketed vessel was calculated to be 311 W/(m^2·K).

The total heating load on the desorber is 7622 W, and this value includes sensible heating of the 60/40 GAP-1m/TEG solvent from 32 °C to 180 °C and heat of desorption of CO_2 from the solvent. The reactor jacket can only deliver ~20% of this heat load, and therefore, a recirculation loop was added to the desorber design. It consists of a high pressure gear pump and shell and tube heat exchanger to deliver all required heat into the system. The flow rate in the recirculation loop can be adjusted from 0 to 30 liters per minute.

The agitator design is presented in Figure 19. The agitator has two sets of 45-degree pitched impellers to provide sufficient mixing and mass transfer between liquid and gas phases.

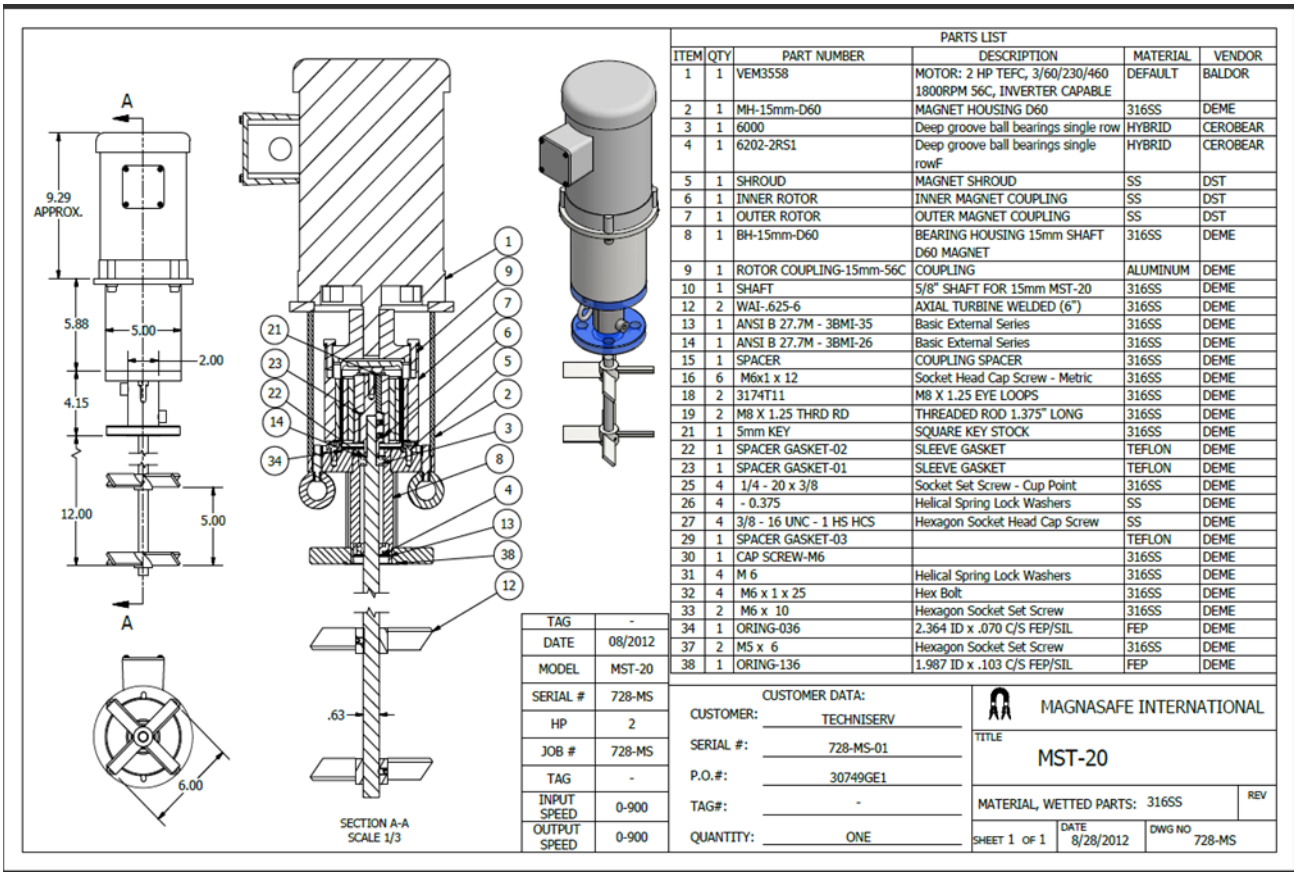

Figure 19. Desorber agitator design.

Design of Bench-Scale System

Figure 20 shows the detailed Piping and Instrumentation Diagram (P&ID) for the bench-scale system. The system consists of a gasoline generator that produces exhaust gas as a proxy for the flue gas from a coal-fired power plant. The exhaust from this generator is chilled in a heat exchanger to lower the water content to that typical of the flue gas from a coal-fired power plant. The exhaust can then be mixed with a variety of gases, such as SO_2, supplied from a gas manifold, to adjust the composition to match the flue gas from coal. The mixture is then heated to 40 to 60 °C. The exhaust, with a flow rate of 50-200 (SLPM), is sent to the bottom of a column, where it flows up, countercurrent to the aminosilicone solution at 1-2 LPM, which captures CO_2. The column is designed in a modular fashion, so that the height of the column can be adjusted, and a variety of different packing materials can be tested. The stripped exhaust exits the top of the column and is sent to a mass spec and CO_2 analyzer for

compositional analysis. The rich solvent leaves the bottom of the column, and is pumped to the high pressure desorber.

The desorber is a jacketed, high-pressure CSTR. It has a recirculation loop, with a heat exchanger. The recirculation loop is designed to provide additional heat input to that provided by the jacketing on the tank. In addition, the recirculation is used to increase mass transfer in the reactor. The lean sorbent leaves the bottom of the desorber and is cooled, dropped in pressure, and sent to a storage tank, before being sent back to the top of the column. The CO_2 produced in the desorber is throttled down in pressure and sent to gas analysis. The system is fully automated, with detailed measurements of all important process variables, including temperatures and pressures.

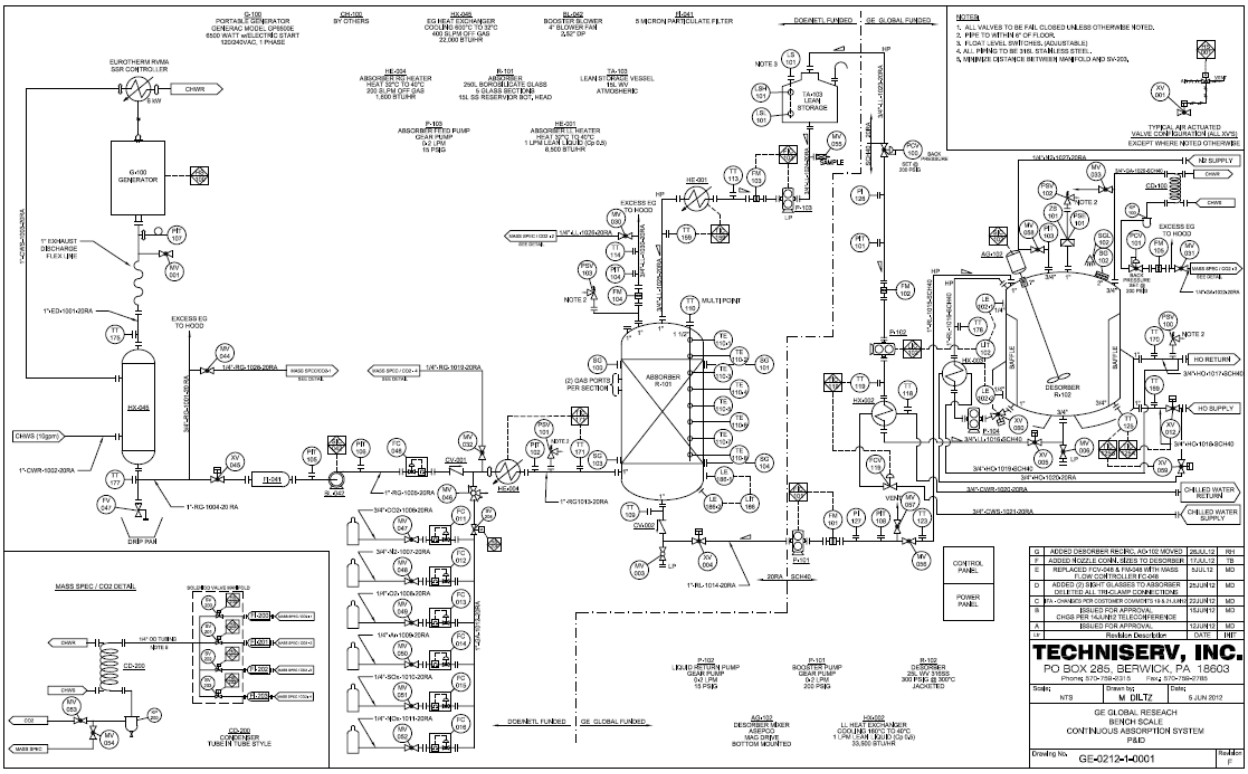

Figure 20. The detailed P&ID for the bench-scale system.

Task 3.2: Build Bench-Scale System

Construction of the bench-scale system was completed by Techniserv in the 4th quarter of 2012. A team from GE GRC traveled to Techniserv from 11/26/2012 to 11/30/2012 to conduct a

factory acceptance test, in which the system was tested to certify proper construction and function. Other than a couple of small deficiencies that were remedied during the test, the system performed as anticipated, and was deemed fully functional. On 12/13/2012, Techniserv delivered the system to GE GRC. Figure 21 shows the bench-scale system during the factory acceptance test at Techniserv.

Figure 21. GEGRC team members completing factory acceptance test of bench-scale system.

Task 3.3: Develop a Bench-Scale Test Plan

The bench-scale system was used to obtain data required for validating a bench-scale model and developing a scale-up plan. The time allotted in the award for this work was six months (Q1 2013 – Q2 2013) and the data to be collected in that time frame included design parameters for both the absorber and the desorber. A bench-scale system test plan was developed to guide the bench-scale system testing. The experiments were prioritized to provide data required for modeling the bench-scale system. Figure 22 shows the timeline for the planned experiments. Each section of the experimental test plan is explained in further detail below.

Task / Experiment	FW																								
	Jan					Feb				Mar				Apr				May				Jun			
	1	2	3	4	5	6	7	8	9	10	11	12	13	14	15	16	17	18	19	20	21	22	23	24	25	26
Install and commision system																									
- install system																									
- write SOP																									
- complete white tag review																									
- clean system with TEG																									
- load system with GAP-S/TEG																									
Baseline system performance																									
- start-up system, determine system setpoints																									
- determine effect of conditions on conc. of CO_2 in liquid																									
Determine $K_G a$ with random packing																									
- vary the G_m/L_m ratio																									
- increase G_m to max																									
- vary the incoming temperature of the solvent																									
- vary the incoming temperature of the gas																									
- vary the lean CO_2 loading																									
Determine desorber performance																									
- vary the stirring rate in the desorber																									
- vary the circulation rate in the desorber																									
- vary the temperature of the desorber																									
- vary the pressure of the desorber																									
Determine effect of water on the system																									
- vary water content in gas stream																									
Determine the effect of NO on the the system / solvent																									
- add NO to the gas and operate system for 5 days																									
- monitor solvent properties / degradation																									
Determine the effect of SO_2 on the the system / solvent																									
- add SO_2 to the gas and operate system																									
- monitor solvent properties / degradation																									
Determine the recommended materials of construction																									
- Install corrosion coupons																									
- Sample / measure corrosion coupons																									
Monitor degradation of solvent																									
- sample and analyze solvent																									

Figure 22. Schedule for bench-scale experimental tests.

Install and Commission System

The installation of the bench-scale system is scheduled to be completed by January 15, 2013. One week is allotted for the white-tag review, where the system and the SOP will be reviewed to verify safe operation. When the white-tag review is successfully completed, the system will be filled with random packing (Intalox® Ultra T™ supplied by Koch-Glitsch LP) and loaded and cleaned with tri-ethylene glycol (TEG) to remove any remaining contaminants from the system. During the cleaning of the system, the system will be tested to ensure that the equipment operates as designed. Testing the system will include circulating both the liquid and the gas, operating the heat exchangers, heating the desorber, and sampling and measuring the composition of the gas. When the system is cleaned and the operation verified using TEG, the system will be filled with a 60/40 (by weight) mixture of GAP-S (GAP-1m supplied by SiVance) and TEG. The corrosion coupons will also be installed at this time. The continuous system will then tested with the 60/40 GAP-S/TEG mixture and the control loops will be tuned.

Baseline System Performance

The goal of this task is to determine a baseline system performance, how the performance changes as a function of reaction conditions (such as liquid and gas flow rates, absorber inlet liquid and gas temperatures, desorber temperatures), and for the operators to gain experience running the system. The range to be studied for each parameter is shown in Table 5.

Table 5. Ranges for parameters to be studied in baseline system performance.

Parameter	Range
Liquid flow rate	0.2 – 2 LPM
Gas flow rate	20 – 200 SLPM
Inlet liquid temperature	30 – 50 °C
Inlet gas temperature	30 – 60 °C
Desorber temperature	100 – 160 °C
Agitator speed	0-100% of max
Recirculation pumping rate	0-100%

During this task, the mass spectrometer and CO_2 analyzer will be brought online. In these experiments, the CO_2 concentration in the liquid exiting the absorber and desorber will be determined as a function of the reaction conditions, and these data will be used to determine the conditions required for targeting desired liquid CO_2 concentrations in the system for

subsequent experiments. The conditions in the absorber to be studied include the liquid and gas flow rates, the inlet liquid and gas temperatures, and the concentration of CO_2 in the inlet liquid. The conditions in the desorber to be studied include desorber temperature, desorber pressure, recirculation pumping rate, agitator speed, and the concentration of CO_2 in the inlet liquid. Based on the results of these baseline experiments, the team will re-evaluated the expected conditions for the experiments planned in the subsequent tasks.

Determine K_Ga with Random Packing

The overall gas phase mass transfer coefficient (K_Ga) will be determined as a function of gas and liquid flow rates, absorber column inlet gas and liquid temperatures, and concentration of CO_2 in the inlet liquid. The liquid flow rate will be varied from 0.5 to 2 LPM, and the gas flow rate will be varied from 50 to 200 SLPM. The inlet gas and liquid temperatures will be varied from 30 to 50 °C. The CO_2 concentration in inlet liquid will be varied by adjusting the desorber conditions (temperature and pressure) as determined in the baseline system performance task. The gas composition will be monitored and recorded at the inlet and outlet of the column, along the height of the column, and at the exit of the desorber. The composition of the liquid will be monitored at the inlet and outlet of the column and the outlet of the desorber. From these data, the overall gas phase mass transfer coefficient will be calculated.

Table 6 gives an example of a set of experiments aimed at determining the effect of gas and liquid flow rates on the overall gas-phase mass transfer coefficient. In this set of experiments, the temperature and the CO_2 concentration in the inlet liquid are held constant. Additional experiments will probe the effect of inlet liquid and gas temperature and CO_2 concentration in the inlet liquid.

Table 6. Example experiments for determining $K_G a$.

Gas flow rate (SLPM)	Liquid flow rate (LPM)	$T_{in,\ gas}$ (°C)	$T_{in,\ liquid}$ (°C)
50	1	40	40
100	1	40	40
150	1	40	40
200	1	40	40
50	0.5	40	40
100	0.5	40	40
150	0.5	40	40
200	0.5	40	40
50	2	40	40
100	2	40	40
150	2	40	40
200	2	40	40

Determine Desorber Performance

The desorption reaction rate constant will be determined by varying the following parameters: the residence time of the solvent in the reactor by adjusting the level set point inside the reactor, temperature of the reactor in the range of 120 °C-180 °C, and the desorber pressure. The recirculation rate in the desorber and the agitator speed will be optimized to minimize the effects due to mass transfer in the desorber. The CO_2 flow rate exiting the reactor will be measured as well as the carbamate loading of the solvent in the reactor inlet and outlet streams. From these data, the reaction rate constant can be calculated and this will enable the confirmation of the optimal reactor design for a large scale unit.

Determine Effect of Water on the System

The water concentration in the gas stream will be varied between 0 and 17 mol% by using bottled gas and/or changing the temperature to which the gas stream exiting the generator is cooled. The amount of water absorbed by the solvent in the liquid can be monitored by measuring the relative humidity of the gas stream entering and exiting the absorption column. The amount of water removed from the liquid in the desorber will be monitored by measuring the water captured in the overhead condenser as well as the relative humidity of the gas stream exiting the desorber. The CO_2 capture performance of the system will also monitored as

the water content in the gas stream is varied to determine the effect of water on the overall system.

Determine the Effect of NO on the System/Solvent

The effect of NO in the gas stream will be determined by conducting test runs with NO. The test run will be conducted for five days. The solvent will be monitored over the course of the experiment to check for degradation in the solvent. Degradation will be monitored using nuclear magnetic resonance (NMR), gas chromatography (GC), and elemental analysis. The performance of the system will be recorded to determine changes in CO_2 net loading.

Determine the Effect of SO_2 on the System/Solvent

The effect of SO_2 in the gas stream will be determined by conducting test runs with SO_2. The solvent will be monitored over the course of the experiment to check for degradation in the solvent. Degradation will be monitored using NMR, GC, and elemental analysis. The performance of the system can be recorded to determine changes in CO_2 net loading.

Determine the Recommended Materials of Construction

The recommended materials of construction are to be determined in various locations in the continuous system. Coupons of carbon steel and 304L stainless will be placed in the absorber sump, the lean storage tank, and the desorber. Coupons are then removed three times over six months, cleaned, and weighed. The corrosion rate will be determined from the weight loss over time. The system will not be operated continuously for the six months. Therefore, the time under each set of conditions will be recorded, and the corrosion rate will be reported as both a function of total time in the system, and time under typical operating conditions.

Monitor Degradation of Solvent

The solvent will be monitored periodically to determine how operating the system affected the solvent performance and properties. The solvent can be sampled during testing and the samples then analyzed by NMR, GC, elemental analysis, heat capacity, viscosity, and equilibrium loading. The purpose of these analyses is to gain a better understanding of how the solvent performance changes over its life, how quickly the solvent degrades under use conditions, and how the solvent properties change as the solvent degrades. As with the materials of construction testing, the system will not be operated continuously for the six months. Therefore, the time under each set of conditions will be recorded, and the degradation rate calculated using the time under typical operating conditions. The intention of these experiments is to fill the system with material and perform all of the experiments with that

initial charge of material to characterize degradation of the solvent under realistic operating conditions.

Task 4: Develop Absorption Material Manufacturing Plan

Task 4.1: Determine Manufacturability, Raw Material Supply Adequacy, and Estimated Price for Top Material Candidates

GE Global Research is developing technology using an aminosilicone based solvent to capture CO_2 from flue gas. In previous work as part of the DOE award # DE-NT0005310, it was found that the best performing material for CO_2 capture was an aminosilicone oligomer known as GAP (3-aminopropyl end-capped polydimethylsiloxane (PDMS)) with a structure shown in Figure 23. It readily reacts with CO_2 to form a carbamate salt, as shown in Figure 24. At elevated temperatures, CO_2 desorbs reversibly, permitting reuse of the CO_2 capture solvent. The best CO_2 capture solvent performance was found with a material with an average value for *x* of 1. As short-hand nomenclature, it will be called GAP-1m. As determined by ^{1}H NMR, GAP-1m consists of approximately 40% GAP-0, 33% GAP-1, 19% GAP-2, and 8% GAP-3, with the average molecular weight being that of GAP-1.

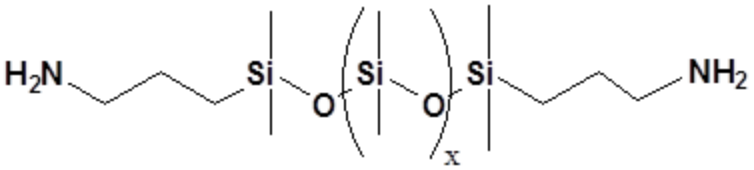

Figure 23. Chemical structure of GAP-x material.

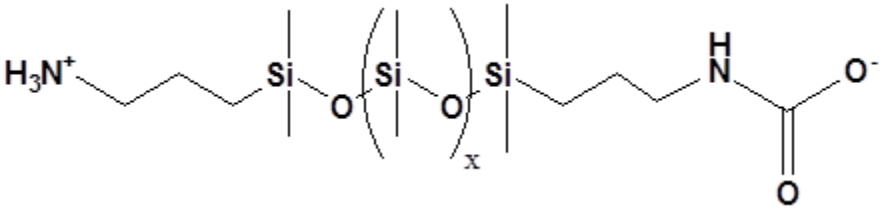

Figure 24. Formation of carbamate by GAP-x material upon absorption of carbon dioxide.

Current Process for Manufacturing GAP-1m

GAP-1m is manufactured by several batch-wise steps. In the first step, chlorodimethylsilane (CDMS) is hydrolyzed with water and condensed to form crude tetramethyldisiloxane, as shown in Figure 25. The crude tetramethydisiloxane is purified to remove any lights (silanes[4], cyclics[5]) or bottoms (water, salts, higher weight polydimethylsiloxanes).

The purified material is charged to a batch reactor with allylamine and Ashby's catalyst (vinyl methyl cyclic platinum[6 7]). As shown in Figure 26, the hydride and double bond react together to form a silicon-carbon bond[8]. Because allylamine has high toxicity, the process is designed where it is the limiting reagent. Ideally, two molecules of allylamine react with one molecule of tetramethyldisiloxane to yield one molecule of product, 1,3-bis(3-aminopropyl)tetramethyldisiloxane. In such cases, x = 0. Preferably, the silane addition occurs at the gamma position, giving the molecule a nickname of gamma-amino propyl or GAP-0. Unfortunately, the reaction does not occur ideally, yielding a mixture of linear and cyclic products. Based upon previous manufacturing experience, the current process uses up to 1.5 molar excess of tetramethyldisiloxane to complete hydrosilation of all the allylamine. While greatly increasing raw material costs, it also complicates downstream processing by creating a wider distribution of molecular weights.

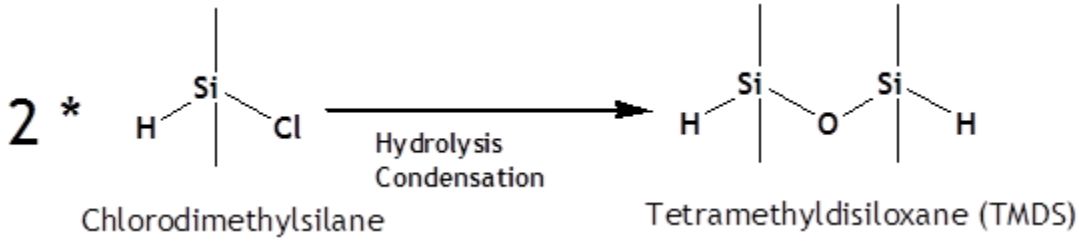

Figure 25. Production of tetramethyldisiloxane.

[4] http://www.britannica.com/EBchecked/topic/544022/silane.
[5] http://www.cyclosiloxanes.eu/index.php?page=cyclic-siloxanes.
[6] *www.platinummetalsreview.com/pdf/pmr-v41-i2-066-075.pdf.*
[7] B.A. Ashby, US4421903, 1983.
[8] N.S. Chu, et al, US 4481364, 1983.

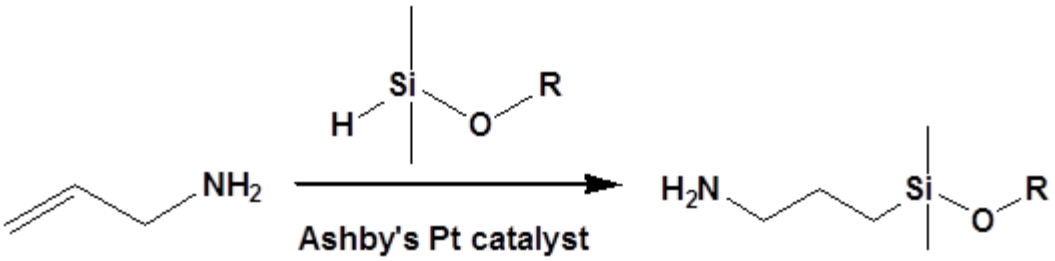

Figure 26. Hydrosilation reaction of allylamine to TMDS (R= dimethylsilyl, hydrogen, or methyl).

Another great difficulty in the reaction is that primary amine-containing compounds poison platinum catalysts.[9] The reaction occurs in an irregular fashion that is difficult to control. To overcome this, large amounts of platinum catalyst are used to keep the reaction going to completion. Since platinum is an increasingly precious metal, the catalyst is a significant cost in the manufacture of the GAP material.

The remaining silicon hydride groups from the excess tetramethyldisiloxane are hydrolyzed with methanol, and the product is washed with sulfuric acid and xylene to remove traces of allylamine. Following the wash, the pH of the material is increased, catalyzing the condensation and insertion of the hydrolyzed material into the GAP-0 material, as illustrated in Figure 27. As a result, the molecular weight distribution increases, with a final average molecular weight of about 1-1.2 and a composition of approximately 40% GAP-0, 33% GAP-1, 19% GAP-2, and 8% GAP-3. For shorthand, this material will be called GAP-1m.

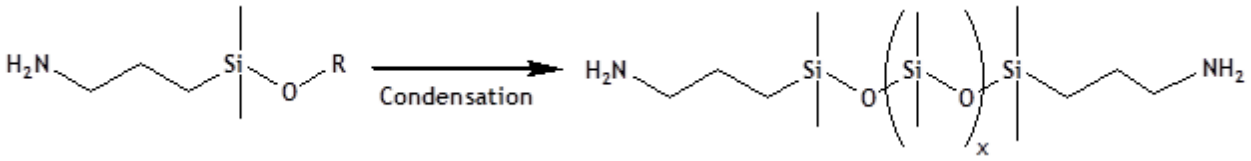

Figure 27. Condensation of the aminopropylsiloxane materials (R= dimethylsilyl or methyl) to form GAP-1m.

Lastly, the GAP-1m is vacuum distilled to remove any traces of organic base, methanol, or xylene, and produce the most effective CO_2 capture solvent.

[9] US 4892918, column 5, line 61.

If pure GAP-0 is desired, it currently must be distilled from the GAP-1m product with a distillation column containing sufficient number of plates for adequate separation. While such distillation is possible at SiVance, much of the remaining material is oxidized, discolored, and damaged for any other use. The large amounts of waste increase costs dramatically to a level not appropriate for CO_2 capture.

2013-2015 Supply Plan

Based upon information from GE Global Research[10], the forecast sales of GAP-1m for CO_2 capture for the next 3 years (2013-2015) is 1000 kg/year, 1000 kg/year, and 5000 kg/year respectively. In the current process, GAP-1m is a crude intermediate for subsequent higher molecular weight commercial products that SiVance have produced for over 20 years. Currently, GAP-1m is still considered to be experimental and is not optimized as a commercial product, especially with respect to purification, volume, and standardization. SiVance currently makes the GAP intermediate in about 1000 kg batches and is fully capable of meeting the technical and supply needs for the GAP-1m solvent in the CO_2 capture process for the next 3 years.

Once specifications are finalized, sales volumes increase, and the product commercialization fully implemented, it will be easier to forecast how much the price will decrease in the future. Price varies greatly with purity, because a crude intermediate is much different than a tightly specified commercial product. SiVance's current equipment is capable of making about 100,000 kg/year, but much of the equipment is currently filled with other products since total annual domestic demand for GAP-1m materials is only about 15,000 kg/yr. For GE, SiVance can make an additional 3,000 kg/year and with sufficiently long lead-time can increase to 10,000 kg/year by shifting the other product mix in the current equipment. Because GAP-1m is currently an experimental product, and priced as such, SiVance explored how to more effectively make the GAP-1m material and enable a lower price in the future.

GE Research and Milliken met March 15th, 2012 to more fully discuss what chemical properties were important for making the best capture materials. It was decided that branching (gamma vs. beta) was a primary variable for investigation. Based upon this discussion, SiVance delivered standard "Normal" product and products with different levels of branching for further testing and evaluation at GE Research.

[10] Robert Perry, GE Global Research, email on 11/28/2012.

Task 4.2: Confirm Small-Scale Synthesis of Top Material Candidates

SiVance/Milliken currently produces a material (known as GAP-S) that is nominally the same as the GAP-1m material that was made in the GE GRC laboratories. Analysis and comparison of GAP-S to GAP-1m prepared at GE GRC is described below. Both materials are made via an equilibration process.

GAP-S, which was prepared via SiVance's commercial process and stripped of most of the MeOH before shipping to GE GRC, was received from SiVance/Milliken. A portion of this material was then subjected to an additional light strip (50 °C, 2 h, 30 mm Hg vacuum) and another aliquot to a deeper devolatilization (70 °C, 6 h, 0.4 mm Hg) step. The materials were then tested for change in composition, heat of reaction with CO_2, and CO_2 uptake. Two samples from each treatment were examined and compared with previous samples for consistency.

Solvent Preparation

GAP-1m was made at GE GRC in one step via the equilibration reaction of GAP-0 and octamethylcyclotetrasiloxane (D4) as shown in Figure 28 below. This reaction results in an equilibrium mixture of GAP-X homologs that, on average have one repeating dimethylsiloxy unit (n = 1). However, this is an average of all components and homologs from n = 0-5 were made in detectable quantities.

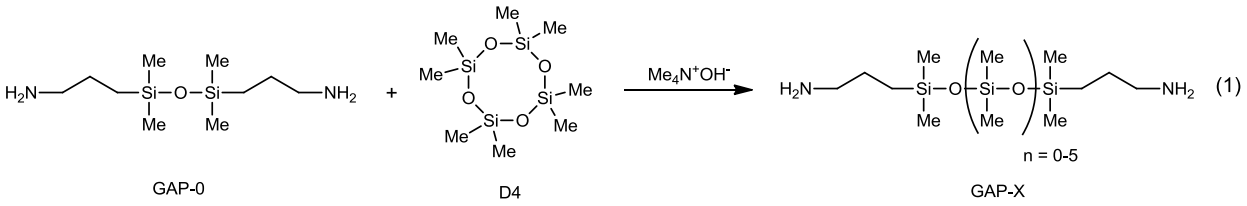

Figure 28. Formation of GAP-1m via the equilibration reaction of GAP-0.

The primary chemistry of GAP-S, as made at Milliken/SiVance is shown in Figure 29.

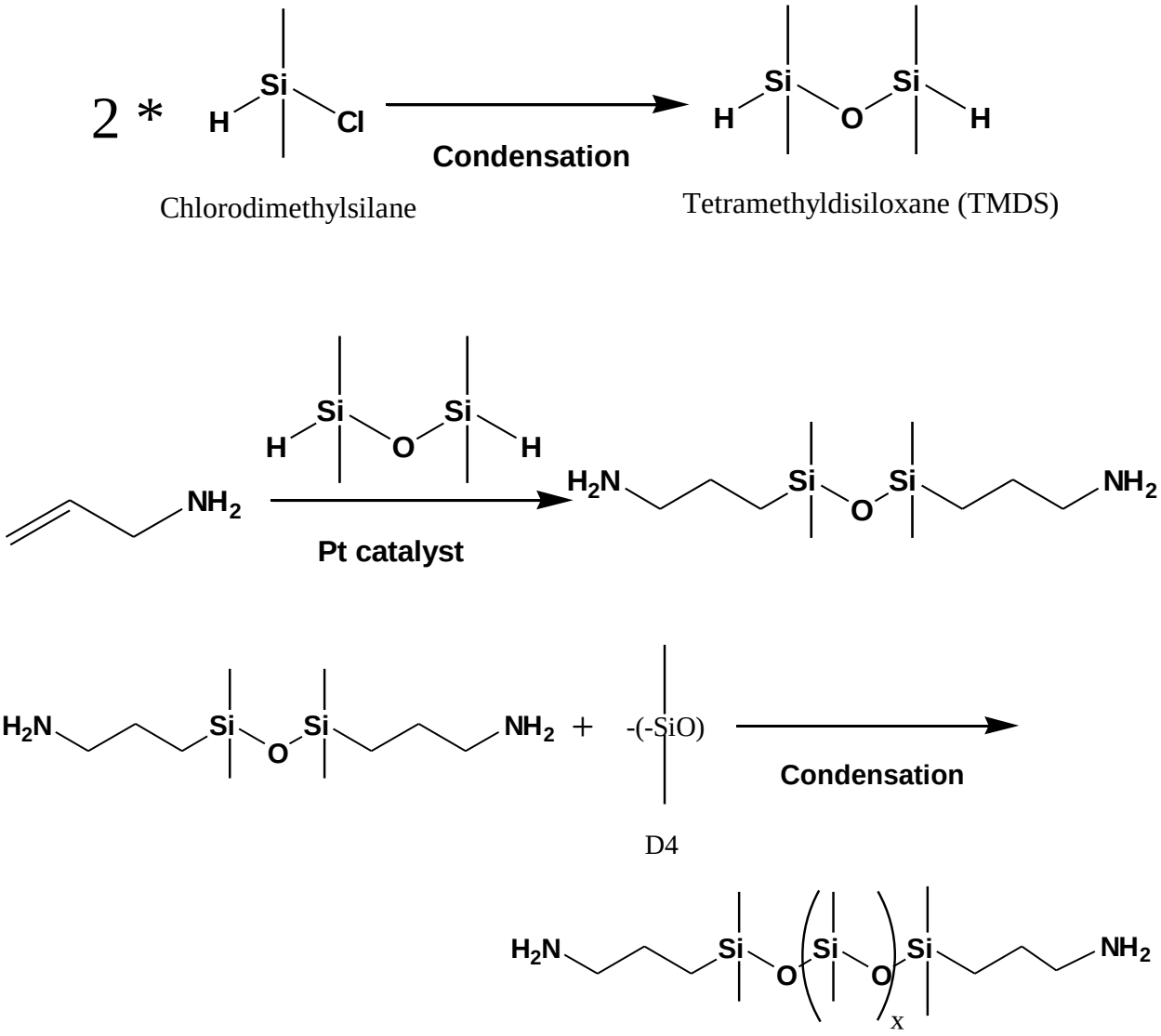

Figure 29. Formation of GAP-S.

GC/Mass Spectral Analysis

GC's were run on a Sample of GAP-S at both the Milliken/SiVance and GE GRC laboratories and are shown in Figure 30 and Figure 31. The traces are quite similar with the exception that the GE GRC chromatogram (Figure 30) shows better resolution and side peaks adjacent to the main peaks are visible.

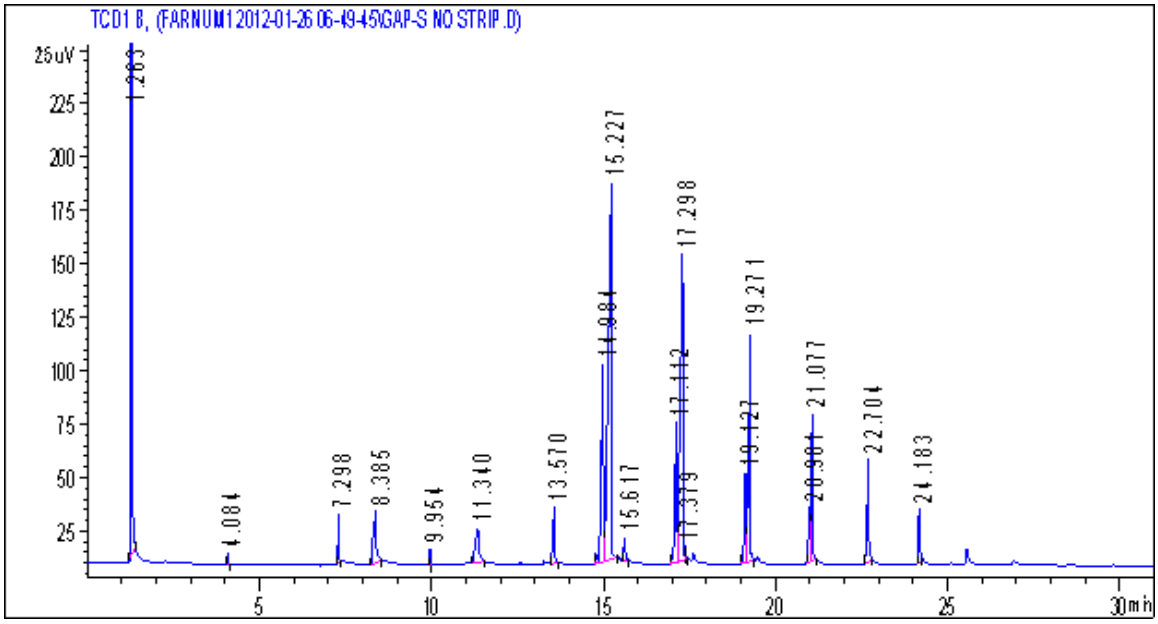

Figure 30. GC trace of GAP-S run at GE GRC.

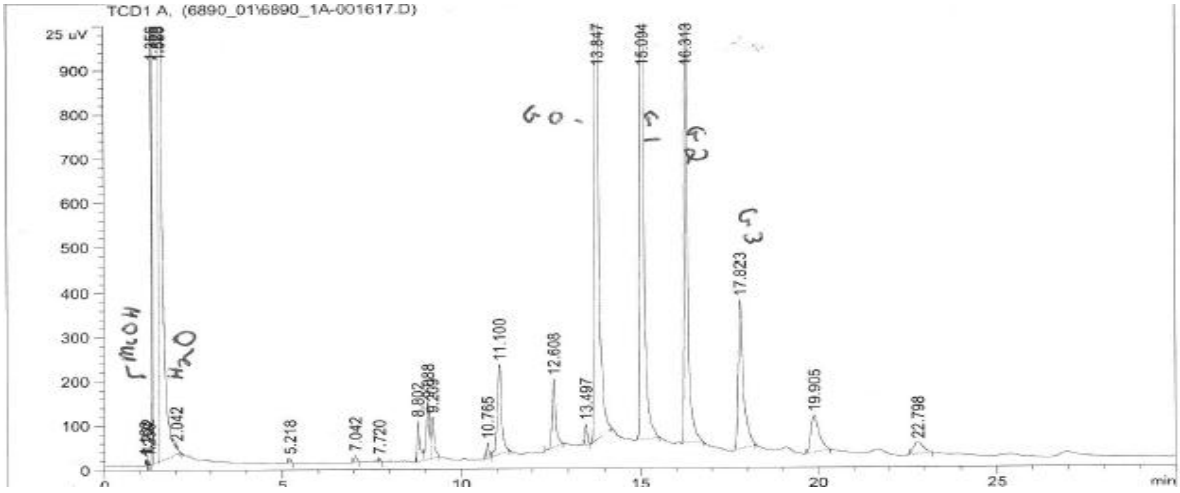

Figure 31. GC Trace of GAP-S run at Milliken/SiVance.

When the sample was subjected to GC/GC/Mass Spec analysis, the GC trace from that instrument further resolved the peaks and a set of three related peaks were observed as seen in Figure 32.

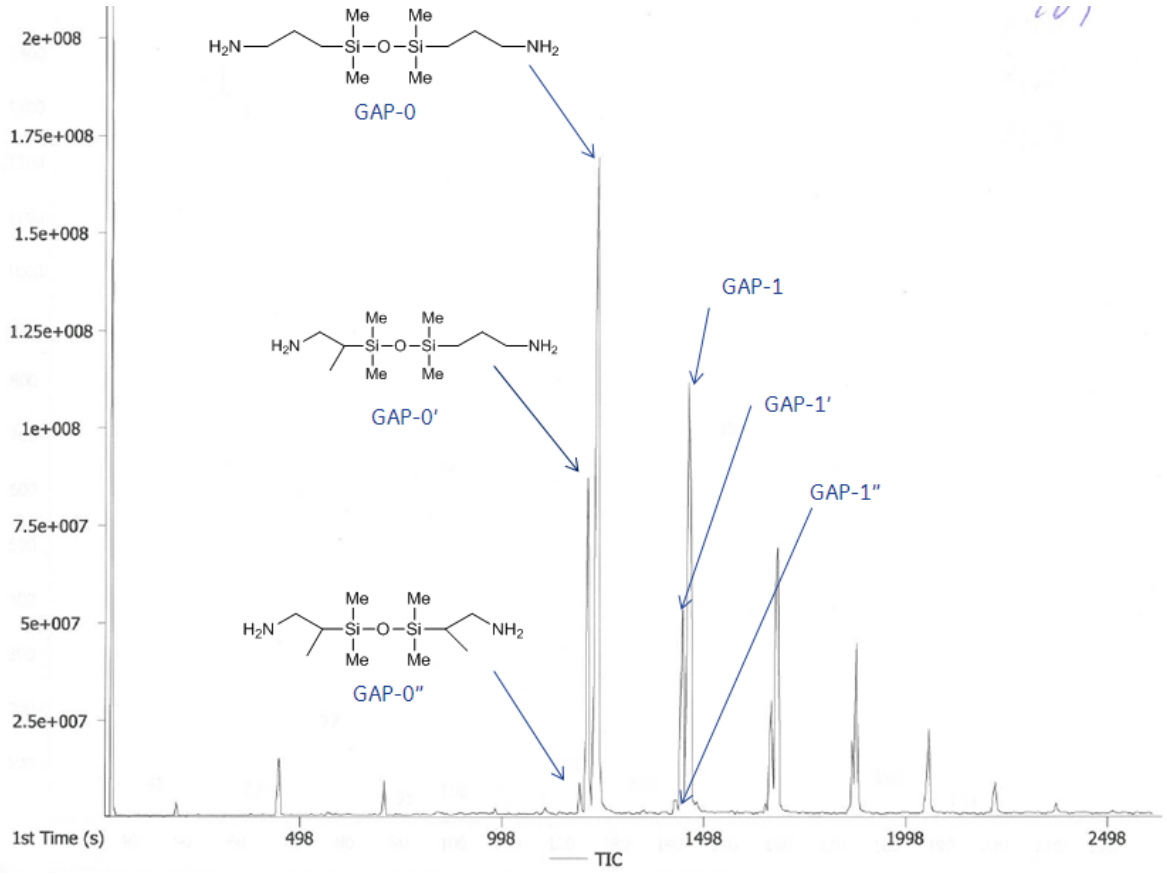

Figure 32. Higher resolution GC trace for GAP-S.

These were determined to be isomers of the parent compound. These isomers arose from addition at both the gamma and beta sites on allylamine as illustrated in Figure 33. Addition is predominately at the less hindered, gamma position.

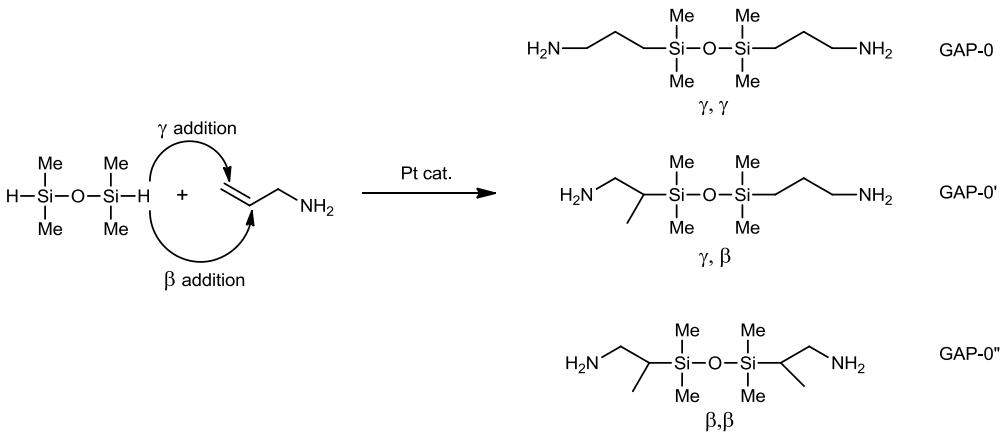

Figure 33. Formation of regioisomers of GAP materials.

The mass spectrometer (MS) analysis also showed the presence of small amounts of other compounds in the GAP-S sample. Figure 34 readily shows the GAP-X isomer series but also small amounts of cyclic dimethylsiloxanes (D4, D5, D6) and very small amounts of an unidentified, moderately polar material.

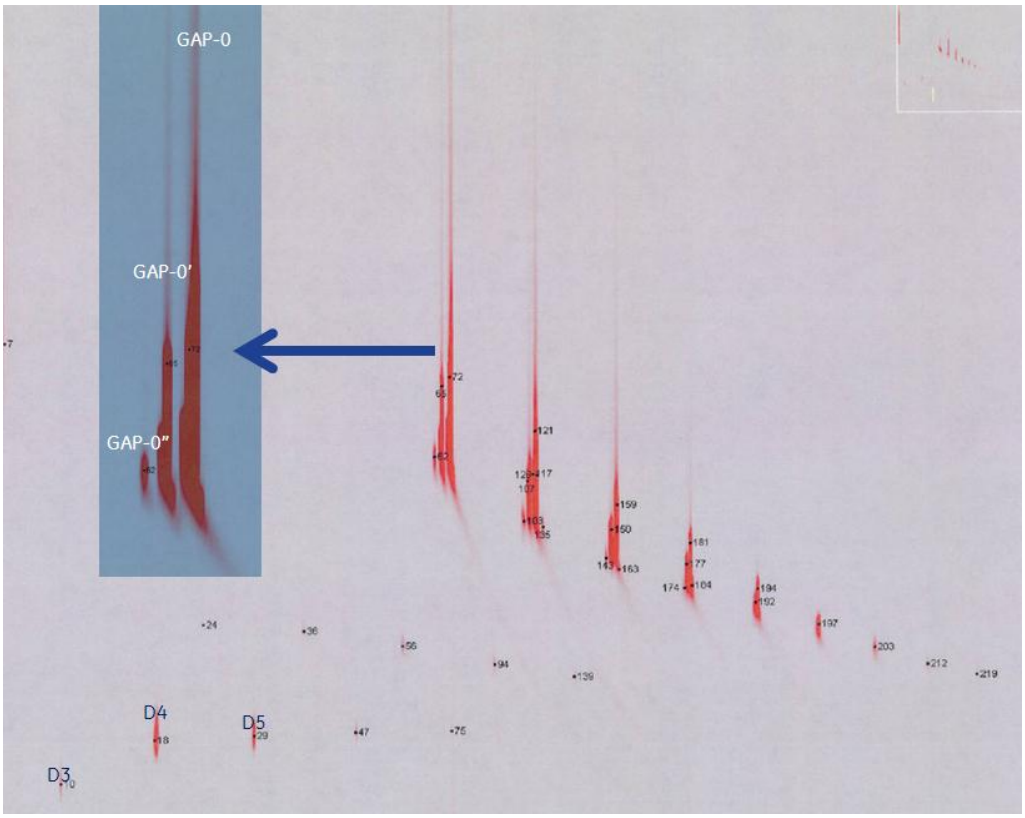

Figure 34. 2-D GC of GAP-S mixture showing other compounds.

In comparison, the GC trace of GAP-1m is shown in Figure 35. There are no beta isomers present. This is not surprising as the starting material for GAP-1m is pure gamma GAP-0.

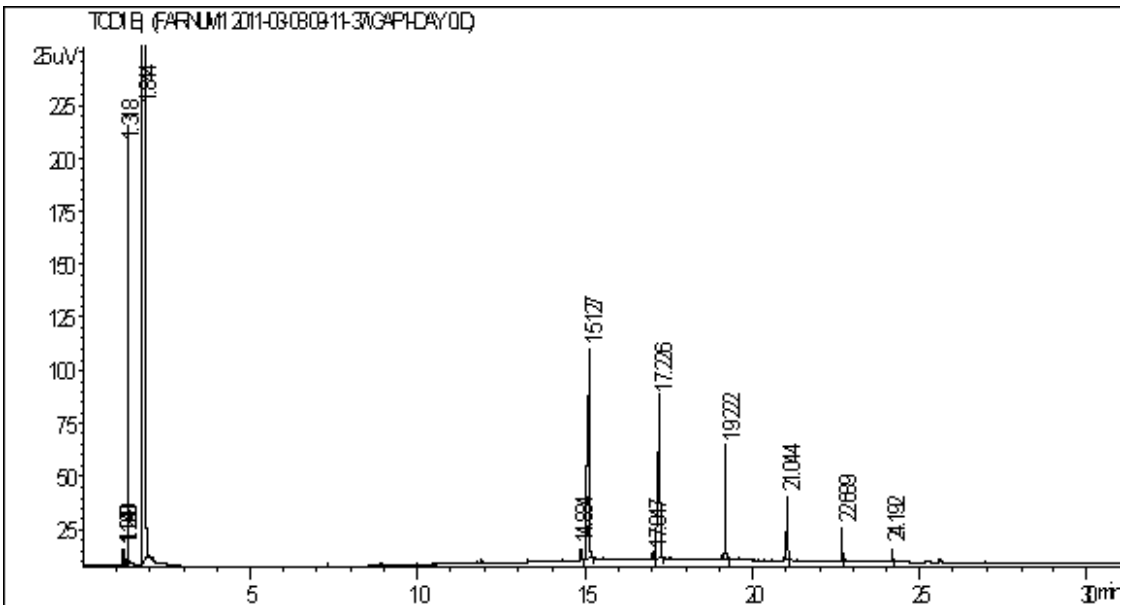

Figure 35. GC of GAP-1m.

Determination of the average chain length for both samples was calculated by using a weighted average of each of the components, as shown in Table 7. Non-aminosilicone impurities were not taken into account and the GAP-S sample was stripped to remove as many volatiles (MeOH) as possible before analysis and performance testing. All isomers of GAP-0, GAP-1, GAP-2, etc. were counted together as the molecular weight of all isomers was the same. Also, the response factors for all the peaks were assumed to be equal.

Table 7. Determination of GAP repeat units.

GAP-S				GAP-1m			
GAP	Area %	MW	% x MW	GAP	Area %	MW	% x MW
0	43.5	248.5	108.10	0	44.8	248.5	111.33
1	28.8	322.5	92.88	1	28.3	322.5	91.27
2	16.0	396.5	63.44	2	14.4	396.5	58.41
3	7.6	470.5	35.76	3	7.1	470.5	33.40
4	3.0	544.5	16.33	4	3.2	544.5	17.42
5	1.1	618.5	6.80	5	1.2	618.5	7.42
		Avg. MW =	323.31			Avg. MW =	319.25
	Avg. repeat unit =		1.01		Avg. repeat unit =		0.96

From the analysis, both materials had nearly identical average compositions. There was some variation in the proportions of individual components with this sample of GAP-1m containing a slightly higher percentage of GAP-0.

NMR Analysis

Both proton and carbon NMR were obtained for GAP-S and GAP-1m. Figures 36 and 37 show the proton spectra of these materials. A more direct comparison is seen in Figure 38. The latter figure shows a number of small resonances indicative of the multiple isomers seen in the GC.

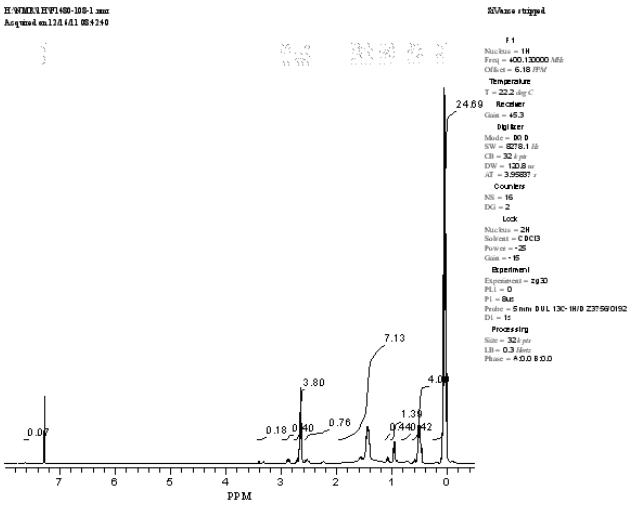

Figure 36. ^{1}H NMR of GAP-S.

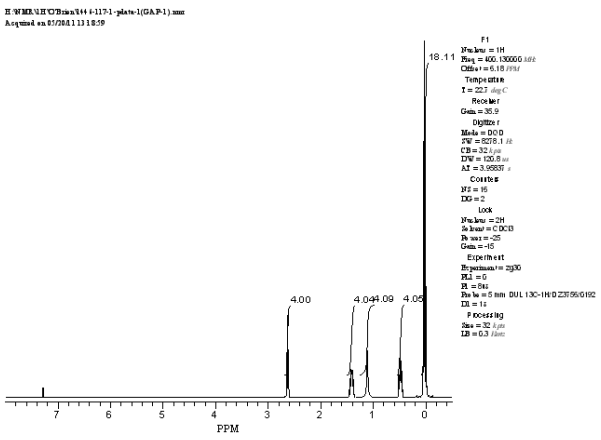

Figure 37. ^{1}H NMR of GAP-1m.

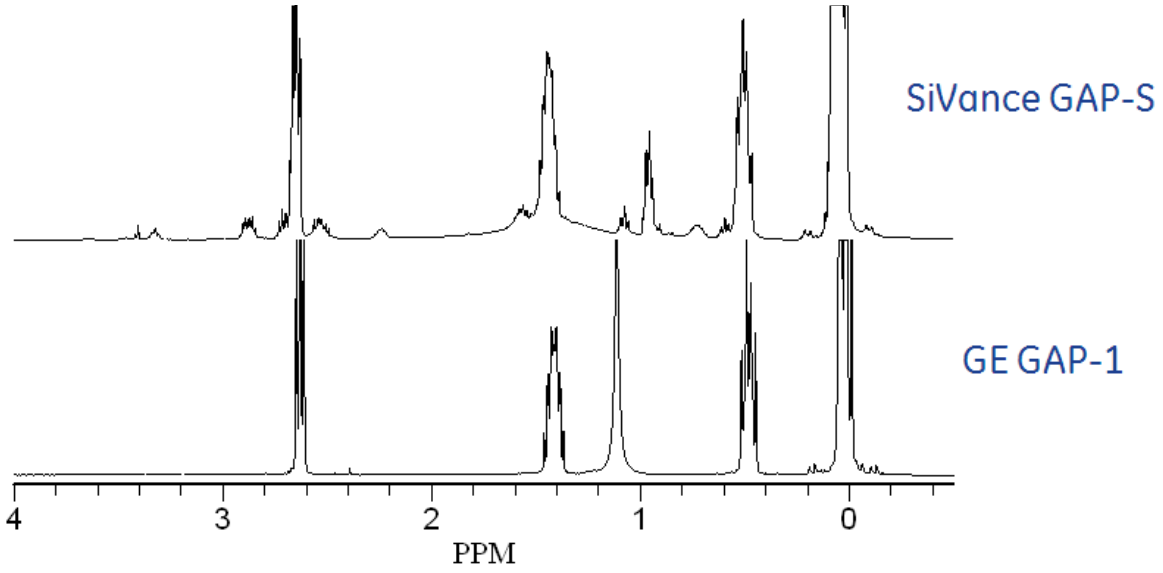

Figure 38. Comparison of GAP-S and GAP-1m ^{1}H NMR spectra.

A similar comparison is seen with the carbon NMR spectra in Figures 39-41. In all cases, the commercially prepared GAP-S contains a large number of other components not seen in the GAP-1m sample.

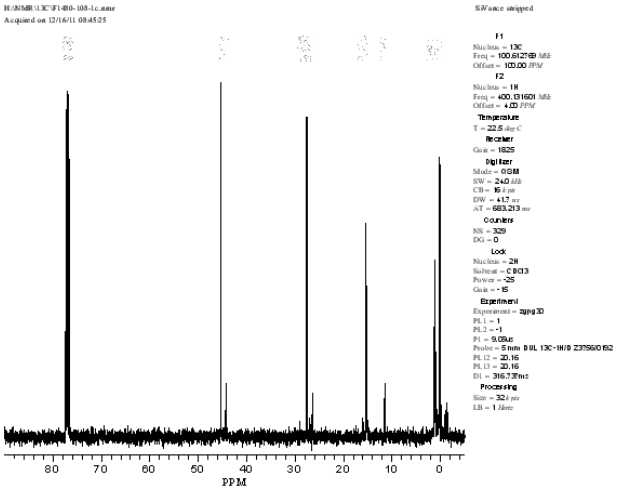

Figure 39. ^{13}C{^{1}H] NMR of GAP-S.

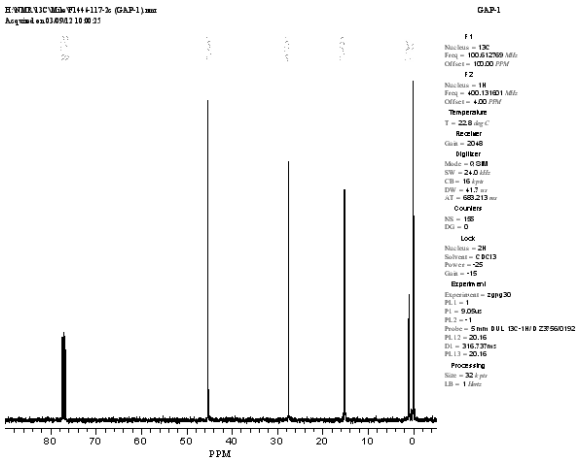

Figure 40. ^{13}C{^{1}H] NMR of GAP-1m.

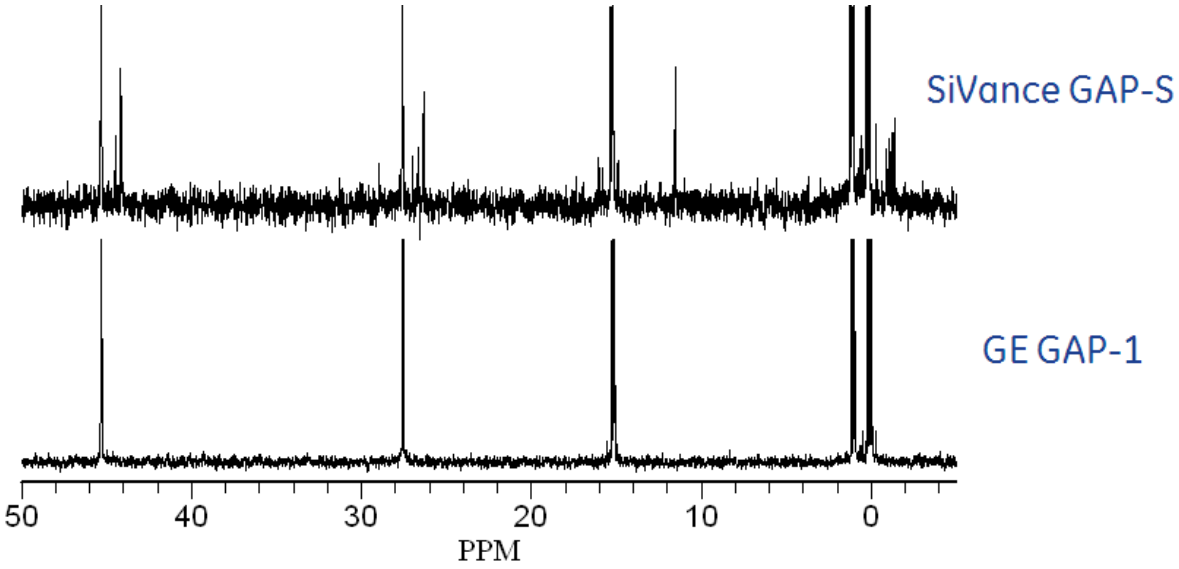

Figure 41. Comparison of GAP-S and GAP-1m $^{13}C\{^{1}H]$ NMR spectra.

Infra-red spectra were acquired on a FT-IR in ATR (attenuated total reflectance) mode and showed no difference between the samples (see Figure 42). This is not surprising as IR is not as sensitive of a method as GC, MS, or NMR for detecting low levels of impurities.

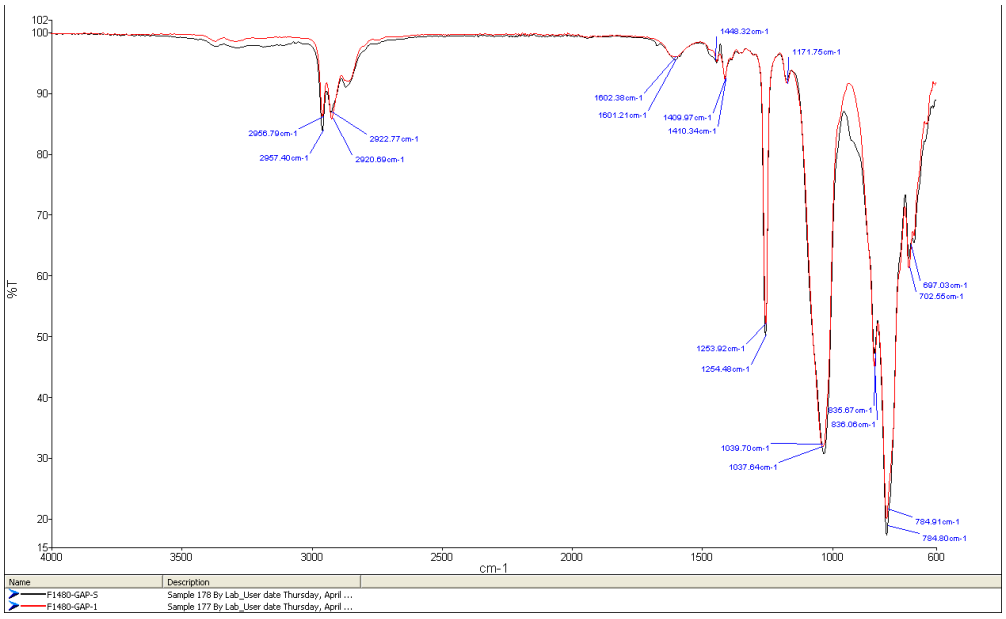

Figure 42. Comparison of FT-IR spectra of GAP-1m and GAP-S.

CO_2 Uptake Experiments

Several preliminary experiments were run to determine the reactivity of the GAP-S solvent in comparison to GAP-1m. Reactions that were neat as well as a 60/40 wt/wt% mixture of GAPm/TEG were examined. A pre-tared 25 mL round bottom flask equipped with a mechanical stirrer, a CO_2 inlet, and a CO_2 outlet (that contained glass wool to capture any fine solid particles that might be formed) connected to a bubbler was charged with the appropriate amount of solvent or solvent mixture (~ 4 grams that were weighed accurately), warmed to 40 °C, and then dry CO_2 (from subliming dry ice that was passed through a Drierite® column) was introduced into the system at a slow rate. After a set period of time (usually 30 min) the flask was re-weighed and the difference was the amount of CO_2 that had been absorbed. The results are shown in Table 8.

Table 8. CO_2 absorption capacity comparison between GAP-1m and GAP-S.

Solvent	Rxn Time (min)	Wt % CO_2 absorbed	% of Theory
GAP-1m neat	30	13.1	96.0
GAP-S neat	30	12.2	90.0
60/40 GAP-1m/TEG	30	8.4	102.6
60/40 GAP-S/TEG	30	7.9	96.9
60/40 GAP-S/TEG	60	7.1	87.9
60/40 GAP-S/TEG	60	7.2	88.9
60/40 GAP-S/TEG	90	7.1	86.9
60/40 GAP-S/TEG	120	6.5	79.7

When the two solvents were run neat, both materials were solid glasses at room temperature but the GAP-S material was a viscous liquid at 40 °C while the GAP-1m has solidified at that temperature. Both did not absorb the theoretical amount of CO_2 because of mass transfer limitations, but the GAP-1m material had about 1% greater pickup.

When 60/40 wt% solutions were exposed to excess CO_2, all reaction products were free flowing liquids. In the case of GAP-1m, it did not matter whether the reaction time was 30 minutes or 2 hours. The weight of the carbamate solution remained constant. However, when GAP-S was used, there was a distinct decrease in the weight over 2 hours as shown in Figure 43. This could be due to loss of volatile components left from the synthesis of the GAP-S.

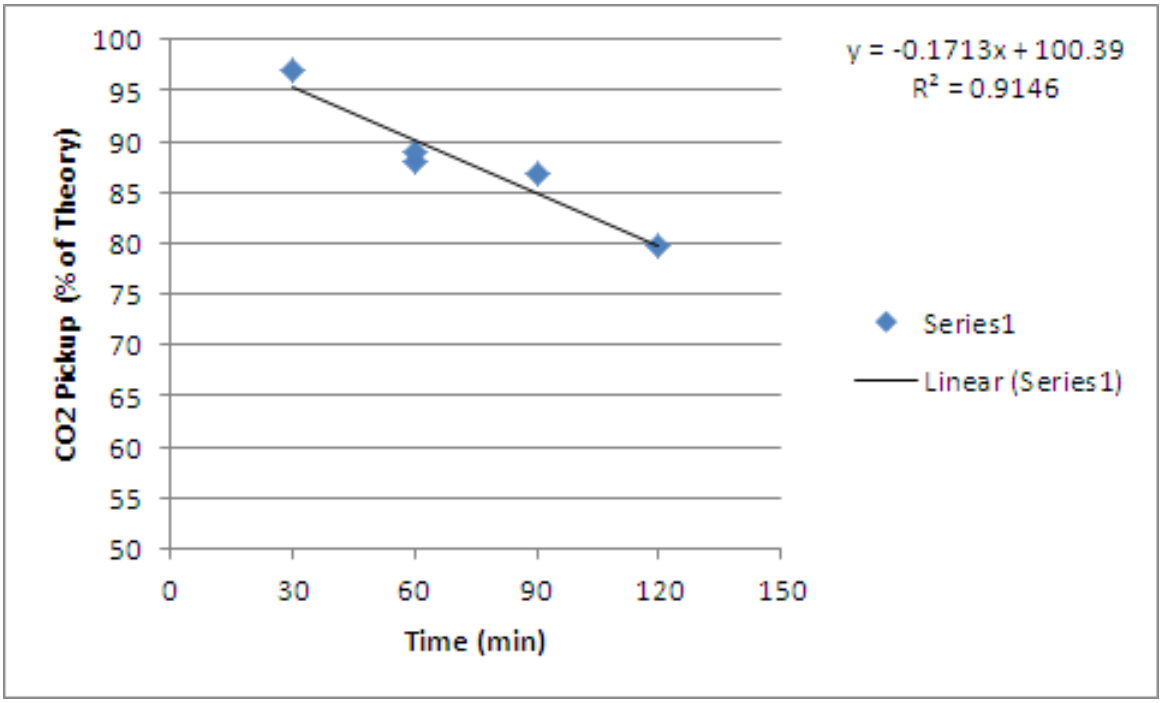

Figure 43. Loss of weight with time for GAP-S carbamate solutions.

GAP Isomers

As described earlier, GAP-1m aminosilicone made in the GE laboratories is a material comprised of only γ-aminopropyl groups, whereas the GAP-S made at SiVance contains 10-15% of the β-isomer. While the SiVance material reacted with CO_2, experiments showed a lower level of CO_2 absorption compared to the GE samples.[11] To determine if the β-isomer content impacted the CO_2 capture capacity, thermal stability, or volatility, a series of GAP-S compounds containing various levels of β-isomer were synthesized and tested.

Three samples were supplied for testing and were designated as low-β, normal-β and high-β content materials. Proton NMR analysis estimated that the beta content of the three samples were <2%, 8%, and 89% as shown in Figure 44.

[11] See Table 8.

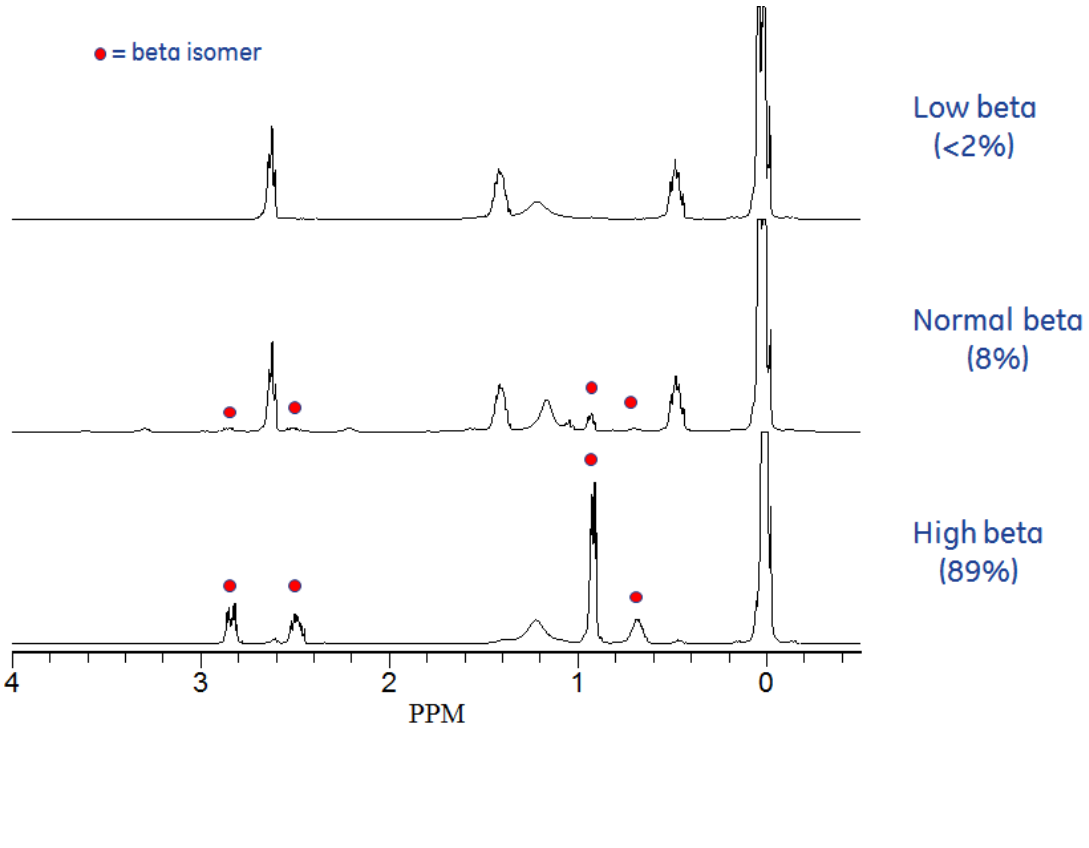

Figure 44. ^{1}H NMR spectra of GAP-S samples.

Figure 45 shows the carbon spectra of the same materials. In both figures, the red dots indicate the beta isomer. It is apparent from both sets of spectra that the low and high beta samples have fewer impurities present.

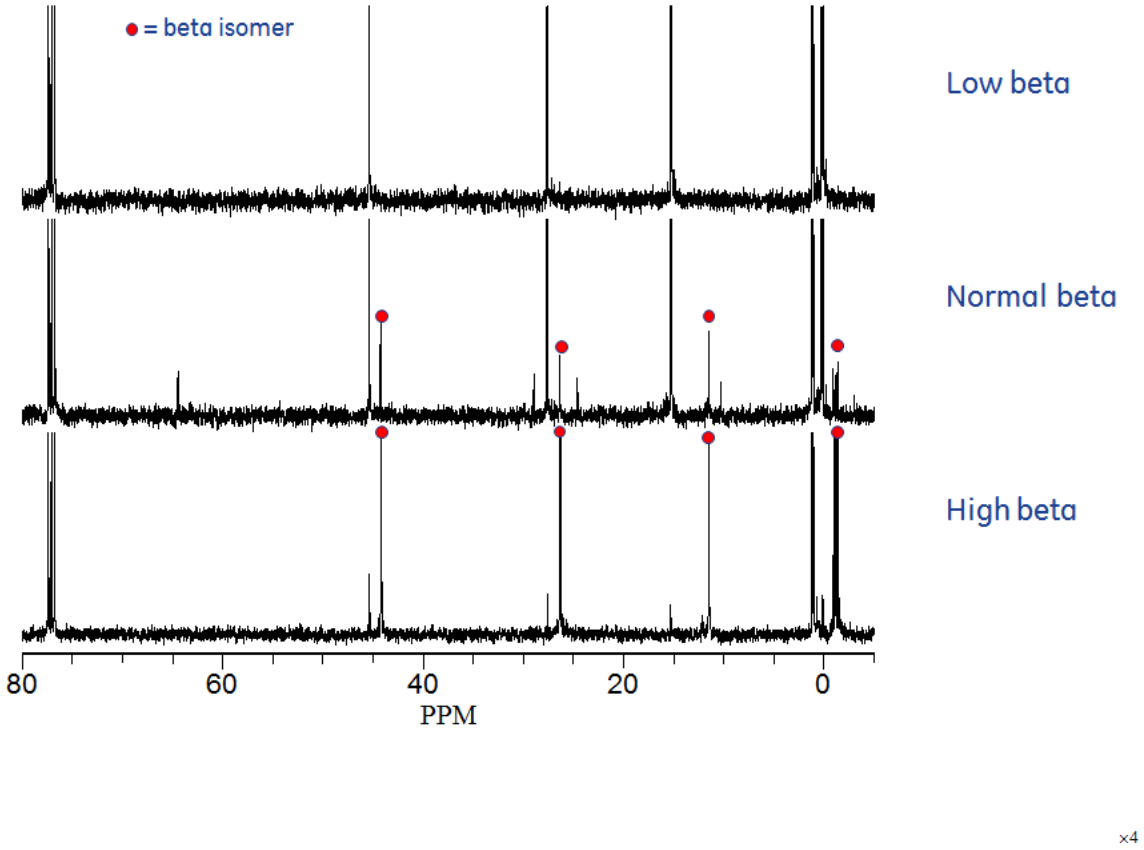

Figure 45. ^{13}C NMR spectra of GAP-S samples.

This is because of the method of preparation. For the low and high test materials, the intermediate methoxydimethylaminopropyl isomers were separated by distillation and then, independently subjected to hydrolysis, condensation, and then equilibration to produce the desired GAP-1(S) derivatives as shown below.

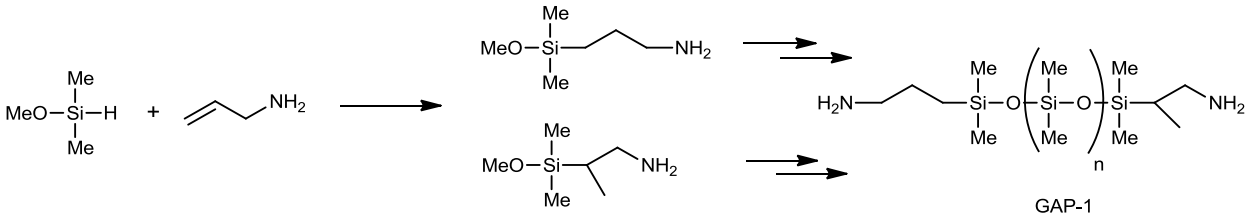

Independent verification of the beta isomer content was performed by GC analysis as shown in Figure 46. For the low beta material, none of the beta isomer was seen by GC. The normal beta had about 10% of the beta isomer which agreed well with the 8% value by NMR. The high beta sample showed 95% by GC and 89% by NMR. While the discrepancy is small, it may be due to peak overlap in the GC traces and inaccurate integration for each species.

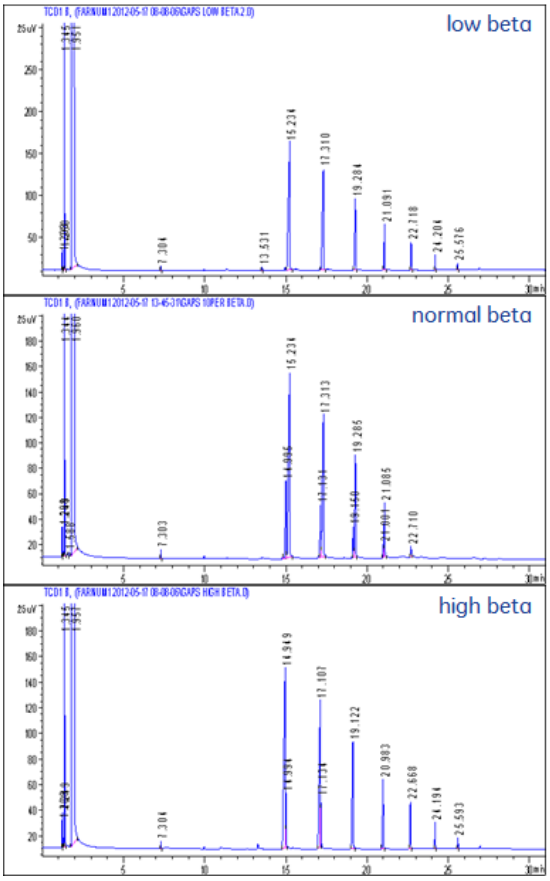

Material/ Retention time	% area, excluding solvent			
	low beta	high beta	10% beta	
D4 (7.304 min)	0.4	0.5	0.5	
Unknown (13.531 min)	0.5	0.0	0.0	
GAP-0'' (14.949 min)	0.0	36.5	0.0	β,β-isomer
GAP-0' (14.994 min)	0.0	3.8	9.4	β,γ-isomer
GAP-0 (15.234 min)	42.0	0.0	36.4	γ,γ-isomer
GAP-1'' (17.107 min)	0.0	25.7	0.0	
GAP-1' (17.134 min)	0.0	2.0	5.8	
GAP-1 (17.313 min)	27.8	0.0	24.6	
GAP-2'' (19.122 min)	0.0	15.9	0.0	
GAP-2' (19.15 min)	0.0	0.0	2.9	
GAP-2 (19.285 min)	15.0	0.0	12.5	
GAP-3'' (20.983 min)	0.0	8.4	0.0	
GAP-3' (21.001 min)	0.0	0.0	1.1	
GAP-3 (21.091 min)	7.7	0.0	5.5	
GAP-4' (22.668 min)	0.0	4.3	0.0	
GAP-4 (22.718 min)	3.9	0.0	1.2	
GAP-5' (24.194 min)	0.0	2.1	0.0	
GAP-5 (24.204 min)	1.9	0.0	0.0	
GAP-6 (25.576 min)	0.8	0.0	0.0	
GAP-6' (25.593 min)	0.0	0.9	0.0	
	0%	95.3%	10.3%	β content

Figure 46. GC analysis of GAP-S samples.

To compare CO_2 uptake for the isomers, 60/40 (wt/wt) mixtures of the GAP-S samples in TEG were made and reacted with CO_2 over 30 minutes at 40 °C. Table 9 shows the results of the preliminary runs in which the samples were used as received. While all materials absorbed over 100% of their theoretical amount of CO_2, the normal GAP-S sample picked up less than the other two (runs 1, 3 and 5). Continuation of the experiment for a total of 1 h showed that the low and high beta samples retained their capture capacity while the normal material dropped from 8.3 to 8.0 wt %.

Table 9. CO_2 absorption in 60/40 GAP-S/TEG samples.

Run	GAP	30 min		1 h		4 h	
		Wt % pickup	% of theory	Wt % pickup	% of theory	Wt % pickup	% of theory
1	Low Beta	8.8	114.4	8.8	113.5	-	-
2	Low Beta (50 °C strip)	8.5	111.2	8.6	112.8	-	-
3	Normal Beta	8.3	100.4	8.0	96.3	-	-
4	Normal Beta (50 °C strip)	8.6	108.6	8.7	109.9	-	-
5	High Beta	8.9	116.2	9.0	117.4	8.6	113.6
6	High Beta (50 °C strip)	9.1	119.5	8.9	116.4	-	-

This may have been due to inefficient stripping of residual volatile impurities and/or the presence of silanol or alkoxy endcaps in the mixture. These materials would be lower molecular weight than the GAP-1 compound and, after reaction, they could be volatilized by the CO_2 gas stream. To examine both possibilities, ^{29}Si NMR was run on all three samples. Figure 47 shows the interpreted spectrum of normal GAP-S and indicates that there are very low levels of silanol in the material.

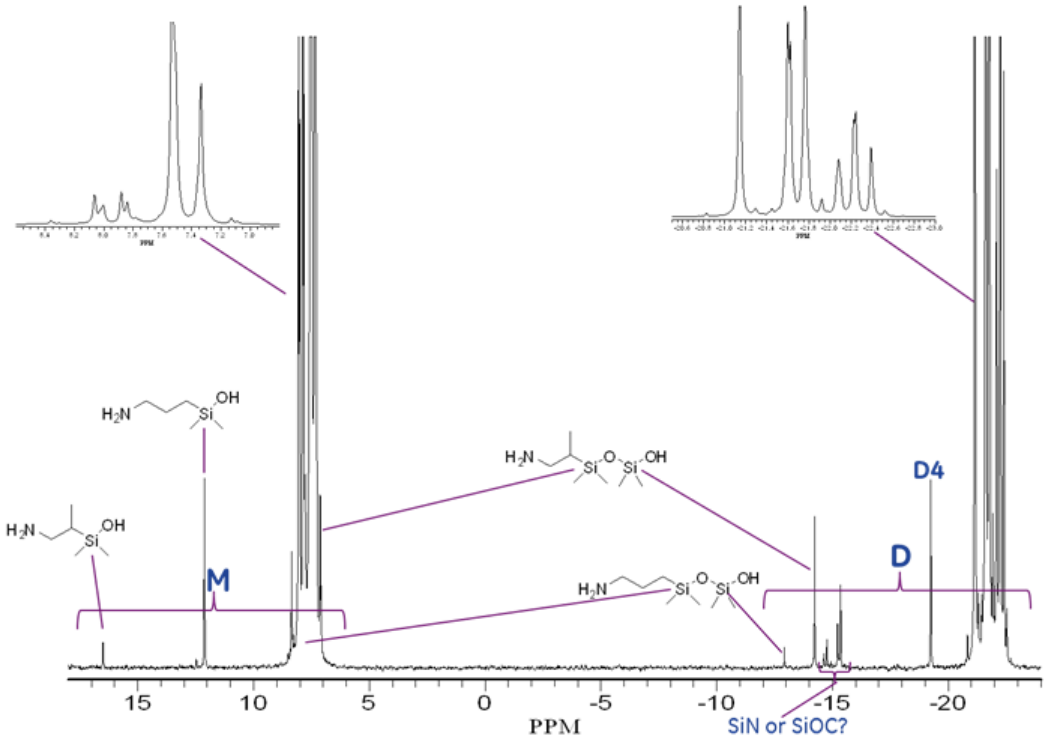

Figure 47. ^{29}Si NMR spectrum of normal GAP-S.

Figure 48 compares the silicone spectra of all three samples. Again, very little silanol is present in any of the materials.

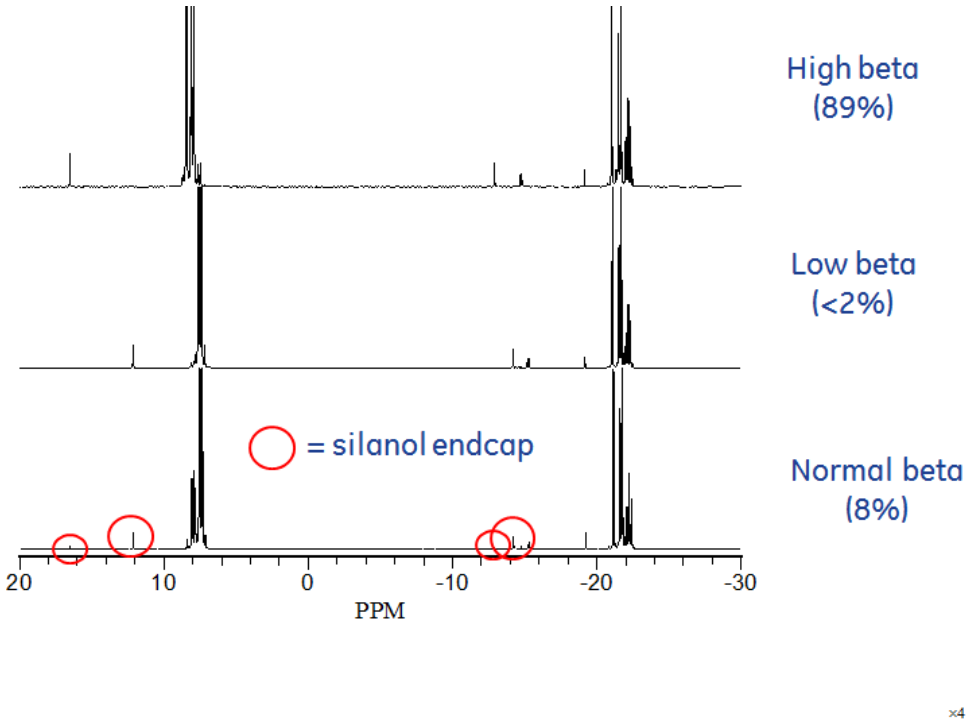

Figure 48. Comparison of ^{29}Si NMR spectra of GAP-S samples.

Aliquots of these three materials were also devolatilized on a rotary evaporator for 1 h at 50 °C/100 mm Hg. When CO_2 uptake experiments were performed, little difference was seen with the high and low beta samples as seen in runs 2 and 6 in Table 9. However, the normal sample maintained its weight gain (run 4) and performed as well as the other two materials. This indicated that the commercially prepared material could be as efficient as the high and low beta compounds if care is taken to remove the volatile species.

Table 10 shows a comparison of all GAP-S samples received from SiVance/Milliken and the analyses performed and includes some average information acquired on GE prepared GAP-1m samples. The first sample received from SiVance/Milliken (189699) was an unstripped sample of their manufactured intermediate and as such had a substantial amount of MeOH present. A 4 h strip at 60 °C removed much of this solvent and provided a material for testing. GE analysis showed nearly 1% of D_4 and D_5 cyclics remained, but also several percent of unidentified low boiling impurities. Also apparent was the presence of β-isomers of the aminopropyl group as previously described.

Table 10. Comparison of SiVance/Milliken GAP-S samples to GE GRC GAP-1m samples.

	Sample	GE GAP-1	189699 1W14R0709	189699 1W14R0709	2670-30A	2670-30A	18969823576 2678-14	18969823576 2678-14	18969823576 2678-14	18969823576 2678-14	18969823576 2678-14	Low Beta 2670-32	High Beta 2670-31
GC Rt(min)	Treatment	Avg 8 runs	as received	stripped 60 C/4h/30 mm Hg	as received	stripped 50 C/1h/30 mm Hg	as received	stripped 50 C/2h/30 mm Hg	stripped 70 C/6.5h/0.4 mm Hg	stripped 50 C/2h/30 mm Hg	stripped 70 C/6.5h/0.4 mm	stripped 50	stripped 50 C/1h/30
	Composition												
1.205	MeOH ?	-	46.60	0.01	-	-	0.29	0.01	0.01	0.01	0.01		
1.242	MeOH ?	-	-	1.86	-	-	-	-	-	-	-	-	-
4.081	?	-	0.20	0.10	-	-	-	-	-	-	-	-	-
7.299	D4	< 0.2	1.00	0.69	0.56	0.57	2.36	2.2	0.16	2.6	0.20	0.40	0.50
9.953	D5	-	0.32	0.25	0.17	0.18	1.01	0.94	-	1.1	-	-	-
11.372	?	-	2.80	1.58	-	-	-	-	-	-	-	-	-
12.602	D6	-	-	-	-	-	0.22	0.2	-	0.24	-	-	-
13.629	?	-	2.29	1.83	-	-	-	-	-	-	-	0.50	-
14.775	GAP-0"	-	-	0.57	-	-	-	-	-	-	-	-	36.5
14.999	GAP-0'	-	9.81	8.67	7.43	7.51	5.43	5.63	5.82	6.14	5.80	-	3.8
15.264	GAP-0	43.4 (1.5)	27.02	27.01	37.77	38.41	20.74	19.84	19.95	22.33	21.05	42.00	-
15.671	?	-	0.85	0.77	-	-	-	-	-	-	-	-	-
17.122	GAP-1"	-	0.32	5.69	0.27							-	25.7
17.349	GAP-1'	-	6.12	21.58	3.19	2.69	3.73	3.81	4.04	4.38	3.92	-	2
17.412	GAP-1	30.2 (2.0)	17.94	0.36	27.26	28.19	21.76	20.62	21.12	23.43	22.32	27.8	-
19.136	GAP-2"	-	-	-		-						-	15.9
19.15	GAP-2'	-	3.27	3.17	1.86	-	2.22	-	2.55	2.7	-	-	-
19.313	GAP-2	14.3 (2.1)	10.62	13.12	13.54	15.09	15.85	17.61	15.56	16.81	18.84	15	-
20.93	GAP-3"	-										-	8.4
21.00	GAP-3'	-	-	-	-	-	-	-	-	-	-	-	-
21.09	GAP-3	7.1 (0.3)	5.92	8.84	6.12	5.92	12.58	12.18	12.45	11.95	12.99	7.7	-
22.67	GAP-4'	-										-	4.3
22.72	GAP-4	3.16 (0.02)	4.19	4.18	1.83	1.44	7.95	8.45	8.35	4.94	8.61	3.9	-
24.199	GAP-5'	-			-	-						-	2.1
24.204	GAP-5	1.02 (0.11)	1.78	1.60	-	-	3.99	4.91	5.26	2.28	4.22	1.9	-
25.576	GAP-6'	-			-	-						-	0.9
25.593	GAP-6	-	1.00	1.00	-	-	2.18	2.39	2.90	1.10	2.03	0.8	-
26.955	GAP-7	-	-	-	-	-	-	1.22	1.34	0.27	0.92	-	-
28.5	GAP-8	-	-	-	-	-	-	-	0.50	-	-	-	-
	% Active	99.8	89.49	95.43	99.27	99.25	97.15	96.66	99.84	96.33	99.80	99.1	99.5
	GAP-X	0.98 (0.04)	1.19	1.23	0.88	0.85	1.78	1.84	1.89	1.48	1.76	1.12	1.18
	wt % N	8.72	8.32	8.24	8.93	9	7.36	7.28	7.21	7.84	7.39	8.46	8.34
	Wt % NH2	9.96	9.5	9.42	10.21	10.29	8.41	8.32	8.24	8.96	8.45	9.67	9.53
	CO2 Uptake (wt %) - neat	14.2	-	12.2	-	-	-	-	-	-	-	-	-
	CO2 Uptake (% of theory) - neat	103.8	-	90	-	-	-	-	-	-	-	-	-
	CO2 Uptake (wt %) -60/40 in TEG	8.5	-	6.4	8.0	8.3	-	6.6	-	-	7.1	8.6	8.8
	CO2 Uptake (% of theory) - 60/40 in TEG	104.3	-	94.7	96	100.4	-	94.3	-	-	102.2	113.6	113.5
	viscosity (cP @ 40 oC)												
	Color (APHA)												
	Heat of Rxn (kJ/kg CO2)	2558 (130)	-	-	-	2580 (28)	2438	-	-	2438	2466	2571 (42)	2585 (116)
	Heat of Rxn (kJ/kg CO2) (40% TEG)	2265 (75)	-	-	-	2295 (25)	2331	-	-	2328	2353	2319 (35)	2304 (44)

The second sample (2670-30A), with nominally the same composition, was a lab prepared sample that contained very little MeOH as it was stripped prior to shipping. It contained low levels of cyclics but no additional unidentified peaks in the GC. The third conventional sample (2678-14) had nearly 3.5% cyclics present as well as a small amount of MeOH. Stripping at 50 °C removed the MeOH but had little effect on the cyclics. A more vigorous strip at 70 °C and low pressure removed essentially all the volatile components. Replicate samples stripped under the same conditions gave GC results that were close. Lab samples that contained low and high

levels of the β-isomer (2670-32 and 2670-31 respectively) showed a small amount of D_4 present.

When comparing the samples, the first striking difference is that there is a wide variation in composition. For ease of viewing, Table 11 shows the aggregated area % (normalized to 100%) of each of the GAP-X homologs from which the volatiles were removed. One can see that the GAP-0 component ranges ~46% to 26% (highlighted). When compared to the average GAP-0 value for the GE prepared GAP-1m materials, at 43.8 +/- 1.5%, this is a huge variation. There was less of a range associated with the GAP-1 component (also highlighted) with a high of 31.1% and a low of 25.2%. This is still significantly larger than the 30.5 +/-2.0% seen with the GE materials.

Table 11. Composition comparison of SiVance/Milliken GAP-S to GE GAP-1m samples.

		GE GAP-1	189699 1W14R0709	2670-30A	18969823576 2678-14	18969823576 2678-14	18969823576 2678-14	18969823576 2678-14	Low Beta 2670-32	High Beta 2670-31		
		Avg 8 runs	stripped 60 C/4h/30 mm Hg	stripped 50 C/1h/30 mm Hg	stripped 50 C/2h/30 mm Hg	stripped 70 C/6.5h/0.4 mm Hg	stripped 50 C/2h/30 mm Hg	stripped 70 C/6.5h/0.4 mm Hg	stripped 50 C/1h/30 mm Hg	stripped 50 C/1h/30 mm Hg	AVG	STDEV
	D4	<.2	0.7	0.6	2.2	0.2	2.6	0.2	0.4	0.5		
	D5		0.3	0.2	0.9		1.1					
	D6				0.2		0.2					
Normalized to 100%	GAP-0	43.8 (1.5)	38.0	46.2	26.4	25.9	29.6	26.7	42.4	40.5	34.46	8.21
	GAP-1	30.5 (2.0)	28.6	31.1	25.3	25.2	28.8	26.2	28.1	27.8	27.63	2.01
	GAP-2	14.4 (2.1)	17.1	15.2	18.2	18.1	20.2	18.8	15.1	16.0	17.34	1.82
	GAP-3	7.1 (0.3)	9.3	5.9	12.6	12.5	12.4	12.9	7.8	8.4	10.22	2.70
	GAP-4	3.16 (0.02)	4.4	1.4	8.7	8.4	5.1	8.5	3.9	4.3	5.59	2.65
	GAP-5	1.02 (0.11)	1.7		5.1	5.3	2.4	4.2	1.9	2.1	3.24	1.56
	GAP-6		1.0		2.5	2.9	1.1	2.0	0.8	0.9	1.60	0.86
	GAP-7				1.3	1.3	0.3	0.9				
	GAP-8					0.5						
	Avg MW	321.2	339.6	311.1	384.8	388.4	357.2	379.6	331.1	335.9		
	GAP-X	0.98	1.23	0.85	1.84	1.89	1.47	1.77	1.12	1.18		
	% N	8.7	8.2	9.0	7.3	7.2	7.8	7.4	8.5	8.3		
	% NH2	10.0	9.4	10.3	8.3	8.2	9.0	8.4	9.7	9.5		
	% NH3	10.6	10.0	10.9	8.8	8.8	9.5	9.0	10.3	10.1		
	% CO2 capture (theory, neat)	13.7	13.0	14.1	11.4	11.3	12.3	11.6	13.3	13.1		
	% CO2 capture (theory, 60% in TEG)	8.2	7.8	8.5	6.9	6.8	7.4	7.0	8.0	7.9		

It appeared that the lab samples that were prepared for the high, low, and normal β content (2670-31, 32, 30A) were very close in composition to the GE materials while the two commercial batches were much lower in GAP-0 content and proportionally higher in the longer homologs. The average for all the GAP-0 content of all GAP-S batches received to date is 34.5 +/- 8.2%.

The variability in GAP-X composition has a huge impact on the CO_2 capture characteristics of the solvent. As seen in Table 11, The GE synthesized GAP-1m had an average repeat unit of 0.98; very close to the desired 1.0 level. This allowed for a theoretical CO_2 capture of 13.7 wt. % for neat material or 8.5% when formulated 60/40 with TEG. In contrast, the GAP-S materials ranged between GAP-0.85 and GAP-1.89 giving a CO_2 uptake potential of 6.8-8.5 wt. % in 60/40 TEG. Historical data is being obtained to determine what the typical range is for the production of GAP-S. With this information, one should be able to determine what controls need to be implemented for production of GAP-S with tighter specifications.

GAP-S materials are considered optimum that have the average structure of GAP-1.0 +/-0.2 with an active content of >99.0% as determined by area % GC analysis. This would minimize the unreactive inert material present as well as the volatile components which would necessitate downstream capture. This also maximizes the capture capacity of the mixture being used (Figure 49). One can see that the CO_2 uptake for GAP-S/TEG mixtures is low for samples that had low % actives (<97%) and/or large repeat unit values (> 1.2).

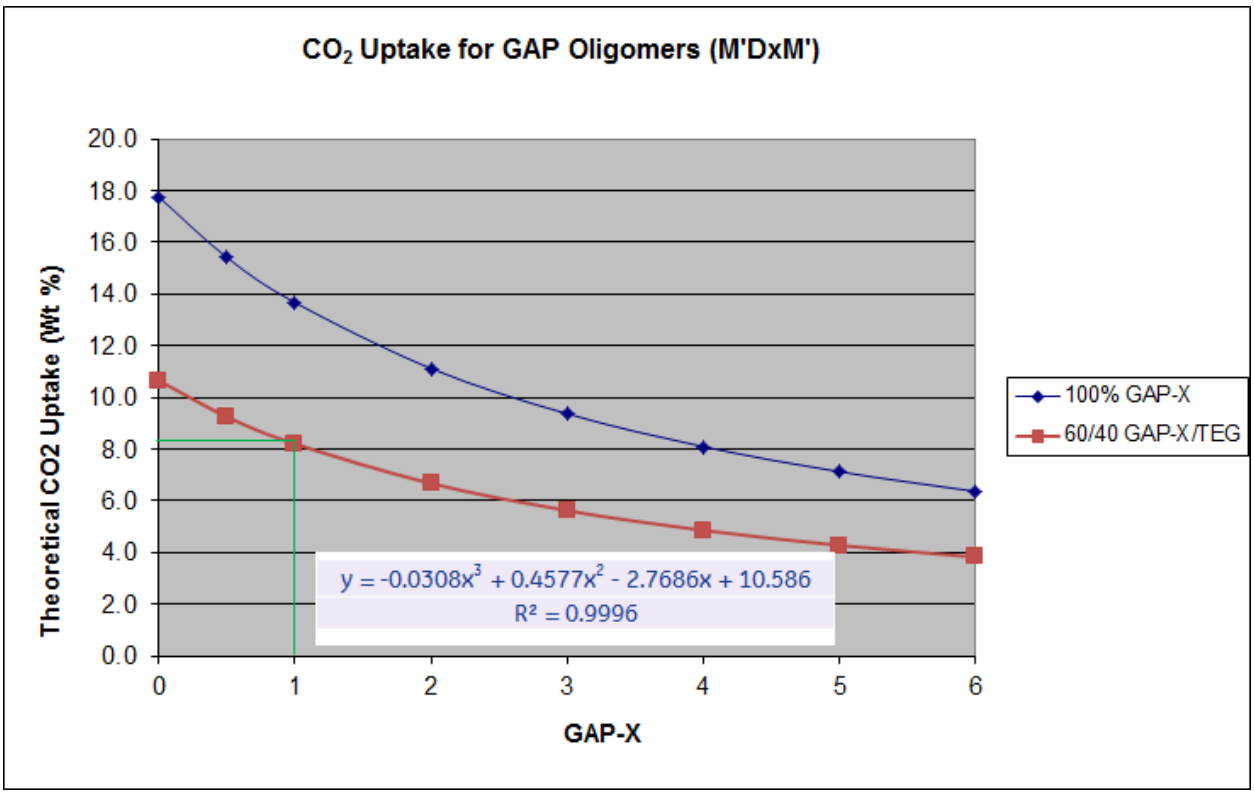

Figure 49. Effect of repeat unit length on theoretical CO_2 uptake.

Material Analysis Experimental Procedures

General

^{1}H and ^{13}C NMR spectra were obtained on a Bruker 400 MHz instrument. FTIR spectra were recorded on a Perkin Elmer Spectrum 100 Spectrometer. The GAP-S and GAP-1m samples were analyzed on an HP-6890 GC equipped with a TCD detector (250 °C). The GC was also equipped with a 7683 series autosampler and 7683 series injector (250 °C). The column was an HP-5 column (length = 30 m, inner diameter = 0.32 mm, film = 0.25 µm). The GC method was initial temperature of 40 °C, hold for 2 minutes then ramp at 10 °C/min to a final temp of 250 °C with a hold for 5 minutes. GC conditions for that used in the MS analysis were: RTx-5 (Restek) 10 m long, 0.18mm ID, 0.2um film thickness (df), 35 °C (0.5 min.), then 5 °C/min. to 270 °C. No solvent was used, so a large split ratio (200:1) and low injection volume was needed to avoid gross overload of this low df column. In the GCxGC application, this column was connected to the MS source with a 1 meter length of RTx-17 phase that is operated at a temperature higher than the first column.

Lab Reactions

Experiments were performed in a 25 mL, 3-neck, round-bottom flask equipped with a mechanical stirrer, gas inlet, and bubbler. The candidate solvent was added, the entire flask assembly was pre-weighed and then allowed to react at 40 °C while being exposed to a constant stream of dry CO_2 generated from dry ice and passed through a drying column. Periodically, the flask was weighed to determine the total weight gained.

1,5-Bis(3-amino[propyl)1,1,3,3,5,5-hexamethyltrisiloxane (GAP-1)

20.0 g of GAP-0 (0.0805 mol) was mixed with 6.0 g octamethylcyclotetrasiloxane (0.0805 mol) and 0.15 g of tetramethylammonium hydroxide pentahydrate. The mixture was heated to 40 °C under vacuum for an hour to remove some of the water from the catalyst. Next, a nitrogen atmosphere was established and the temperature was increased to 90-95 °C and allowed to react overnight. The reaction mixture was then heated to 150 °C for 30 minutes and then a vacuum was carefully applied (house vacuum). Heating was then continued to 165 °C and the most volatile species were stripped off. After cooling, ca. 25 g (96%) of product was obtained as a light yellow oil with an average composition of M'DM'.

Thermal Stability Experiments

Thermal stability tests of the aminosilicones were necessary to determine the maximum operating temperature for the desorber. Table 12 summarizes all aminosilicones for which

thermal stability experiments have been completed. The materials were heated to either 150 °C or 180 °C in sealed vials placed in silicone oil baths. Samples were typically collected every 1-3 weeks. Analysis was conducted on a GC equipped with a thermal conductivity detector (TCD). Since the samples are periodically exposed to air, the conditions in these experiments should be considered aggressive.

Table 12. List of thermal stability experiments.

Material	Structure	Temperature (°C)	Duration of experiment
GAP-S	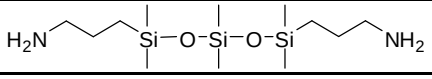	150	56 days
60% GAP-1m in TEG	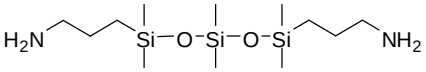	150	78 days
60% GAP-1m in TEG	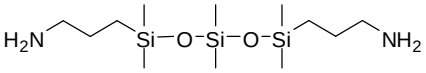	180	78 days
GAP-1m carbamate	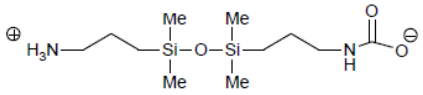	150	28 days

GAP-S at 150 °C

GAP-S is a GAP-1m material made by SiVance/Milliken for testing at GE Global Research to determine if SiVance's synthesis techniques produce a material with similar properties to the GAP-1m made at GE Global Research. The composition of the starting material is provided in Table 13. The starting material showed the presence of isomers of several of the aminosilicone peaks (designated as GAP-0', GAP-0'', GAP-1', etc.). These isomers have not been detected in the GAP-1m materials synthesized at GE Global Research.

Table 13. GAP-S starting material composition.

Component	% area in starting material from TCD analysis
D4	0.7
D5	0.3
GAP-0''	0.3
GAP-0'	10.1
GAP-0	28.5
GAP-1''	0.2
GAP-1'	7.2
GAP-1	21.1
GAP-2'	4.0
GAP-2	12.1
GAP-3'	2.2
GAP-3	6.4
GAP-4	4.1
GAP-5	1.2
Unidentified peak	1.6

As of the end of the experiment on day 91, as shown in Figure 50, the GAP-0 peak continued to show a decrease relative to the other aminosilicone peaks, with GAP-1 showing a slightly higher % area than GAP-0. The CO_2 uptake was measured to be 11.1% at the end of the experiment. This was 91% of what was measured in the lab at GRC and 81-82% of theory.

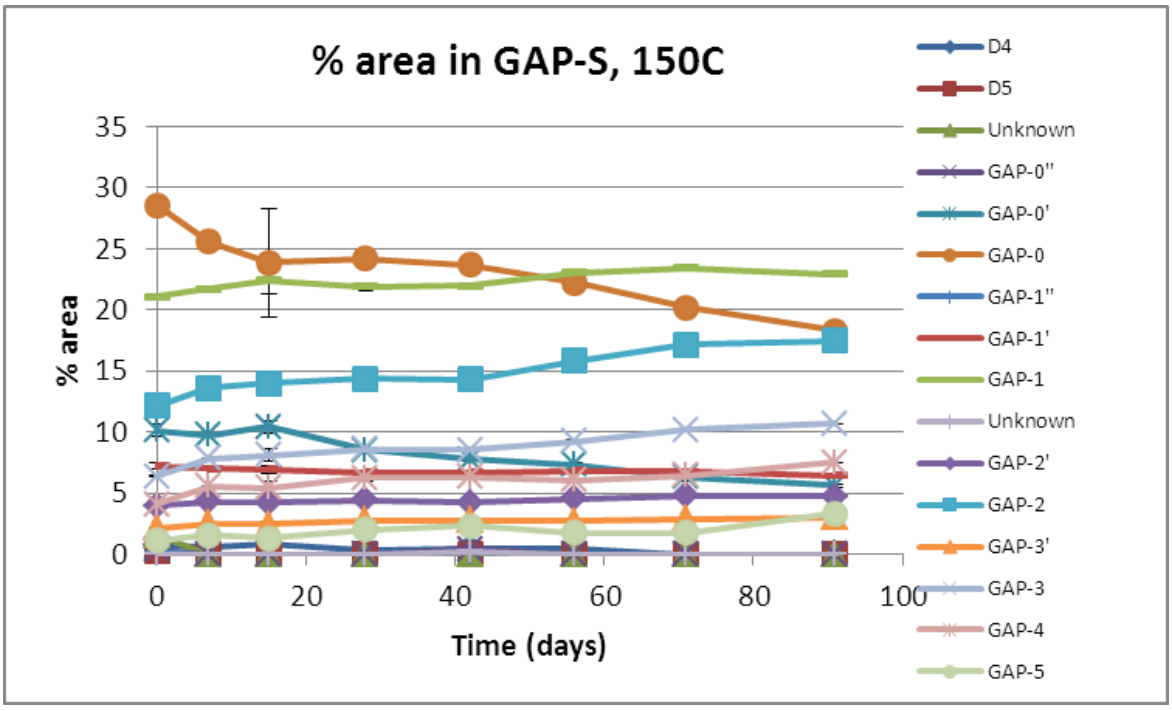

Figure 50. Composition of GAP-S at 150 °C over time.

60/40 (wt/wt) GAP-1m/TEG at 150 °C

The results for this experiment are provided in Figure 51. The starting material contained TEG, GAP-0, GAP-1, GAP-2, GAP-3, GAP-4, and GAP-5. At the end of the experiment on day 91, a few minor peaks have been detected (D4 and D5), with no significant changes observed in the aminosilicone peaks. The CO_2 uptake was measured to be 4.8% at the end of the experiment, which is 61% of theory.

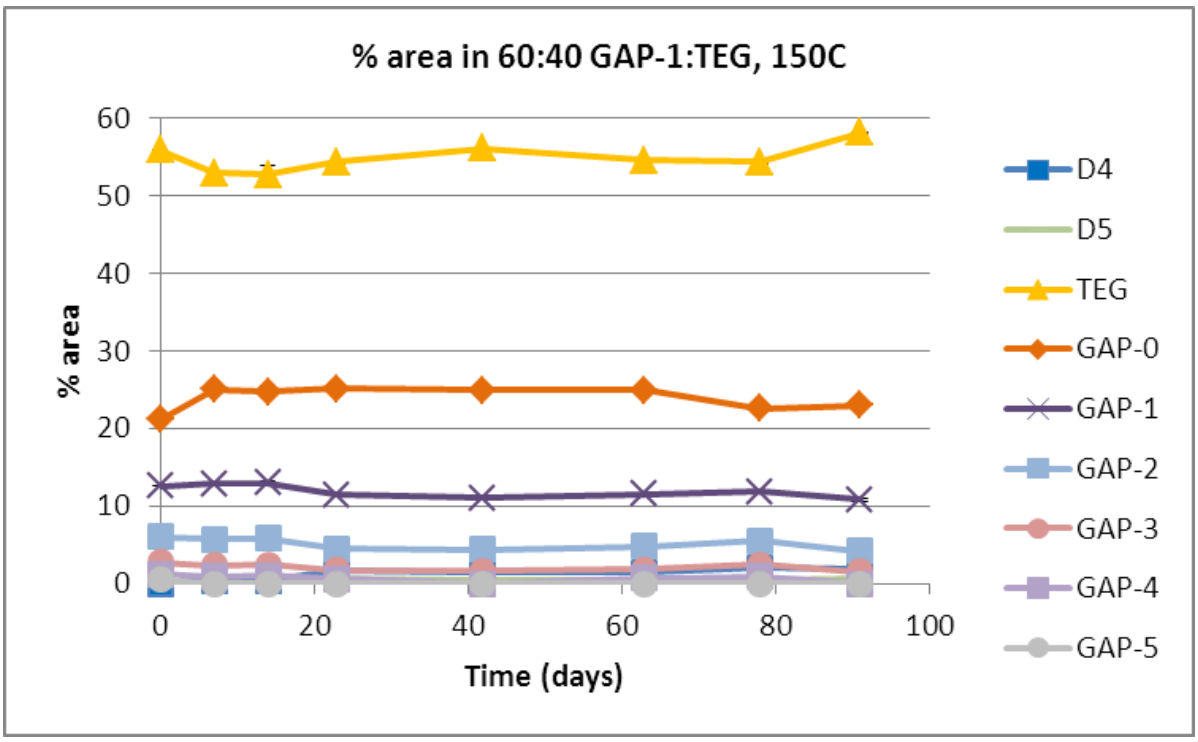

Figure 51. Composition of 60/40 (wt/wt) GAP-1m/TEG at 150 °C over time.

60/40 (wt/wt) GAP-1m/TEG at 180 °C

The results for this experiment are provided in Figure 52. The starting material contained D4, TEG, GAP-0, GAP-1, GAP-2, GAP-3, GAP-4, and GAP-5. As of the end of the experiment on day 91, one small, unidentified peak was detected in addition to the peaks present in the starting material. GAP-4 and GAP-5, which are relatively small compared to the other peaks in the starting material, were no longer detected. The most significant change in the GC-TCD (thermal conductivity detector) results was the steady increase in TEG relative to the aminosilicone peaks. This increase was observed since the beginning of the experiment. TEG increased from 48.9% area in the starting material to 72.2% area as of day 91. The CO_2 uptake was measured to be 5.4% at the end of the experiment, which is 69% of theory.

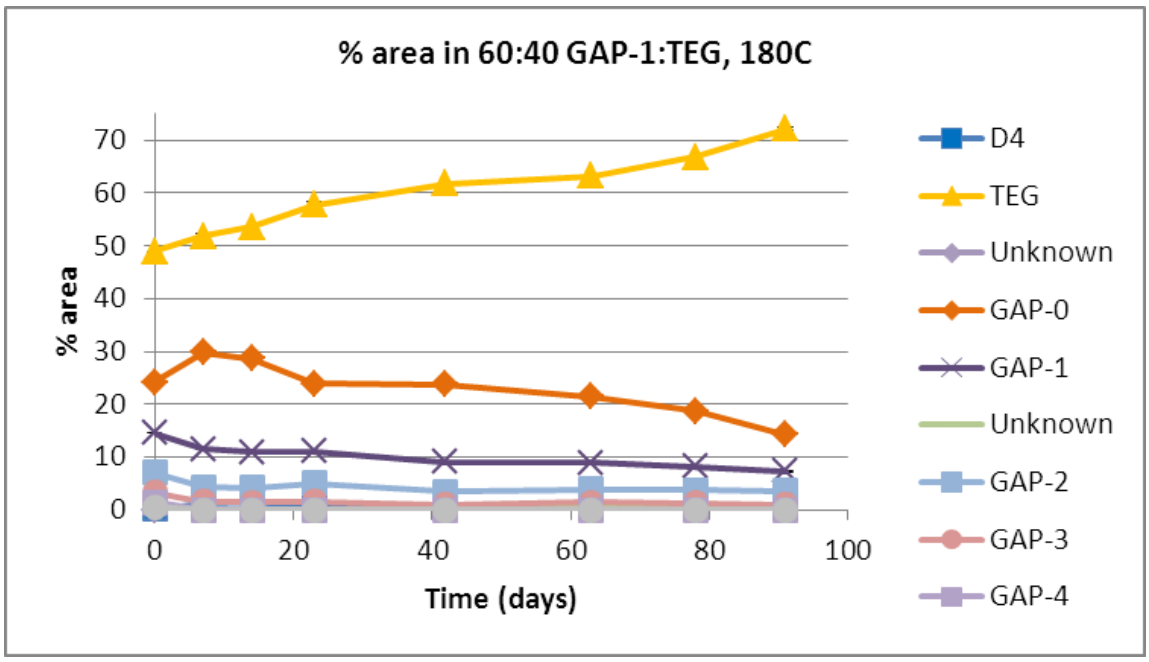

Figure 52. 60% GAP-1m in TEG at 180 °C results over time.

GAP-1m Carbamate at 150 °C

The results for GAP-1m carbamate are provided in Figure 53. The starting material primarily consisted of GAP-0, GAP-1, and higher oligomers. Four separate treatments were set up for this experiment. Each treatment is sacrificed upon sampling, since the vessel needs to be open to air and CO_2 will desorb. Samples were scheduled for 7, 14, 28 and 56 days. As of the 28 day sample, the GAP-0 peak showed a steady decrease relative to the other aminosilicone peaks and a few small, unidentified peaks were detected. It should be noted that, though the GAP-1m carbamate is not soluble in chloroform prior to the experiment, the material removed from the vessel after heating was observed to be soluble in chloroform.

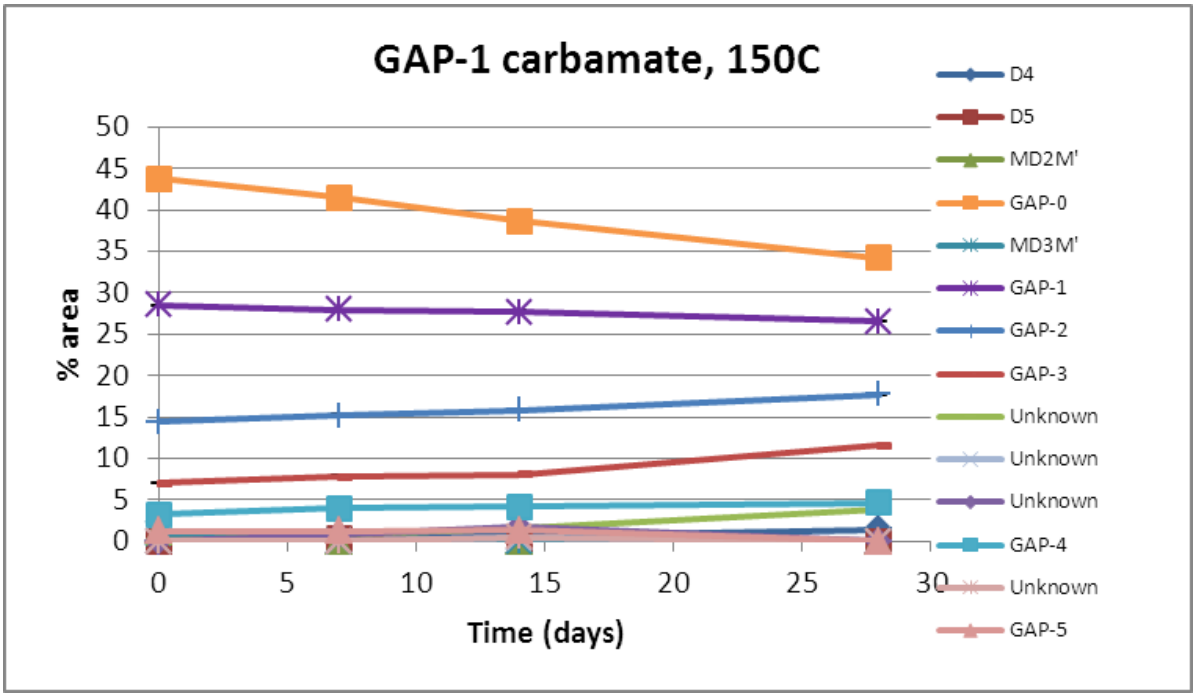

Figure 53. Composition of GAP-1m carbamate at 150 °C over time.

Vapor Pressure

Vapor pressure measurements were completed for GAP-S (GAP-1m made by SiVance) with 10% beta isomer, GAP-S with high beta isomer, and GAP-S with low beta isomer. Figure 54 shows a diagram of the system. The system was fitted with a high temperature 0-15 psia pressure transducer, as the vapor pressures of the materials of interest are low. The oil bath had the capability to reach 180 °C, and the temperature and pressure were continuously monitored throughout the experiment. The sample holder and valve were designed to be submersible in the oil bath, to maintain a consistent system temperature.

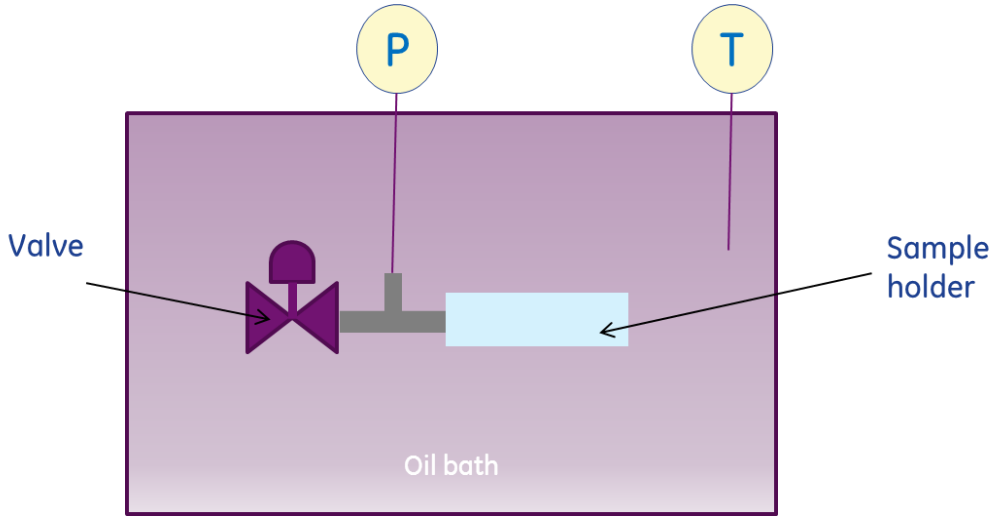

Figure 54. Vapor pressure measurement system.

Prior to completing the temperature ramps, nitrogen is bubbled through the material for 2-3 hours. The material is then loaded into the apparatus, placed with only the sample holder in the oil bath and hooked up to vacuum. Different methods have been used for pulling the vacuum with the aminosilicone materials, depending on the material being studied. For these materials, the vacuum was pulled for 1 hour while the sample was held at 120 °C.

Each temperature ramp ranged from room temperature (approximately 25 °C) to 180 °C. It should be noted that at the lower temperatures on the ramp, the pressure is less than the sensitivity of the pressure transducer. Results for each material tested are provided with the sensitivity of the transducer and the baseline results for pure MEA indicated on each of the graphs. The method used to pull the vacuum on the apparatus is also noted for each test.

The results for GAP-S with 10% beta isomer, GAP-S with high beta isomer and GAP-S with low beta isomer are provided in Figures 55, 56, and 57, respectively.

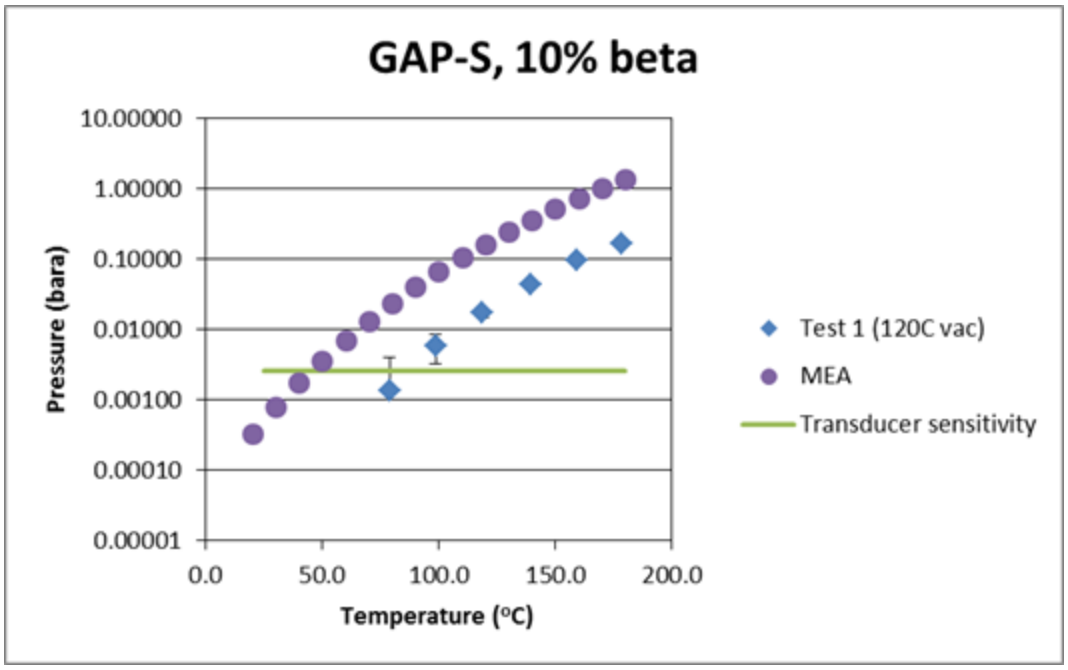

Figure 55. Vapor pressure results for GAP-S, 10% beta isomer.

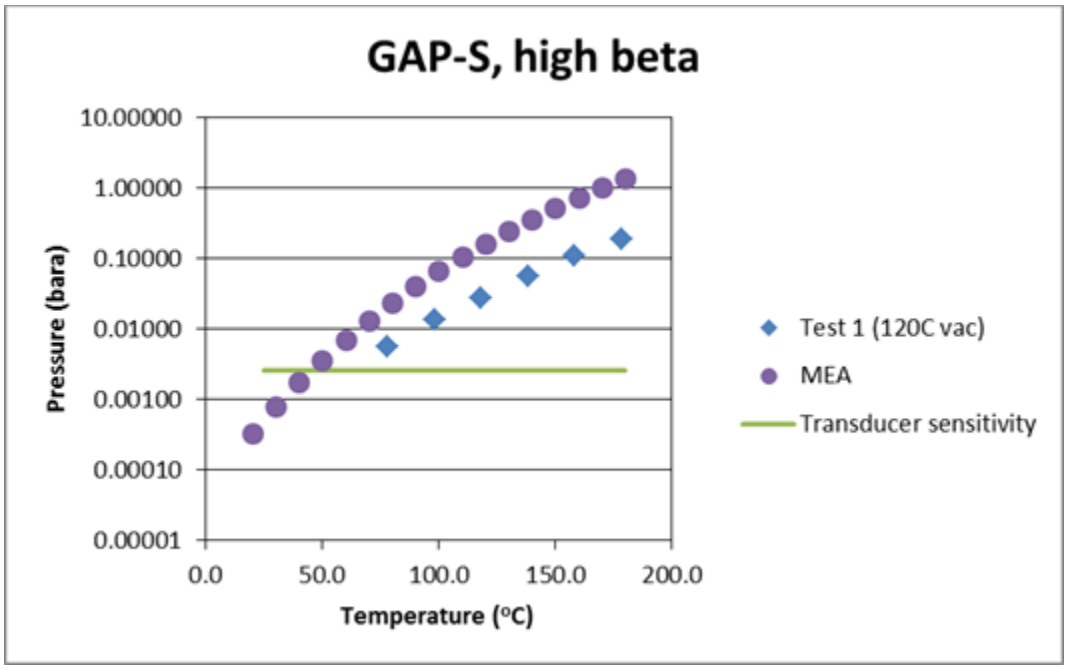

Figure 56. Vapor pressure results for GAP-S, high beta isomer.

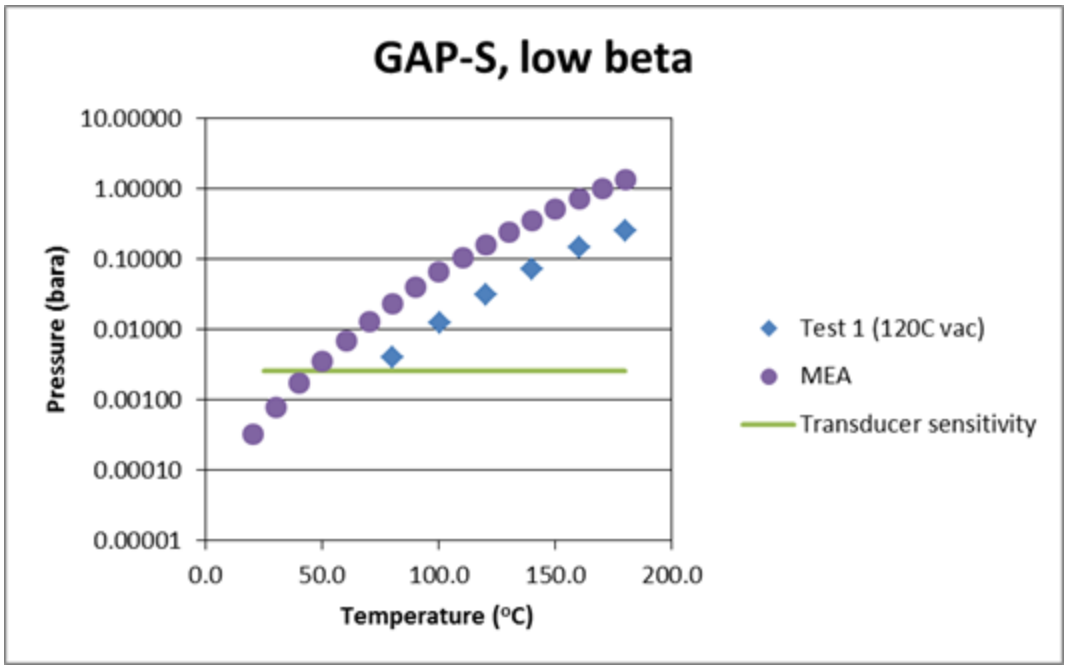

Figure 57. Vapor pressure results for GAP-S, low beta isomer.

Figure 58 shows the comparison of the three GAP-S materials studied. GAP-1m (made by GE GRC) is also included on the figure. GAP-1m was tested using 80 °C and 180 °C vacuums. The data for both vacuum temperatures are provided on the graph for comparison.

The three GAP-S materials showed similar vapor pressures. The vapor pressures were higher than GAP-1m with a 180 °C vacuum, but showed very similar results to GAP-1m with 80 °C vacuum. All of the materials measured have significantly lower vapor pressures than pure MEA.

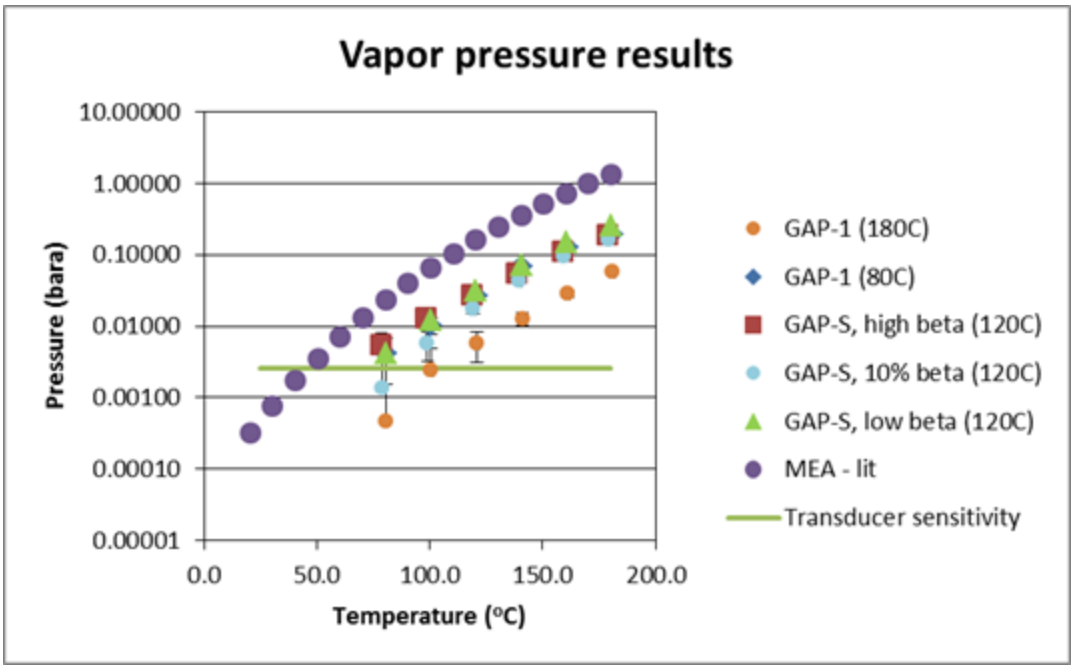

Figure 58. Comparison of vapor pressure results for GAP-1m and GAP-S materials.

Task 4.3: Develop Cost Effective Plan for Large-Scale Manufacture

Review of Alternative Pathways for Synthesis of GAP-1m for a Commercialized CO_2 Capture System

In the process pathway shown in Figure 29, far more platinum catalyst and tetramethyldisiloxane (TMDSO) is used than desired. Excessive platinum is used because the primary amine portion of allylamine poisons the catalyst sites, lowering reactivity. Common hydrosilations require only 1-4 mg/mol of product to affect hydrosilation. The current process uses about 13 mg/mol, a great waste. Excessive tetramethyldisiloxane is used to try to drive the reaction thermodynamically and complete the consumption of the allylamine. It would be more preferable to use as little TMDSO as necessary, substituting octamethylcyclotetrasiloxane (D4) to grow the siloxane chain for GAP-1m. D4 is about 10x cheaper than TMDSO. Thus, allylamine causes many problems, especially since it is expensive when compared to other monomers like acrylonitrile or allyl chloride.

The strategy for improving the synthesis pathway is to 1) use less catalyst by minimizing the poisoning, 2) use less tetramethyldisiloxane by increasing the reaction efficiency, and 3) use less or replace allylamine.

Replace Allylamine with Allyl Chloride

Hydrosilation

One option is to replace allylamine with allyl chloride. This proved to be more difficult than originally imagined. The most common methods of hydrosilation use platinum as a catalyst. Unfortunately with allyl chloride, the hydrosilation reaction competes with allyl chloride reduction and double bond migration.[12] Low yields of the desired bis-chloropropyl tetramethyldisiloxane result.

Fortunately, two other catalysts have been found that do not catalyze the competitive reactions, copper[13] and iridium[14]. For copper, the reaction requires undesirably high temperatures (200 °C) and pressurized conditions for long reaction times (45 hours). For iridium, the results are much better. The reaction can be run under reflux conditions at atmospheric pressures for several hours to obtain a high yield (>90%) of bis-chloropropyl tetramethyldisiloxane material. While iridium is an expensive metal, Y. Tonomura[15] and others[16] [17] [18] [19] suggest that co-catalysts can suppress deactivation, increasing lifetime.

The reaction was performed several times at the Milliken & Company laboratories to understand what would be necessary for scale-up. Hydrosilation with tetramethyldisiloxane (TMDSO) (hydrolyzed chlorodimethylsilane) did not work as well as hydrosilation with chlorodimethylsilane. As shown in Figure 59, a chlorodimethylsilane reaction required approximately 100 ppm of iridium to complete the reaction after 4 hours. The conversion was measured with GC-MS, comparing the area under each curve. This amount of catalyst is still higher than desired since it is also expensive.

[12] M. Jankowiak, et al, Journal of Organometallic Chemistry, 690 (2005) 4478-4487.
[13] B.T. Nguyen, et al, US6713644, Oct. 3, 2002.
[14] J.M. Quirk, et al, US4658050, March 31, 1986.
[15] Y. Tonomura, et al, US6359161, May 11, 2001.
[16] T. Kornek, et al, US7208618, June 12, 2003.
[17] A. Bauer, et al, US7956210, Feb. 25, 2008.
[18] K. Ramdani, et al, US7655813, April 7, 2008.
[19] N. Guennouni, et al, US7884225, July 16, 2008.

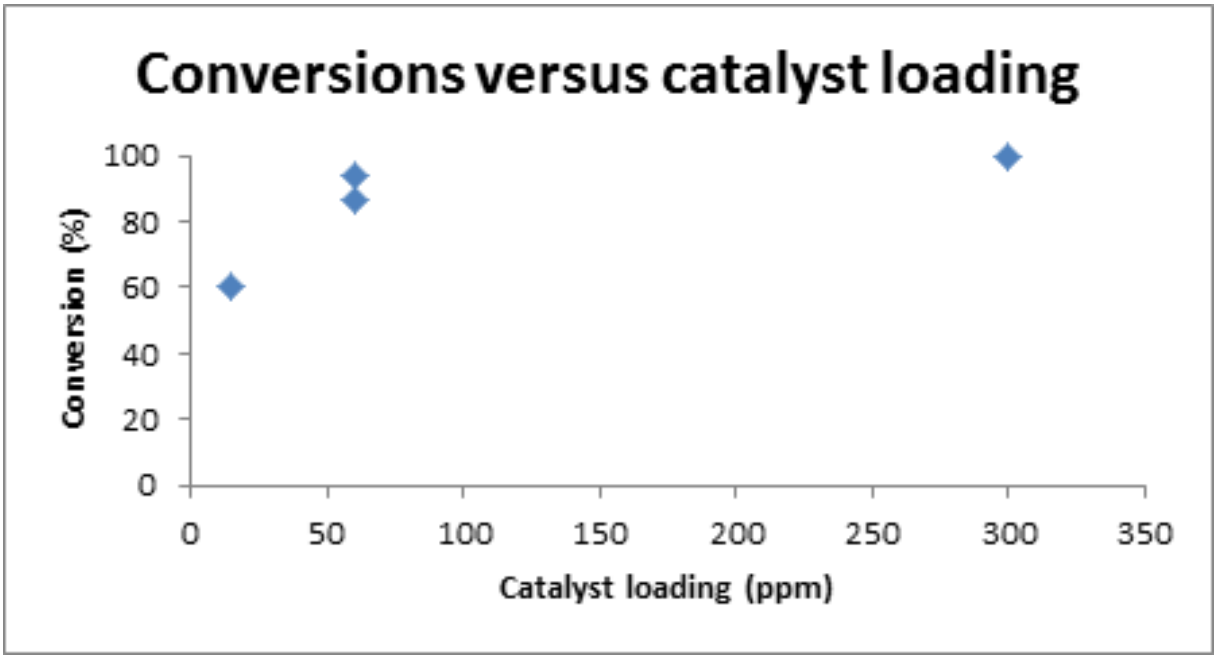

Figure 59. Effect of iridium catalyst loading on conversation for the hydrosilation of allyl chloride to chlorodimethylsilane.

When using allyl chloride to make GAP-1m, the conversion of the chloro- group into a primary amine must also be accomplished. After studying the literature, SiVance investigated a) substitution of chlorine by concentrated ammonia to form primary amine,[20] and b) transformation of chlorine on bis-chloropropyl tetramethyldisiloxane to carbamate functionality and subsequent hydrolysis to primary amine.[21]

Convert Chloro- to Amino- with Ammonia

For substitution by ammonia, two possible methods were disclosed in the literature. First, the chloropropylchlorodimethylsilane can be hydrolyzed into bis(3-chloropropyl) tetramethyldisiloxane, which can be treated with excess ammonia to form GAP-0. The difficulty is that secondary and tertiary amines are usually formed even if the concentration (pressure) of ammonia is very high. A couple of experiments showed that a large distribution of various products is made, even with a large excess of ammonia. Separation and purification were difficult, making this process less desirable.

[20] http://www.docbrown.info/page06/OrgMechs2.htm#ammonia.
[21] E. Fritz-Langhals, US Pat. Appl. 2012/0004436, March 23, 2009.

Alternatively, the chloropropylchlorodimethylsilane can be treated with excess ammonia before hydrolysis to form a cyclic silazane that converts to GAP-0 when hydrolyzed.[22] This process also requires a very high excess of ammonia to insure that a cyclic disilazane forms without any secondary or tertiary amines. A second series of experiments confirmed that again a wide distribution of products is made, even with a large excess of ammonia.

The high concentration and pressure of ammonia that is required in both of these processes decreases the possible yield per batch, making this process less desirable because a large capital investment would be needed to make a full batch of GAP material. Experiments also suggested that the subsequent separation and purification would be difficult. Thus, work on using ammonia was discontinued.

Convert Chloro- to Amino- via Carbamate

Fritz-Langhals[21] disclosed a process that uses potassium cyanate to convert the chloro- group on bis(3-chloropropyl)tetramethyldisiloxane to carbamate. These are then hydrolyzed to primary amines by refluxing in strong acid or base to release carbon dioxide, producing GAP-0. A possible disadvantage of the process is that the yields disclosed in the patent application ranged greatly, sometimes as low as 50%.

<u>Protect Allylamine and Prevent Poisoning of Catalyst</u>

Literature

A second thought is to protect the amine and prevent it from poisoning the catalyst. Others have looked for similar improvement. US3642854[23] and US4584393[24] describe changing the sequence of manufacture by reacting the dimethylchlorosilane with excess allylamine first to form N- allyl-dimethylsilazane. After removal of the allylamine hydrochloride salt and remaining excess allylamine, platinum catalyst is added to affect intramolecular hydrosilation. The resulting oily material can then be hydrolyzed to form the desired bis(3-aminopropyl)-tetramethyldisiloxane product.

Unfortunately, this technique suffers from two issues. First, the process uses excess allylamine. Allylamine is a cardiovascular health hazard that must be handled carefully, and preferably used as the limiting reagent. Second, it is difficult to control the reaction to form only the preferred monosilazane product as opposed to a mixture of mono- and di-silazanes. The monosilazane is preferred because it hydrolyzes to pure bis(3-aminopropyl)tetramethyldisiloxane. With the

[22] L. Brader, et al, US6531620, Sept. 27, 2001.
[23] V.P. Kozjukov, et al, US3642854, claim 12, Feb. 15, 1972.
[24] J.L. Webb, et al, US4584393, April 22, 1986.

mono- and disilazane blend, a mixture of oligomers is produced, comparable to that found with the current process described above. This reaction was performed several times, and the difficulties handling the excess allylamine and hydrochloride salt were confirmed. Further work was abandoned because this method did not produce much improvement over the current process.

In other work, Webb[25] suggests that the yield of the desired GAP product can be improved by first reacting dimethylchlorosilane with ammonia to preferably form tetramethyldisilazane. That product is then reacted with allylamine to form the N-allyl-dimethylsilazane. After hydrosilation and hydrolysis, the product is primarily GAP-0. This has advantages that only stoichiometric amounts of allylamine are needed, and the final product has higher purity. Its disadvantages come from the need to manufacture tetramethyldisilazane which can be expensive. The chemistry necessary to limit the initial reaction to monosilation on the allylamine nitrogen can also be difficult.

More interestingly, US4892918[26] suggests that secondary amines do not poison the platinum hydrosilation catalyst as much as primary amines. They reported that they could hydrosilate N-methyl allyl amine with dimethylchlorosilane without any catalyst poisoning.

This suggests that protection[27] of the amine could aid the hydrosilation reaction and lower catalyst usage. As shown in Figure 60, the general reaction scheme changes the primary amine of allylamine with another reactant (X') to form a secondary or tertiary amine. After hydrosilation, the protecting group (X) must be removed, restoring the primary amine functionality.

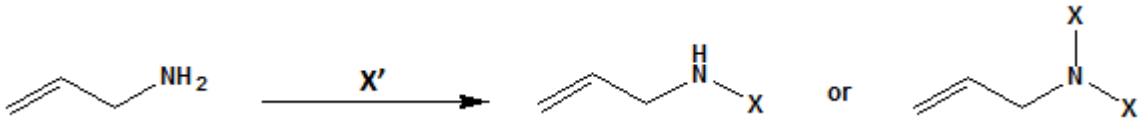

Figure 60. General protection reaction scheme converting the primary amine of allylamine into a secondary or tertiary amine.

Several specific reaction schemes are published in the literature, but a careful choice is important because many protection/deprotection processes are expensive and not likely suited

[25] J.L. Webb, US4565885, Jan. 21, 1986.
[26] H.S. Ryang, US4892918, Jan. 9, 1990.
[27] http://www.organic-chemistry.org/synthesis/C1N/amines/protectedprimaryamines.shtm.

for the projected volumes of aminosilicone solvent needed for power plants. For example, Figure 61 and Figure 62 show schemes where allylamine is reacted with phthalic acid to form a phthalimide[28] or reacted with hexamethyldisilazane to create allyl hexamethyldisilazane.[29] In both cases, the protection "shrubbery" is too expensive to be practical for this application.

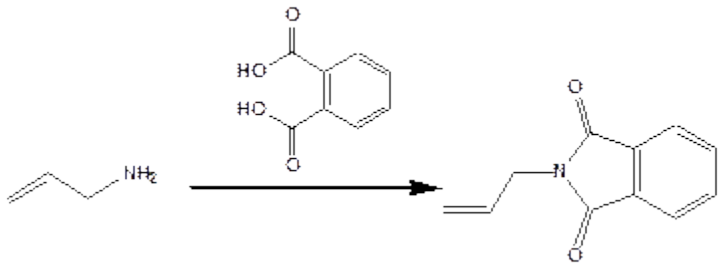

Figure 61. Protection reaction scheme where phthalic acid is used to convert the primary amine of allylamine into a phthalimide, a tertiary amine.

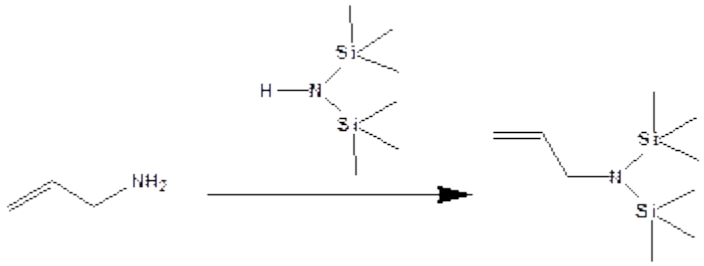

Figure 62. Protection reaction scheme where hexamethyldisilazane is used to convert the primary amine of allylamine into a tertiary amine.

A more promising reaction scheme is the reaction of methyl chloroformate with allylamine to make methyl N-allylcarbamate[30] [31] as shown in Figure 63. In this case, the resulting protection "shrubbery" is methanol and carbon dioxide, less expensive materials that may make this process more feasible.

[28] Michael Palucki, et al., US6262268, 2001.
[29] B.N. Ghose, Journal of Organometallic Chemistry, 1979, Vol. 164, p. 11-18.
[30] T. W. Greene, Protective Groups in Organic Synthesis, 1981, p. 224.
[31] P. J. Kocienski, Protecting Groups, 2000, p. 191-192.

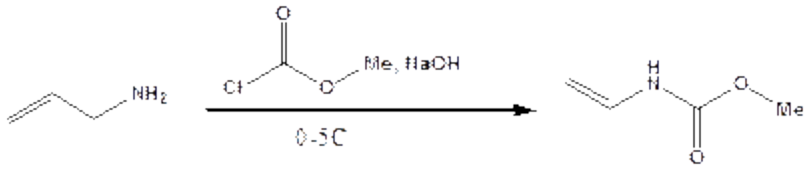

Figure 63. Protection reaction scheme where methyl chloroformate is used to convert the primary amine of allylamine into a secondary amine, methyl N-allylcarbamate.

Laboratory – Minimize excessive use of platinum catalyst and TMDSO

SiVance conducted experiments where methyl chloroformate was added drop-wise to a mixture containing allylamine and sodium hydroxide cooled in an ice/water bath. Because the reaction was exothermic, the chloroformate was added at a low enough rate to ensure that the reaction did not overheat. Once the addition was complete, the mixture was stirred for 30 minutes, diluted with diethyl ether, and filtered. The aqueous layer was separated, extracted once with ether, and the organic layers were dried over $MgSO_4$. Following solvent evaporation, the material was distilled (74-76 °C at 12-15 mm Hg). Representative ^{1}H-NMR and IR are shown in Figure 64 and 65, respectively.

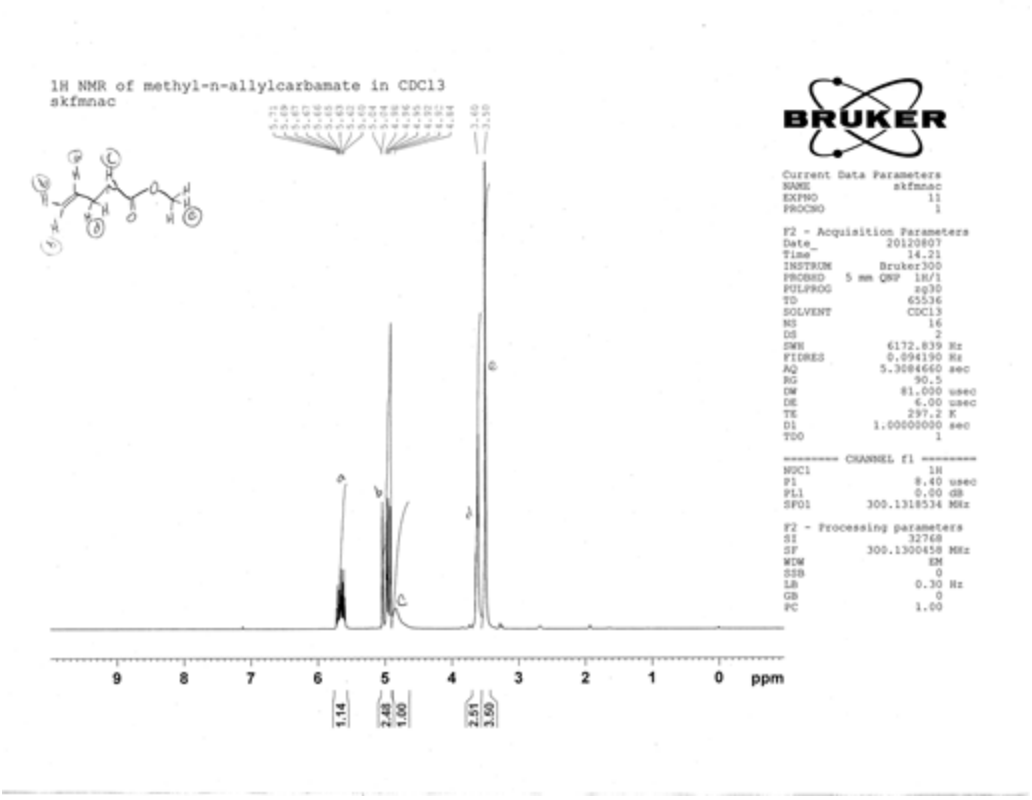

Figure 64. Representative H-NMR of methyl-N-allylcarbamate in chloroform.

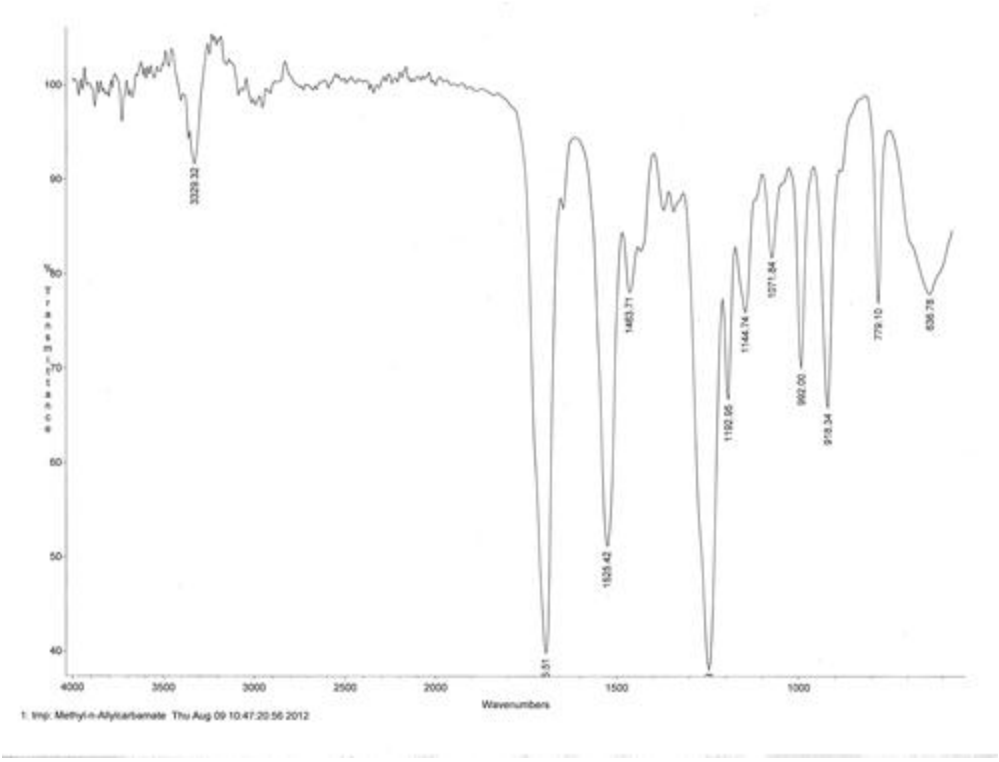

Figure 65. Representative IR of methyl-N-allylcarbamate.

From here, a route was developed to make the GAP product using hydrosilation[32 33], as shown in Figure 66. In the first step, one of three methods was used where the hydrosilation reaction attached the carbamate moiety to the siloxane. In the first method, methyl-N-allylcarbamate (4.74 mL, 0.04 mols) was syringed into a three-neck round-bottom-flask backfilled with nitrogen. Platinum catalyst (0.004605 g, 4.61 mL 20 ppm with respect to methyl-N-allylcarbamate) was added via syringe. Then 1,1,3,3-tetramethyldisiloxane (4.60 mL, 0.026 mols)[TMDSO] was added drop-wise using a syringe pump over 4 hrs at 100 °C (at a rate of 0.019 mL/min). The reaction was monitored via GC-MS and ^{1}H NMR after one hour from start of reaction. The reaction was allowed to run overnight and again analyzed by IR, ^{1}H NMR, and GC-MS. The product was named "bis(methoxycarbonyl)-GAP" or "GAP-carbamate" for shorthand. Representative spectra are included in Figure 67, 68, and 69.

[32] H.S. Ryang, US4892918, 1987.

[33] V.F. Mironov, et al., "Carbofunctional organosilicon compounds containing isocyanate, chloroformate, and carbamate groups by hydrosilylation", Doklady Akademii nauk SSSR, 178 (2), 1968, p.358-61.

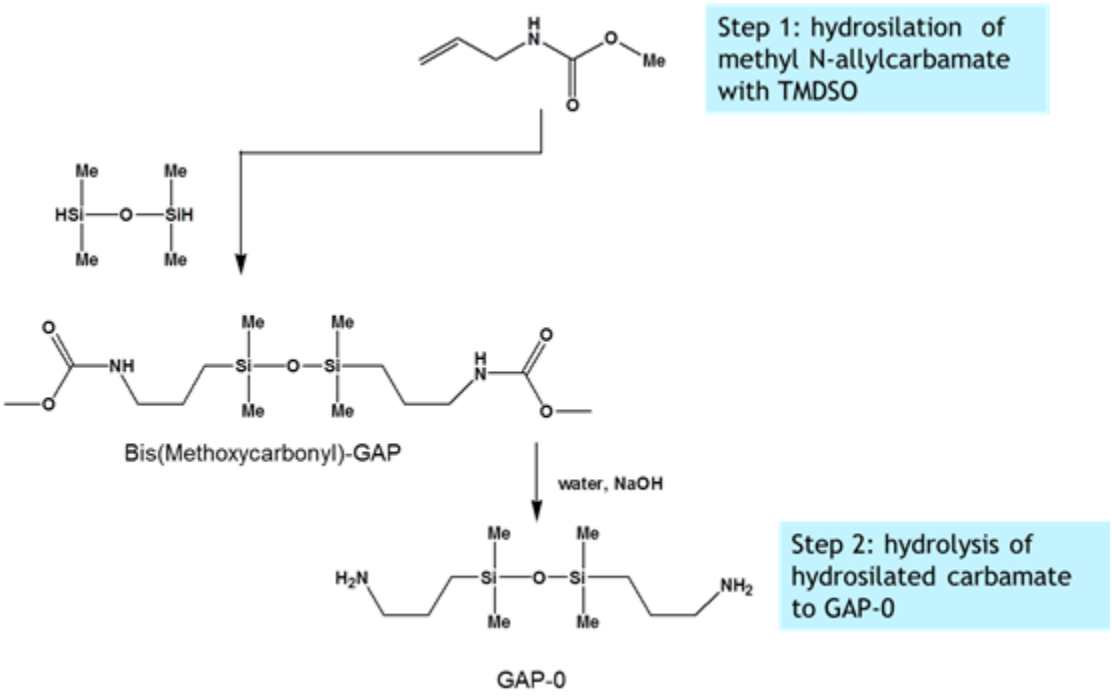

Figure 66. Reaction scheme where methyl N-allylcarbamate is hydrosilated and subsequently hydrolyzed to make GAP-0.

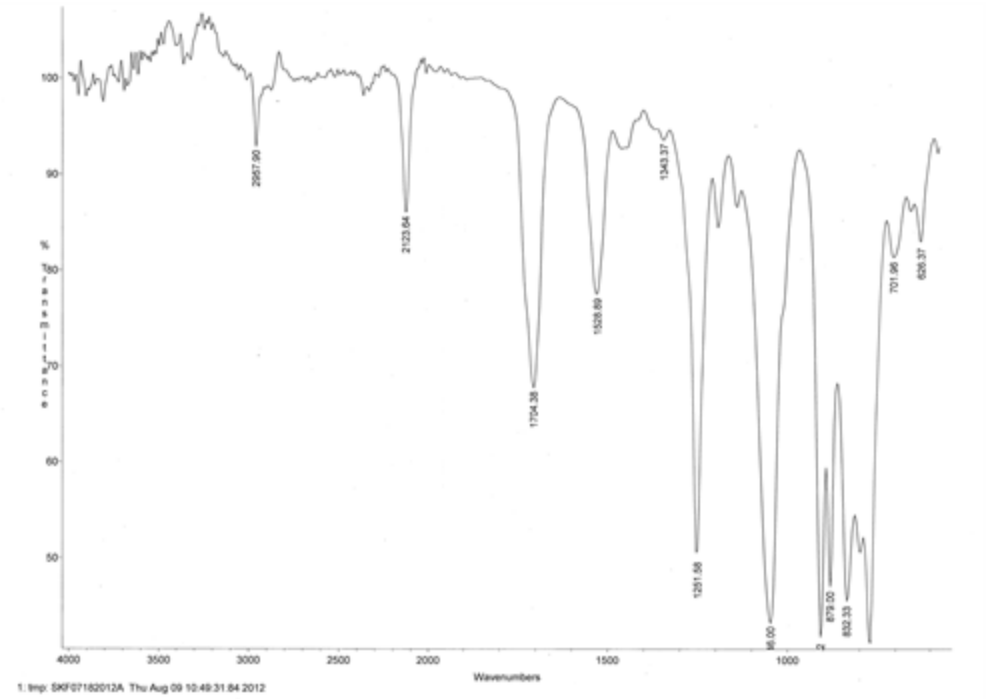

Figure 67. Representative IR of "bis(methoxycarbonyl)-GAP" or "GAP-carbamate" for shorthand.

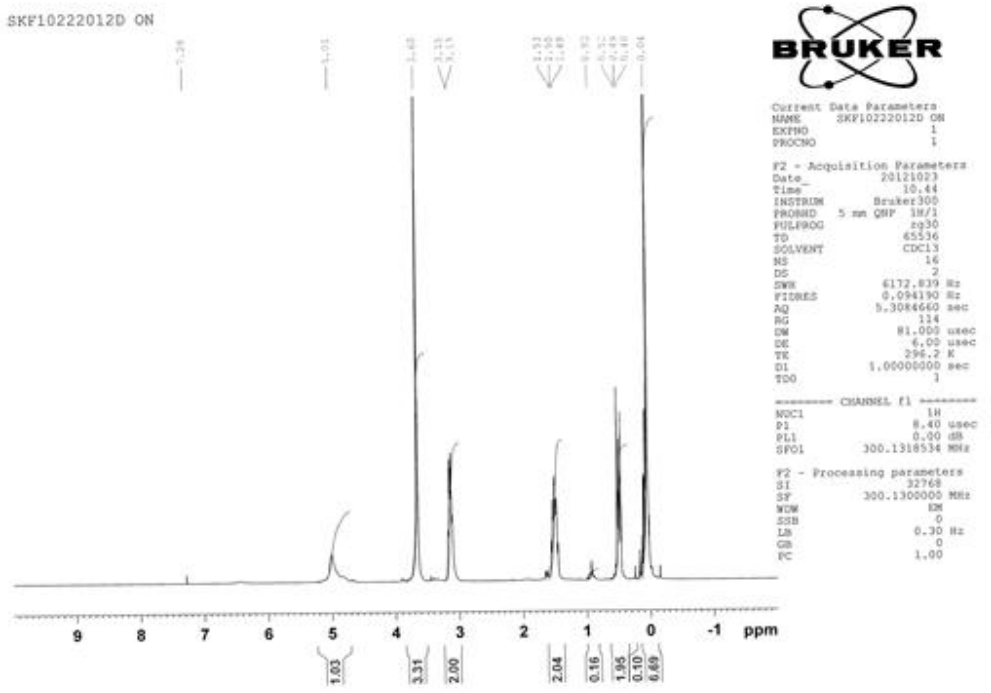

Figure 68. Representative ^{1}H-NMR of "bis(methoxycarbonyl)-GAP" or "GAP-carbamate" for shorthand. The peak at 3.66 is from the carbamate hydrogens.

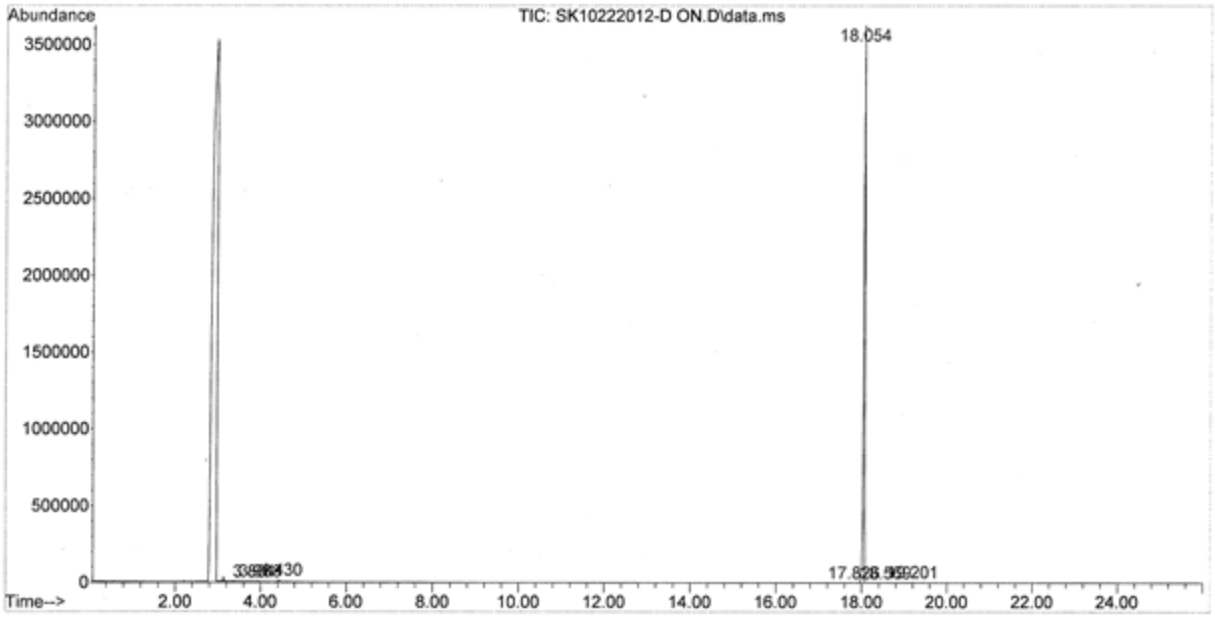

Figure 69. Representative GC of "bis(methoxycarbonyl)-GAP" or "GAP-carbamate" for shorthand. The peak at 2.75 is the solvent; the peak at 18.054 is GAP-carbamate.

In the second method, methyl-N-allylcarbamate (2.3026 g, 0.02 mols) and 1,1,3,3-tetramethyldisiloxane (1.3432 g, 0.01 mols)[TMDSO] were added to a glass pressure vial. Platinum catalyst (2.26 mL 20 ppm with respect to methyl-N-allylcarbamate) was added to the mixture. The reaction mixture was heated to 100 °C and run overnight in a closed glass system with a Teflon™ top. Reaction progression was checked via ^{1}H NMR and GC-MS in the morning. Again, the product was named "bis(methoxycarbonyl)-GAP" or "GAP-carbamate" for shorthand.

The results of the new process are quite successful. It was possible to decrease the concentration of platinum catalyst from 13 mg/mol of product in the current process to as low as 2.5 mg/mol product in the new process. It was also possible to achieve essentially complete hydrosilation with much lower levels of excess TMDSO, as shown in Table 14. Under some conditions, it was possible to even go as low as a mol ratio of 1:1, another large cost savings.

Table 14. Results of hydrosilation of methyl N-allylcarbamate to tetramethyldisiloxane (TMDSO).

Silane	Molar Ratio	Hydrosilation	γ,γ-Bis(methoxycarbonyl)-GAP-0
TMDSO	1:1.3	96	---
TMDSO	1:1.2	96.8	94.5
TMDSO	1:1.1	94.6	92.9
TMDSO	1:1.05	97.5	96.3
TMDSO	1:1	98.7	98.2

Following hydrosilation, the GAP-carbamate products were treated with sodium hydroxide in a 2.1:1 molar ratio, where the sodium hydroxide solution is 15-50% NaOH. Aliquat 336™ was used as a phase transfer catalyst at 5 wt% based upon water. It was reacted at 130 °C under pressure for 4-18 hours. The water layer was separated, extracted once with diethyl ether, and GAP-0 product was collected by evaporating the solvent. As shown in Table 15, the purity was high, and the yield was greater than 70% for small 10g reactions. This should be even better for larger scale reactions.

Table 15. Results of deprotection of carbamate group with aqueous sodium hydroxide, generating GAP-0.

NaOH Conc (2.1/1 mol ratio)	10 g batch Yield %	H-NMR Purity %
50%	70%	100%
35%	63%	100%
25%	79%	100%
20%	83%	100%
15%	74%	98%
10%	NA	93%
5%	NA	97%

The results of this new process show that it is effective for: 1) minimizing the poisoning of the catalyst, allowing lower usage, and 2) improving the reaction efficiency, allowing less tetramethyldisiloxane to be used. This successfully meets the first two objectives of the project's strategy.

Replace Allylamine and Generate Methyl-N-Allylcarbamate

The third leg of the strategy focuses on replacing both allylamine and methyl chloroformate in the reaction scheme shown in Figure 70. While effective on smaller scale, they are too expensive to meet the lower cost targets of CO_2 capture.

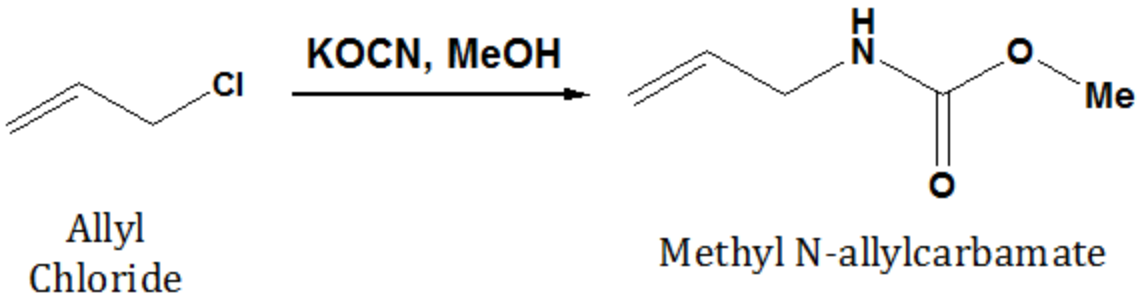

Figure 70. Reaction scheme where allyl chloride is reacted with potassium cyanate and methanol to make methyl N-allylcarbamate.

Literature

As discussed earlier, allyl chloride would be more preferred if the process to convert chloride to carbamate and then to primary amine was cheaper than the difference in raw material costs. Fortunately in the late 1940's, Kaiser discovered that allyl chloride can be reacted with potassium cyanate[34] and methanol to produce methyl-N-allylcarbamate, as shown in Figure 71.[35] As discussed above, carbamate can be converted to amine by hydrolysis with strong acid or base.[36] This is promising because the cost of these raw materials are quite low.

[34] Over 20,000 tons of potassium cyanate are used per year for manufacturing pesticides, drugs, and detergents; P.M. Schalke, et al.,"Cyanates, Inorganic Salts", Ullmann's Encyclopedia of Industrial Chemistry, 2006, Wiley-VCH, Weinheim.
[35] D.W. Kaiser, US2647916, 1953.
[36] E. Fritz-Langhals, US Pat. Appl. 2012/0004436, March 23, 2009.

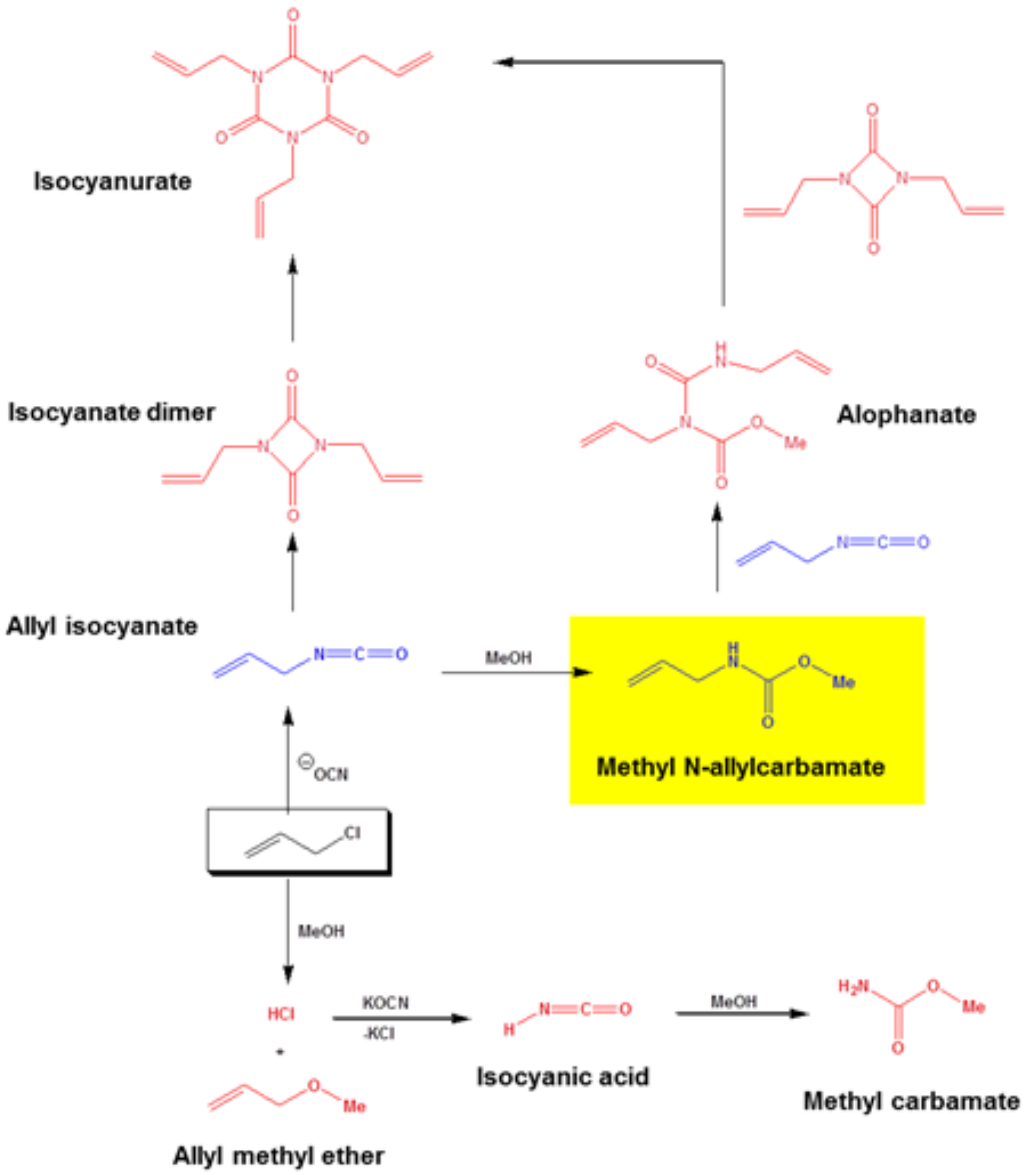

Figure 71. Possible reaction pathways, including undesired by-products, obtained after numerous laboratory reactions under various conditions.

Laboratory – Replace Allylamine with Methyl-N-Allylcarbamate

As shown in Figure 71, it was found that control of the process was very important because many side reactions that lower yield can occur. For example, the intermediate, allyl isocyanate, can dimerize or trimerize to form isocyanurate, a non-recoverable byproduct. Methanol must be controlled to a sufficient concentration to prevent the isocyanate side reactions.

Unfortunately, excessive amounts of methanol will substitute onto the allyl chloride to create allyl methyl ether and hydrochloric acid. The acid reacts further with potassium cyanate to make isocyanic acid that reacts with methanol to make methyl carbamate. By carefully controlling the temperature and solubility of the potassium cyanate through solvent choice, it is possible to minimize the formation of the undesired byproducts to an acceptable level.

Manufacturing Plan for GAP-1m for a Commercialized CO_2 Capture System

Due to the success in the laboratory, a reaction scheme has been developed to address all three legs of SiVance's strategy: 1) minimize the catalyst poisoning, 2) use less tetramethyldisiloxane by increasing the reaction efficiency, and 3) replace allylamine. In the first step of the scheme, allyl chloride was converted to methyl-N-allylcarbamate with KOCN and methanol. Secondly, the methyl-N-allylcarbamate was hydrosilated with TMDSO and a low amount of platinum catalyst. Thirdly, the secondary amine of the carbamate was converted into the desired primary amine with sodium hydroxide, generating GAP-0. Lastly, the GAP-0 was polymerized with octamethylcyclotetrasiloxane (D4) to grow the siloxane chain for the desired product: GAP-1m. For ease of reference, the reaction scheme will be called "GAP-Carb" during further discussion.

It is estimated that about 1.8 MM kg of GAP-1m will be required for initial start-up of a 550 MW plant, with an additional 300,000 to 400,000 kg/year of make-up primarily due to thermal decomposition and deactivation by sulfur in the flue gas. In SiVance's discussions with GE Global Research[37], GE predicted commercialization of the aminosilicone CO_2 capture system to occur sometime after 2015 at a rate of:

Year 1: 1 x 550 MW plant @ 2.2MM kg

Year 2: 3 x 550 MW plants (1 existing plant and 2 new ones) @ 4.7 MM kg

Year 3: 5 x 550 MW plants (3 existing and 2 new) + 1 x 1GW plant @ 9.7 MM kg

At those sales volumes, Milliken & Company/SiVance plans to use the more efficient GAP-Carb reaction scheme that was developed as part of this DOE project. In 2012, Milliken & Company/SiVance created the new process at the exploratory 10-100g exploratory scale. In 2013, Milliken & Company has decided to continue scale-up of this process outside of this GE/DOE cooperative agreement because such work was not included in the 2013 phase of the project.

[37] Robert Perry, GE Global Research, email on 11/30/12.

Raw Material Supply Plan for GAP-1m for a Commercialized CO_2 Capture System

Milliken & Company/SiVance's Global Purchasing Group was able to find a stable supply chain for all raw materials that are used in the GAP-Carb process. Their comments include:

Methanol - No supply concerns. It is a global commodity with 75 million metric ton annual capacity. Six approved manufacturers and availability through multiple regional distributors; multiple suppliers have announced plans to build plants in the US to take advantage of US low global natural gas feedstock pricing due to shale gas.

Allyl Chloride - No supply concerns. It is produced domestically by Dow (794 MM pounds) and Solvay (400 MM pounds) and internationally by 11 others. It is a major raw material for Milliken with multiple approved sources.

KOCN - No supply concerns. It is a global commodity that Milliken buys from a regional distributor (Aceto) who has ongoing relationships with both domestic producers and offshore importers. The global supply exceeds 20,000 tons. When the CO_2 capture process becomes commercial, Milliken would become a key consumer in the Southeastern US with significant market leverage.

Dimethylchlorosilane (DMCS) - Milliken & Company/SiVance has two approved suppliers (Dow Corning, Momentive) and others available internationally (Wacker, Blue Star, Shin Etsu, and Asian). Occasionally Milliken & Company/SiVance has experienced supply delays when suppliers have large internal demands.

Sodium Hydroxide - No supply concerns. It is a global commodity. Milliken buys from multiple regional distributors who have ongoing relationships with both domestic producers and offshore importers. Milliken is a key consumer in the Southeastern US with significant market leverage.

Platinum Catalyst – No supply concerns are expected because the amount necessary for the CO_2 Capture application is tiny compared to the total amount necessary for the silicone industry. Milliken & Company/SiVance synthesizes their own catalyst using the basic raw material, platinum chloride. Metal catalysts, including platinum, are becoming increasingly limited in availability and are termed "critical elements" by the National Research Council.[38] As discussed above, this limitation is being addressed by minimizing the amount that is used. Some

[38] D. Friedman, et al, The Role of the Chemical Sciences in Finding Alternatives to Critical Resources: A Workshop Summary, www.nap.edu/catalog.php?record_id=13366.

academic research is seeking alternatives to platinum for hydrosilation, but nothing is as globally effective as platinum has been found today.[39]

Task 5: Supply Materials for Bench-Scale Testing

The goal of Task 5 was for Milliken/SiVance to synthesize and deliver to GE GRC aminosilicone materials for bench-scale testing. Milliken/SiVance completed this task.

Task 5.0: Large-Scale Synthesis of Materials for Bench-Scale Testing

Milliken/SiVance delivered the first order of 60 kg of GAP-1m on 2/4/13. A second order for 120 kg of GAP-1m shipped on 2/15/13 and was received by GE GRC.

This task is complete. All aminosilicone solvents for bench-scale testing were delivered.

Task 6: Perform Technology EH&S Risk Assessment

A cross-functional team from SiVance and GE Global Research was assembled to conduct the EH&S technology risk assessment for the CO_2-capture process using the aminosilcone-based solvent. The EH&S assessment was conducted in accordance with Attachment 4 of U.S. DOE funding opportunity announcement DE-FOA-0000403.

Task 6.0: Perform Technology EH&S Risk Assessment

Introduction – Completion of Task 6.0: Technology EH&S Risk Assessment

GE Global Research is developing technology to capture carbon dioxide (CO_2) from flue gas using an aminosilicone-based liquid solvent. As part of the DOE award #DE-NT0005310, GE identified 3-aminopropyl end-capped polydimethylsiloxane as a preferred aminosilicone solvent for CO_2 capture. Its structure is shown in Figure 72. It is commonly identified as GAP-x, where x is the number of dimethylsiloxane segments. X can be 0, 1, 2, 3, 4, etc. GE Global Research found that the desired GAP material is a mixture of GAP-x oligomers with x = 0, 1, 2, 3, and 4, but an average molecular weight of x = 1. For simplicity, the aminosilicone material will be identified as GAP-1m.

GE Global Research found that GAP-1m readily reacts with CO_2 to form a carbamate salt. At elevated temperatures, the aminosilicone-carbamate salt releases CO_2, permitting reuse of the solvent and capture of the CO_2. GE also found that addition of triethylene glycol (TEG) as a co-

[39] Hydrosilylation: A Comprehensive Review on Recent Advances, Springer, 2009.

solvent prevents solidification of the aminosilicone salt after absorption of CO_2.[40] This liquid mixture works well as a solvent in a CO_2 capture process.

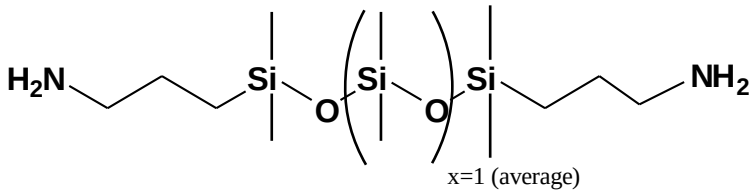

Figure 72. Chemical structure of aminosilicone material.

In this project, GE Global Research's objective was to build, operate, and test a bench-scale continuous CO_2 absorption/desorption system using aminosilicone/triethylene glycol as the solvent. Milliken & Company (SiVance LLC) was sub-contracted to supply the aminosilicone material for the bench-scale system and conduct an Environmental, Health, and Safety (EH&S) assessment for full scale operation.

Air, Water, and Solid Waste Identification for the Aminosilicone-based CO_2 Capture System for a 550 MW Coal-Fired Power Plant

This section describes the potential ancillary or incidental air, water, and solid wastes from the proposed technology and identifies and estimates their magnitude for a 550 MW coal-fired power plant. In addition to the absorption solvents, the possible by-products, waste products, and flue gas contaminants were considered. The CO_2 capture system was designed to minimize possible environmental degradation products and bioaccumulation thereof. The design also examined the full-scale conditions at the point of discharge to the environment.

The chemical composition of the solvent system for a future large - scale power plant installation can be predicted from the materials delivered for the bench scale study of award number DE-FE0007502. The aminosilicone solvent used in the continuous CO_2 absorption/desorption process is a 60%wt GAP-1m/40%wt TEG mixture. The triethylene glycol (CAS #112-27-6) was supplied by Greenchem Industries, LLC. Greenchem's technical bulletins, materials safety data sheets (MSDS's), and additional EH&S paperwork requested from Greenchem suggest that the triethylene glycol does not contain any contaminants.

[40] B. Wood, Technical Proposal In response to DE-FOA-0000403, AOI B1: Bench-Scale Silicone Process for Low-Cost CO2 Capture, March 20, 2011, p. 4.

The GAP-1m was supplied by Milliken & Company (SiVance LLC), Item #2700210000, DAP-0. GAP-1m has some methanol and xylene contaminants that come from SiVance's manufacturing process. To estimate the concentration of the contaminants, the composition of 5 delivered lots of GAP-1m was measured with an Agilent 6890 gas chromatogram (GC) and a model 5973 mass spectrometer (MS). The methanol was less than 100 ppm, and the xylene concentration was less than 50 ppm in the 5 lots. However due to statistical analysis of the capability of the current manufacturing process, SiVance specified the concentration limits to be 500 ppm for each, as shown in Table 16. Thus, 500 ppm will be used as the de-facto concentration in the mass balance discussed below. The molecular weight distribution of GAP-1m was also measured, showing a mixture of X=0, 1, 2, 3, and 4 as included in Table 17. The GAP-0 and GAP-(1-4) components of GAP-1m have been registered separately as CAS#2469-55-8 and CAS#106214-84-0, respectively.

Table 16. Composition range and specifications of GAP-1m delivered to GE Global Research, 2013.

	Methanol ppm	**Xylene ppm**	**Molecular Weight (g/mol)**	**Total Amine Activity (%)**
Specification	<500	<500	<345	>96%
Range of 5 lots	<100[41]	<50[42]	301-317	96-100

Table 17. Distribution of GAP-1m components delivered to GE Global Research, 2013.

GAP-0	**GAP-1**	**GAP-2**	**GAP-3**	**GAP-4**
44%	30%	15%	8%	3%

To make the final solvent, the GAP-1m and TEG are mixed batch-wise before use.

The final solvent composition fed into the CO_2 absorption/desorption process is summarized in Table 18.

[41] Jose Valle, SiVance GAP-1m Method detection limit for Methanol, personal communication, Dec. 16, 2013.
[42] Jose Valle, SiVance GAP-1m Method detection limit for Xylene, personal communication, Dec. 16, 2013.

Table 18. Composition of the aminosilicone solvent for the continuous CO_2 absorption/desorption system.

CO_2 Capture Solution	**GAP-1m (60%wt)**				**TEG (40%wt)**
Components	GAP-0	GAP 1-4	Methanol	Xylene	Triethylene glycol
CAS #	2469-55-8	106214-84-0	67-65-1	1330-20-7	112-27-6
% wt Composition in CO_2 Capture System	24 wt %	36 wt %	<300 ppm	<300 ppm	40 wt %

Milliken & Company collaborated with GE Global Research to create a process flow and mass balance diagram for a continuous CO_2 absorption/desorption system for a 550 MW coal-fired power plant. The balance, included as Figure 73, is based upon knowledge learned from GE Global Research's operation of the bench scale system. The flue gas composition for the 550 MW plant was taken from the award between GE Global Research and the DOE.[43] Before entering the CO_2 absorption/desorption system, flue gas is cleaned and prepared with Flue-Gas Desulfurization (FGD), pre-scrubber, cooler, and condenser units. The gas, labeled 1 in Figure 73, is fed into the CO_2 absorption unit (Absorber). The composition and flow rate of the gas is included in Table 19. It is primarily CO_2, nitrogen (N_2), water (H_2O), and oxygen (O_2), with smaller contaminants of sulfur oxides (SO_x) and nitrogen oxides (NO_x).

[43] DOE-GE Global Research Cooperative Agreement; Award Number DE-FE0007502.

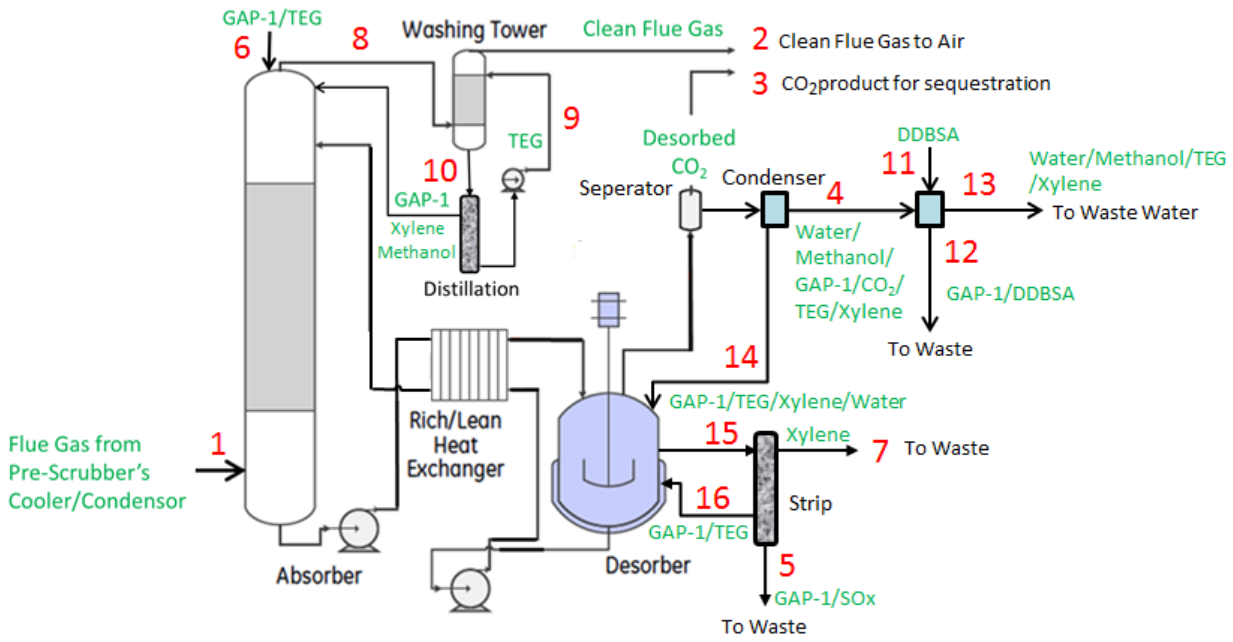

Figure 73. Continuous CO_2 absorption/desorption system for a 550 MW coal-fired power plant.

Table 19. Composition and flow rate of stream 1, inlet flue gas.

Fluegas from Chiller (1)

Flow rate = 4.77E+06 lb/hr
Flow rate = 1.60E+05 lbmol/hr

	vol frac	lbmol/hr	MW	lb/hr
CO2	1.48E-01	2.37E+04	44.01	1.04E+06
H2O	7.31E-02	1.17E+04	18.02	2.11E+05
N2	7.53E-01	1.21E+05	28.01	3.38E+06
O2	2.62E-02	4.20E+03	32.00	1.34E+05
SOx	4.69E-05	7.52E+00	64.07	4.82E+02
NOx	8.26E-05	1.33E+01	46.01	6.10E+02

As the gas enters the absorber, it mixes with the 60%wt GAP-1m/40%wt TEG absorption solvent. The gas passes upward through the column while the liquid flows down. As it mixes, the GAP-1m reacts with CO_2 to make a carbamate salt. The column is designed to capture 90% of the inlet CO_2. The salt is soluble in the liquid and is carried down to the bottom of the column

with the solvent. The GAP-1m also reacts with the SO_x gases to form heat stable salts. This reaction is very efficient, and all of the incoming SO_x is removed from the gas stream. This amino-sulfate salt is dispersed into the solvent and carried to the bottom of the column with the solvent. Since water and triethylene glycol are miscible, a large amount of water vapor dissolves into the solvent and is carried with the liquid to the bottom of the column. Meanwhile, none of the N_2, O_2, or NO_x dissolves or reacts with the solvent, as confirmed by GE Global Research's bench-scale studies.[44] As the cleaned flue gas exits the top of the column, a small amount of GAP-1m, TEG, xylene, and methanol may exit with the gases. To prevent release to the environment, these are captured with a TEG wash tower. The GAP-1m, xylene, and methanol are separated from the TEG with a distillation column and returned to the top of the absorption column. The TEG is returned to the TEG wash tower. The cleaned flue gas, shown as stream 2 in Figure 73, is released to the atmosphere via a stack. Its composition and flow rate is shown in Table 20.

Table 20. Composition and flow rate of stream 2, cleaned flue gas.

Clean Fluegas Out (2)

Flow rate = 3.78E+06 lb/hr
Flow rate = 1.36E+05 lbmol/hr

	vol frac	lbmol/hr	MW	lb/hr
CO2	1.73E-02	2.37E+03	44.01	1.04E+05
H2O	6.58E-02	8.97E+03	18.02	1.62E+05
N2	8.86E-01	1.21E+05	28.01	3.38E+06
O2	3.08E-02	4.20E+03	32.00	1.34E+05
SOx	0.00E+00	0.00E+00	64.07	0.00E+00
NOx	9.72E-05	1.33E+01	46.01	6.10E+02
GAP-1m	0.00E+00	0.00E+00	322.67	0.00E+00
TEG	0.00E+00	0.00E+00	150.17	0.00E+00

Meanwhile, the liquid at the bottom of the absorption column is pumped through a heat exchanger into a desorption vessel (Desorber). Here, the liquid is heated until the carbamate salt decomposes, releasing CO_2 gas. Some GAP-1m, TEG, water, xylene, and methanol may also

[44] Benjamin Wood, GE Global Research, personal communication, Oct. 22, 2013.

vaporize with the CO_2 product. The gas stream goes through a series of condensers and compressors to remove the contaminants from the gas stream. The clean gas stream, shown as stream 3 in Figure 73, is collected as the CO_2 product. See Table 21 for composition and flow rate. A second stream rich in GAP-1m, TEG, xylene, and a fraction of water, is recycled to the Desorber. A third condensed stream, stream 4 in Figure 73, is mostly water and methanol with a small amount of GAP-1m, TEG, and xylene (see Table 22). This stream will be treated with a stream of dodecylbenzenesulfonic acid (DDBSA) (stream 11), detailed in Table 23, and allowed to settle. A small stream of GAP-1m/DDBSA salt (stream 12), detailed in Table 24, is then removed from the water and disposed of as industrial, non-hazardous solid waste. Stream 13 (see Table 25), which contains water, methanol, TEG, and xylene, would also be disposed of as non-hazardous solid waste, which could include sending it to a wastewater treatment facility, depending on site-specific considerations. This would not be an option if GAP-1m were still present in this waste stream.

Table 21. Composition and flow rate of stream 3, CO_2 product.

CO2 Out (3)

Flow rate = 9.37E+05 lb/hr
Flow rate = 2.13E+04 lbmol/hr

	vol frac	lbmol/hr	MW	lb/hr
CO2	9.99E-01	2.13E+04	44.01	9.37E+05
H2O	7.91E-04	1.69E+01	18.02	3.04E+02
N2	0.00E+00	0.00E+00	28.01	0.00E+00
O2	0.00E+00	0.00E+00	32.00	0.00E+00
SOx	0.00E+00	0.00E+00	64.07	0.00E+00
NOx	0.00E+00	0.00E+00	46.01	0.00E+00
GAP-1m	0.00E+00	0.00E+00	322.67	0.00E+00
TEG	0.00E+00	0.00E+00	150.17	0.00E+00

Table 22. Composition and flow rate of stream 4, Desorber condensate.

Desorber Condensate (4)

Flow rate = 5.06E+04 lb/hr
Flow rate = 2.74E+03 lbmol/hr

	mol frac	lbmol/hr	MW	lb/hr
H2O	1.44E-01	2.74E+03	18.02	4.93E+04
GAP-1m	2.10E-04	3.98E+00	322.67	1.28E+03
TEG	1.43E-06	2.71E-02	150.17	4.07E+00
Methanol	3.06E-06	5.79E-02	32.04	1.86E+00
Xylene	8.41E-08	1.59E-03	106.16	1.69E-01

Table 23. Composition and flow rate of stream 11, DDBSA stream.

DDBSA Stream (11)

Flow rate = 2.60E+03 lb/hr
Flow rate = 7.96E+00 lbmol/hr

	mol frac	lbmol/hr	MW	lb/hr
DDBSA	1.00E+00	7.96E+00	326.49	2.60E+03

Table 24. Composition and flow rate of stream 12, GAP-1m/DDBSA stream.

GAP-1m/DDBSA Stream (12)

Flow rate = 3.88E+03 lb/hr
Flow rate = 3.98E+00 lbmol/hr

	mol frac	lbmol/hr	MW	lb/hr
GAP-1m/DDBSA	1.00E+00	3.98E+00	975.65	3.88E+03

Table 25. Composition and flow rate of stream 13, waste water.

Waste Water (13)

Flow rate = 4.93E+04 lb/hr
Flow rate = 2.74E+03 lbmol/hr

	mol frac	lbmol/hr	MW	lb/hr
H2O	1.44E-01	2.74E+03	18.02	4.93E+04
TEG	1.43E-06	2.71E-02	150.17	4.07E+00
Methanol	3.06E-06	5.79E-02	32.04	1.86E+00
Xylene	8.41E-08	1.59E-03	106.16	1.69E-01

A second exit stream (stream15) from the Desorber prevents buildup of GAP-1m/SOx and xylene waste products in the system. This stream has the same composition as the material in the Desorber. It is rich in GAP-1m and TEG but contaminated with GAP-1m/SOx compounds and xylene. To remove the contaminants, the material is vacuum-distilled. The bottoms will consist of GAP-1m/SOx compounds (stream 5, Table 26) and the lights will consist of xylene (stream 7, Table 27). Stream 5 would be disposed of as industrial, non-hazardous waste and stream 7 would be disposed of under Subpart C of RCRA as hazardous waste. The remaining GAP-1m and TEG is returned to the Desorber. A third, cleaned exit stream is recycled back to the Absorber as part of the continuous CO_2 removal system. Lastly, GAP-1m and TEG are added to the Absorption tower (stream 6) to replenish that lost in waste streams 5 and 12. See Table 28 for flow rate and composition.

Table 26. Composition and flow rate of stream 5, Desorber purge stream.

Purge Stream (5)

Flow rate = 2.91E+03 lb/hr
Flow rate = 7.52E+00 lbmol/hr

	mol frac	lbmol/hr	MW	lb/hr
GAP-1m/SO2	1.00E+00	7.52E+00	386.74	2.91E+03

Table 27. Composition and flow rate of stream 7, xylene waste stream.

Xylene Stream (7)

	mol frac	lbmol/hr	MW	lb/hr
Xylenes	1.51E-03	1.59E-02	1.06E+02	1.84E+00

Table 28. Composition and flow rate of stream 6, solvent make-up stream.

GAP-1m/TEG Make-up Stream (6)

Flow rate = 3.72E+03 lb/hr
Flow rate = 1.16E+01 lbmol/hr

	mol frac	lbmol/hr	MW	lb/hr
GAP-1m	9.91E-01	1.15E+01	322.67	3.71E+03
Methanol	4.99E-03	5.79E-02	32.04	1.86E+00
Xylenes	1.51E-03	1.75E-02	106.16	1.86E+00
TEG	2.34E-03	2.71E-02	150.17	4.07E+00

Toxicological Effects of Components in the Continuous CO_2 Absorption/Desorption Process

The following section details a description of the various toxicological effects of the substances identified above. A thorough literature search was conducted to examine potential human health effects and eco-toxicity. Where information was lacking for a particular material, the material was either compared to similar substances or Quantitative Structure Activity Relationships (QSARs) models[45] were used to predict toxicity levels of the particular chemical. The EPA has worked with various computer programming companies to develop numerous QSARs programs to predict the hazard and toxicological effects of many chemicals. However, it is important to note that the predictability of these QSAR models is currently uncertain for complex toxicological endpoints, such as developmental toxicity or non-genotoxic carcinogenicity.

[45] http://www.epa.gov/nrmrl/std/qsar/qsar.html

The substances of interest in Figure 73 are GAP-1m, xylene, methanol, TEG, GAP-1m/SO_x, and DDBSA. As shown in Table 18, GAP-1m can be considered as a mixture of two compounds, CAS #2469-55-8 (GAP-0) and CAS #106214-84-0 (GAP-(1-4)). The GAP-1m/SO_x salt is not a registered compound, and toxicity information is not readily available. Typically, acid/primary amine salts are less toxic than the free amine itself. For example, 1, 4 diaminobutane is a linear alkyl amine similar in structure to the GAP materials, except it is a carbon chain. Its National Fire Protection Association (NFPA) rating is Health hazard: 4, Fire: 2, Reactivity Hazard: 0, on a scale of 0-4 where 4 is severe. In contrast, its acid salt, 1, 3-Diaminopropane dihydrochloride, has a NFPA rating of Health hazard: 2, Fire: 0, Reactivity Hazard: 0. The acid salt is much less severe. Thus, for analysis here the toxicity of GAP-1m/SO_x is assumed to be less than or equal to its components, GAP-1m and SO_x. Thus, the substances considered here are the components of GAP-1m (CAS #2469-55-8 (GAP-0) and CAS #106214-84-0 (GAP-(1-4)), xylene, methanol, TEG, and DDBSA.

Several literature resources were searched including: MSDS, ATMI[46], REACH compliance registration[47], and SAP EHS Regulatory Content Substance Reports[48]. Much of the requested toxicology data has not been measured or published for CAS #2469-55-8 (GAP-0) and CAS #106214-84-0 (GAP-(1-4)). Instead, the QSAR models ECOSAR, EPIWIN, TOXTree, PBT Profiler, and T.E.S.T were used to predict potential human health effects and eco-toxicity for these materials. These models use the physical characteristics of the various parts of the chemical structure to predict the characteristics of the whole molecule. For example, molecules that contain the primary amine group, -NH_2, are known to have toxicity to fish. The siloxane group is known to be hydrophobic and decompose slowly in the environment. These and other "molecular descriptors" are combined through a series of mathematical equations to predict the hazard and toxicity properties of the entire molecule.

Through the years, the EPA has learned that the accuracy of the aquatic toxicity models (ECOSAR) is limited for very hydrophobic molecules. As the molecule becomes more hydrophobic, less disperses into water, preventing the chemical from contacting aquatic life. A common method of measuring hydrophobicity is the octanol/water partition coefficient (K_{ow}). It is defined as the ratio of a chemical's concentration in n-octanol to its concentration in water at

[46] http://www.supplier.milliken.com/en-us/EHS/atmivpep.pdf

[47] REACH is the Regulation on Registration, Evaluation, Authorization and Restriction of Chemicals. It is the regulative framework on chemicals for the European Union (EU). CAS# 2469-55-8 (GAP-0) is scheduled for REACH registration in 2018. Until then, no compliance information is available to the public. CAS #106214-84-0 (GAP-(1-4)) is not scheduled for registration until sometime after 2018, suggesting that its toxicity profile is considered to be less than that for GAP-0. No compliance information is available from REACH to the public at this time.

[48] SAP NetWeaver Portal (https://erc-viewer.sap.com/irj/portal/ajax); SAP America Inc 3999 West Chester Pike Newtown Square, PA 19073 USA.

equilibrium. Since the number is small, the log K_{ow} is more commonly reported. When the log K_{ow} is less than or equal to 5.0 for fish and daphnid, or 6.4 for green algae, ECOSAR provides reliable toxicity estimates for acute effects. If the log K_{ow} exceeds those general limits, the decreased water solubility of these oleophilic chemicals limits the acute toxicity effects during a 48-hour to 96-hour test. For chronic exposures, the applicable log K_{ow} range is extended up to log K_{ow} = 8.0. If the log K_{ow} of the chemical exceeds 8.0, no chronic toxic effects are expected even with long-term exposures.[49]

The following sections summarize the results of various tests used to estimate their toxicity to humans and the environment. When available, experimental data were included. If not available, modeling data were included and are indicated as predicted in the tables below. Resource information was also provided for clarification of how the data were obtained.

GAP-1m: CAS# 2469-55-8 (GAP-0) and CAS# 106214-84-0 (GAP-1-4)

Some of the ingestion, eye, and skin effects for GAP-1m have been experimentally tested previously as shown in Table 29 and 30. Generally, GAP-1m is a severe skin and eye irritant but has low ingestion toxicity.

[49] Tolls, J; Müller, M; Willing, A, et al. (2009) "A New Concept for the Environmental Risk Assessment of Poorly Water Soluble Compounds and Its Application to Consumer Products", Integr Environ Assess Manag 5(3), 2009, p. 374-378.

Table 29. GAP-0 toxicity.

CAS# 2469-55-8, GAP-0	Toxicity Test Result	Species	Time (hrs)	Resource/Model Software
Ingestion LD_{50} (mg/kg)	500	Rat	N/A	SiVance MSDS[50]
Intraperitoneal LD_{50} (mg/kg)	80	Mouse	N/A	SiVance MSDS[50]
Eye Irritation/Damage	Severe Irritant	Rabbit	24 hours (500 µL)	SiVance MSDS[50]
Dermal LD_{50} (mg/kg)	>2 g/kg	N/A	N/A	SiVance MSDS[50]
Skin Corrosion/Irritation	Severe Irritant	Rabbit	24 hours (500 µL)	SiVance MSDS[50]
Predicted Octanol Water Partition Coefficient, log K_{ow}	4.27	N/A	N/A	ECOSAR
Predicted Genotoxicity	Negative	N/A	N/A	TOXTree
Predicted Nongenotoxic Carcinogencity	Negative	N/A	N/A	TOXTree
Predicted Mutagencity	Negative	N/A	N/A	TEST
Predicted Fish Toxicity LC_{50} (ppm)	1.54	N/A	96	ECOSAR
Predicted Fish Toxicity LC_{50} (ppm), chronic	0.74	N/A	N/A	ECOSAR
Predicted Daphnia LC_{50} (ppm)	0.24	Daphnia	48	ECOSAR
Predicted Daphnia Toxicity LC_{50} (ppm), chronic	0.020	Daphnia	N/A	ECOSAR
Predicted Algae EC_{50} (ppm)	0.12	N/A	N/A	ECOSAR
Predicted Algae Toxicity EC_{50} (ppm), chronic	1.02	N/A	N/A	ECOSAR
Predicted Biodegradability	Not readily biodegradable	N/A	N/A	EPIWIN
Predicted Soil Adsorption Coefficient, K_{oc} (L/kg)	1751	N/A	N/A	EPIWIN
Predicted Bioconcentration Factor (BCF)	305	N/A	N/A	EPIWIN

[50] SiVance, LLC MSDS for DAP-0.

Table 30. GAP-1-4 predicted toxicity based on molecular modeling.

CAS# 106214-84-0, GAP-1-4	Toxicity Test Result	Species	Time (hrs)	Resource/Model Software
Predicted Ingestion LD_{50} (mg/kg)	>2444	Rat	N/A	T.E.S.T.
Intraperitoneal LD_{50} (mg/kg)	80	Mouse	N/A	SiVance MSDS[50]
Eye Irritation/Damage	Severe Irritant	Rabbit	24 hours (500 µL)	SiVance MSDS[50]
Skin Corrosion/Irritation	Severe irritant	Rabbit	24 hours (500 µL)	SiVance MSDS[50]
Predicted Octanol Water Partition Coefficient K_{ow}	See Figure 3	N/A	N/A	ECOSAR
Predicted Developmental Toxicity	Positive	N/A	N/A	TOXTree - GAP1-3
Predicted Genotoxicity	Negative	N/A	N/A	TOXTree - GAP1-4
Predicted Nongenotoxic Carcinogencity	Negative	N/A	N/A	TOXTree - GAP1-4
Predicted Mutagencity	Negative	N/A	N/A	TEST - GAP1-4
Predicted Fish Toxicity LC_{50} (ppm), chronic	0.000279	N/A	N/A	ECOSAR - GAP-2
Predicted Daphnia LC_{50} (ppm), chronic	0.000967	N/A	N/A	ECOSAR - GAP-2
Predicted Algae EC_{50} (ppm), acute	0.014	N/A	96	ECOSAR – GAP-1
Predicted Algae EC_{50} (ppm), chronic	0.000841	N/A	N/A	ECOSAR - GAP-2
Predicted Biodegradability	Not readily biodegradable	N/A	N/A	EPIWIN
Predicted Soil Adsorption Coefficient, K_{oc} (L/kg)	>11,250	N/A	N/A	EPIWIN
Predicted Bioconcentration Factor (BCF)	See Figure 4	N/A	N/A	EPIWIN

TOXTree and TEST models were used to predict the carcinogenic and mutagenic toxicity of the GAP-1m compounds. The models suggest low probability of genotoxic, carcinogenic, and mutagenic toxicity.

Since much of the aquatic toxicity data for the GAP-1m materials needed to be derived from modeling, the log K_{ow} values were calculated to determine if the models are valid for this material. Specifically, the log K_{ow} was calculated for the GAP-x series of x = 0, 1, 2, 3, and 4, the components of GAP-1m. These are plotted in Figure 74. It shows that the log K_{ow} values are directly proportional to the molecular weight of the GAP species. The log K_{ow} validity limits are also plotted for fish, daphnia, and algae. ECOSAR model predictions are valid for the CAS# 2469-55-8 (GAP-0) component of GAP-1m for acute and chronic toxicity to fish, daphnia, and algae. The CAS# 106214-84-0 (GAP-1-4) component is more complex. The molecules become less water soluble as x increases. Thus for x = 1, only acute algae and chronic toxicity predictions are valid. For x = 2, only chronic toxicity predictions are valid. For x = 3 & 4, none of the predictions are valid. Knowing this information, the toxicity predictions were calculated and the results included in Table 29 for CAS# 2469-55-8 (GAP-0) and Table 30 for CAS# 106214-84-0 (GAP-1-4). Since GAP-(1-4) (CAS# 106214-84-0) is a mixture of x = 1-4, the worst valid toxicity result was used to represent the mixture. The results suggest that the GAP-1m material can be quite toxic to aquatic ecosystems. This concurs with the results found with analogous organic amines that are known to be harmful to aquatic wildlife.

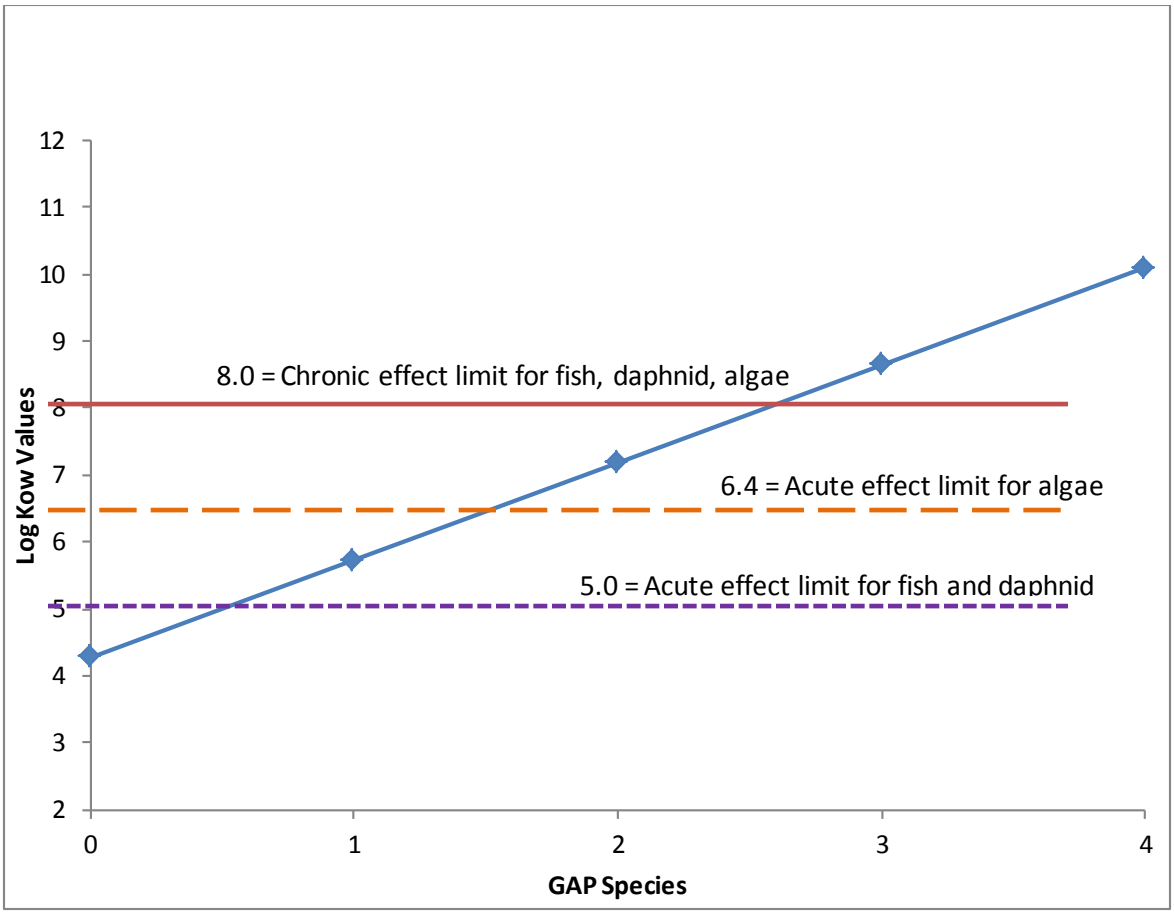

Figure 74. Log K_{ow} values of GAP-0-4 with ECOSAR validity limits.

A second model, EPIWIN, predicted the effect of GAP-1m on soil-based environments. It suggests that it does not biodegrade easily, tending to persist in the environment. Compounds with siloxane segments are known to degrade slowly.[51] The lipophilic structure of the siloxane chain also tends to adsorb well to soil. A KoD > 500 L/kg suggests that it blends and adheres well to most soils. The results show that both CAS# 2469-55-8 (GAP-0) and CAS# 106214-84-0 (GAP-1-4) adhere well to soil, making it difficult to remove.

The modeling results for Bio-Concentration Factor, graphed in Figure 75, are interesting. Bio-Concentration Factor (BCF) is the measure of how readily a chemical moves in and out of the lipid layer of fish. This is important because humans eat fish, possibly consuming concentrated amounts of the chemical. In the model, the BCF values are most affected by the molecular weight, structure, and solubility partition of the compound between non-polar, fatty

[51] http://www.wiley-vch.de/books/biopoly/pdf_v09/vol09_15.pdf

substances and water. The BCF values for GAP-1m (x = 0-4) are plotted in Figure 75, showing a bell shaped curve. The GAP-0 and GAP-4 have the lowest BCF values while GAP-2 has the highest. It is possible that the molecular weight of GAP-0 is low enough that the fish can excrete the compound without it concentrating in the fat layers. GAP-4 is likely too big to be absorbed. GAP 1, 2, and 3 (especially 2) are small and lipophilic enough to be absorbed and difficult to excrete. As a result, they concentrate in the lipid layer of the fish.

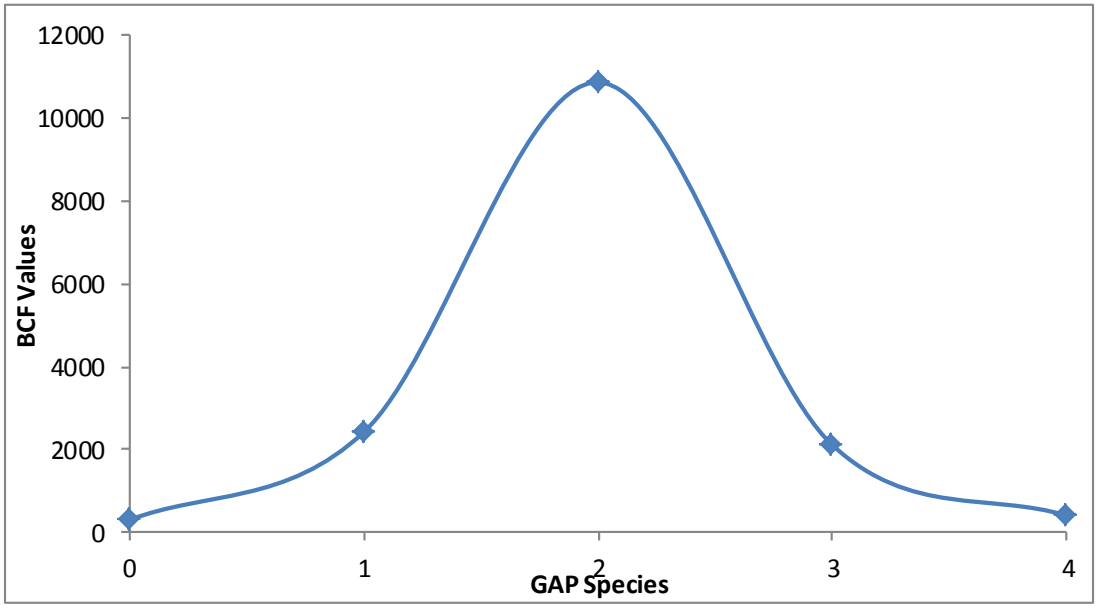

Figure 75. Predicted BCF values of GAP-0-4.

Xylene (CAS # 1330-20-7) Toxicological Data

Toxicological data for xylene is more widely available and is included in Table 31. Based on the ingestion, dermal and inhalation data, proper ventilation and protective equipment is recommended when using large volumes of xylene. Also, xylene is a severe eye irritant. Proper splash goggles should be worn around xylene. In the Integrated Risk Information System (IRIS), the EPA has documented the oral reference doses (RfD) and the inhalation reference concentration (RfC), defining the daily oral exposure (mg/kg/day) and continuous inhalation exposure (mg/m^3), respectively, that are likely to be without appreciable risk of health effects

during a lifetime. RfD and RfC values only address the risk of non-cancer effects. For xylene, IRIS has stated "data are inadequate for an assessment of human carcinogenic potential."[52]

Table 31. Xylenes toxicological data.

	Toxicity Test Result	Species	Time (hrs)	Resource
Ingestion LD_{50} (mg/kg)	4,300	Rat	N/A	Ashland MSDS[53]
Inhalation LC_{50} (ppm)	6,700	Rat	4	Ashland MSDS[53]
Dermal LD_{50} (mg/kg)	>2,000	Rabbit	N/A	Ashland MSDS[53]
Developmental Toxicity	Data Inadequate	N/A	N/A	Acros MSDS[54]
Carcinogencity	Data Inadequate	N/A	N/A	Acros MSDS[54]
Mutagencity	Data Inadequate	N/A	N/A	Acros MSDS[54]
Skin Irritation	Moderate	Rabbit	24	Acros MSDS[54]
Eye Irritation	Severe	Rabbit	24	Acros MSDS[54]
Reference Concentration (RfC) (mg/m^3)	0.1	N/A	24	IRIS[52]
Reference Dose (RfD) (mg/kg/day)	0.2	N/A	24	IRIS[52]
Biodegradability	readily biodegradable	N/A	N/A	EPA[55]
Soil Adsorption Coefficient, K_{oc} (L/kg)	196-311	N/A	N/A	EPA[56]
Bio-concentration Factor (BCF)	2.14-2.20	N/A	N/A	EPA[56]

[52] http://www.epa.gov/iris/subst/0270.htm
[53] http://www.sfm.state.or.us/cr2k_subdb/MSDS/XYLENE_5_AROMATIC_SOLVENT.PDF
[54] http://cnl.colorado.edu/cnl/images/MSDS/fisher%20xylene.pdf
[55] http://www.epa.gov/safewater/pdfs/factsheets/voc/tech/xylenes.pdf.
[56] http://www.epa.gov/superfund/health/conmedia/soil/pdfs/appd_k.pdf.

Octanol Water Partition Coefficient K_{ow}	3.16	N/A	N/A	Ashland MSDS[53]
Fish Toxicity LC_{50} (mg/L)	23.53 – 29.97	Pimephales Promelas	96	Ashland MSDS[53]
Daphnia LC_{50} (mg/L)	>100-<1,000	Daphnia magna	24	Ashland MSDS[53]

The octanol/water partition coefficient of 3.16 suggests that xylene is not very water soluble, but approximately 25 mg/L (LC_{50}) is toxic to fish. The BCF value for xylene is a range from 2.14-2.20 to include the three isomeric forms of xylene, suggesting that it is not bio-accumulative in fish (since BCF is less than 1,000). The data also suggests that it is readily biodegradable and does not adsorb well to soil. Regardless, it is recommended that xylene not be released to the environment without proper waste treatment.

Methanol (CAS # 67-65-1) Toxicological Data

Like xylene, toxicological data for methanol are more readily available and are shown in Table 32. The inhalation value of 83.2 mg/L suggests that proper ventilation and respiration protection equipment are needed when working with large volumes of methanol.

Table 32. Methanol toxicological data.

	Toxicity Test Result	**Species**	**Time (hrs)**	**Resource**
Ingestion LD_{50} (mg/kg)	5,628	Rat	N/A	Thermo Fisher Scientific MSDS[57]
Inhalation LC_{50} (mg/L)	>83.2	Rat	4	Thermo Fisher Scientific MSDS[57]
Dermal LD_{50} (mg/kg)	15,800	Rabbit	N/A	Thermo Fisher Scientific MSDS[57]

[57] http://www.fishersci.com/ecomm/servlet/msdsproxy?productName=A4134&productDescription=METHANOL+NF+4L&catNo=A413-4+%3Cimg+src%3D%22%2Fglyphs%2Fgsa_glyph.gif%22+width%3D%2230%22+height%3D%2213%22+alt%3D%22Available+on+GSA%2FVA+Contract+for+Federal+Government+customers+only.%22+title%3D%22Available+on+GSA%2FVA+Contract+for+Federal+Government+customers.%22++border%3D%220%22%3E%26%23160%3B&vendorId=VN00033897&storeId=10652

Oral LD_{50} (mg/kg)	5,600	Rat	N/A	Airgas MSDS[58]
Intravenous LD_{50} (mg/kg)	2,131	Rat	4	Airgas MSDS[58]
Intraperitoneal LD_{50} (mg/kg)	7,529	Rat	N/A	Airgas MSDS[58]
Carcinogenicity	Negative	N/A	N/A	Methanol Toxicology Review[59]
Mutagenicity	Negative	N/A	N/A	Methanol Toxicology Review[59]
Reference Concentration (RfC) (mg/m^3)	20	N/A	24	IRIS[60]
Reference Dose (RfD) (mg/kg/day)	2.0	N/A	24	IRIS[60]
Octanol Water Partition Coefficient K_{ow}	-0.74	N/A	N/A	Thermo Fisher Scientific MSDS[57]
Biodegradability	readily biodegradable	N/A	N/A	EPA[61]
Soil Adsorption Coefficient, K_{oc} (L/kg)	9	N/A	N/A	EPA[61]
Estimated Bio-concentration Factor (BCF)	0.2	N/A	N/A	EPA[61]
Fish Toxicity LC_{50} (mg/L)	29,400	Pimephales Promelas	96	Airgas MSDS[58]
Daphnia LC_{50} (mg/L)	23,400	Daphnia magna	48	Thermo Fisher Scientific MSDS[57]

The octanol/water partition coefficient is very low because methanol is miscible with water. It readily interacts with aquatic life when mixed with water. The low aquatic toxicity as shown by the >10000 mg/L LC_{50} for fish and Daphnia suggest that use of proper wastewater treatment techniques can be an effective method to eliminate this waste.

[58] http://www.airgas.com/documents/pdf/006043.pdf
[59] http://www.hpa.org.uk/webc/hpawebfile/hpaweb_c/1194947357226
[60] http://www.epa.gov/iris/subst/0305.htm
[61] http://www.epa.gov/chemfact/s_methan.txt.

TEG (CAS# 112-27-6) Toxicological Data

Toxicological data shown in Table 33 suggests that TEG is not very harmful. An inhalation value of >5.2 mg/kg suggests that proper ventilation or respiration protection equipment are needed when exposed to mists or vapors of TEG.

Table 33. TEG toxicological data.

	Toxicity Test Result	Species	Time (hrs)	Resource
Ingestion LD_{50} (mg/kg)	17,000	Rat	N/A	Sigma Aldrich MSDS[62]
Inhalation LC_{50} (mg/kg)	>5.2	Rat	N/A	Raw Material Supplier Form
Dermal LD_{50} (mg/kg)	>22,500	Rabbit	N/A	Sigma Aldrich MSDS[62]
Skin Irritation	Mild Skin Irritation	Human	24	Sigma Aldrich MSDS[62]
Eye Irritation	Mild Eye Irritation	Rabbit	24	Sigma Aldrich MSDS[62]
Fish Toxicity LC_{50} (mg/L)	10-100	Fish	96	Raw Material Supplier Form
Daphnia LC_{50} (mg/L)	48,900	Daphnia magna	48	Dow MSDS[63]
Algae EC_{50} (mg/L)	>100	Pseudokirchneriella subcapitata	168	Dow MSDS[63]
Biodegradability	readily biodegradable	N/A	N/A	Dow MSDS[63]
Estimated Soil Adsorption Coefficient, K_{oc} (L/kg)	10	N/A	N/A	Dow MSDS[63]
Estimated Bio-concentration Factor (BCF)	<100	N/A	N/A	Dow MSDS[63]

[62] http://www.sigmaaldrich.com/MSDS/MSDS/DisplayMSDSPage.do?country=US&language=en&productNumber=90390&brand=FLUKA&PageToGoToURL=http%3A%2F%2Fwww.sigmaaldrich.com%2Fcatalog%2Fproduct%2Ffluka%2F90390%3Flang%3Den.

[63] http://aglayne.com/wp-content/uploads/2010/10/Triethylene-Glycol-MSDS.pdf.

Estimated Octanol Water Partition Coefficient K_{ow}	-1.75	N/A	N/A	Dow MSDS[63]
Carcinogenicity	Negative	Lab Animals	N/A	Dow MSDS[63]
Developmental Toxicity	Negative	Lab Animals	N/A	Dow MSDS[63]
Reproductive Toxicity	Negative	Lab Animals	N/A	Dow MSDS[63]
Genotoxicity	Negative	Lab Animals	N/A	Dow MSDS[63]

The fish toxicity of 10-100 mg/L suggests that use of proper wastewater treatment techniques is needed before it can be released to the environment.

DDBSA (CAS # 27176-87-0) Toxicological Data

The toxicological data for DDBSA are provided in Table 34. The predicted fish toxicity LC_{50} and predicted Algae EC_{50} values are listed as no effects at saturation (NES). According to ECOSAR, no effects are expected if these values are greater than 10 times the solubility in water, which is predicted to be 0.7032 mg/L. Since these values were predicted to be above that limit, they are not included in the table. It should be noted that the other aquatic toxicity values listed in the table are also above the solubility of DDBSA in water, though below the 10X solubility limit required for NES classification. The BCF is significantly below 1000, so very little bioaccumulation in fish is expected. DDBSA is a severe irritant and is known to cause burns to skin, eyes, the digestive tract and respiratory system.

Table 34. DDBSA toxicological data.

	Toxicity Test Result	Species	Time (hrs)	Resource/Model Software
Ingestion LD_{50} (mg/kg)	650	Rat	N/A	MSDS[64]
Eye Irritation/Damage	Severe irritant	N/A	N/A	MSDS[64]
Skin Corrosion/Irritation	Severe irritant	N/A	N/A	MSDS[64]
Predicted Octanol Water Partition Coefficient, log K_{ow}	4.784	N/A	N/A	ECOSAR
Predicted Genotoxicity	Negative	N/A	N/A	TOXTree
Predicted Nongenotoxic Carcinogenicity	Negative	N/A	N/A	TOXTree
Predicted Mutagenicity	Negative	N/A	N/A	TEST
Predicted Fish Toxicity LC_{50} (ppm)	NES	N/A	96	ECOSAR
Predicted Fish Toxicity LC_{50} (ppm), chronic	1.121	N/A	N/A	ECOSAR
Predicted Daphnia LC_{50} (ppm)	6.218	Daphnia	48	ECOSAR
Predicted Daphnia Toxicity LC_{50} (ppm), chronic	1.24	Daphnia	N/A	ECOSAR
Predicted Algae EC_{50} (ppm)	NES	N/A	96	ECOSAR
Predicted Algae Toxicity (ppm), chronic	6.225	N/A	N/A	ECOSAR
Predicted Biodegradability	Not readily biodegradable	N/A	N/A	EPIWIN
Predicted Soil Adsorption Coefficient, K_{oc} (L/kg)	3707	N/A	N/A	EPIWIN
Predicted Bioconcentration Factor (BCF)	71	N/A	N/A	EPIWIN

Physical Properties of the Chemical Materials

The volatility, flammability, chemical reactivity, corrosivity and other physical property data were collected from various databases and included in Table 35 below. Data were collected for

64 http://www.fishersci.com/ecomm/servlet/msdsproxy?productName=AC240885000&productDescription=DODECYLBENZENE+SULFONIC+500GR&catNo=AC240885000&vendorId=VN00032119&storeId=10652.

GAP-1m, TEG, xylenes, methanol, and DDBSA. The information aids in the design and engineering of the CO_2 absorption/desorption system. It also helps in understanding how to handle and work with each chemical compound. The volatility and flash point data suggest that GAP-1m and TEG are not very volatile or flammable, but xylene and methanol are. All of the compounds react with oxidizing agents. GAP-1m and DDBSA are corrosive materials, but TEG, xylenes, and methanol are not.

Table 35. Physical properties of the CO_2 capture solution components.

	GAP-1m[50] Stream 6, Figure 2	**TEG[65] Stream 6, Figure 2**	**Xylenes[54] Stream 7, Figure 2**	**Methanol[57] Stream 4, Figure 2**	**DDBSA[64] Stream 4, Figure 2**
Volatility (Evap. Rate)	<1 (butyl acetate = 1)	<0.001 (butyl acetate = 1)	0.86 (butyl acetate = 1)	4.6 (butyl acetate =1))[66]	Not available
Flash point	>100 °C	177 °C	26.66 °C	53.6 °F 12 °C	> 200°C
Lower explosion limit/upper explosion limit	Not available[67]	0.9 % (V)/ 9.2 % (V)	1.0 % (V)/ 7.0 % (V)	6.0 % (V)/ 31.00 % (V)	Not available
Auto-ignition temperature	No data available	349 °C	527 °C	455 °C	Not available
Chemical Reactivity	May react with oxidizing agents	May react with oxidizing agents	May react with oxidizing agents	May react with oxidizing agents	May react with metals, strong oxidizing agents, strong bases
Corrosivity	Corrosive	Not Corrosive	Not Corrosive	Not Corrosive	Corrosive
State, STP	Liquid	Liquid	Liquid	Liquid	Liquid
Color	Brownish	Colorless	Colorless	Colorless	Brown
Odor	Amine-like	Odorless	Mild, aromatic	Alcohol-like	Sulfur dioxide odor
Melting point	~ -90 °C	-7 °C	-47.00 °C	-98 °C	10°C

[65] http://msdssearch.dow.com/PublishedLiteratureDOWCOM/dh_004d/0901b8038004d042.pdf.
[66] http://www.erowid.org/chemicals/alcohol/alcohol_data_sheet.shtml.
[67] With the flash point being >100C, the material is considered to be non-flammable. The LEL and UEL have not been determined.

Boiling point	>155 °C	288.0 °C	137-140 °C	64.7 °C	315°C
Vapor pressure	<0.13 kPa @ 20 °C	<0.001kPa @ 20 °C	0.93 kPa @ 20 °C[68]	12.8 kPa @ 20 °C	Not available
Vapor density	>1 (Air = 1.0)	5.2 (Air = 1.0)	3.66 (Air = 1.0)	1.11 (Air = 1.0)	Not available
Density	0.93 g/cm^3@ 20 °C	1.124 g/ cm^3 @ 20 °C	0.86 g/cm^3 @20 °C	0.791 g/ cm^3 @ 20 °C	1.2 g/cm^3
Water solubility	Very slightly soluble in cold water	Soluble in water	Negligible (practically insoluble)	Soluble in water	Soluble in water
Solubility Properties	Soluble in chloroform, toluene, hexanes	Soluble in ethanol, benzene, ether	Ether; soluble in many organic liquids, alcohol	Ethanol, ether and many other organic solvents[69]	Not available
Viscosity, dynamic	4.092 cP @ 25 °C	49.0 cP @ 20 °C	0.59 cP @ 20 °C	0.55 cP @ 20 °C	Not available

U.S. EH&S Law Compliance and Regulation Implications

The compliance of the chemicals used in and potential emissions from the proposed continuous CO_2 absorption/desorption system to United States Environmental, Health, and Safety regulations is summarized below. The resulting implications on the proposed technology are also addressed. The applicable U.S. EH&S laws addressed include Toxic Substances Control Act (TSCA), Comprehensive Environmental Response and Liability Act of 1980 (CERCLA), Clean Water Act (CWA), Clean Air Act (CAA), Superfund Amendments and Reauthorization Act (SARA) Title III, the Occupational Safety and Health Act (OSHA), and the Resource Conservation and Recovery Act (RCRA).

Table 36 summarizes the initial list of streams from the process (Figure 73) that were considered in preparing the regulatory review.

[68] http://www.ppci.com.ph/msds2k10/17_xylene.pdf
[69] http://oehha.ca.gov/air/chronic_rels/pdf/67561.pdf

Table 36. Streams considered for regulatory review.

Stream #	Components	Comments
1	Flue gas	This stream would come directly from the plant and is not included in the regulatory review of this specific process.
2	Clean flue gas – see Table 5	This process does not add any components to this stream. It is not discussed further in the regulatory review.
3	CO_2 product	This stream is not a concern for the regulatory review and is not discussed further in this section.
5	GAP-1m/SOx salts	--
6	GAP-1m/TEG make-up stream, includes xylene and methanol	--
7	Xylene	--
12	GAP-1m, DDBSA	--
13	Water, TEG, methanol, xylene	--

The following individual components are the primary focus of this review, based on the summary in Table 36.

- GAP-0
- GAP-1-4
- TEG
- Xylene
- DDBSA
- Methanol
- GAP-1m/SOx salts

A summary of the applicable regulations for each of these components is provided in Table 37. Each regulation in Table 37 is discussed separately in the following sections.

In Table 37, all substances are marked as being regulated by RCRA. This indicates that all of these materials are potential waste products of this process and would, therefore, be regulated under RCRA Subpart C or D. This table does not indicate hazardous or non-hazardous waste classification. For a detailed discussion of those classifications for each waste stream, see the RCRA section of this report.

Table 37. Environmental and hazard compliance data.

	TSCA	CERCLA RQ (lbs)	CWA	CAA HAP	CAA VOC	SARA 302 EHS	SARA 311/312	SARA 313	OSHA Regulated	RCRA
CAS#2469-55-8, GAP-0	Y	N	N	N	N	N	Acute Fire	N	Y	Y
CAS#106214-84-0, GAP-1-4	Y	N	N	N	N	N	Acute	N	Y	Y
CAS#1330-20-7, Xylene	Y	100	Y	Y	Y	N	Acute Chronic Fire	Y	Y	Y
CAS#67-65-1, Methanol	Y	5000	N	Y	Y	N	Acute Chronic Fire	Y	Y	Y
CAS#112-27-6, TEG	Y	N	N	N	N	N	Acute	N	Y	Y
CAS#27176-87-0, DDBSA	Y	1000	Y	N	N	N	Acute	N	Y	Y
GAP-1m/SOx salts	N	N	N	N	N	N	N	N	Y	Y

TSCA

GAP-0, GAP-1-4, xylene, methanol, TEG, and DDBSA are all on EPA's TSCA Inventory allowing companies to manufacture and use the chemical commercially. The CAS numbers for each are included in Table 37.

CERCLA

CERCLA hazardous substances are considered severely harmful to human health and the environment.[70] RQ is the minimum release quantity that must be reported.[71] CAS#2469-55-8 (GAP-0), CAS#106214-84-0 (GAP-1-4), and triethylene glycol are not listed as CERCLA hazardous substances, but xylene, methanol, and DDBSA are. The minimal reportable quantities are 100 lbs/day, 5000 lbs/day, and 1000 lbs/day for xylene, methanol, and DDBSA, respectively.

Xylene leaves this process through streams 7 and 13. The total amount of xylene leaving the process in both of these streams is estimated to be 45 lbs/day, which is expected to be the maximum potential quantity that could be released. This is below the reportable quantity so is unlikely to be a concern for this process.

Methanol leaves this process through stream 13. The estimated amount of methanol leaving this process is also 45 lbs/day, which is expected to be the maximum potential quantity that could be released. This is below the reportable quantity so is unlikely to be a concern for this process.

Though DDBSA leaves the process through streams 12, there is also the potential for spills of the pure material stored on-site for use in the process. This would need to be stored on-site in quantities greater than the reportable quantity. This emphasizes the importance of safe handling and storage of this material. In future, materials that could be substituted for DDBSA for treatment of stream 4 will also be investigated.

Clean Water Act

Xylene and DDBSA are designated as hazardous substances to the water supply in accordance with Section 311(b)(2)(A) of 40 CFR 116, the Clean Water Act (CWA).[72] As with CERCLA, the minimum reportable quantities for xylene and DDBSA are 100 lbs/day and 1000 lbs/day (40 CFR § 117.3), respectively.

Clean Air Act

Xylene and methanol are also both regulated Hazardous Air Pollutants (HAPs) and Volatile Organic Compounds (VOCs) under the Clean Air Act (CAA).[73] The potential release rate for a 550 MW power plant is lower than required for reporting.

[70] http://www.epa.gov/oem/docs/er/302table01.pdf
[71] http://www.epa.gov/superfund/policy/release/rq/index.htm#levels
[72] EPA 2005b 40 CFR 116.4.
[73] EPA 2004b 42 USC 7412.

SARA

None of these chemicals pose an immediate hazard to a community upon release as described by EPA's SARA 302 list. For Safety Data Sheet reporting (SARA 311/312), GAP-0, GAP-1-4, xylene, methanol, TEG, and DDBSA are considered as acute, immediate health hazards. Xylene and methanol are considered to be chronic, delayed health hazards, and GAP-0, xylene, and methanol are considered as fire hazards. SARA 313 rules require reporting chemical releases of xylene and methanol to public and government officials.[74]

OSHA

All of the chemicals are regulated by OSHA, requiring proper safety data sheet, handling, shipping, and storage equipment.

RCRA

The relevant sections of RCRA are Subparts C and D of 40 CFR Part 260.

Subpart D deals with municipal solid waste and non-hazardous waste, including that generated by industry, such as power plants. Waste not categorized under Subpart C as a hazardous waste is disposed of under Subpart D. Specific requirements for disposal for Subpart D would depend on the power plant location and a detailed discussion of local requirements is outside the scope of this document. Specific disposal methods would need to be reviewed on a site-specific basis.

For the purpose of this review, only federal RCRA requirements are considered. These are the minimum requirements for RCRA. Some states administer their own programs, which are at least as stringent as the EPA's. This EH&S assessment does not include a detailed review of all the state programs. These requirements would vary based on power plant location and an extensive review of all state RCRA programs is considered to be outside the scope of this document.

To determine if Subpart C applies to a given stream, the following questions must be answered (in order):

---

74 http://nepis.epa.gov/Exe/ZyNET.exe/100038G4.txt?ZyActionD=ZyDocument&Client=EPA&Index=1991%20Thru%201994&Docs=&Query=&Time=&EndTime=&SearchMethod=1&TocRestrict=n&Toc=&TocEntry=&QField=&QFieldYear=&QFieldMonth=&QFieldDay=&UseQField=&IntQFieldOp=0&ExtQFieldOp=0&XmlQuery=&File=D%3A%5CZYFILES%5CINDEX%20DATA%5C91THRU94%5CTXT%5C00000007%5C100038G4.txt&User=ANONYMOUS&Password=anonymous&SortMethod=h%7C-&MaximumDocuments=1&FuzzyDegree=0&ImageQuality=r75g8/r75g8/x150y150g16/i425&Display=p%7Cf&DefSeekPage=x&SearchBack=ZyActionL&Back=ZyActionS&BackDesc=Results%20page&MaximumPages=1&ZyEntry=5

1. Is the material in question a solid waste?
2. Is the material excluded from the definition of solid waste or hazardous waste?
3. Is the waste a listed or characteristic hazardous waste?
4. Is the waste delisted?

If a stream is excluded from RCRA's definition of a solid or hazardous waste by answering one of these questions, it is not necessary to proceed through the remaining questions.

Each of these questions is discussed in detail for the following streams (Figure 73):

- Absorber: Streams 8, 9, and 10
- Desorber: Streams 5, 7, 12, 13, 14, 15, and 16

The overall conclusions for each stream are summarized at the end of this section in Table 39.

Absorber

Streams 8, 9 and 10

The flue gas in stream 8 goes through the TEG wash tower to remove GAP-1m, xylenes, and methanol. A stream containing GAP-1m, xylene, methanol, and TEG then undergoes a distillation step to separate into TEG (stream 9), which is recycled back to the wash tower, and GAP-1m, xylene, and methanol (stream 10), which is recycled back to the absorber.

Question 1: Is the material in question a solid waste?

Since these streams are involved in a distillation step before returning to the process and distillation is included in RCRA's definition of reclamation, streams 8, 9, and 10 would be considered solid waste.

Question 2: Is the material excluded from the definition of solid waste or hazardous waste?

An exclusion is provided by RCRA for Closed loop recycling (40 CFR § 261.4(a)(8)). This excludes materials from the definition of solid waste if they are being reclaimed and recycled to the process through an enclosed system of pipes and tanks. This exclusion would apply to streams 8, 9, and 10 since the material will be recycled back to the process. Therefore, all three streams are excluded from the RCRA definition of solid waste.

Desorber

Streams 5, 7, 15, and 16

To purge the GAP-1m/SOx salts from the system, stream 15 is removed from the desorber. It undergoes a vacuum distillation. This produces the GAP-1m/SOx salt stream (Stream 5), the xylene stream (stream 7), and the GAP-1m/TEG stream (stream 16). Stream 16 is recycled back to the desorber.

Question 1: Is the material in question a solid waste?

Streams 5, 7, 15, and 16 are considered to be solid wastes since a reclamation step is required before the GAP-1m/TEG can be recycled back to the desorber.

Question 2: Is the material excluded from the definition of solid or hazardous waste?

The GAP-1m/TEG in streams 15 and 16 is excluded from the definition of solid waste by the closed loop recycling exclusion, since the reclamation step will be fully enclosed and the GAP-1m/TEG stream (stream 16) will be returned directly to the desorber after reclamation.

Streams 5 and 7 will not return to the process and will require disposal and are, therefore, considered to be solid wastes.

Question 3: Is the material a listed or characteristic hazardous waste?

Stream 5 (GAP-1m/SOx salts) is not a listed waste. This stream also does not exhibit the characteristics listed in Table 38 so is not considered a characteristic waste. This waste will be disposed of under RCRA Subpart D as industrial, non-hazardous waste in accordance with local regulations at the plant in question.

Table 38. Criteria to be considered characteristic waste under RCRA Subpart C.

Characteristic	Criteria
Ignitability	Liquid wastes with flashpoints below 60 °C
Corrosivity	Aqueous with pH ≤ 2 or ≥ 12.5
Reactivity	Explode or cause violent reactions or react to release toxic gas or fumes when exposed to water or under normal handling conditions
Toxicity	Presence of chemical above TCLP regulatory levels

Stream 7 contains primarily xylene. This is on the U list, but only if the xylene is pure, unspent solvent. It is also on the F list, but only if the solvent is being used in pure form or in a mixture with specifically named solvents. Xylene is present in low levels in the GAP-1m material and is not used in the process as a pure solvent or as a mixture with any of the other solvents listed under the F003 designation. In this process, xylene is not a listed waste. Xylene does exhibit the ignitability characteristic with a flashpoint below 60°C. Stream 7 is, therefore, a characteristic hazardous waste.

Question 4: Is the waste delisted?

Stream 7 is a characteristic hazardous waste, and not a listed hazardous waste. Therefore, question 4 does not apply. Stream 7 would need to be disposed of under Subpart C of RCRA as hazardous waste. The Subpart C requirements are discussed in more detail later in this section as they apply to this process.

<u>Stream 12</u>

Stream 12 is a GAP-1m/DDBSA stream produced from the treatment of stream 4 condensed out of the exit gas from the desorber.

Question 1: Is the material in question a solid waste?

Stream 12 is not returned to the process and would require disposal. It is, therefore, considered to be a solid waste.

Question 2: Is the material excluded from the definition of solid or hazardous waste?

Stream 12 is not excluded and is, therefore, considered to be solid waste.

Question 3: Is the material a listed or characteristic hazardous waste?

GAP-1m and DDBSA are not on the F, K, P, or U lists. They are not considered listed hazardous wastes.

The GAP-1m/DDBSA stream would not exhibit any of the criteria in Table 38. It is not a characteristic hazardous waste. This waste will be disposed of under RCRA Subpart D as industrial, non-hazardous waste in accordance with local regulations at the plant in question.

Stream 13

Stream 13 contains primarily water and TEG, with some methanol, and xylene after treatment of stream 4.

Question 1: Is the material in question a solid waste?

Stream 13 is not returned to the process and would require disposal. It is, therefore, considered to be a solid waste.

Question 2: Is the material excluded from the definition of solid or hazardous waste?

Stream 13 is not excluded and is, therefore, considered to be solid waste.

Question 3: Is the material a listed or characteristic hazardous waste?

Methanol and xylene are on the U list, but this process does not use pure, unspent solvent so the designation would not apply in this case. Xylene is on the F list, but this process does not use the pure solvent and it is not mixed with the other solvents in the F003 definition so the designation would not apply. TEG is not on the F, K, U or P lists. Stream 13 is not considered to be a listed waste.

To be considered a characteristic waste, at least one of the criteria in Table 38 would need to apply. The flashpoints for pure xylene and pure methanol are below 60 °C. However, these chemicals are only present in trace amounts in Stream 13. Stream 13 would not cause an ignitability concern. The other criteria are not applicable to this stream either. Therefore, stream 13 would be considered industrial, non-hazardous solid waste under RCRA and would be disposed of under Subpart D in accordance with local regulations at the plant in question, which could include sending it to a wastewater treatment facility.

Stream 14

Stream 14 contains GAP-1m, TEG, xylenes, and some water that is condensed out of the gas exiting the desorber.

Question 1: Is the material in question a solid waste?

Since stream 14 is recycled directly back to the desorber and does not require reclamation, it is not considered solid waste.

An overall summary of the RCRA classifications for each of the streams discussed in this section is provided in Table 39.

Table 39. Summary of RCRA classifications.

Stream Number	Materials	Classification and other relevant RCRA Information
Absorber		
8	Flue gas, GAP-1m, xylene and methanol	Not solid waste under Closed loop recycling exclusion
9	TEG	Not solid waste under Closed loop recycling exclusion
10	GAP-1m, xylene, and methanol	Not solid waste under Closed loop recycling exclusion
11	TEG	Industrial, non-hazardous solid waste to be disposed of under Subpart D
Desorber		
5	GAP-1m/SOx salts	Industrial, non-hazardous solid waste to be disposed of under Subpart D
7	Xylene	Characteristic hazardous waste based on ignitability to be disposed of under Subpart C
12	GAP-1m, DDBSA	Industrial, non-hazardous solid waste to be disposed of under Subpart D
13	Primarily water and TEG, with	Industrial, non-hazardous

	some xylene, and methanol	solid waste to be disposed of under Subpart D
14	GAP-1m, TEG, xylene, and water	Not considered solid waste since directly recycled to desorber without reclamation
15	GAP-1m, TEG, xylene, GAP-1m/SOx salt	Not solid waste under Closed loop recycling exclusion
16	GAP-1m, TEG	Not solid waste under Closed loop recycling exclusion

RCRA Subpart C requirements

Generator requirements

Specific requirements for hazardous waste handling depend on the generator classification based on the quantity of hazardous waste generated per month. The only stream from this process for which the Subpart C requirements are relevant is stream 7.

The quantity of xylene generated based on the mass balance for stream 7 is estimated to be 1380 lbs per month (assuming a 31 day month), or 626 kg per month. This would classify this process as a Small Quantity Generator (SQG) based on the RCRA definition. Depending on the classification of the overall power plant, large quantity generator (LQG) requirements may be applicable since it would add to existing hazardous waste streams at the power plant. In general, both SQGs and LQGs need to do the following:

- Identify and count waste
- Obtain an EPA ID number
- Comply with accumulation and storage requirements
- Prepare the waste for transportation
- Track the shipment and receipt of such waste
- Meet recordkeeping and reporting requirements

Since the exact requirements for hazardous waste disposal would vary based on plant classification and plant location, they are not discussed in detail in this assessment, but would need to be evaluated on a site-specific basis.

TSDF

RCRA excludes generators from the permit requirements for transport, storage, and disposal facilities (TSDF) as long as the generators accumulate waste on-site in accordance with the generator regulations. It is assumed that this process would comply with the necessary generator requirements and would, therefore, not be subject to TSDF regulations.

Engineering Analysis and Controls

The entire system requires some plant-wide engineering controls. Many of these are common in the chemical industry but might be new for a power plant facility. For example:

1) To protect groundwater, a double containment drain system is necessary. These keep rainwater separated from any chemical drainage system, not allowing them to mix. The containment system should be built with chemical resistant, high strength concrete.

2) A volatile vapor detection sampling and monitoring system is necessary to identify when leaks occur. This is especially important for VOC's like xylene and methanol.

3) A pressure/relief, vapor condensation/recovery system should be considered for all vessels. This prevents undesired backflow from one vessel to another, and it is required to minimize leaks and meet VOC release standards.

4) The equipment and piping arrangement chosen for the system should be designed to minimize leaks. For example, a shell & tube heat exchanger is much better than a plate & frame heat exchanger for minimizing leaks. The large number of gaskets in the plate & frame are all potential VOC emission points.

5) The gas streams, #2 and #3 in Figure 73, require a final gas polishing process like an activated carbon absorption bed. This removes any remaining VOCs, lowering potential emissions.

6) The thermal oxidizer equipment requires its own safety failure analysis. Equipment like detonation arrestors, back-flow valves, etc. is needed. Vendors of such equipment are well versed in the requirements and design of a specific unit is outside to scope of this task. [75]

Handling and Storage

This section describes the precautions necessary for safe handling and storage of the chemicals used in the CO_2 absorption/desorption system. The applicable rules and standards of the

[75] http://www.oxidizerservice.com/ccs/; http://rto.american-environmental.us/Lower-Explosive-Limit.html.

Occupational Safety and Health Act (OSHA) are summarized, including safe storage, incompatibilities with other materials, waste treatment and offsite disposal options, accidental release measures, and protective equipment suggestions. The following section provides handling and storage recommendations for GAP-1m, TEG, xylene, methanol, sulfur dioxide, and DDBSA. As discussed above, the toxicity of GAP-1m/SO_x is assumed to be less than or equal to its components, GAP-1m and SO_x. Details of handling and storage of GAP-1m/SOx are not available but are assumed to be less rigorous than those needed for its components.

a) GAP-1m (CAS# 106214-84-0 and 2469-55-8)

GAP-1m is classified as a hazardous chemical by the OSHA Standard. It is regulated under both DOT and IATA as a corrosive liquid. Its HMIS Classification is a 3 for health hazard, 1 for flammability, and 0 for physical hazards.[50]

1) Storage and Handling Recommendations

GAP-1m should be stored in a phenolic lined drum or pail and away from acids and oxidizers. When it is burned, it decomposes into carbon monoxide, carbon dioxide, nitrogen oxides, and silicone dioxide. The material should be used in an area with adequate ventilation.[50]

2) Accidental Release Measures

When a spill occurs, one should evacuate the area and alert trained spill officials. Those trained to work with spills should wear a respirator when ventilation is not adequate and wear proper personal protect equipment. The spill team should keep those untrained and unprotected from entering the spill area. Also they should prevent others from touching or walking through the contaminated area. For environmental protection, do not allow the material to be dispersed or come in contact with drains, sewers, soil or any water source. Use an absorbent barrier to prevent contamination into the environment. When or if the material comes in contact with the environment, notify the local authorities immediately.[50]

3) Health Effects

It is corrosive to the skin, eyes, digestive tract, and respiratory system and may cause burns. Use the material in a well-ventilated area.[50]

4) Exposure Limits and Effects

Overexposure to GAP-1m can cause respiratory irritation, coughing, stomach pains, skin redness, and watering or redness of the eyes.[50] The PEL has not been established for this chemical. Since GAP-1m has a high boiling point, the amount that vaporizes at ambient conditions is very low.

5) Respiratory Protection Recommendation

If the vapor concentration of GAP-1m exceeds 2000 ppm, a full-faced respirator with an olive cartridge is recommended. A cartridge designed for amines is recommended.[76]

6) Hand and Eye Protection Recommendation

When using GAP-1m, chemical resistant gloves should be worn. Butyl rubber and neoprene are recommended. These gloves have an estimated breakthrough time of more than 8 hours. The recommended eye protection is splash goggles or a face shield.[50]

7) Skin and Body Protection Recommendation

The risk of exposure for the production area needs to be evaluated to determine proper body protection. For low risk exposure of only hands, butyl or neoprene gloves are recommended. For high risk exposure, a rubberized acid suit is recommended.[50,76]

b) Triethylene Glycol (CAS# 112-27-6)

Triethylene Glycol (TEG) is not known as an OSHA hazard. Its HMIS Classification is a 0 for health hazard, 1 for flammability and 0 for physical hazards. It is not regulated by the Department of Transportation (DOT) or International Air Transport Association (IATA).[62]

1) Storage and Handling Recommendations

It is recommended that the material be kept in a tightly closed container in a dry, well-ventilated area. Triethylene glycol is hygroscopic, requiring a storage container that minimizes exposure to moisture. Iron can contaminate the material. To avoid contamination from iron, the use of stainless steel, aluminum, phenolic, or epoxy resin lined vessels is recommended.[77] Avoid storing this chemical near strong oxidizing agents, strong acids, or bases because triethylene glycol reacts with these materials. An

[76] Carlton Dill, SiVance, LLC, personal communication, December 9, 2013.

[77] http://www.huntsman.com/portal/page/portal/performance_products/Media%20Library/a_MC348531CFA3EA9A2E040EBCD2B6B7B06/Products_MC348531D0B9FA9A2E040EBCD2B6B7B06/Glycols_MC348531D11A3A9A2E040EBCD2B6B7B06/files/teg_triethylene_glycol_.pdf

exothermic reaction can take place when TEG mixes with strong acids and oxidizing agents. These reactions often produce a toxic, flammable gas and could lead to an explosion. Special examples of common chemicals that should be avoided are acetic acid and anhydrides.[78] In a fire, triethylene glycol can decompose to carbon monoxide and carbon dioxide.[62]

2) Accidental Release Measures

In the case of a spill or accidental release, evacuate personnel to a safe area. Ensure adequate ventilation and inform trained clean-up professionals of the spill. Only allow these trained officials to enter the spill area wearing the proper protective equipment (including a respirator, if necessary).[62]

Barriers should be placed around the spill to prevent TEG from entering drains or other water sources. Inert absorbent material should be used to cleanup and contain the spill. Contaminated material should be disposed as hazardous waste in closed containers.[62]

3) Health Effects

If triethylene glycol is inhaled, it may cause respiratory tract irritation. It may also cause skin and eye irritation.[62]

4) Exposure Limits and Effects

The material is not classified as hazardous under OSHA. No exposure limit data was available.

5) Respiratory Protection Recommendation

At room temperature, exposure to vapor is expected to be small due to low volatility, but at elevated temperatures, vapors may cause irritation of the upper respiratory tract (nose and throat). In such cases, respiratory protection should be worn when exposure to TEG vapors and mists are likely. In misty atmospheres, use an approved air purifying respirators with an organic vapor cartridge and a particulate pre-filter.[79]

6) Hand and Eye Protection Recommendation

Triethylene glycol should be handled with gloves. They should be inspected prior to use. If one is going to be in full contact with TEG, nitrile rubber gloves with a minimum layer

[78] http://www.pttgcgroup.com/src/download/products/eo_based/TEG_MSDS.pdf
[79] http://aglayne.com/wp-content/uploads/2010/10/Triethylene-Glycol-MSDS.pdf

thickness of 0.11 mm are recommended. The nitrile gloves have a break through time of >480 minutes. For splash protection when working with TEG, a nitrile rubber apron should also be worn. For eye protection, safety glasses with side shields are recommended.[62]

7) Skin and Body Protection Recommendation

Prolonged skin contact is unlikely to result in absorption of harmful amounts. Massive contact with damaged skin or of material sufficiently hot to burn skin may result in absorption of potentially lethal amounts. Still, avoid contact with skin and clothing. Wash thoroughly after handling. Use protective clothing chemically resistant to this material, including such items as gloves, face-shields, boots, apron, or a full-body suit, depending upon the task. When handling hot material, protect skin from thermal burns as well as from skin absorption.[62]

c) Xylene (CAS# 1330-20-7)

Xylene is classified as a hazardous chemical by the OSHA Standard. It is regulated under both DOT and IATA as a flammable liquid (hazard class 3) with the proper shipping name xylenes. Its HMIS Classification is a 2 for health hazard, 3 for flammability, and 0 for physical hazards.[53]

1) Storage and Handling Recommendations

Xylene is a flammable liquid (flash point is 80 ^{o}F/26.7 ^{o}C). Handle material away from heat, flames and sparks. When handling xylene, vessels need to be grounded before transfer or use of material. The material should be used in a cool, dry, and well, ventilated area. Xylene should not be handled near alkalis, strong acids, and strong oxidizing agents.[53]

2) Accidental Release Measures

When a spill occurs, spill team authorities should be alerted. All personnel should be evacuated to a safe area away from the spill. Unauthorized individuals should not be allowed to enter the area without proper protective equipment. Xylene is a flammable material; therefore, all sources of ignition (fire, electrical sparks, etc.) should be eliminated. Prevent vapors from building up by providing proper ventilation.[53]

Xylene spills should be contained by non-combustible absorbent materials. Some examples of these materials are sand, vermiculite, and diatomaceous earth. The contaminated absorbent material should be disposed in accordance with national and

local regulations pertaining to waste disposal. Xylene should be kept from entering drains and not flushed into the sewer system during the clean-up process. If the material is not able to be contained and gets into the environment, local authorities must be notified immediately.[53]

3) Health Effects

Xylene may affect the central nervous system leading to dizziness, headache, or nausea. It may cause mild eye irritation with symptoms include stinging, tearing, or redness. It can also cause skin and respiratory tract irritation. Prolonged skin exposure may lead to burns, redness and cracking of the skin. Swallowing the material may lead to lung inflammation or other lung injury. Breathing small amounts (below the permissible exposure limits) of the material will not likely cause any harmful effects. Some symptoms from exposure to xylene include: nausea, vomiting, diarrhea, redness of the skin, inhalation irritation, chest discomfort, shortness and slowness of breath, lack of coordination and memory, irregular heartbeat, narcosis, coma, central nervous system excitation followed by depression. Exposure to xylene may aggravate pre-existing medical issues relating to the lung, kidney heart, skin, central nervous system, male reproductive system, and auditory system.[53]

4) Exposure Limits and Effects

Overexposure to xylene by laboratory animals led to the following effects: testis damage, kidney and liver damage, effects on hearing, cardiac sensitization and harm to animal fetuses. Also overexposure can lead to effects on the central nervous system. For xylenes, the PEL is 100 ppm or 435 mg/m^3 during 8 hrs. The Short Term Exposure Limit (STEL) is 150 ppm or 655 mg/m^3 over 15 minutes. Another test, Immediately Dangerous to Life and Health Concentration (IDLH), resulted in 900 ppm.[53]

5) Respiratory Protection Recommendation

Typically, the PEL and IDLH are used to determine the threshold limit for implementation of respirators. From 100 to 900 ppm, an approved air-purifying respirator with an organic vapor cartridge is required. A full-faced respirator with organic cartridges is required when emptying a vessel of xylene, reducing the risk of exposure to vapors and in case of a flash fire. [80]

6) Hand and Eye Protection Recommendation

[80] http://www.ccohs.ca/oshanswers/chemicals/chem_profiles/xylene.html#_1_12

When working with xylene, one should wear butyl or neoprene gloves which should be inspected prior to use. Wash hands after glove removal. Either a face shield or splash goggles is recommended when working with xylene.[53]

7) Skin and Body Protection Recommendation

Since xylene is a flammable material, one should wear flame resistant protective clothing, especially when handling large quantities. The proper protective attire should be determined by the amount of the chemical being handled and the environment of the plant.[53]

d) Methanol (CAS# 67-56-1)

Methanol is classified as a hazardous chemical by the OSHA Standard. It is regulated under both DOT and IATA as a flammable liquid (hazard class 3) with the proper shipping name methanol. Its HMIS Classification is a 2 for health hazard, 3 for flammability, and 0 for physical hazards.[57]

1) Storage and Handling Recommendations

Due to the flammability of methanol (flash point is 53.6 °F/12 °C), it should be handled away from hot surfaces, ignition sources, and open flames. When handling methanol, containers storing the material should be grounded or electrically bound before transfer or use of material. The material should be used in a cool, dry, and well ventilated area.[57]

Methanol should not be handled near strong acids, acid anhydrides, acid chlorides, strong bases metals, peroxides or strong oxidizing agents.[57]

2) Accidental Release Measures

When a spill occurs, spill team authorities should be alerted. All personnel should be evacuated to a safe area away from the spill. Unauthorized individuals should not be allowed to enter the area without proper protective equipment. Methanol is a flammable material; therefore, all sources of ignition (fire, electrical sparks, etc.) should be eliminated. Prevent vapors from building up by providing proper ventilation.[57] Methanol spills should be contained by inert absorbent materials. The contaminated absorbent material should be collected and stored in suitable containers for disposal. These containers shall be disposed of in accordance with national and local regulations pertaining to flammable waste disposal. Methanol should be kept from entering drains and not flushed into the sewer system during the clean-up process. If the material is not

able to be contained and gets into the environment, local authorities must be notified immediately.[57]

3) Health Effects

The organs targeted by methanol are the central nervous system, eyes, skin, respiratory system, optic nerve, liver, kidney, spleen, blood, and the gastrointestinal tract (GI). The acute effects are irritation to eyes, skin, and respiratory tract. Research has shown, prolonged exposure (inhalation, dermal, and ingestion) can lead to serious irreversible effects. Methanol has been shown to cause liver and kidney problems along with reproductive toxicity effects.[57]

4) Exposure Limits and Effects

The PEL is 200 ppm or 260 mg/m^3 during 8 hrs. The Short Term Exposure Limit (STEL) is 250 ppm or 325 mg/m^3 over 15 minutes. Another test, Immediately Dangerous to Life and Health Concentration (IDLH), resulted in 6000 ppm.[57]

5) Respiratory Protection Recommendation

A full-faced respirator with organic cartridges is recommended.

6) Hand and Eye Protection Recommendation

Methanol should be handled with butyl rubber or neoprene gloves. Wash hands after glove removal. Tightly fitting safety goggles or splash goggles are recommended.[57]

7) Skin and Body Protection Recommendation

Since methanol is a flammable material, one should wear flame retardant or resistant antistatic protective clothing and boots, especially when handling large quantities. The proper protective attire should be determined by the amount of the chemical being handled.[57] The Methanol Institute recommends the following:

> "For routine unloading of methanol where splashing or skin absorption is not anticipated, natural fiber clothing (cotton) is adequate. Avoid wearing synthetic fiber clothing when there is a risk of fire from handling methanol. A chemical resistant apron, butyl or nitrile rubber gloves, and rubber boots, and a full face-shield worn over goggles for additional protection, (but not as a substitute for goggles), may be needed where there is a risk of splashing, such as in coupling and uncoupling hoses or lines. Chemical-resistant clothing/materials should be worn if repeated or prolonged skin contact with methanol is expected.

Respiratory protection should be selected based on hazards present and the likelihood of potential exposure. Air purifying respirators with organic vapor (OVA) cartridges are not appropriate protection against methanol vapors due to the very short service life of the OVA cartridge before it becomes saturated, and there are no means of knowing when the vapors break through and the cartridge is no longer offering protection. The use of a supplied air respirator with a full face piece operated in a pressure-demand or other positive-pressure mode is the recommended respiratory protection. Personal protection equipment for the responders should, at a minimum, include chemical splash goggles and face shield, butyl or nitrile gloves, rubber boots, chemical resistance coveralls, and provision for supplied fresh breathing air, such as full face, positive pressure SCBA. Fire resistant clothing is only necessary when fighting a fire. For more information on methanol personal protective equipment consult Chapter 4.2.2 of the Methanol Institute's Methanol Safe Handling Manual."[81]

e) DDBSA (CAS# 27176-87-0)

DDBSA is classified as hazardous by the OSHA Standard based on corrosivity.[82] It is regulated under both DOT and IATA as a corrosive material. Its HMIS Classification is a 3 for health hazard, 0 for flammability, and 0 for physical hazards.

1) Storage and Handling Recommendations

This material should be stored in a cool, dry place and the container kept closed when not in use. It should be kept away from oxidizing materials, metals, and alkaline substances. It should be used in a well-ventilated area.[82]

2) Accidental Release Measures

In the case of a spill, personnel should be evacuated to a safe area and trained spill control officials should be notified. The area should be ventilated and the material absorbed with inert materials (e.g. vermiculite, sand or earth). For environmental protection, precautions should be taken to avoid any runoff into drains, storm sewers, or ditches.[82]

3) Health Effects

[81] http://www.methanol.org/health-and-safety/frequently-asked-questions.aspx
[82] http://datasheets.scbt.com/sc-226619.pdf

DDBSA causes severe burns to skin and eyes and may cause irreversible eye injury. It is harmful to the digestive tract and respiratory system. The material should be used in a well-ventilated area.[82]

4) Exposure Limits and Effects

No OSHA PEL has been established for this chemical.[82]

5) Respiratory Protection Recommendation

No specific recommendations for exposure limits for respirator usage were available. When risk assessment indicates it is necessary, respirators should meet OSHA 29 CFR 1910.134 and ANSI Z88.2 requirements.[82]

6) Hand and Eye Protection Recommendations

Appropriate gloves and safety glasses/splash goggles should be worn during use.[82]

7) Skin and Body Protection Recommendation

At a minimum, gloves should be worn. The need for additional protective clothing should be evaluated based on the concentration and amount of chemical used.[82]

Task 7: Perform Bench-Scale Testing

Using the bench-scale system designed and built in Task 3, testing was performed with the aminosilicone-based CO_2-capture solvent. For these tests exhaust from a gasoline home generator was used as a proxy for the flue gas from a pulverized coal power plant. This bench-scale system was used to investigate the effect of the primary process variables on system performance. Updated correlations between the primary system variables and system performance were generated at this scale and a comparison between the performance of the bench-scale system and the lab-scale system (as determined in the previous project, DE-NT0005310) were made to determine scale-up effects. Tests necessary to determine physical properties of the aminosilicone CO_2-capture solvent needed for eventual design at the next scale were performed during this task. Various materials of construction were tested to determine the best materials to use at larger scales.

Task 7.1: Obtain Engineering Data

Baseline System Performance

Experiments designed to test the baseline system performance of both the absorption column and the desorber were completed. In the set of experiments to test the absorption column performance, the desorber conditions were set so that the concentration of CO_2 in the liquid would be approximately constant for all runs in the design of experiments. The parameters set as constants are shown in Table 40 and the set of completed experiments is shown in Table 41.

Table 40. Constant parameters for baseline system performance experiments.

Parameter	Units	Value
Desorber temperature	°C	160
Desorber agitator speed	RPM	300
Desorber recirculation loop pump speed	% of max	50
Desorber level	in H_2O	7.5
Desorber pressure	psig	0
Inlet absorber temperature (gas and liquid)	°C	40
Absorber sump level	in H_2O	5.0
Total gas flow rate	SLPM	185

Table 41. Initial results for baseline system performance tests.

Liquid flow rate (LPM)	Inlet gas CO_2 conc (vol%)	Actual % CO_2 in	Actual desorber P (psig)	% CO_2 captured (from gas)	% GAP-1m reacted in column (gas mass balance)	% GAP-1m reacted in column (liquid mass balance)	mol % CO_2 in liquid exiting absorber	mol % CO_2 in liquid entering absorber	mol % CO_2 in liquid exiting desorber
0.5	9%	7.2%	0.7	82.6%	53.8%	55.7%	24.7%	2.9%	2.9%
0.5	16%	16.0%	0.8	49.0%	70.5%	66.8%	28.9%	3.2%	2.7%
1	5%	4.7%	2.2	99.6%	21.2%	18.1%	10.3%	3.3%	2.8%
1	9%	8.8%	2.1	99.4%	39.3%	36.5%	13.8%	3.6%	2.5%
1	16%	16.3%	1.3	84.8%	57.7%	61.8%	26.4%	2.6%	3.0%
1.5	5%	1.6%	1.9	100.0%	13.9%	11.1%	5.8%	2.2%	2.5%
1.5	9%	9.0%	1.0	100.0%	27.1%	22.3%	11.6%	2.9%	3.0%
1.5	16%	16.2%	4.4	99.3%	48.3%	49.5%	22.3%	3.0%	3.0%

The inlet gas CO_2 concentration listed in Table 41 is achieved by mixing either N_2 or CO_2 with the exhaust gas from the generator. The concentration of CO_2 in the generator exhaust is measured and the flow rate of either N_2 or CO_2 needed is calculated based on the total gas flow rate and the CO_2 in the exhaust stream.

During each test, the CO_2 concentration in the gas phase is monitored at the inlet of the column, and liquid samples are taken periodically from the absorber sump, the desorber, and the lean storage tank and analyzed using FTIR. The temperatures in the absorber are also monitored. When the CO_2 concentrations in the liquid and the absorber temperatures have stabilized, the system has reached steady state, and the gas-phase CO_2 concentrations at the exit of the column and the exit of the desorber are measured. From these data, the amount of CO_2 captured in the absorption column can be calculated and the amount of CO_2 in the liquid-phase can be calculated based on both the FTIR data and the CO_2 analyzer data.

In the baseline experiments, by varying the liquid and gas flow rates, CO_2 capture efficiencies ranging from 49% to 100% were demonstrated and GAP-1m reacted in the absorption column ranged from 14% to 71%. The CO_2-capture efficiencies and the amount of GAP-1m that reacted in the absorption column to obtain those capture efficiencies can be correlated to the molar excess of GAP-1m fed to the column, compared to the amount of CO_2 fed to the column, as shown in Figures 76 and 77. In each of these figures, a negative % excess GAP-1m indicates an excess of CO_2 in the column. Figure 76 demonstrates that in general, as the excess of GAP-1m fed to the column increases, the amount of GAP-1m reacted in the column decreases. Figure 77 demonstrates that as the excess of GAP-1m fed to the column increases, the capture efficiency also increases, and that at a certain % excess GAP-1m, all of the CO_2 can be captured in the column. For this set of conditions, that occurs at around 100 mol% excess GAP-1m.

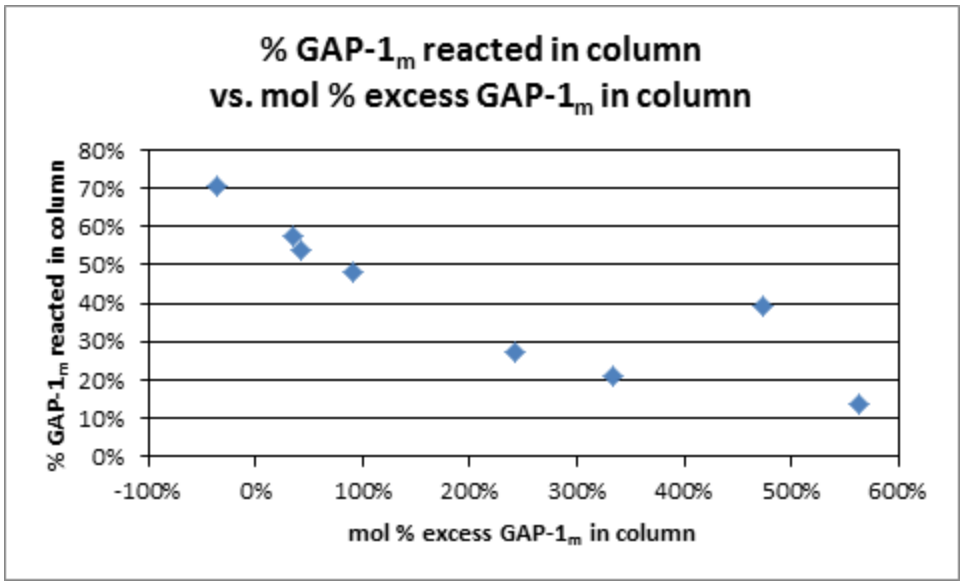

Figure 76. Comparison of GAP-1m reacted in the column and mol% excess of GAP-1m in column.

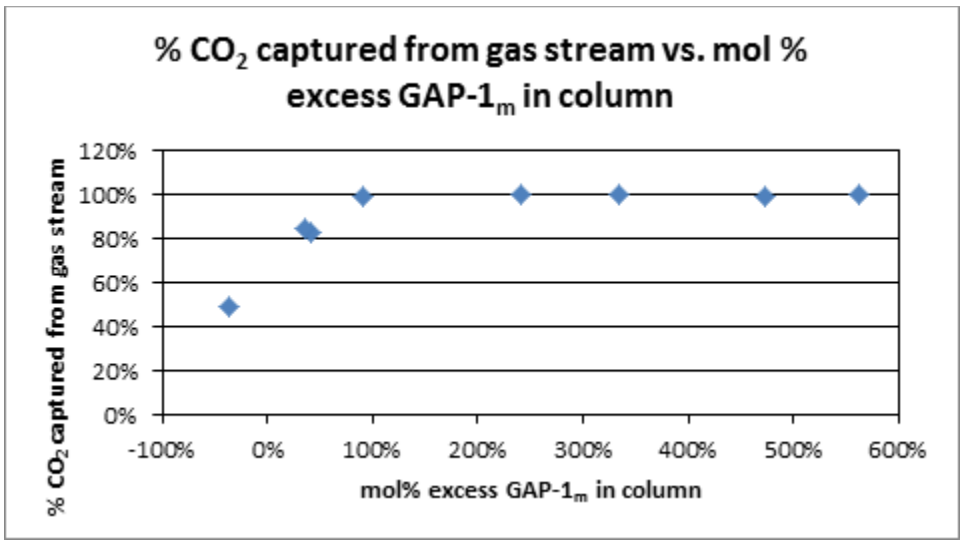

Figure 77. Comparison of CO_2 capture efficiency and mol% excess of GAP-1m in column.

Absorber Performance

A series of experiments were performed to determine the effect of system conditions on the absorption of CO_2. In this set of experiments, the desorber was operated at 160 °C and 0 psig

with a stir rate of 300 RPM and a recirculation pump speed of 50%, so that the CO_2 concentration in the lean solvent exiting the desorber was minimized and to maintain a consistent liquid CO_2 concentration entering the absorber. The target CO_2 concentration in the gas entering the absorber was 16%. This was achieved for these experiments by mixing bottled CO_2 and N_2. The absorber inlet temperatures (both liquid and gas) were maintained at 40 °C. In these experiments, the liquid and gas flow rates were varied from 0.5 to 1.5 LPM and 50 to 119 SLPM, respectively. By varying the liquid and gas flow rates within these ranges, the molar L_m/G_m ratio is varied from between 0.4 and 3.1. The concentration of CO_2 in the liquid stream was monitored by FTIR. Liquid samples were collected at the bottom of the absorber, the desorber exit, and from the lean storage tank. The concentration of CO_2 in the gas stream was monitored using a CO_2 analyzer and by mass spectrometry. The gas was analyzed at the exit of the generator, at the bottom of the absorption column, at five points along the absorption column, at the top of the absorption column, and at the desorber exit. From the CO_2 concentrations measured in the gas phase at the top and bottom of the column, the percentage of CO_2 captured from the gas stream can be calculated and from that value, the amount of GAP-1m reacted in the absorption column can be determined based on the gas phase mass balance. The amount of GAP-1m reacted in the absorption column can also be determined from the FTIR analysis of the liquid samples, and these values are compared to determine consistency between the two methods. Table 42 gives the parameters used for this set of experiments and Table 43 summarizes the results.

Table 42. Parameters for absorption column experiments.

Parameter	**Units**	**Value**
Desorber temperature	°C	160
Desorber agitator speed	RPM	300
Desorber recirculation loop pump speed	% of max	50
Desorber level	in H_2O	7.5
Desorber pressure	psig	0
Inlet absorber temperature (gas and liquid)	°C	40
Absorber sump level	in H_2O	5.0
CO_2 concentration in inlet gas to column	mol%	16
Gas source		bottled

Table 43. Absorption column experiment results.

Liquid flow rate (LPM)	Gas flow rate (SLPM)	Actual % CO_2 in	Actual desorber P (psig)	% CO_2 captured (from gas)	% GAP-1_m reacted in column (gas mass balance)	% GAP-1_m reacted in column (liquid mass balance)	mol % CO_2 in liquid exiting absorber	mol % CO_2 in liquid entering absorber	mol % CO_2 in liquid exiting desorber
0.5	50	16.2%	1.6	99.8%	38.9%	44.6%	19.7%	2.2%	2.2%
0.5	75	16.1%	0.7	95.4%	55.8%	60.2%	27.4%	3.9%	3.8%
0.5	100	16.3%	0.8	80.1%	62.5%	67.3%	30.1%	3.7%	3.9%
0.5	119	16.3%	0.8	66.2%	61.3%	66.8%	30.9%	4.7%	4.9%
1.5	50	15.9%	0.3	100.0%	13.2%	14.8%	11.2%	5.4%	5.6%
1.5	50	15.8%	3.1	100.0%	12.9%	15.1%	19.8%	13.5%	12.9%
1.5	75	16.2%	2.5	100.0%	19.7%	22.3%	17.2%	8.4%	8.5%
1.5	100	16.2%	2.2	100.0%	26.0%	28.8%	28.3%	9.0%	9.5%
1.5	100	16.4%	0.2	100.0%	26.9%	27.6%	23.3%	12.5%	12.5%
1.5	119	16.2%	4.4	99.3%	48.3%	49.5%	22.3%	3.0%	3.0%
1	50	15.7%	0.1	100.0%	19.3%	20.9%	19.0%	10.8%	11.2%
1	75	15.7%	0.3	100.0%	28.6%	31.5%	24.2%	11.8%	11.8%
1	100	16.0%	0.8	97.7%	38.3%	41.1%	28.7%	12.6%	12.5%
1	119	16.1%	0.7	89.2%	42.0%	42.4%	30.0%	13.5%	12.9%

As was shown for the baseline system performance runs, the % GAP-1m reacted in the column correlates well with the excess GAP-1m fed to the column, as shown in Figure 78. As was the case with the baseline system performance experiments, when approximately 100 mol% excess of GAP-1m is fed to the column, all of the CO_2 is captured from the gas phase.

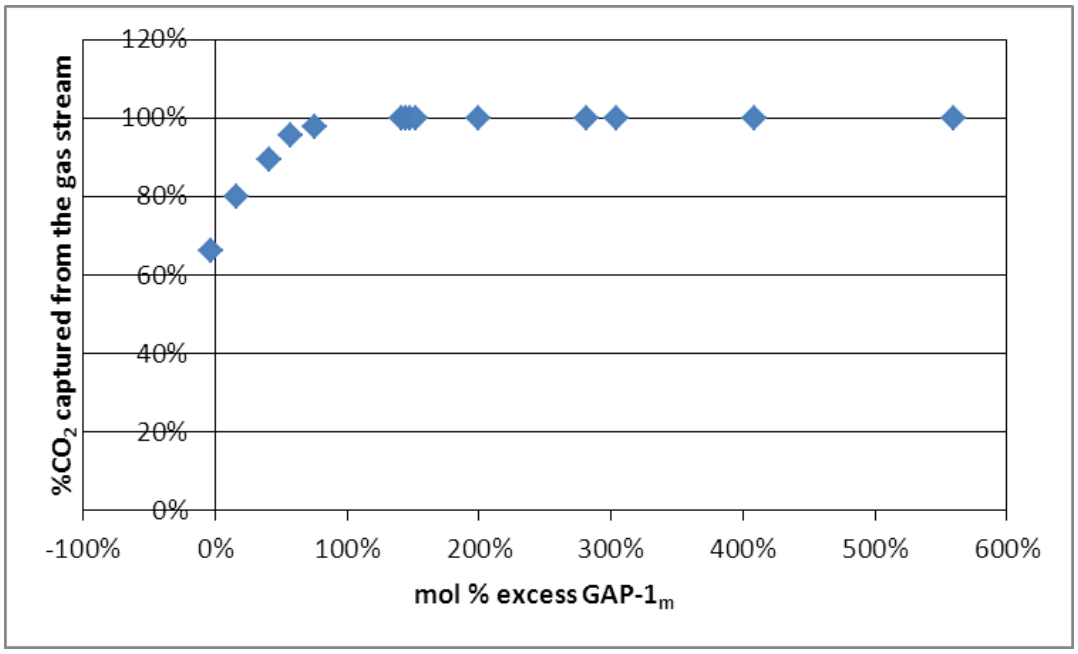

Figure 78. Comparison of CO_2 capture efficiency and mol% excess of GAP-1m in column.

The CO_2 captured from the gas stream can also be viewed as a function of liquid and gas flow rates, as shown in Figures 79 and 80. Figure 79 shows the % CO_2 captured from the gas stream is fairly insensitive to the gas flow rates studied at liquid flow rates of 1 and 1.5 LPM, but is very sensitive to the gas flow rates at 0.5 LPM. Figure 80 demonstrates this dependency more clearly.

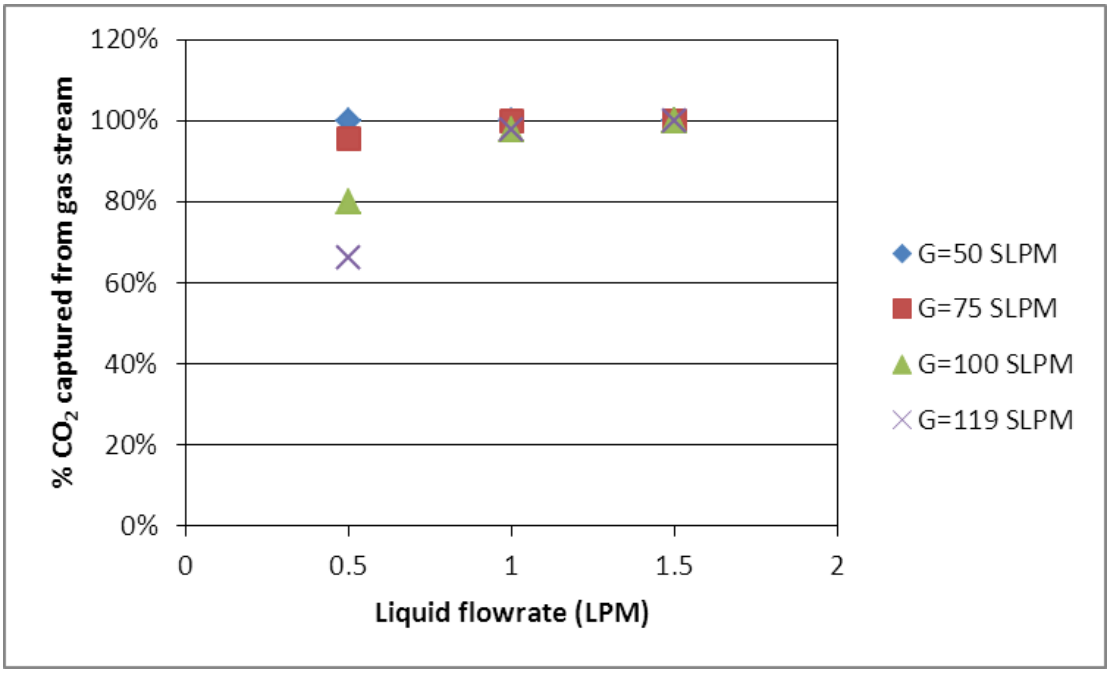

Figure 79. %CO_2 captured from the gas stream as a function of both liquid and gas flow rates.

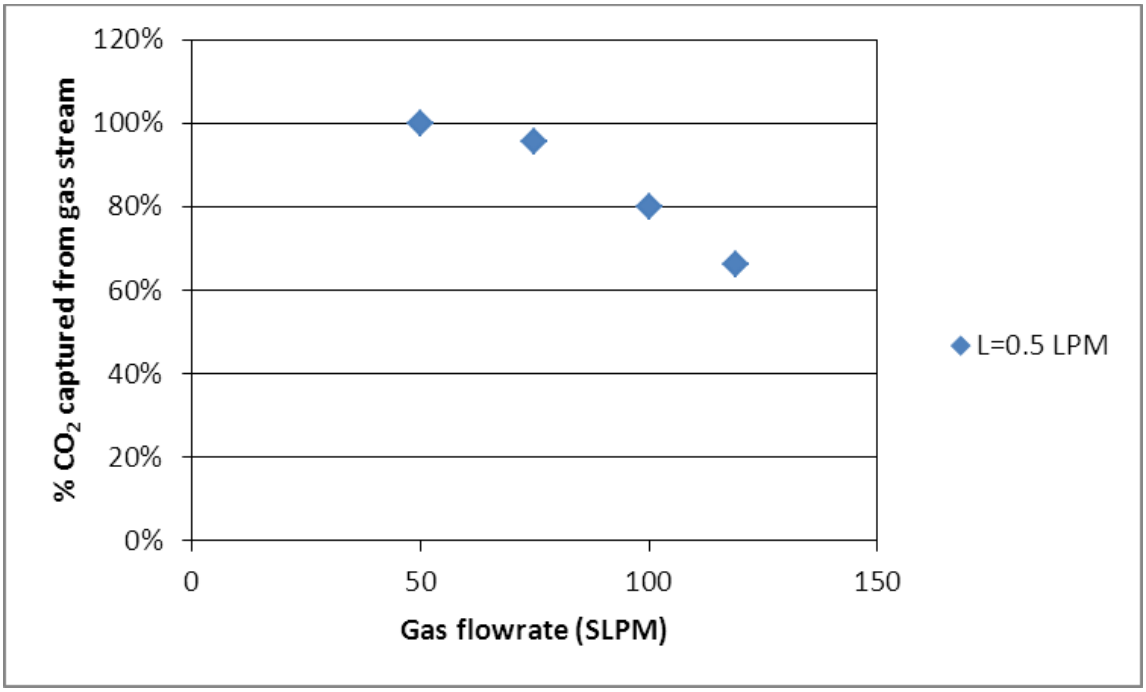

Figure 80. %CO_2 capture from the gas stream at a liquid flow rate of 0.5 LPM.

The temperature profile in the column is also measured for each run. The temperature profiles for most the experiments in this series are shown in Figure 81. The temperature profile data is not available for the experiments performed at a liquid flow rate of 0.5 LPM and gas flow rates of 50 and 75 SLPM. For better legibility, Figures 82-86 show the temperature profiles for each liquid flow rate and gas flow rate studied. These charts show that for a given liquid flow rate, as the gas flow rate increases, the temperature in the column increases. The majority of the experiments in this series are run with an excess of GAP-1m, and so when the gas flow rate is increased, more CO_2 is available to react with the GAP-1m, and because the reaction of CO_2 and GAP-1m is exothermic, heat is generated. For a given gas flow rate, as the liquid flow rate decreases, the temperature in the column increases. The reproducibility of the temperature measurements is also demonstrated in Figures 84 and 85.

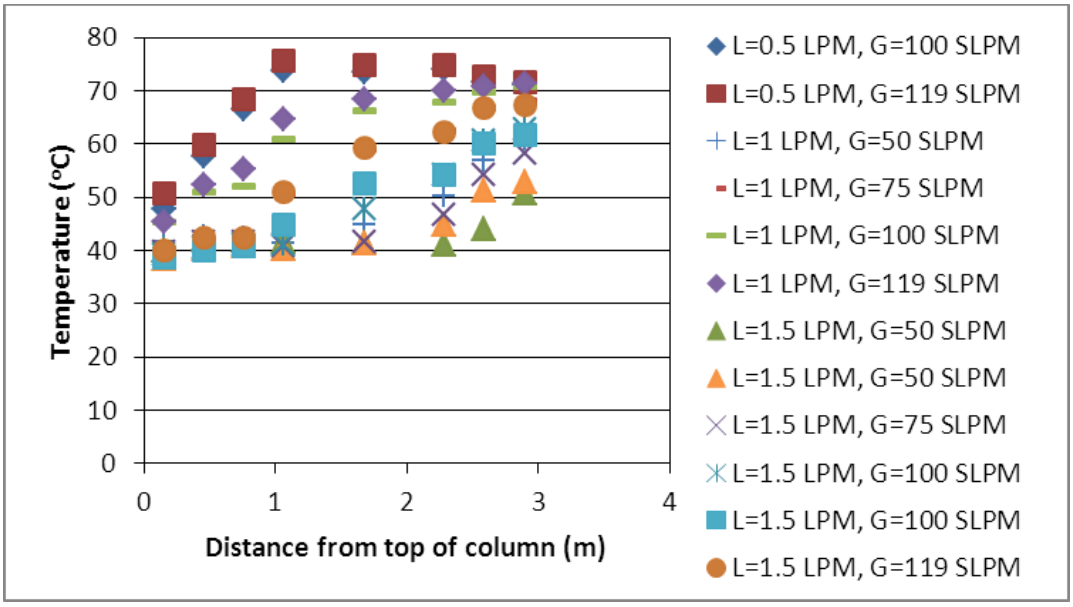

Figure 81. Temperature profile in absorption column.

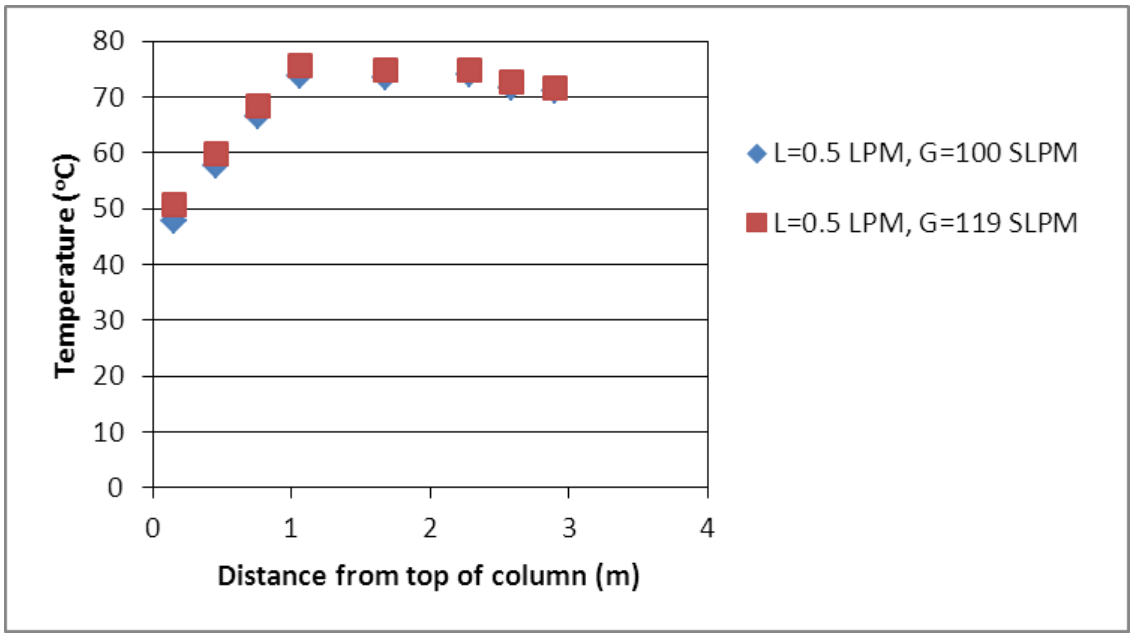

Figure 82. Temperature profiles for 0.5 LPM liquid flow rates.

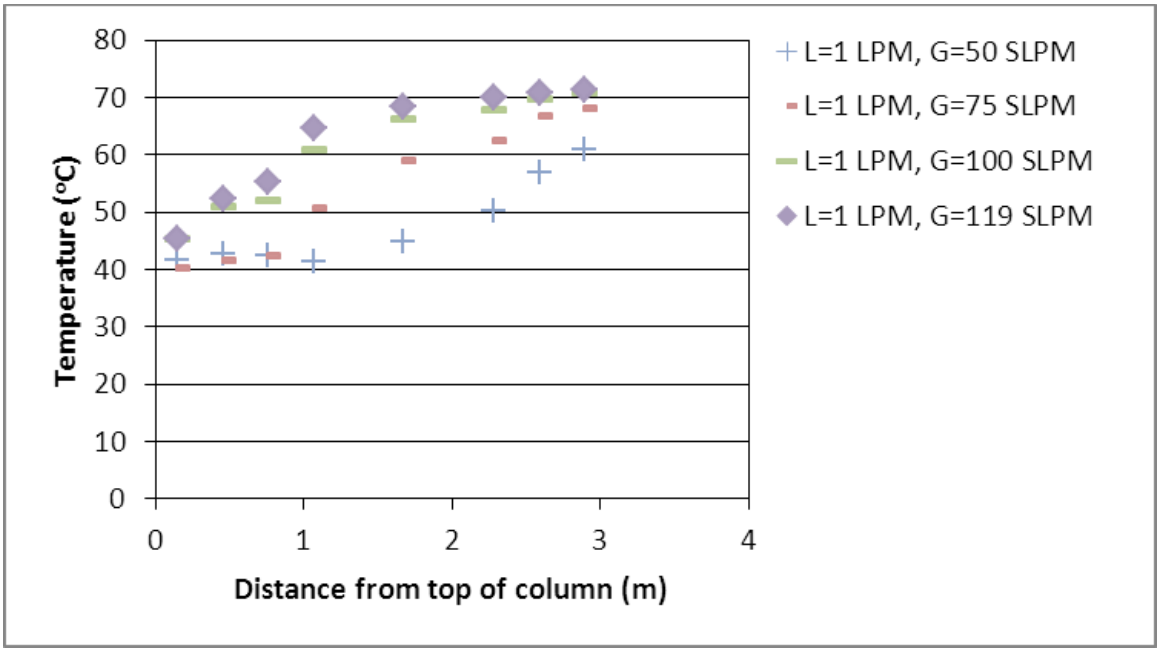

Figure 83. Temperature profiles for 1.0 LPM liquid flow rates.

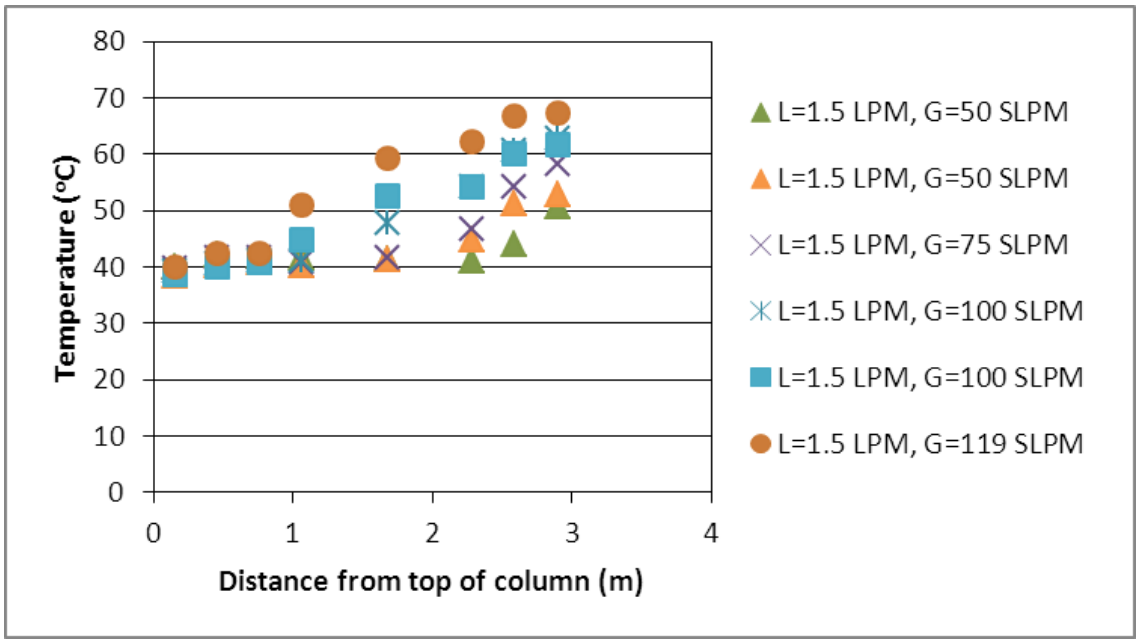

Figure 84. Temperature profiles for 1.5 LPM liquid flow rates.

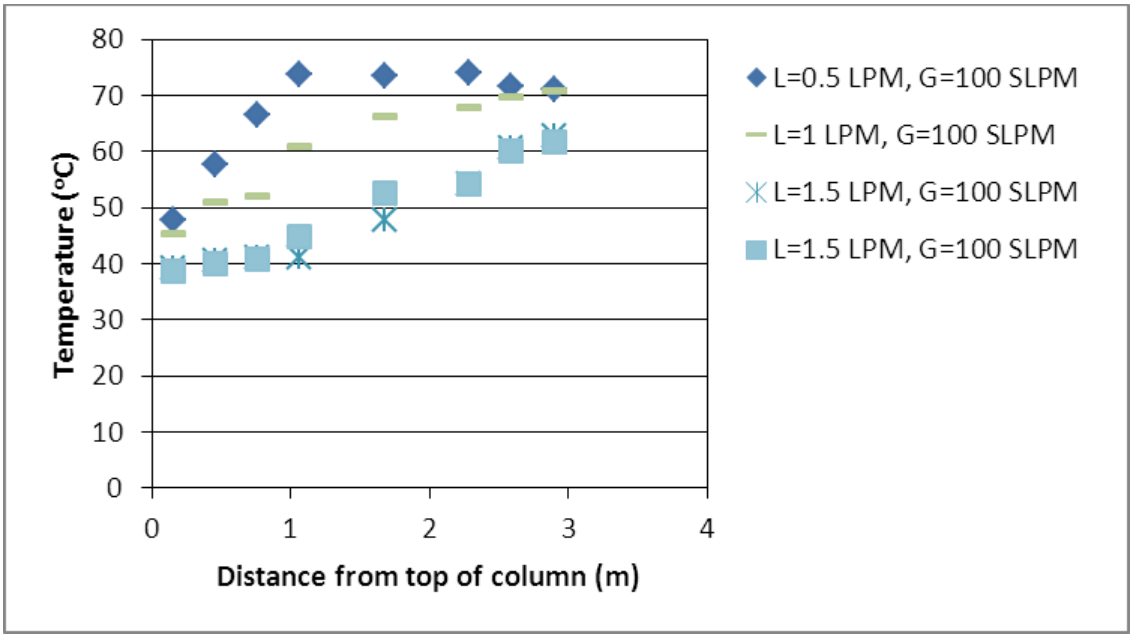

Figure 85. Temperature profiles for 100 SLPM gas flow rates.

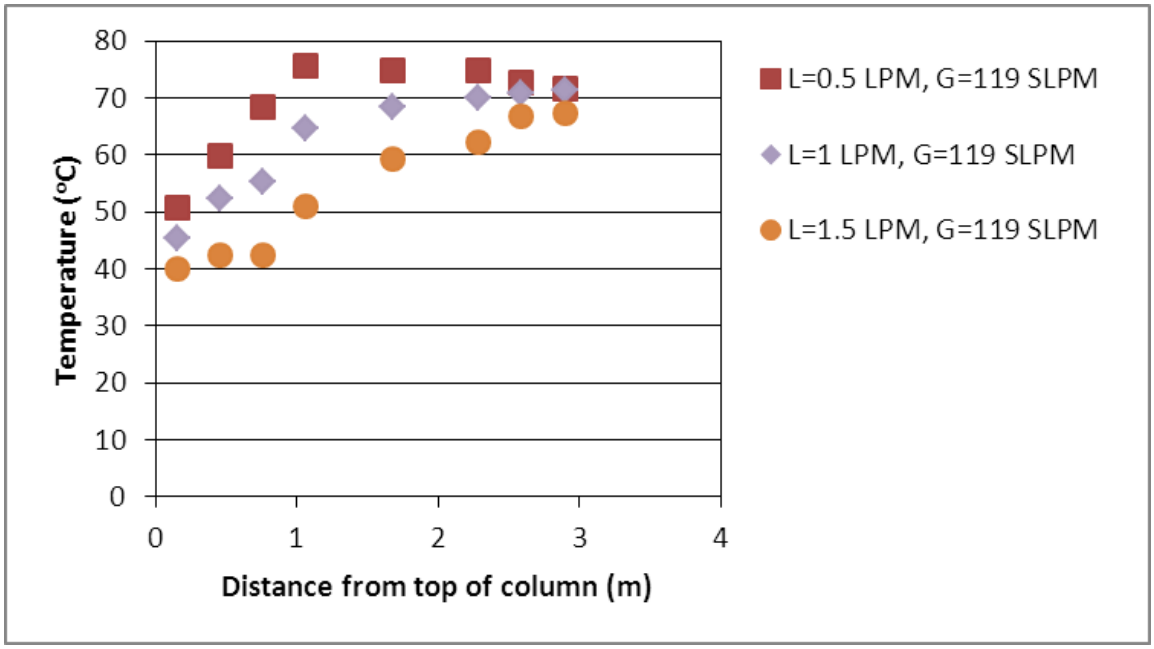

Figure 86. Temperature profiles for 119 SLPM gas flow rates.

In addition to the temperature profiles in the column, CO_2 concentrations in the gas phase as a function of column height were also measured and are shown in Figures 87. Figures 88-94 show the CO_2 concentration profiles for each liquid and gas flow rate studied in this series of experiments. Figures 88-90 show that, in general, for a given liquid flow rate, as the gas flow rate decreases, the amount of CO_2 captured at the same point in the column increases. In other words, as the residence time of the gas in the column increases, more CO_2 is removed from the column. Figures 91-94 show that, in general, for a given gas flow rate, as the liquid flow rate decreases, the rate at which CO_2 is absorbed in the column also decreases. This effect is most apparent at the lower gas flow rates (50 and 75 SLPM). Interestingly, at the lowest gas flow rates (50 and 75 SLPM) and lowest liquid flow rate (0.5 LPM), the CO_2 concentration drops significantly in the first 0.3 meters from the bottom of the column, after which the rate of CO_2 absorption slows significantly.

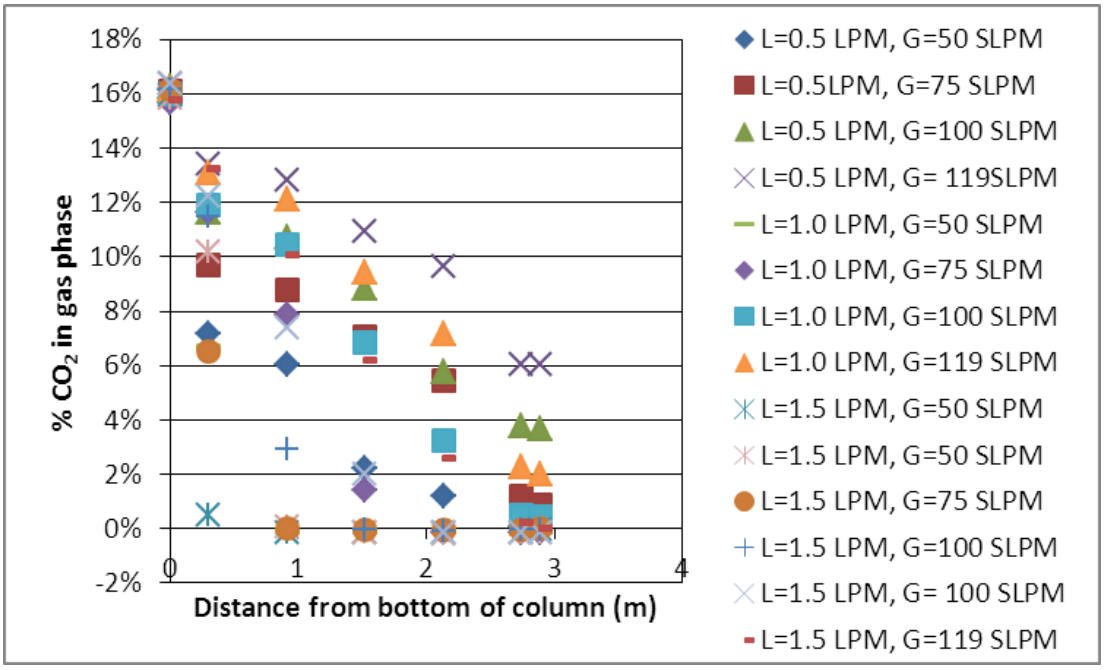

Figure 87. CO_2 concentration in the gas phase as a function of absorption column height.

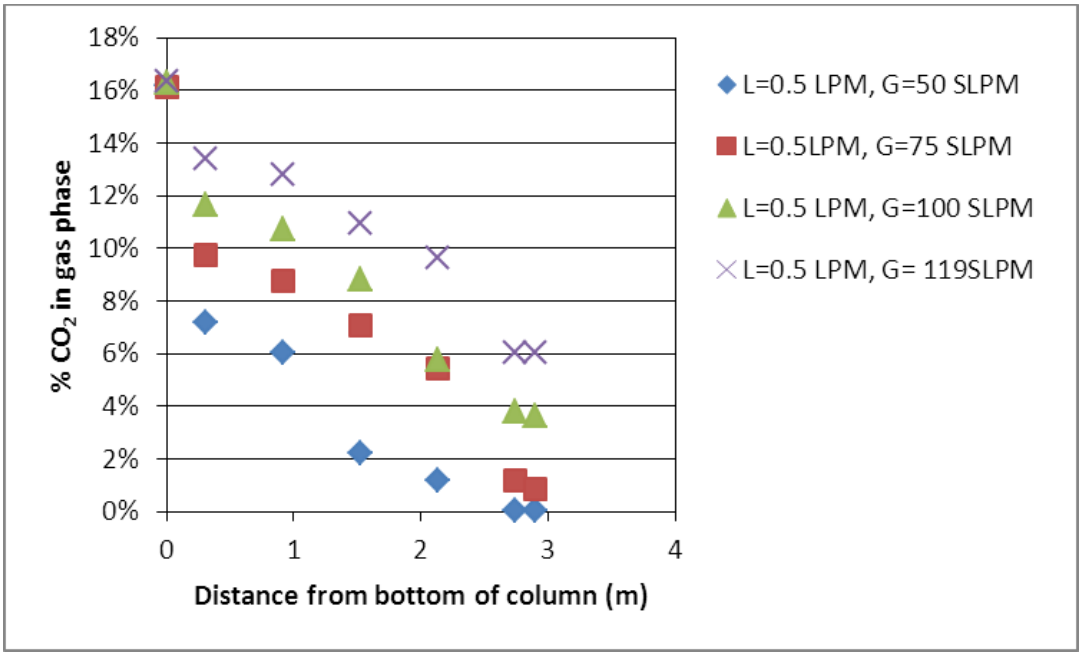

Figure 88. CO_2 concentration profile for L=0.5 LPM.

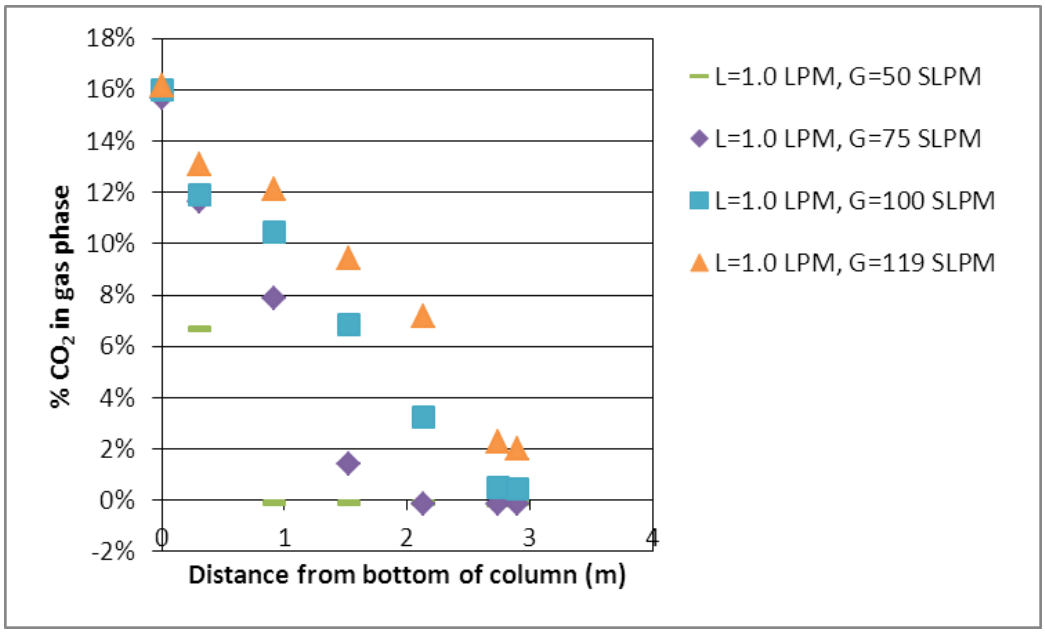

Figure 89. CO_2 concentration profile for L=1.0 LPM.

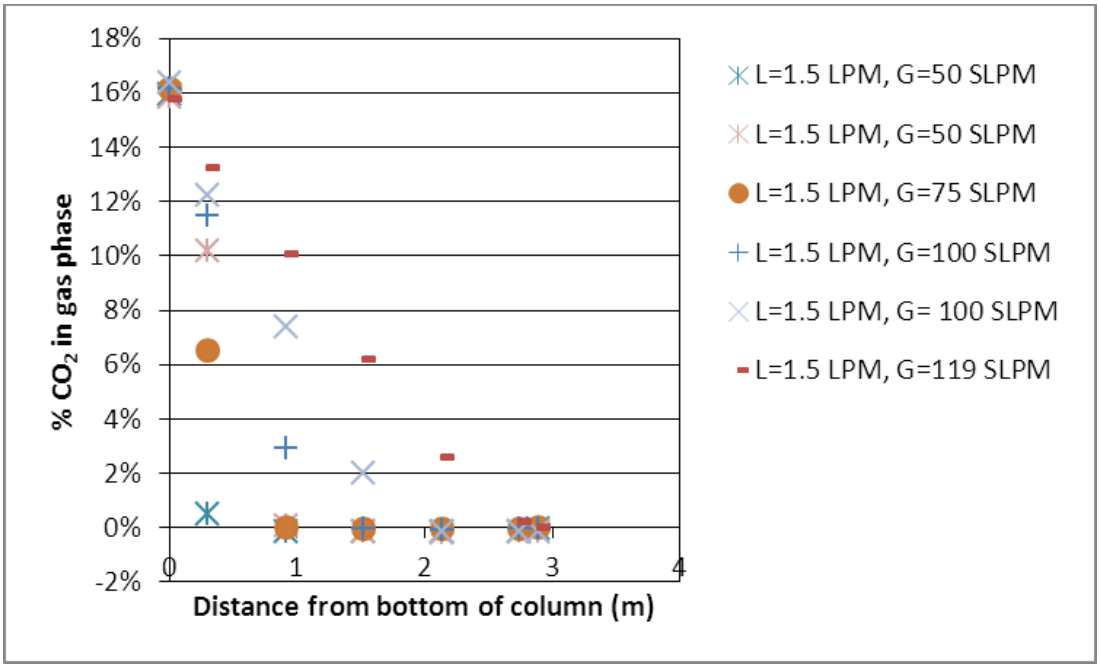

Figure 90. CO_2 concentration profile for L=1.5 LPM.

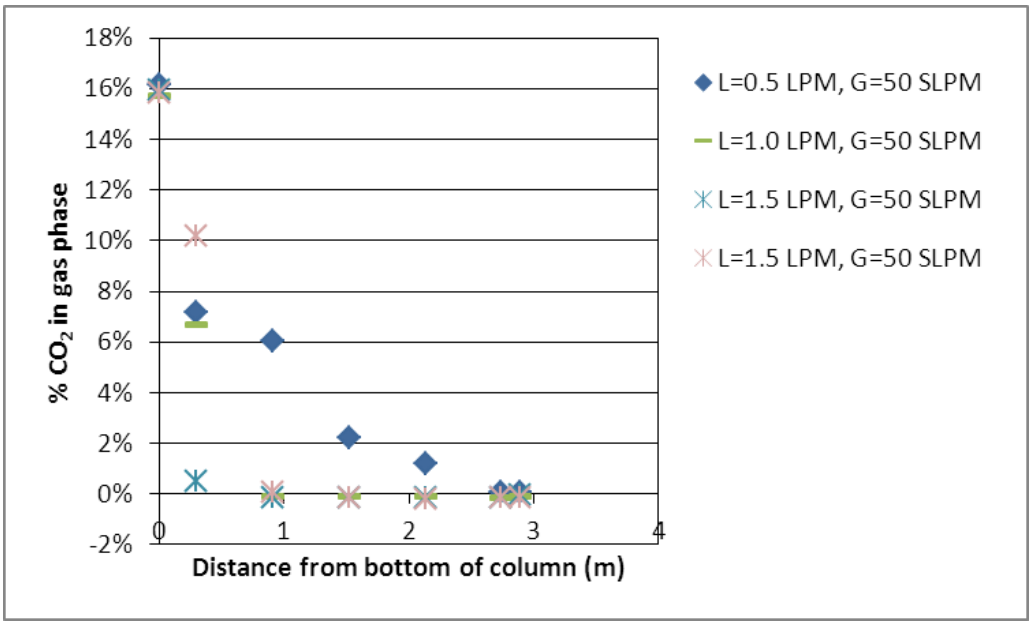

Figure 91. CO_2 concentration profile for G = 50 SLPM.

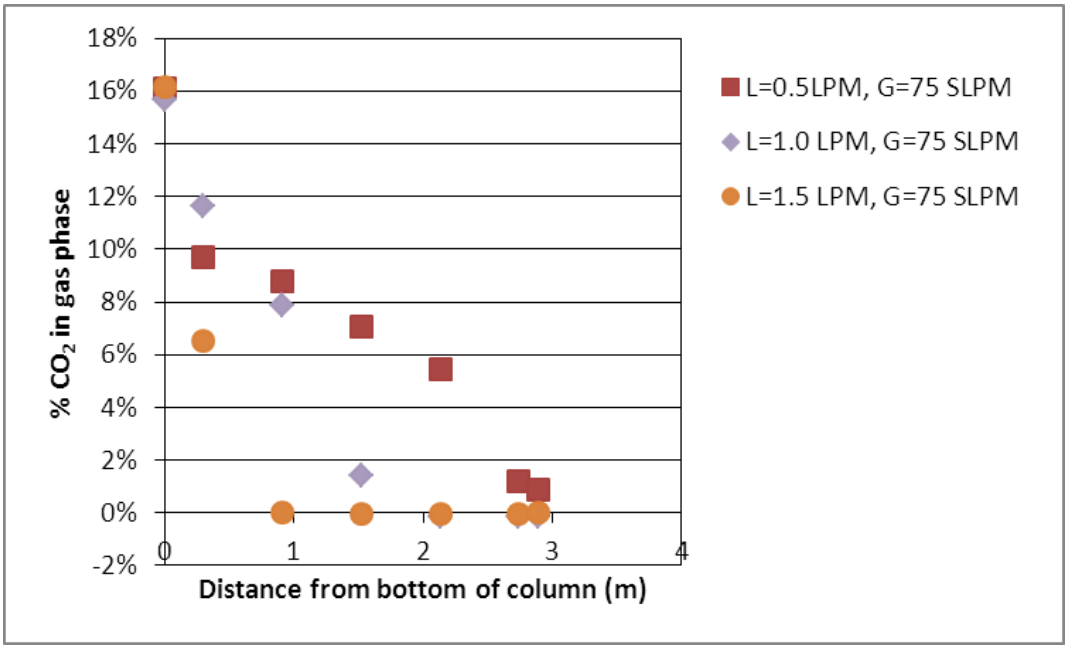

Figure 92. CO_2 concentration profile for G = 75 SLPM.

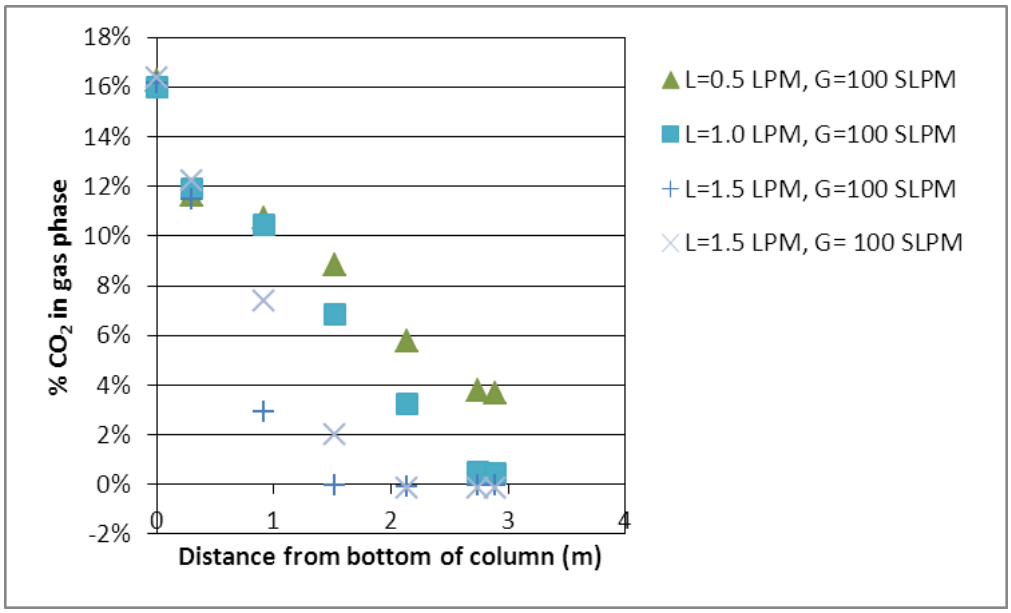

Figure 93. CO_2 concentration profile for G=100 SLPM.

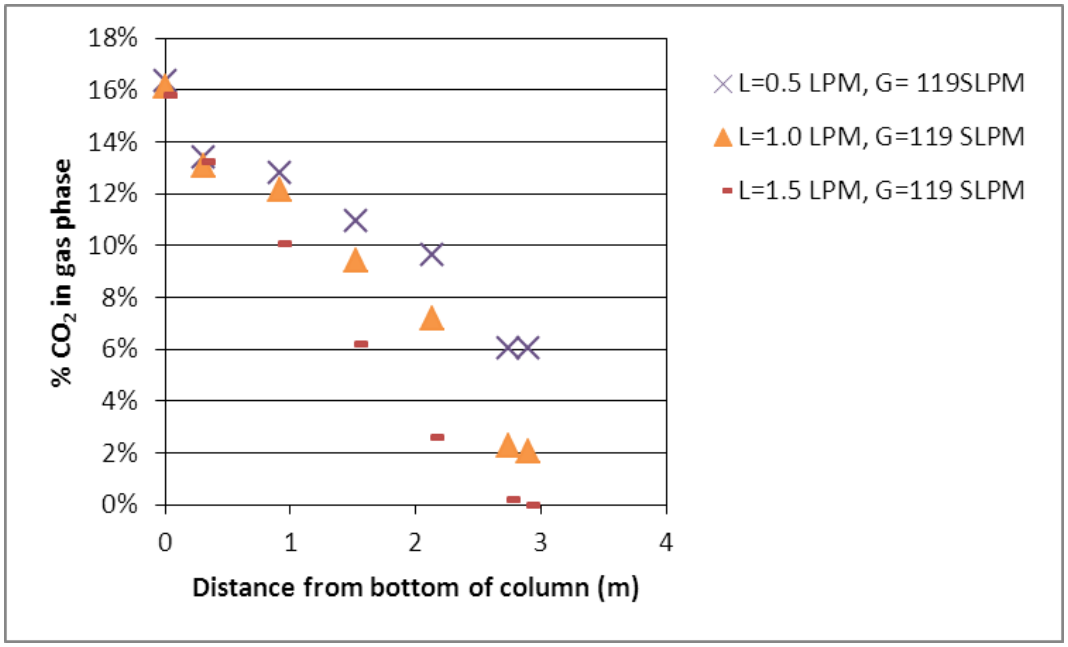

Figure 94. CO_2 concentration profile for G = 119 SLPM.

Effect of Inlet Temperature to the Absorber

The effect of the inlet temperature to the absorber on the temperature profile and concentration of CO_2 removed from the gas phase was studied. The effect on the temperature profile in the column is shown in Figure 95 and the effect on the concentration profile is shown in Figure 96. All the experiments shown in Figures 95 and 96 used bottled gases (low water), a liquid flow rate of 0.5 LPM, a gas flow rate of 112 SLPM, a desorber temperature of 140 °C, and a desorber pressure of 45 psig. The only factor changing in these experiments is the inlet liquid and gas temperatures to the absorber. Figure 95 shows a significant difference in the temperature profile in the column. However, a significant difference in the CO_2 absorption was not observed, as shown in Figure 96.

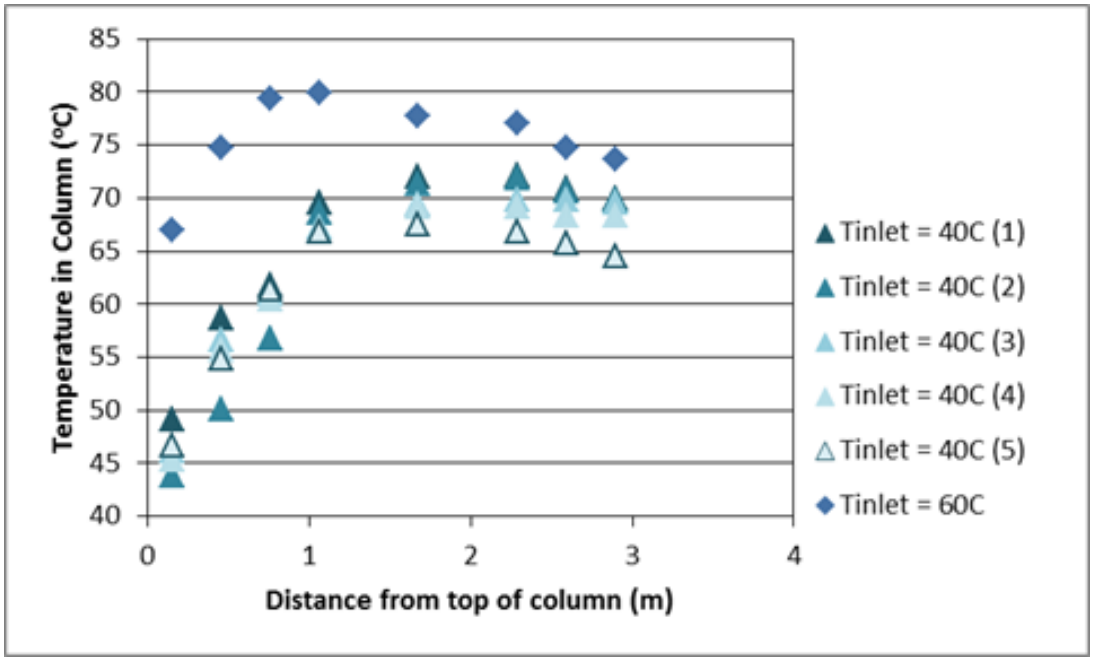

Figure 95. Effect of inlet temperature to absorption column on temperature profile in column.

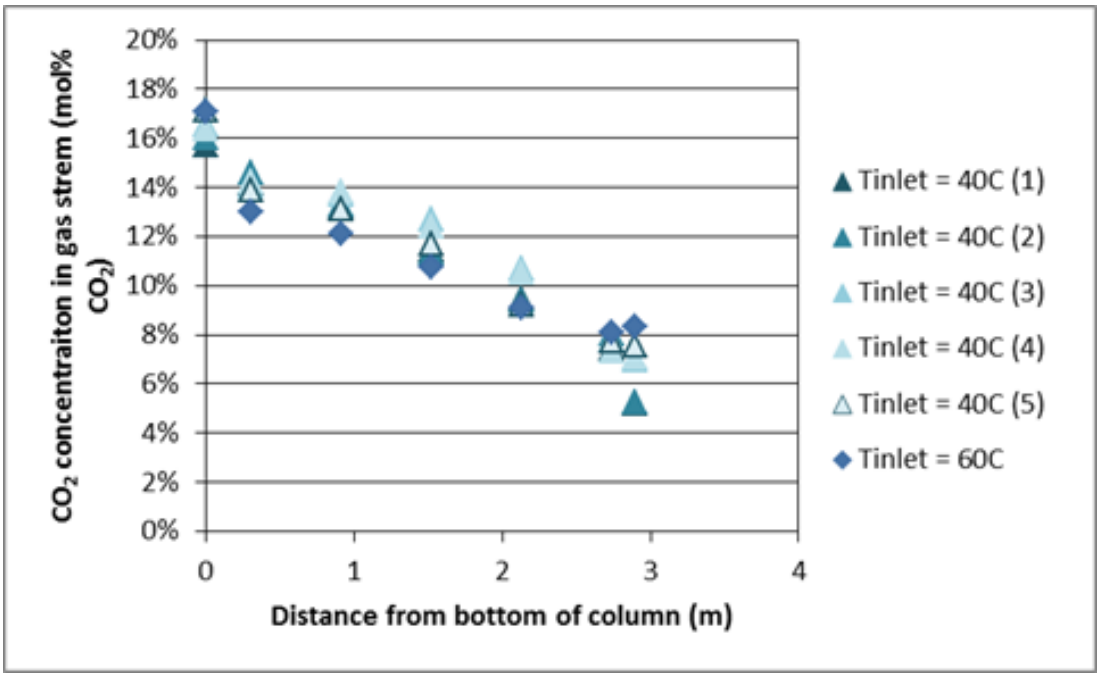

Figure 96. Effect of inlet temperature to absorption column on concentration profile in column.

Desorber Performance

A series of experiments were performed to determine the effect of system conditions on the desorption of CO_2. In this set of experiments, the absorber was operated at 40 °C for both the liquid and gas inlet temperatures, a liquid flow rate of 0.5 LPM, a gas flow rate of 112 SLPM, and a gas phase CO_2 concentration of 16 mol%. The inlet CO_2 concentration was achieved by mixing bottled CO_2 with the exhaust gas from the gasoline generator. These conditions were used to maximize the liquid CO_2 concentration exiting the absorber and maintain a consistent inlet liquid CO_2 concentration to the desorber. Several desorber parameters were studied to determine their effect on desorption. These include mixing in the desorber, which can be controlled by varying both the stirring rate of the agitator and the speed of the recirculation pump, temperature, pressure, and residence time, which can be controlled by both liquid flow rate and level of liquid in the desorber. In addition, the reproducibility of the experimental system was also explored.

<u>Mixing in the Desorber</u>

The nominal stirring rate in the desorber is 300 RPM and the nominal pump speed for the desorber recirculation loop is 50% of maximum pump speed. To probe the effect of mixing in the desorber, both the agitator rate and the pump speed were increased to near their

maximum values (550 RPM and 90%, respectively). As is shown in Figure 97, changing the mixing conditions did not change the amount of CO_2 desorbed in the reactor, suggesting that at an agitator stir rate of 300 RPM and a recirculation pump speed of 50%, the desorption reaction is not mass transfer limited.

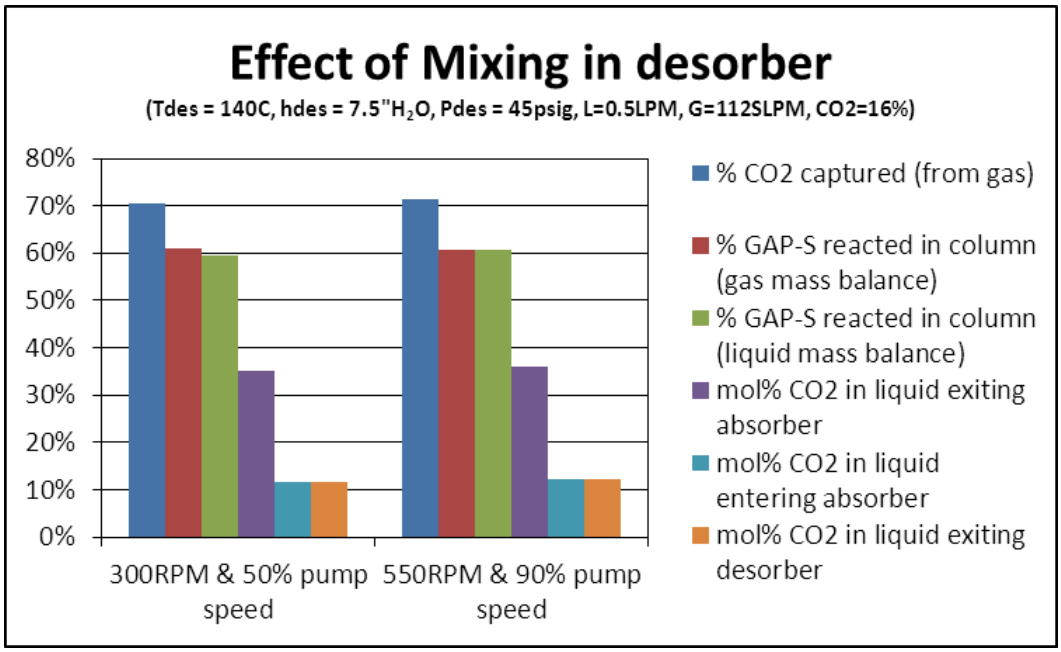

Figure 97. Effect of mixing conditions on the desorption of CO_2.

Desorption Temperature

The effect of desorption temperature on the system was studied by varying the temperature of the desorber from 120 °C to 150 °C. For this set of experiments, the desorption pressure was set at 45 psig. As shown in Figure 98, as the temperature of desorption increases, the amount of CO_2 desorbed from the liquid increases, as is expected. Figure 98 also illustrates that as the amount of CO_2 desorbed increases, so does the working capacity of the fluid and Figure 99 shows that as the working capacity increases, the amount of CO_2 captured from the gas stream in the column also increases.

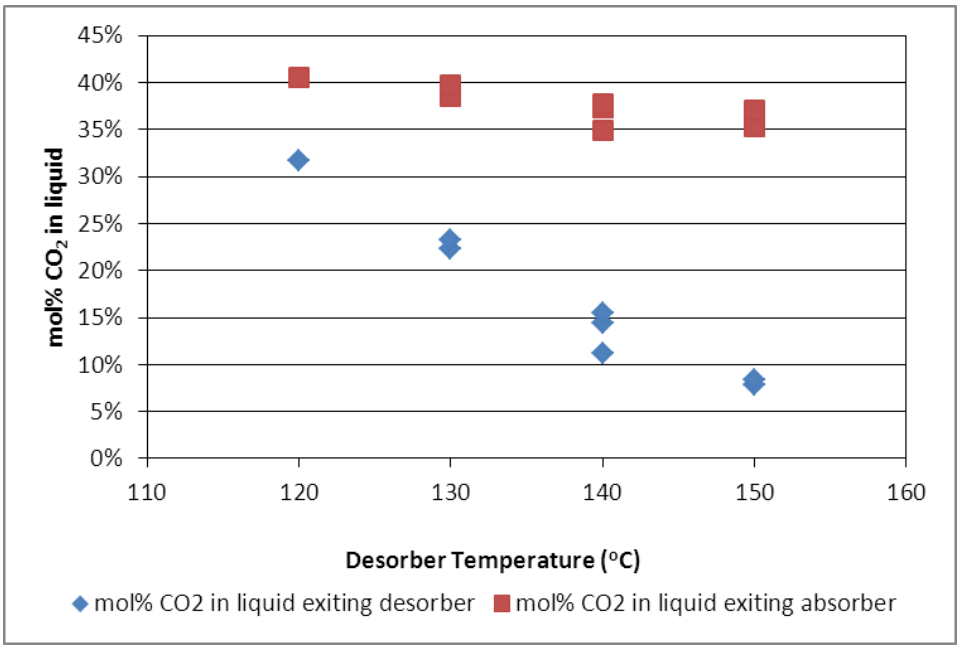

Figure 98. Effect of desorber temperature on CO_2 desorption and working capacity.

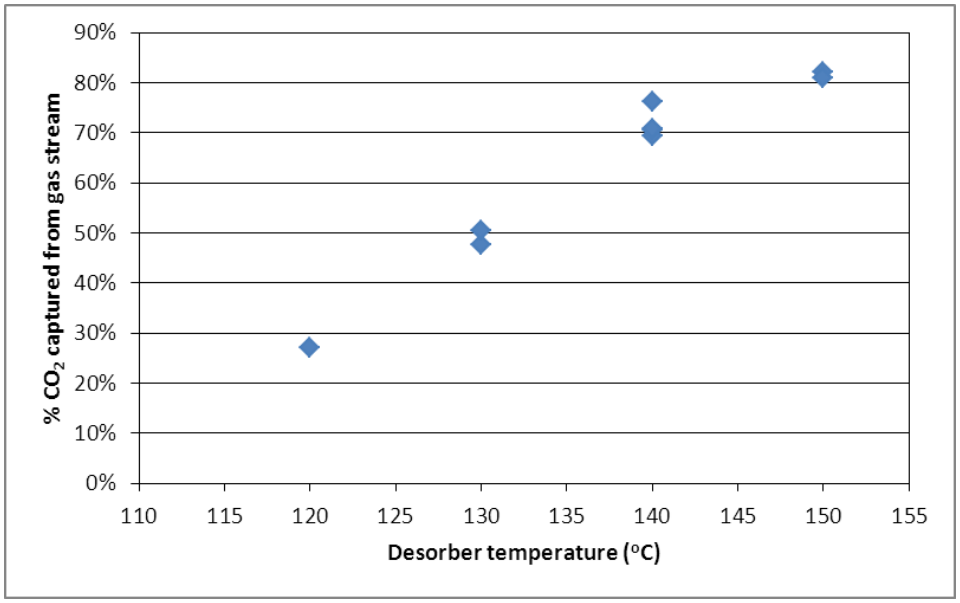

Figure 99. Effect of desorber temperature on CO_2 capture efficiency.

Figures 98 and 99 also illustrate the reproducibility of the experimental system, as several of the experiments were repeated. Figures 100 through 102 also demonstrate the reproducibility of the experiments.

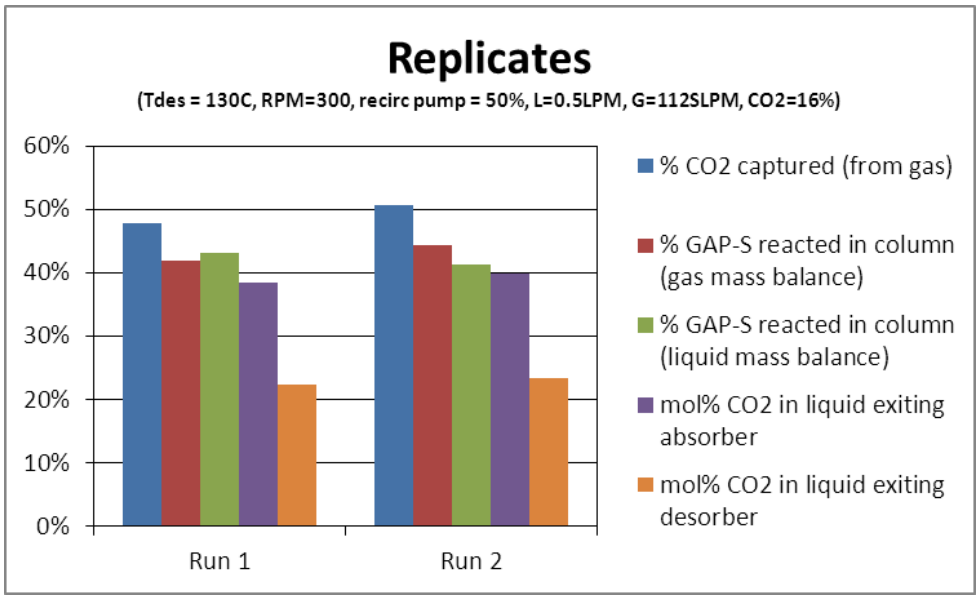

Figure 100. Reproducibility of experiments at a desorber temperature of 130 °C.

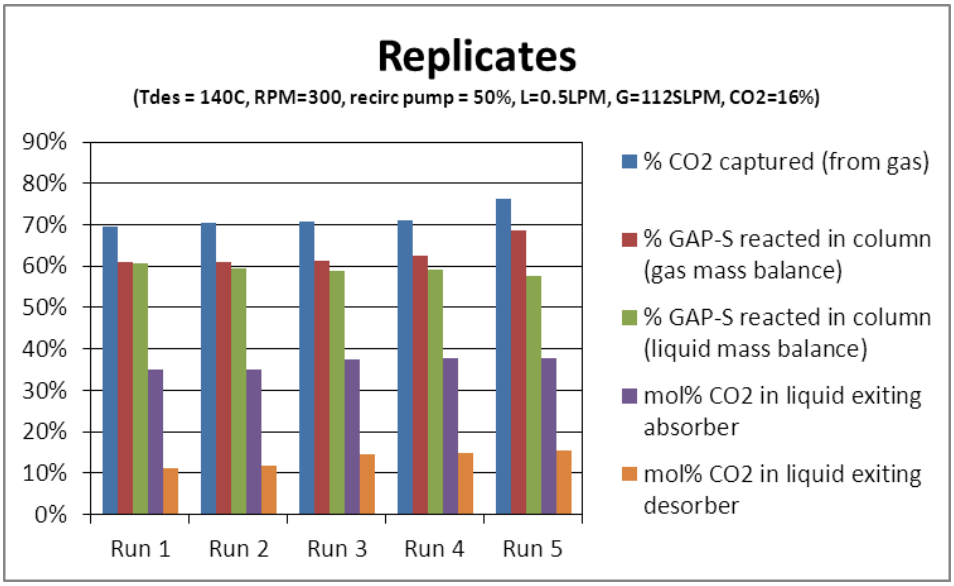

Figure 101. Reproducibility of experiments at a desorber temperature of 140 °C.

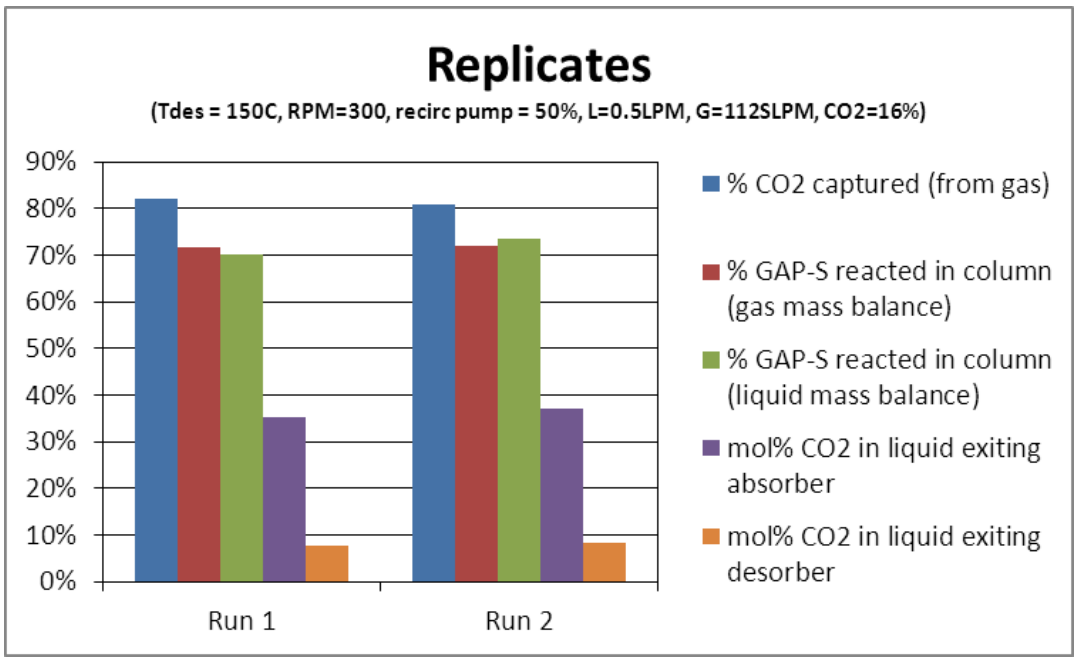

Figure 102. Reproducibility of experiments at a desorber temperature of 150 °C.

Desorption Pressure

Desorption pressures of 0.7 and 45.1 psig were studied. For these experiments, the desorber temperature was 140 °C, the agitation rate was 300 RPM, the recirculation pump speed was 50%, and the height of the liquid in the desorber was 7.5" H_2O. Figure 103 shows that as the desorber pressure increases, the concentration of CO_2 in the liquid exiting the desorber increases, as is expected. However, interestingly, the concentration of the CO_2 in the liquid exiting the absorber also increases, resulting in only a small working capacity penalty for operating under pressure under these conditions. There is a maximum capacity for CO_2 in the liquid, so this trend could not continue indefinitely. However, it would be interesting to determine the highest operating pressure that still gives an acceptable working capacity.

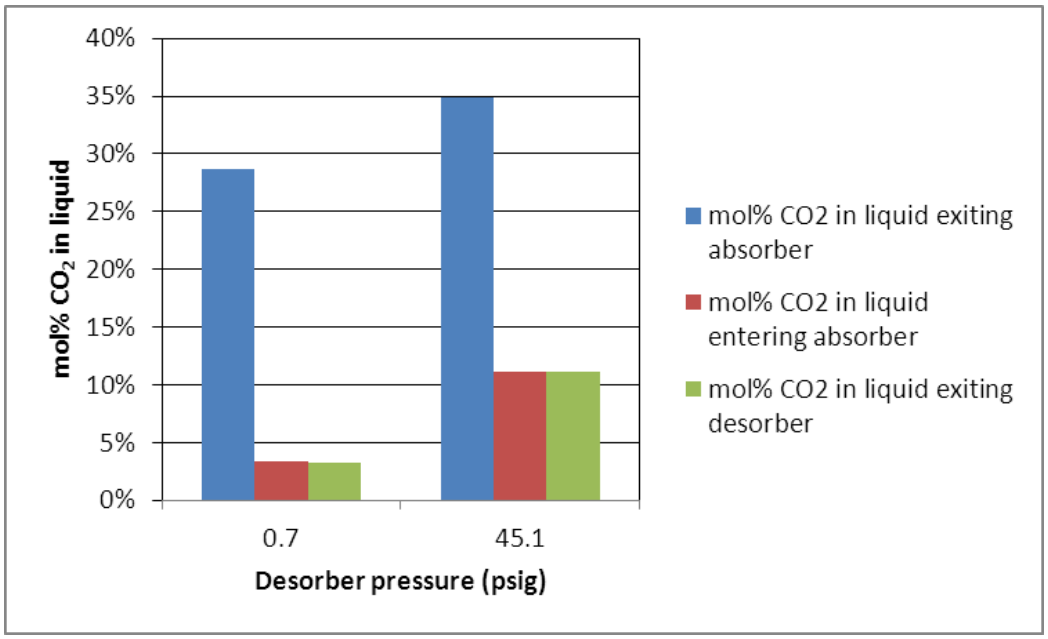

Figure 103. Effect of desorber pressure on the desorption of CO_2.

Effect of Desorber Residence Time

When the initial model of the desorber was developed, the model used the same residence time as the desorber assembly (CSTR plus recirculation loop) in the bench-scale system (58 minutes). However, when scaling-up the bench scale model to use it for determining the economics of the full-scale system, it was determined that the residence time in the desorber in the bench scale was likely much longer than was actually needed to achieve sufficient desorption, and that a smaller desorber with a shorter residence time could be used. It was necessary to obtain data at shorter residence times to compare to the modeling results to confirm desorber sizing on the larger scale.

The most effective method of achieving different residence times in the desorber is to change the liquid flow rate. The maximum achievable liquid flow rate in the bench-scale system (limited by cooling capacity of the heat exchanger that cools the liquid at the desorber exit) is 1.8 LPM. When using bottled gases, the maximum gas flow rate is 120 SLPM, which means the lowest achievable molar L/G for the maximum liquid flow rate is approximately 1.5. Experiments were performed holding L/G constant at approximately 1.5 and varying the residence from 16 to 58 minutes, and the desorber pressure from 0 to 60 psig. Figures 104 and 105 show the effect of the residence time on the amount of GAP-1m reacted in the column for both desorber pressures of 45 psig and 60 psig. As the desorber residence time decreases, it

was expected that the concentration of CO_2 in the liquid exiting the desorber would increase. While a slight increase is seen in both figures, data at residence times shorter than 16 minutes would be required to determine if this trend is real.

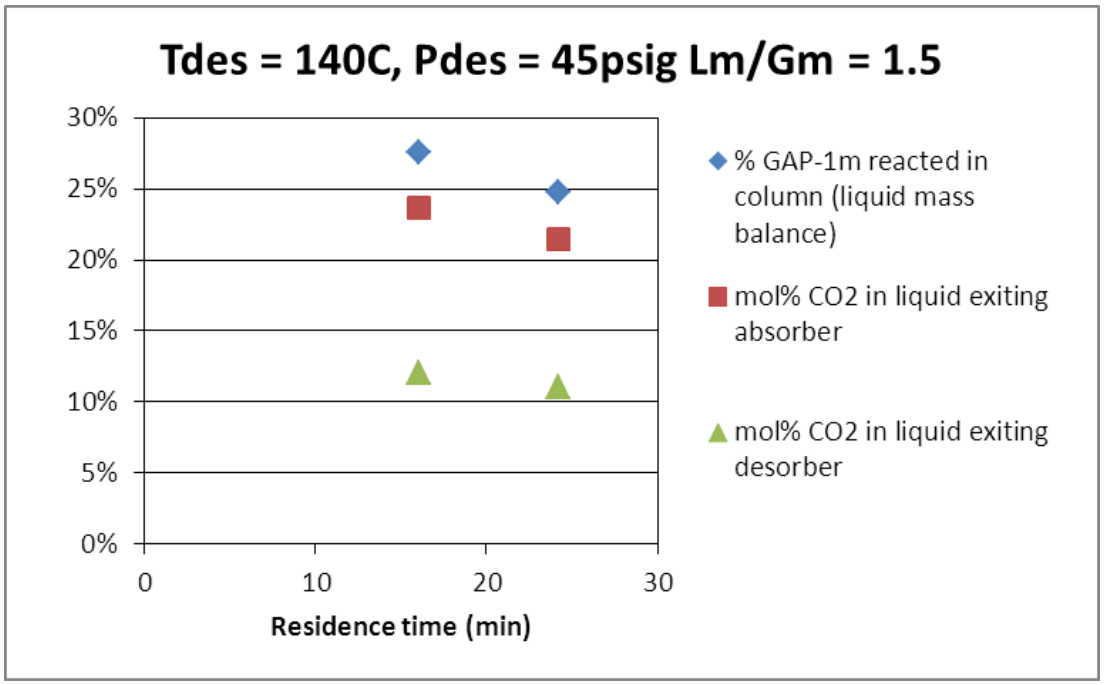

Figure 104. Effect of desorber residence time on desorption of CO_2 at 45 psig and 140 °C.

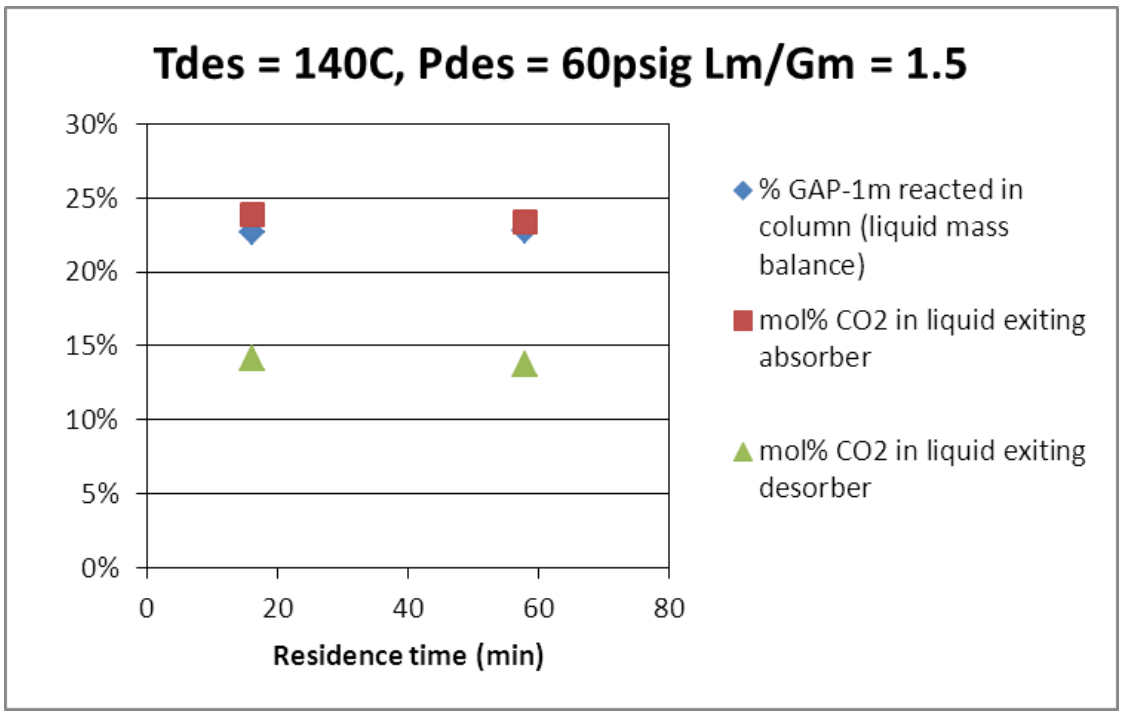

Figure 105. Effect of desorber residence time on desorption of CO_2 at 60 psig and 140 °C.

The current system cannot operate at desorber residence times of less than 16 minutes without modifying the equipment. Additional experiments were performed to determine if the conditions in the desorber can be altered to change the amount of CO_2 desorbed in order to validate the model at equilibrium. Both the temperatures and pressures in the desorber were varied and the effect on the desorption of CO_2 was observed, as seen in Figures 106 and 107. As expected, as the desorber pressure increases, the amount of CO_2 desorbed decreases, and as the desorber temperature increases, the amount of CO_2 desorbed increases.

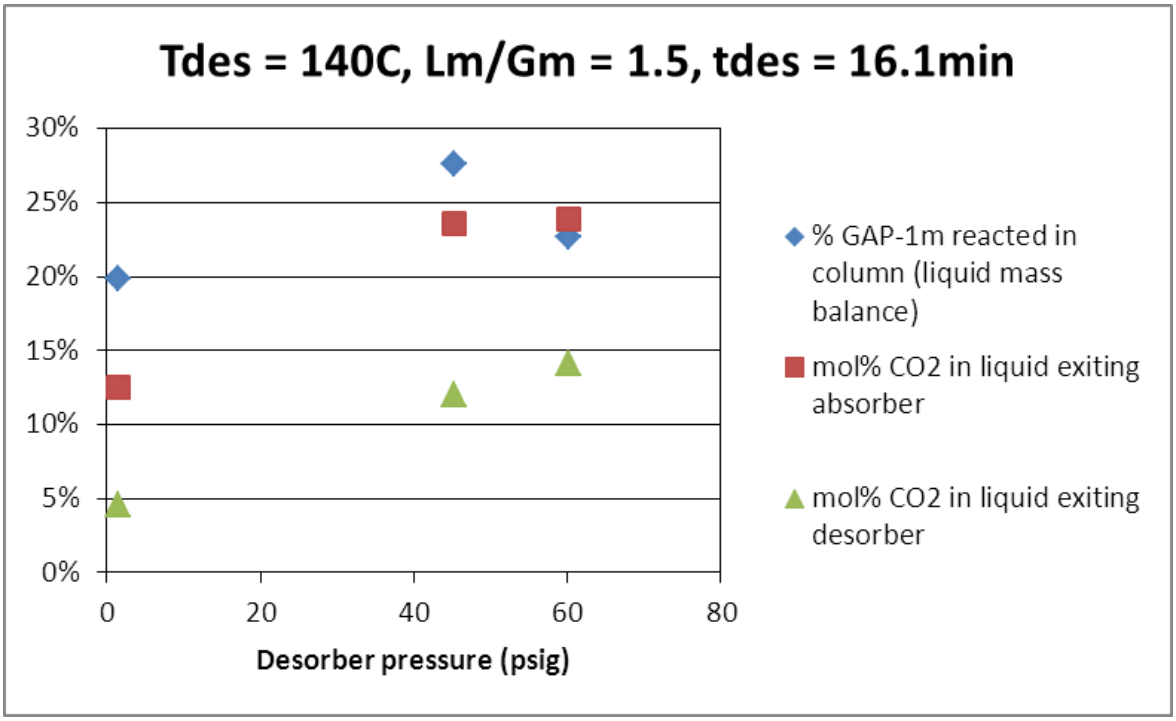

Figure 106. Effect of desorber pressure on desorption of CO_2 at 140 °C, Lm/Gm = 1.5, and residence time of 16.1 minutes.

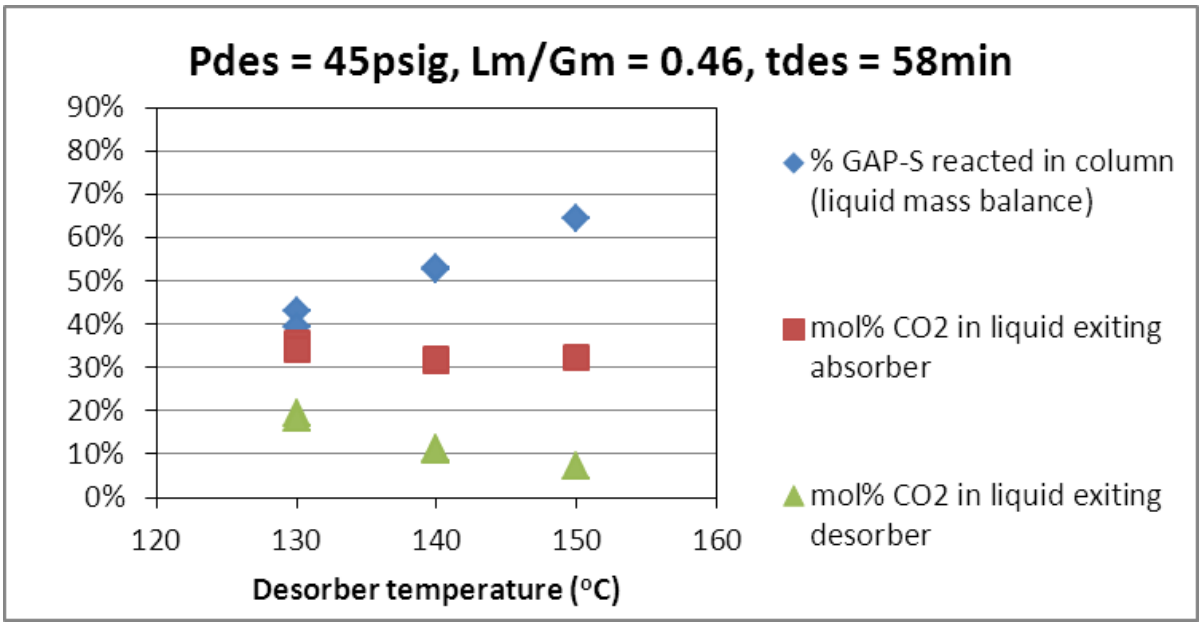

Figure 107. Effect of desorber temperature on desorption of CO_2 at 140 °C, Lm/Gm = 0.46, and residence time of 58 minutes

Solvent Degradation

As the series of experiments shown in Table 42 were being performed and the data analyzed, it was observed that the lean liquid CO_2 concentrations were drifting over time (Figure 108). This was not observed for the baseline system performance experiments (Figure 109). Both Figures 108 and 109 show the molar liquid concentration of CO_2 in run number order in the lean storage tank (entering absorber) and in the absorber (exiting absorber) as measured by FTIR. The analysis of the FTIR data for this calibration involves correcting the baseline for each dataset, finding the maximum absorbance in the range of 1570 to 1600 cm^{-1}, and using the calibration curve to determine the concentration of CO_2 in the liquid. Several causes of this drift were investigated and are listed in Table 44.

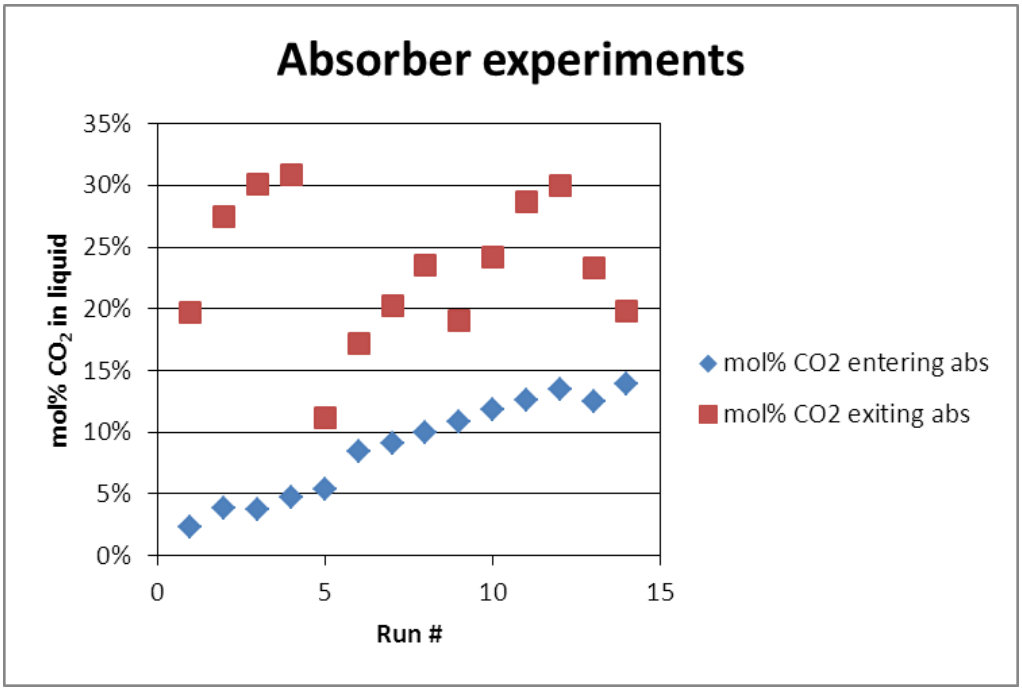

Figure 108. CO_2 concentration in liquid as a function of run order for absorber experiment runs.

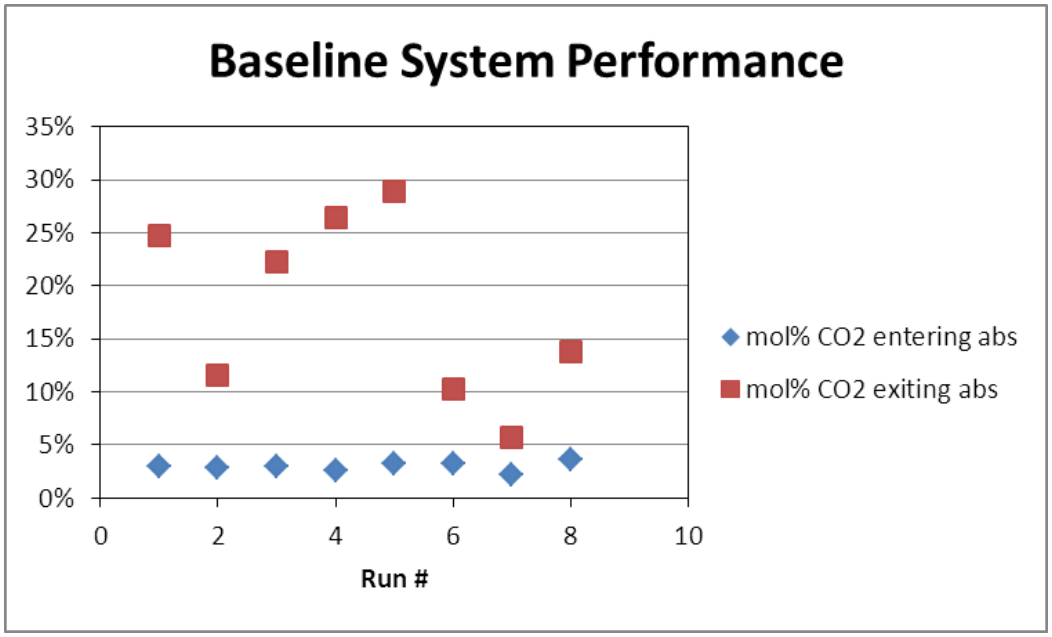

Figure 109. CO_2 concentration in liquid as a function of run order for baseline system performance runs.

Table 44. Potential causes liquid CO_2 concentration drift.

Potential cause	Investigation	Result
Drift in the IR instrument	Remeasure original calibration samples	No drift observed – IR working properly
CO_2 not desorbing completely in desorber	Heat sample from system and observe weight loss	No weight loss observed after heating
Material degrading and degradation peaks obscuring calibration peak	Compared raw IR curves for experiments to raw calibration IR curves	See Figure 110

As can be seen in Figure 110, for the original calibration curve, using the maximum absorbance between 1570 and 1600 cm^{-1} did not pose an issue. However, from the raw IR curves, it is observed that an additional peak is appearing very near the calibration peak and growing larger as a function of time in the system. Since a maximum in that region is used, as the new peak grew, it began obscuring the original peak, causing an artificially high absorbance number and resulting in an elevated liquid CO_2 concentration measurement.

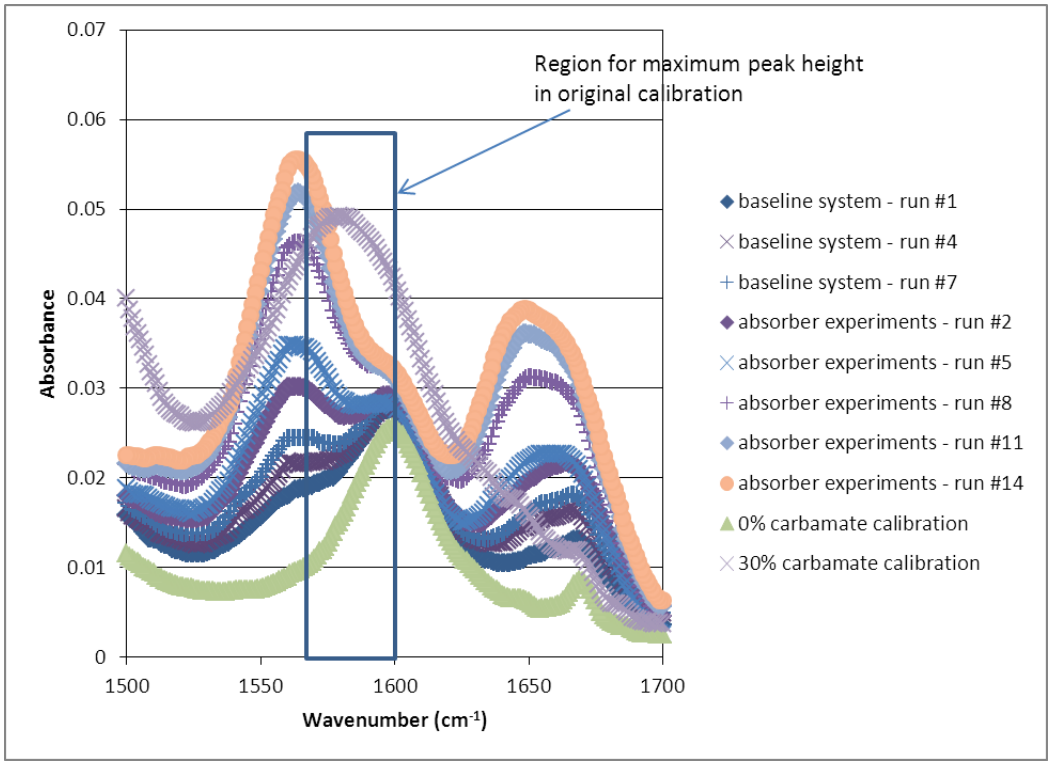

Figure 110. FTIR trace for samples exiting desorber.

To determine if the degradation of the solvent was only affecting the IR results or if the performance of the material was different due to the degradation, absorption experiments were completed using the same experimental setup that was previously used for the absorption isotherm for GAP-1m and GAP-S diluted in TEG. Aged material from the skid experiments, which was exposed to 160 °C temperatures for an extended period of time, was used for these experiments to compare to the performance of the fresh material. All experiments were completed using a partial pressure of CO_2 of 2.41 psi. Temperatures of both 30 °C and 45 °C were investigated. One experiment was also completed after the material was heated to 160 °C for one hour to ensure that all CO_2 was removed from the sample.

30 °C Experiments

The results for the experiments completed at 30 °C are provided in Figure 111. This figure shows the comparison of fresh 60% GAP-S in TEG to the material that was aged in the skid. The aged sample that was heated prior to the absorption experiment to remove CO_2 is also included. This additional heating did not significantly change the results. In both cases, the aged material showed a significantly lower CO_2 absorption than was observed for the fresh sample.

The fresh sample showed approximately 8.9% weight gain. The aged samples with and without additional heating showed % weight gains of 5.2% and 5.4%, respectively.

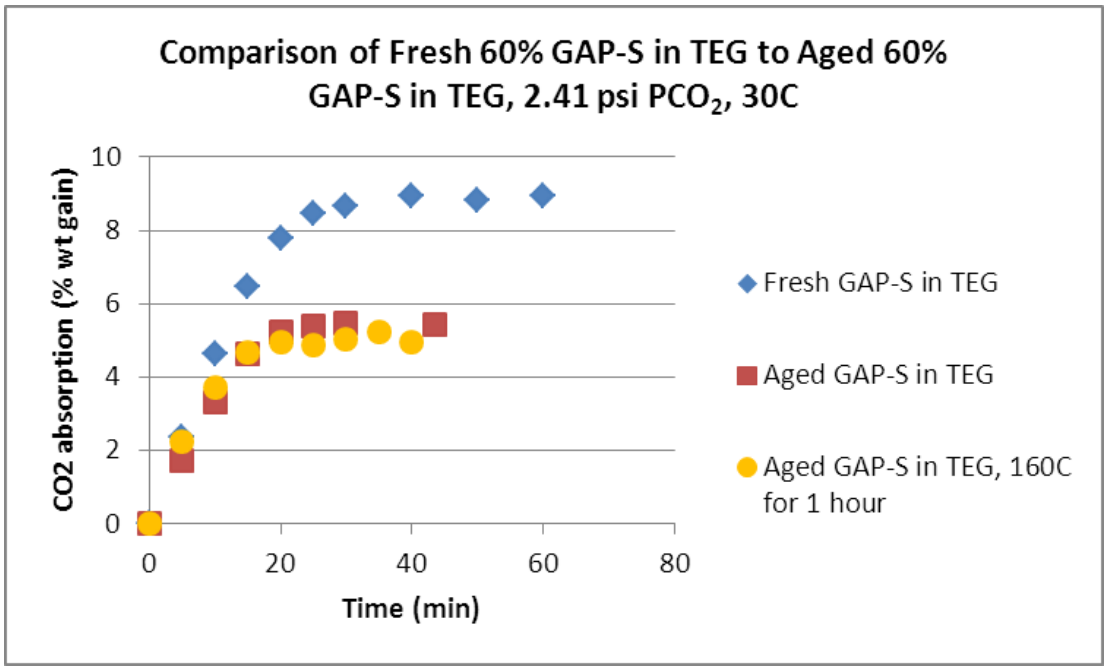

Figure 111. 30 °C absorption results for fresh vs. aged 60% GAP-S in TEG.

45 °C Experiment

The results for the experiments completed at 45 °C are provided in Figure 112. These results were consistent with the trend observed for the 30 °C experiments and showed that the CO_2 absorption was also significantly lower for the aged material when compared to the fresh sample. The fresh samples showed % weight gains of 6.6-7.4%. For the aged sample, a % weight gain of 4.9% was observed.

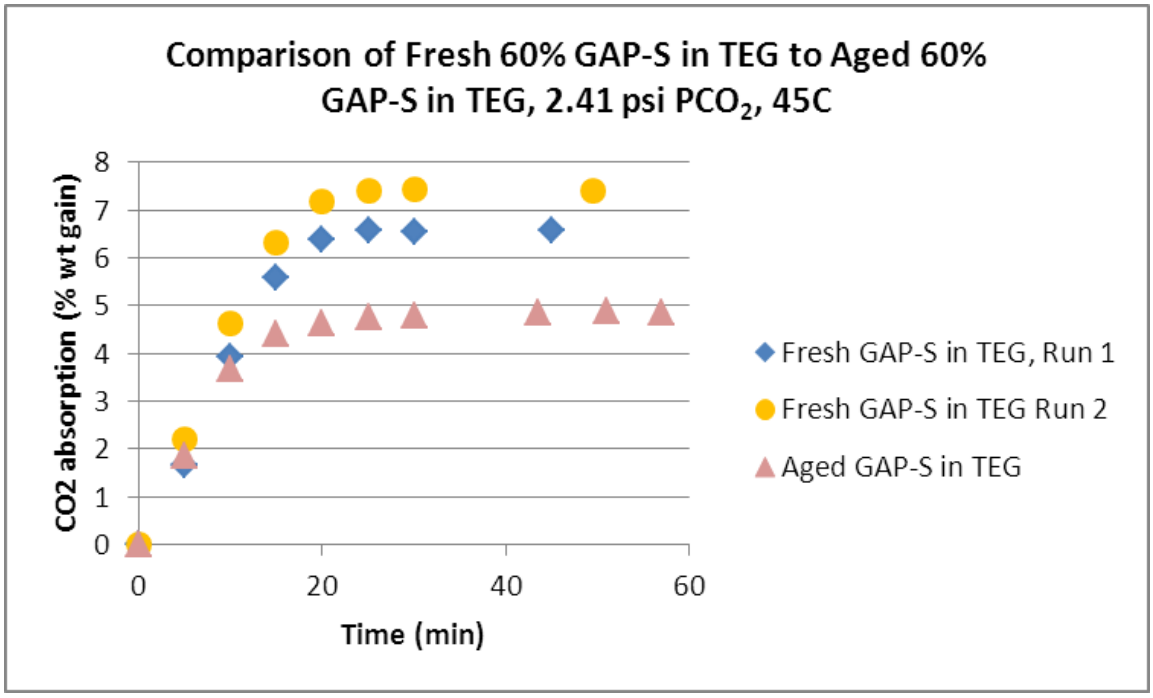

Figure 112. 45 °C absorption results for fresh vs. aged 60% GAP-S in TEG.

For the majority of the early experiments on the bench-scale system, the temperature of the desorber was set at 160 °C. To achieve 160 °C, the hot oil to the desorber heat exchanger needed to be set between 185 °C and 192 °C which would cause the solvent to encounter temperatures greater than 160 °C at the heat exchanger wall. The decision was made to replace the solvent in the system, and operate at a temperature of 140 °C in the desorber. To achieve this desorber temperature, the hot oil to the desorber heat exchanger was set between 153 °C and 155 °C, limiting the temperature the solvent would encounter. Initial FTIR results from the new solvent with the desorber temperature limited to 140 °C are shown in Figure 113. No new degradation peak was observed after ten experiments with the fresh solvent in the system.

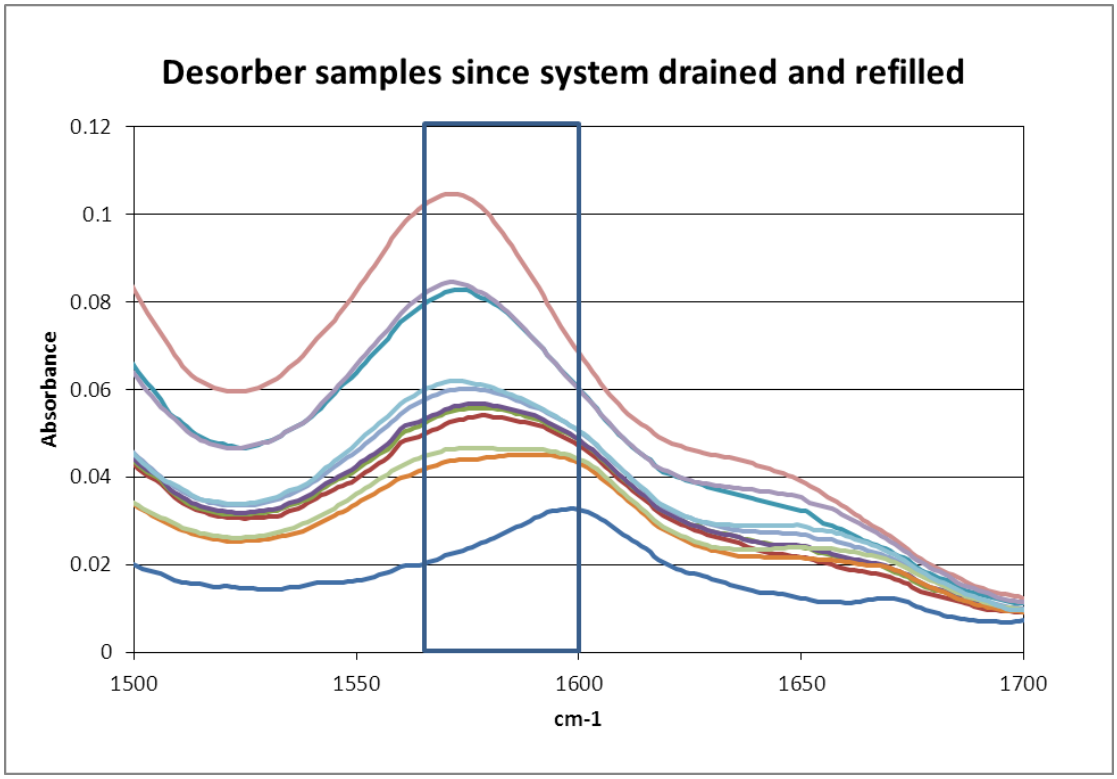

Figure 113. FTIR trace for samples exiting desorber with new solvent limited to an operating temperature of 140 °C.

Table 45 summarizes four thermal stability experiments that were completed for 60% GAP-1m in TEG. The materials were heated to 160 °C in sealed pressure vessels placed in silicone oil baths. Samples were collected every 1-3 weeks. Sample analysis was completed primarily using FT-IR, with some supplemental analyses completed with NMR and GC equipped with a thermal conductivity detector (TCD).

Table 45. Thermal stability experiments.

Material	Structure	Temperature (°C)	Analyses completed
60% GAP-1_m in TEG	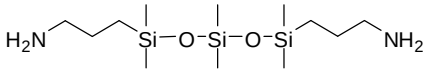	160	IR (days 7, 14, 31, 42, 56, 72 and 91) GC (days 31, 56 and 91) NMR (days 31, 56 and 91)
60% GAP-1_m in TEG + 4% water	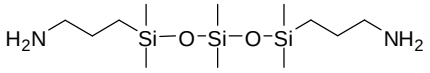	160	IR (days 7, 14, 31, 42, 56, 72 and 91) GC (days 31, 56 and 91) NMR (days 31, 56 and 91)
60% GAP-1_m in TEG + 0.04% TEMPO	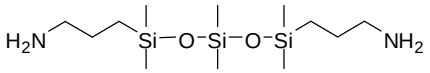	160	IR (days 7, 14, 31, 42, 56, 72 and 91) GC (days 31, 56 and 91) NMR (days 31, 56 and 91)
60% GAP-1_m in TEG + 4% water + 0.035% TEMPO	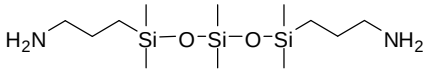	160	IR (days 7, 14, 31, 42, 56, 72 and 91) GC (days 31, 56 and 91) NMR (days 31, 56 and 91)

The purpose of the experiments was to determine if the additional peaks observed in the IR results for the aged material from the bench-scale system could be replicated under similar temperature conditions in the lab. Figures 114-117 show the IR results over time in the region of interest, with no significant changes observed in any of the experiments as of day 91. Significant changes were not observed in either the GC or the proton NMR results. Note that TEMPO is an additive to increase the thermal stability of the aminosilicone solvent.

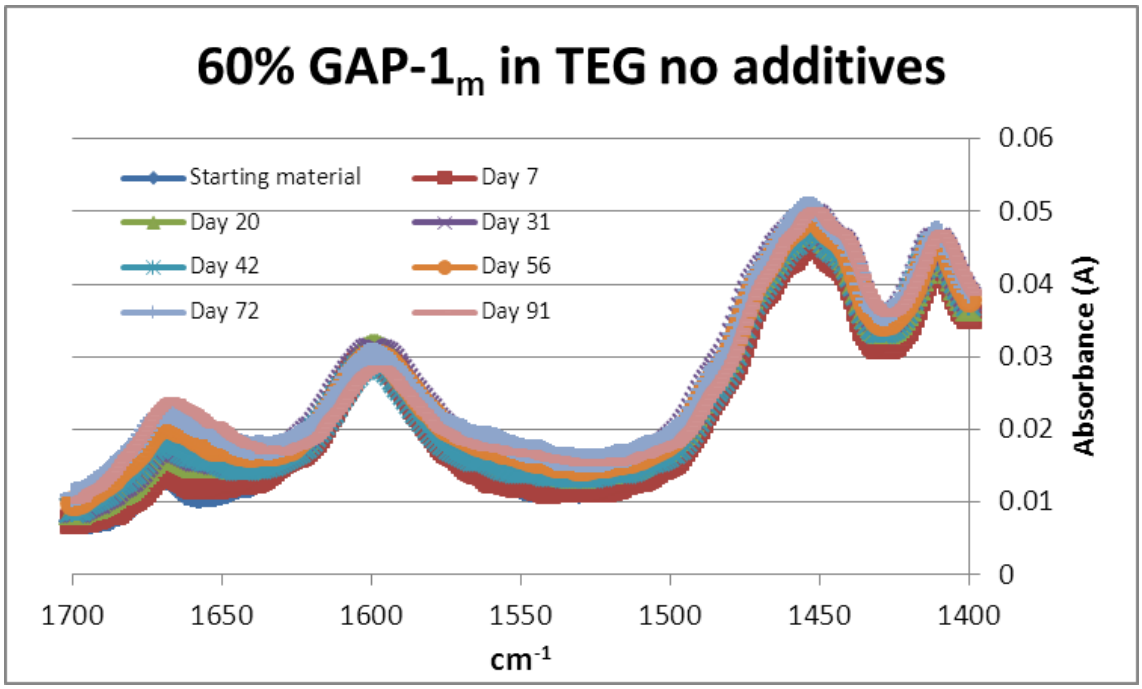

Figure 114. 60% GAP-S in TEG IR results at the end of the experiment.

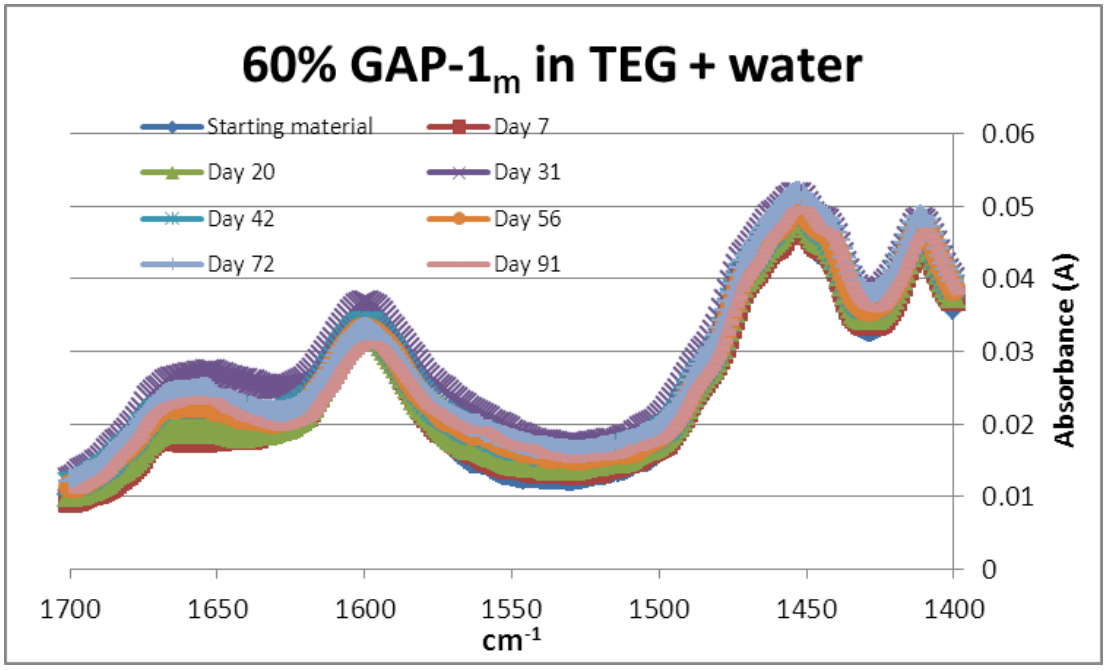

Figure 115. 60% GAP-S in TEG + water IR results at the end of the experiment.

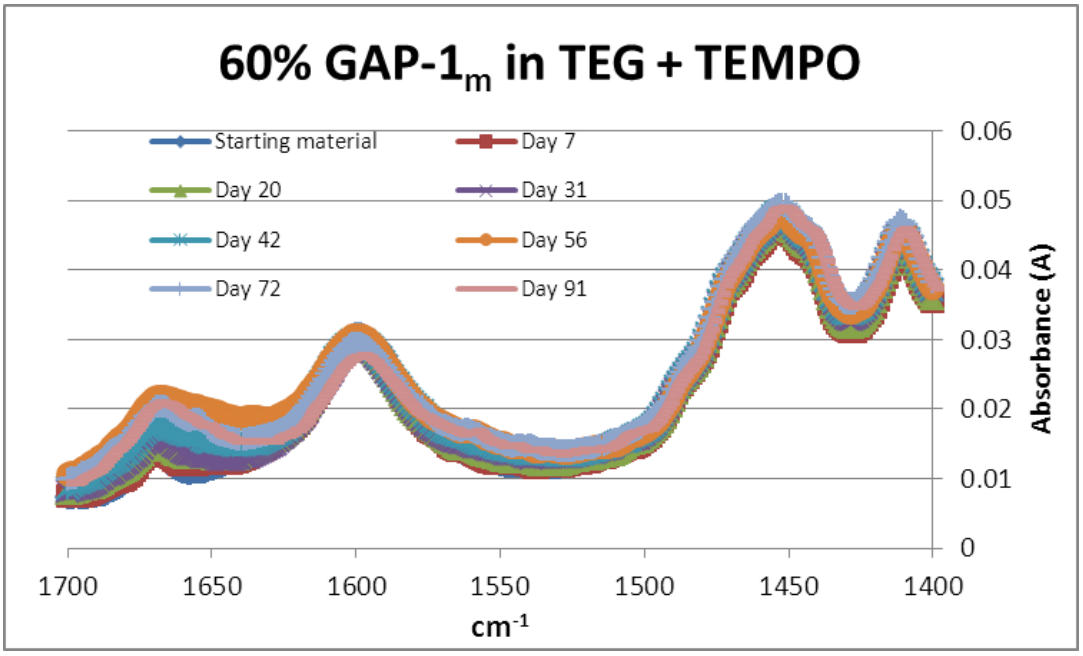

Figure 116. 60% GAP-S in TEG + TEMPO IR results at the end of the experiment.

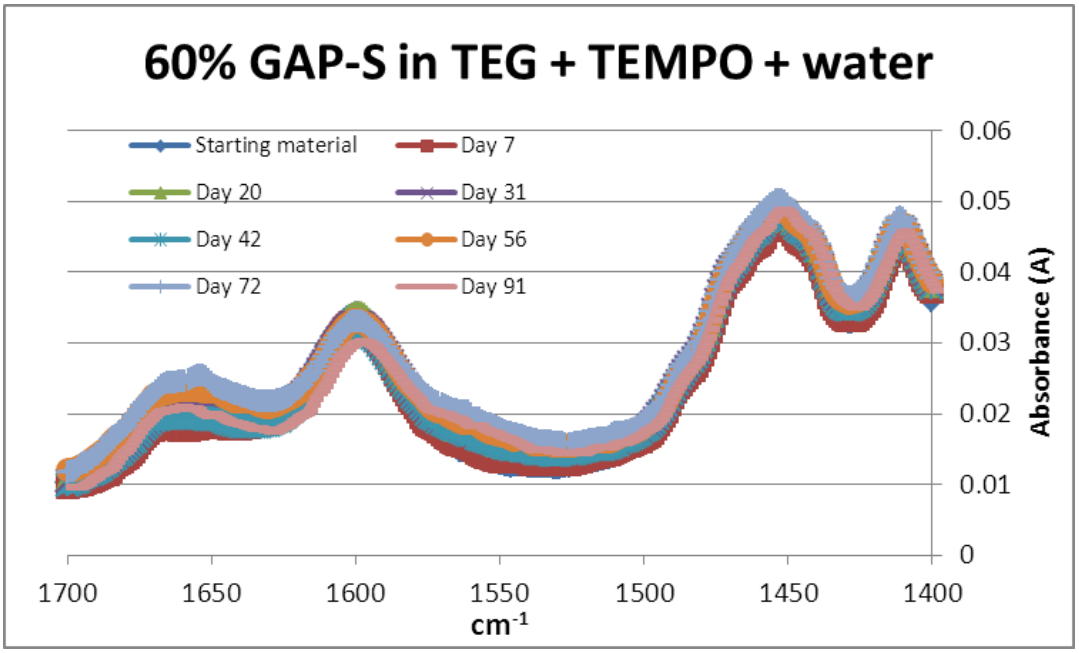

Figure 117. 60% GAP-S in TEG + TEMPO + water IR results at the end of the experiment.

CO_2 absorption experiments were also completed at the end of the experiment. The results of these tests are summarized in Table 46. These experiments were completed using the same method as that used for the absorption isotherms for this program and were only completed at 30°C. The fresh GAP-1m showed a % weight increase of 8.9%. The four treatments showed similar % weight increases, ranging from 6.65 to 7%.

Table 46. CO_2 absorption experiments.

Experiment	% weight increase in 30 °C experiments
60% GAP-1m in TEG	6.65%
60% GAP-1m in TEG + water	6.75%
60% GAP-1m in TEG + TEMPO	6.76%
60% GAP-1m in TEG + TEMPO + water	7.02%

NMR Analysis of Heat Aged GAP-1m/TEG Samples in the Presence of Water and TEMPO

NMR spectroscopy was also used to analyze the thermally treated samples of GAP-1m/TEG that had been exposed to water and/or TEMPO during heating. Figure 118 shows the proton spectra of the samples and, other than the shifting of the amine protons at ~2.8 ppm, no significant changes were noted. Silicone NMR (Figure 119) also showed little change in the composition of the samples with the exception of the amount of Si-O-TEG component (at 19 and -12 ppm) nearly absent in the water and TEMPO sample. The ratio of M:D units remained relatively constant between these experiments (2.42-2.51) indicating there was little decomposition of the siloxane chain to form branches or cross-links.

Thermally Aged (91 days) GAP-S Samples

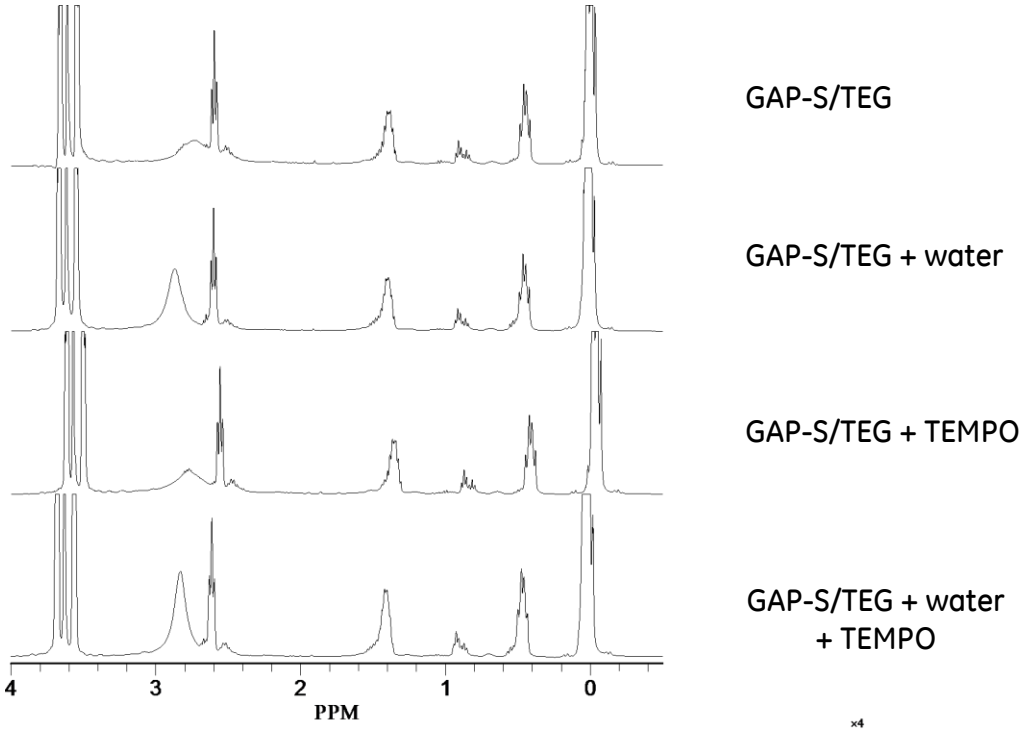

Figure 118. ^{1}H NMR of GAP-1m/TEG mixtures exposed water and/or TEMPO.

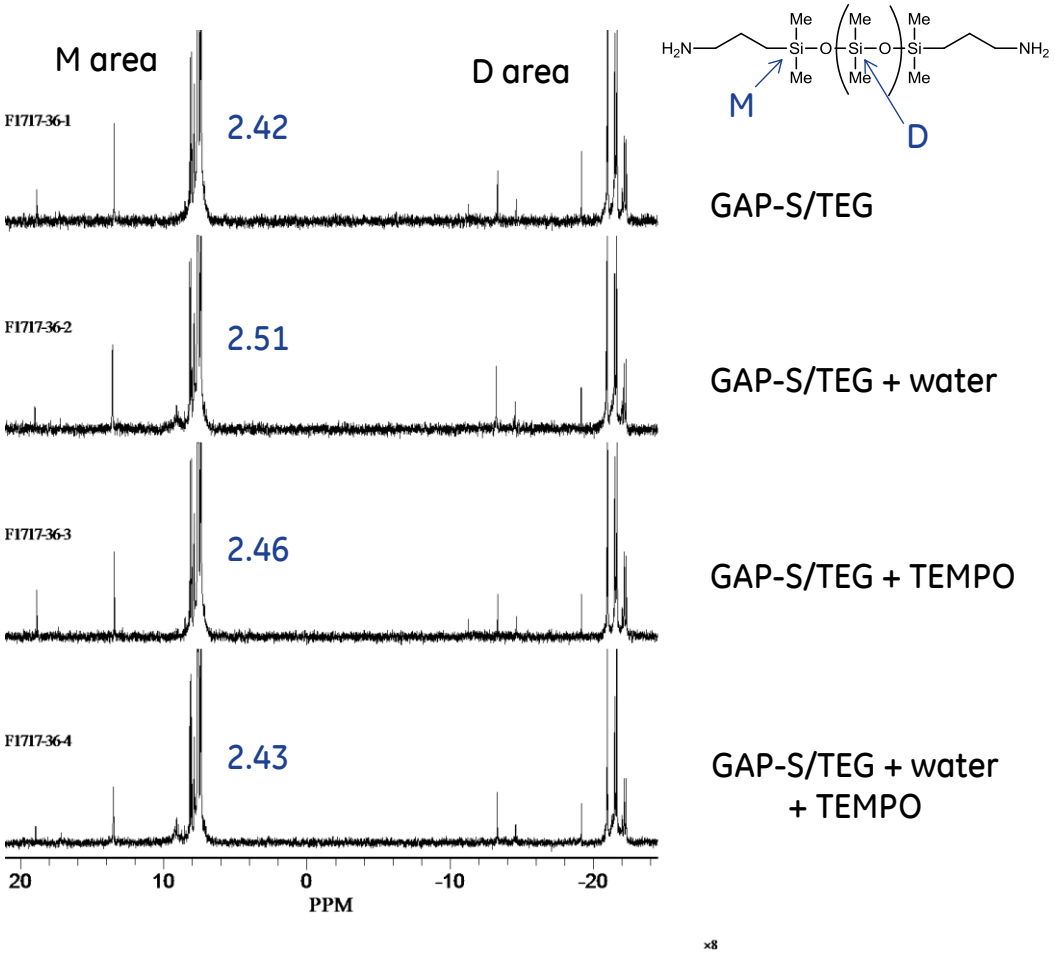

Figure 119. ^{29}Si NMR of GAP-1m/TEG mixtures exposed water and/or TEMPO.

IR Calibration

The errors in the liquid CO_2 concentration measurement highlighted the need for an improved IR calibration. Two alternative methods were investigated.

Alternative Method #1 – There is a peak between 1430 and 1500 that did not appear to be affected by the degradation peak growing into the FTIR curve. This method is similar to the original method in that the curve is corrected for the baseline, and then the maximum absorbance between 1430 and 1500 cm^{-1} is found. The calibration curve is shown in Figure 120.

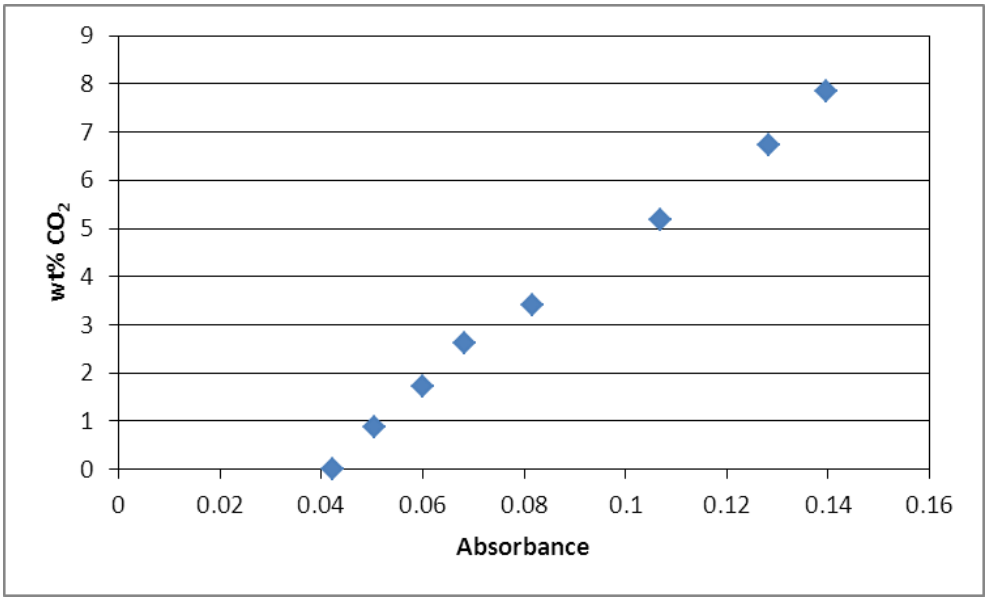

Figure 120. FTIR calibration curve based on peak between 1430 and 1500 cm^{-1}.

Alternative Method #2 – The region in the IR spectrum between 1500 and 1700 cm^{-1} was fit to 6 Lorentzian curves centered at 1426, 1558, 1570, 1599, 1645, and 1670 cm^{-1}. It was found that the area under the Lorentzian curve centered at 1570 cm^{-1} correlated strongly with the wt% of CO_2 in solution, as shown in Figure 121.

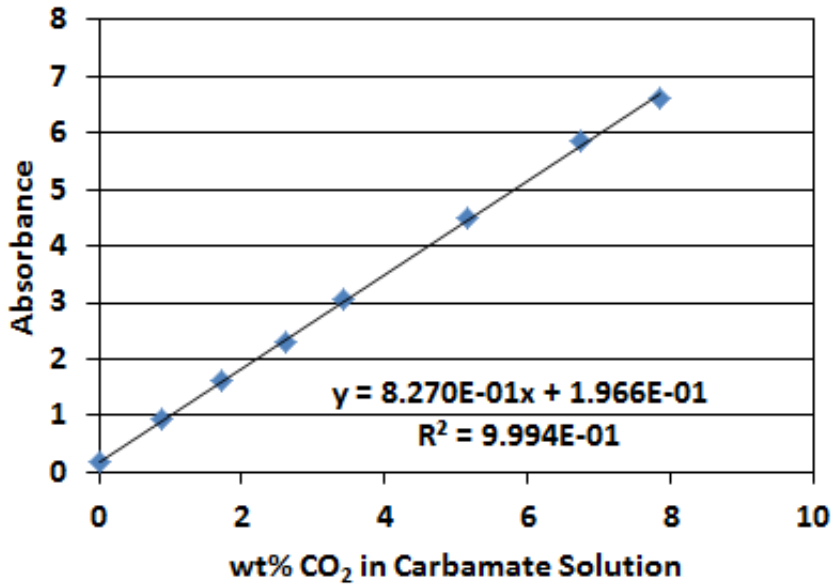

Figure 121. Absorbance for IR band at 1570 cm^{-1} with increasing wt% of CO_2 in solution.

Comparison of Methods

A comparison of the three different analysis methods is shown in Figures 122 and 123. Figure 122 gives examples of this comparison for the old solvent that had degraded in the system, and Figure 123 gives examples of this comparison for the new solvent that had not yet degraded.

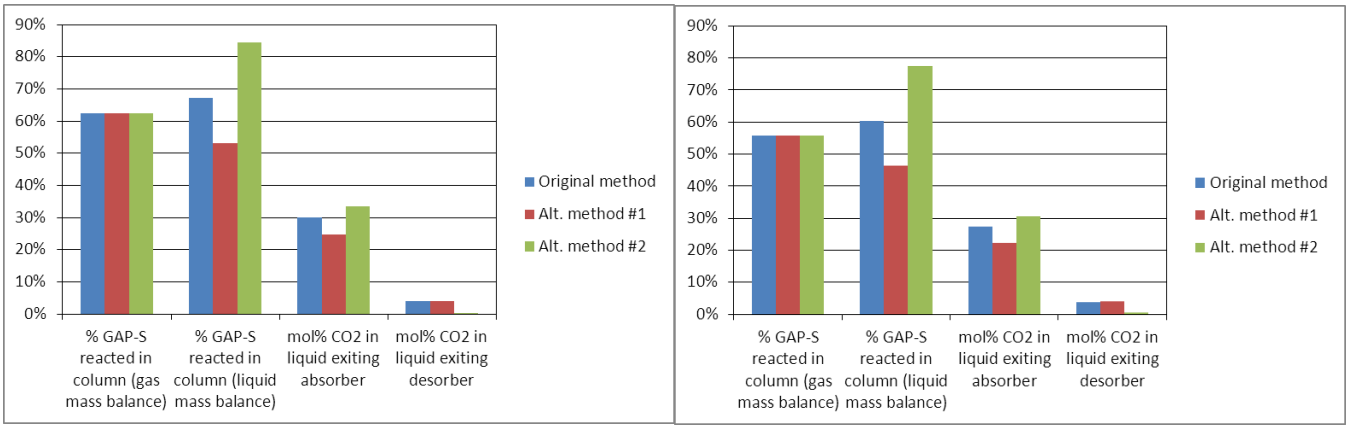

Figure 122. FTIR method comparison for degraded solvent from two different samples.

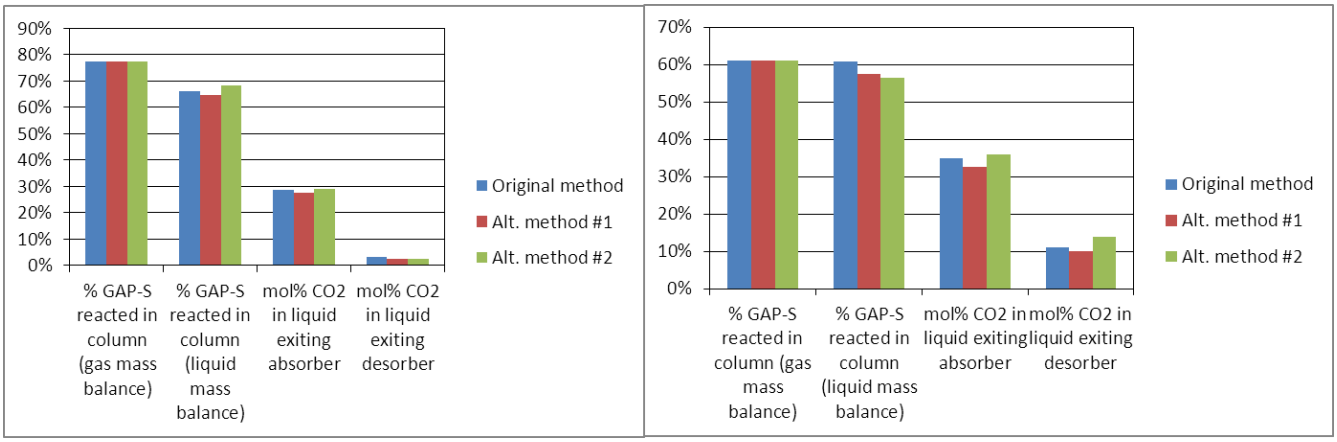

Figure 123. FTIR method comparison for fresh solvent from two different samples.

For the analysis with the degraded solvent, the analysis method appears to significantly affect the results. However, for the analysis with the fresh solvent, all analysis methods give similar results.

Analysis of Solvent Decomposition and Contaminants on Bench-Scale System Performance

Analyses of aged samples from the bench-scale unit were initiated. Given the large number of components present in the GAP-1m/TEG mixture, an analytical technique that produced a 2-dimensional contour plot of the species was used. This process used two GC (gas chromatography) columns to effect separation based on both boiling point and polarity. Mass spectrometry (MS) was used to determine the molecular weight of the fragments produced in the MS.

Figure 124 shows the 2-D GC plot of the starting GAP-1m/TEG mixture prior to use. Some of the smearing of the peaks is due to severe column overload so that very minor components could be seen. The largest signals are due to the TEG co-solvent and the homologous GAP-X series. For GAP-0, one can see a small side peak that is due to the β-isomer. Generally, all the β and γ isomers appeared as a single peak. Also seen in the chromatogram are a series of peaks labeled C-D3, C-D4, etc. These are the cyclic dimethylsiloxanes shown in Figure 125. These were formed in the GAP-1m manufacturing process.

Also visible in the chromatograph are several small peaks that have been circled. They are estimated to exist at the ppm level and were not identified. By MS analysis, the peak directly below the TEG signal appeared to have elements of ethylene oxide (EO) present and was likely a TEG derivative. Exact identification of the unidentified materials is difficult as the MS data does not generally give a molecular ion.

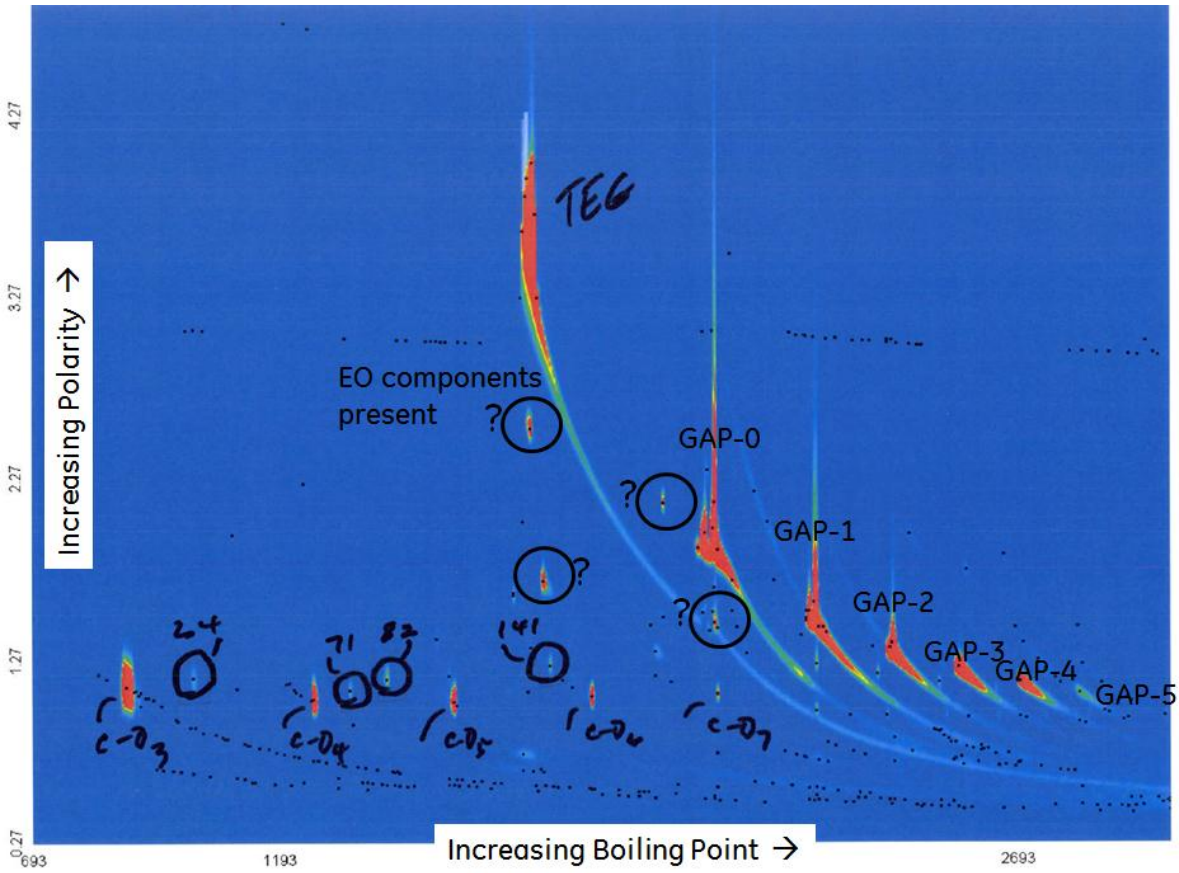

Figure 124. 2-D GC contour plot of starting solvent mixture.

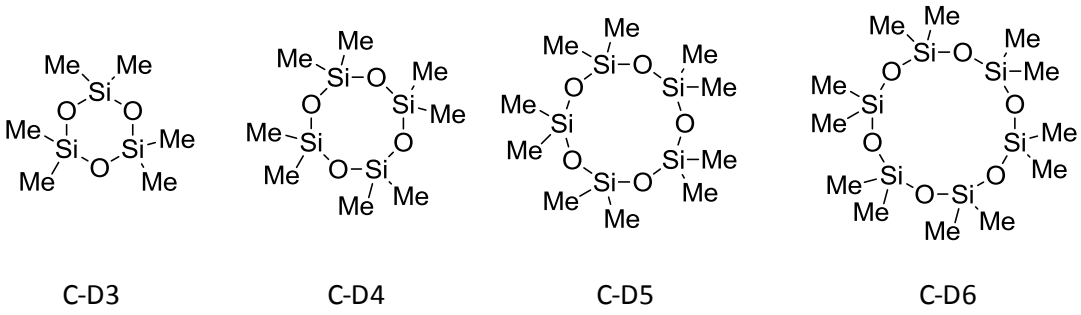

Figure 125. Cyclic dimethylsiloxanes.

After recirculation of the GAP-1m/TEG solvent mixture through the bench-scale reactor for approximately 1 month, a sample was pulled from the lean storage tank and subjected to the same analytical procedure. Figure 126 shows that several new peaks were present in the chromatogram. A long streak denoted as 259 was tentatively identified as the cyclic compound

shown in the figure. This material could have formed via a back-biting mechanism as shown in Equation 3.

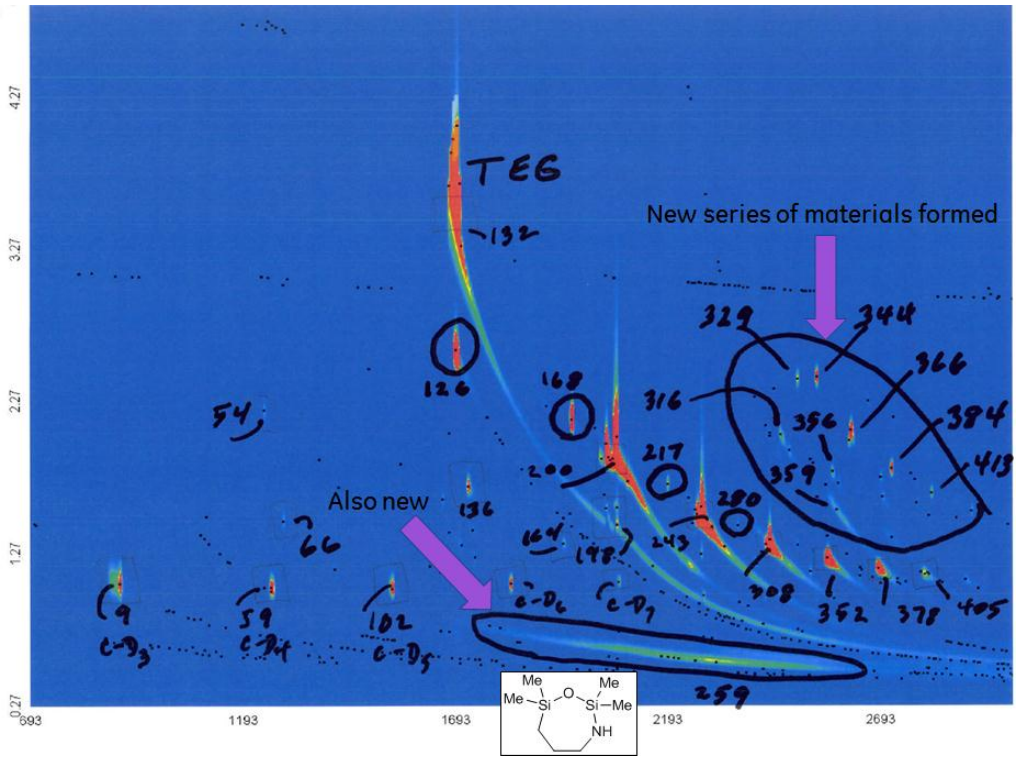

Figure 126. 2-D GC contour plot of aged (1 month) solvent mixture.

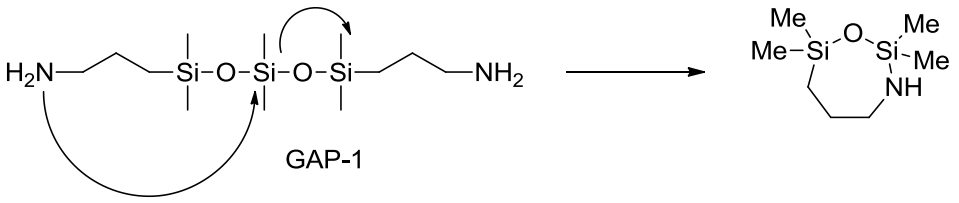

(3)

Also seen was another series of small peaks that are circles in Figure 126. While not identified yet, they appear to be a related series of compounds that have some characteristics of both TEG and the GAP materials. This tentative identification is supported by ^{29}Si NMR data seen in Figure 127.

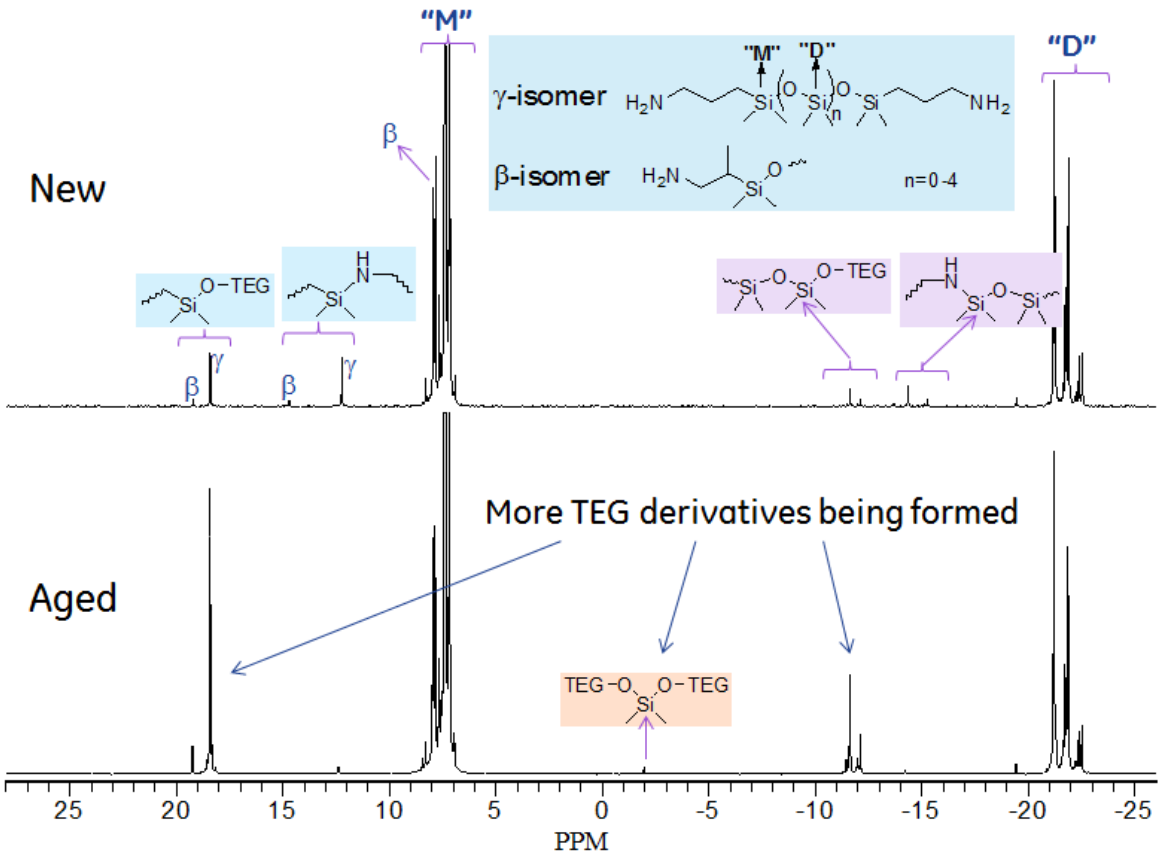

Figure 127. ^{29}Si NMR Spectra of new and aged GAP-1m/TEG solvent mixtures.

For the new sample it was possible to differentiate between the β and γ-isomers of the aminopropyl group on the GAP substrate. However, more interesting was the increase in peaks assigned to Si atoms that were attached to an ethyleneoxy unit. The arrows point to the increased abundance of the silicone-TEG adducts in the aged sample. This was expected to occur to some degree as the hydroxyl end groups of TEG can participate in exchange reactions with Si-O-Si bonds as shown in Equation 4. However, these side-products are also capable of reacting with CO_2 and do not diminish the ability of the solvent to capture CO_2.

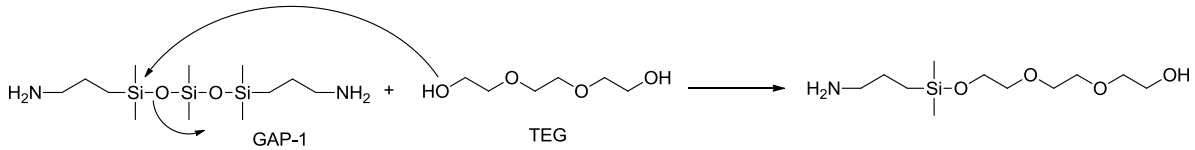

(4)

Also apparent is a small amount of Si-N linkages which can be explained by amine "back-biting" illustrated in Equation 3.

Effect of NO on System Performance

The effect of NO on the CO_2-capture efficiency of the aminosilicone solvent system was studied using the bench-scale system. Five experiments were performed using bottled gases, mixing 16 vol% CO_2, 89 ppm (by vol) NO, and the balance N_2. The results of these experiments were compared to a set of baseline experiments having the same total liquid and gas flow rates, CO_2 inlet gas concentration, absorber inlet temperatures, and desorber temperature, pressure, and mixing conditions. Figure 128 shows that there is no statistically significant difference in the amount of CO_2 captured from the gas stream between the baseline and NO experiments.

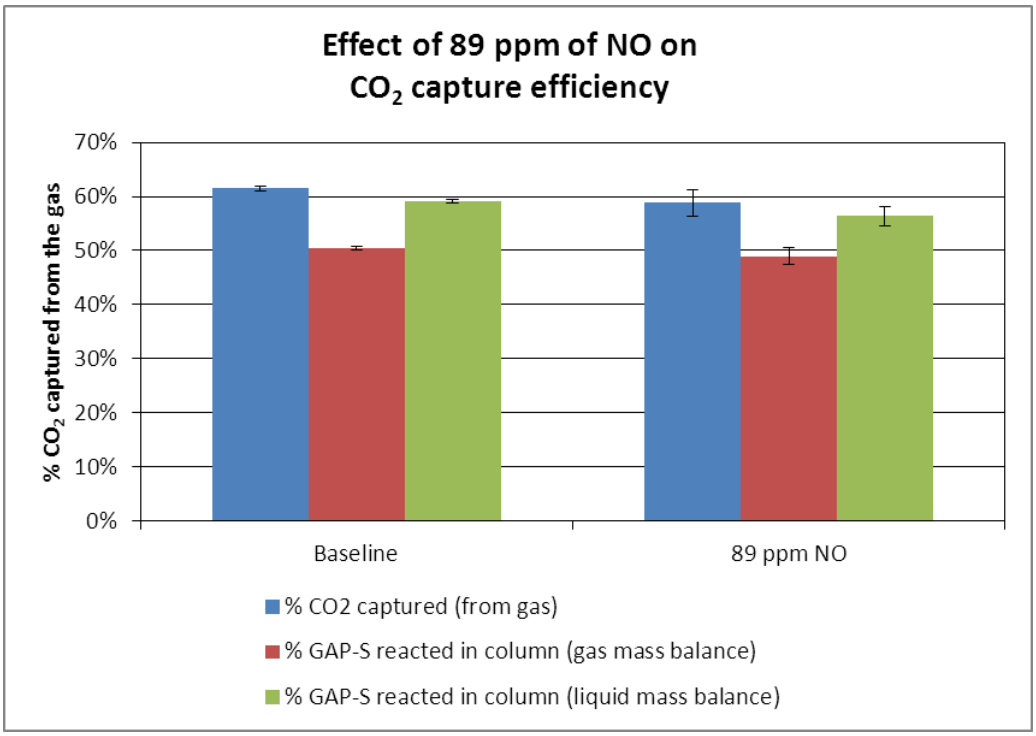

Figure 128. Effect of 89 ppm of NO on CO_2 capture efficiency.

The equilibrium uptake of CO_2 in the GAP-1m/TEG before and after it was exposed to NO in the system was measured using the same experimental setup that was previously used for the absorption isotherms for GAP-1m diluted in TEG. These experiments were completed using a partial pressure of CO_2 of 2.41 psi and temperatures of both 30 °C and 45 °C were investigated. Table 47 summarizes the results. No effect of NO exposure on equilibrium CO_2 uptake by the solvent was observed.

Table 47. Equilibrium weight gain of 60/40 GAP-1m/TEG upon exposure to CO_2 before and after exposure to NO.

	% weight gain at 30 °C upon exposure to CO_2 (P_{CO2} = 2.41 psi)	% weight gain at 45 °C upon exposure to CO_2 (P_{CO2} = 2.41 psi)
Fresh sample	8.9%	6.6-7.4%
Aged sample not exposed to NO	7.7%	7.6%
Aged sample exposed to NO	7.6%	7%

Effect of SO_2 on System Performance

The effect of SO_2 on the CO_2-capture efficiency of the aminosilicone solvent system was studied using the bench-scale system. Five experiments were performed using bottled gases, mixing 16 vol% CO_2, 45 ppm (by vol) SO_2, and the balance N_2. The results of these experiments were compared to a set of baseline experiments having the same total liquid and gas flowrates, CO_2 inlet gas concentration, absorber inlet temperature, and desorber temperature, pressure, and mixing conditions. Figure 129 shows that exposure to SO_2 significantly decreases the CO_2 capture efficiency of the solvent.

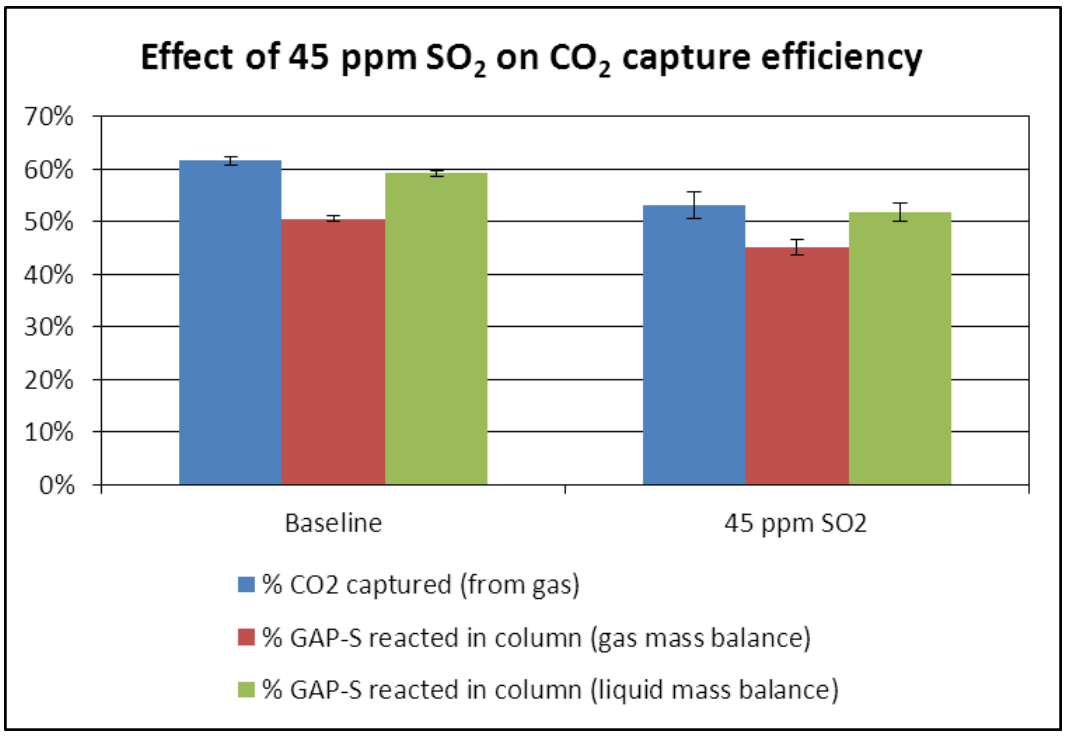

Figure 129. Effect of 45 ppm of SO_2 on CO_2 capture efficiency.

Figure 130 shows the CO_2 capture efficiency as a function of experiment number. The capture efficiency appears to drop rapidly compared to the baseline with the first SO_2 experiment and then gradually level off. From the SO_2 analyzer, all of the SO_2 fed to the bottom of the column was absorbed in the column, and no measureable amount was detected leaving the desorber. Figure 131 compares the actual drop in performance from the baseline with the calculated loss in available GAP-1m in the system due to complete irreversible absorption of SO_2 into the solvent. The actual loss in performance is much greater than what can be explained from SO_2 absorption alone.

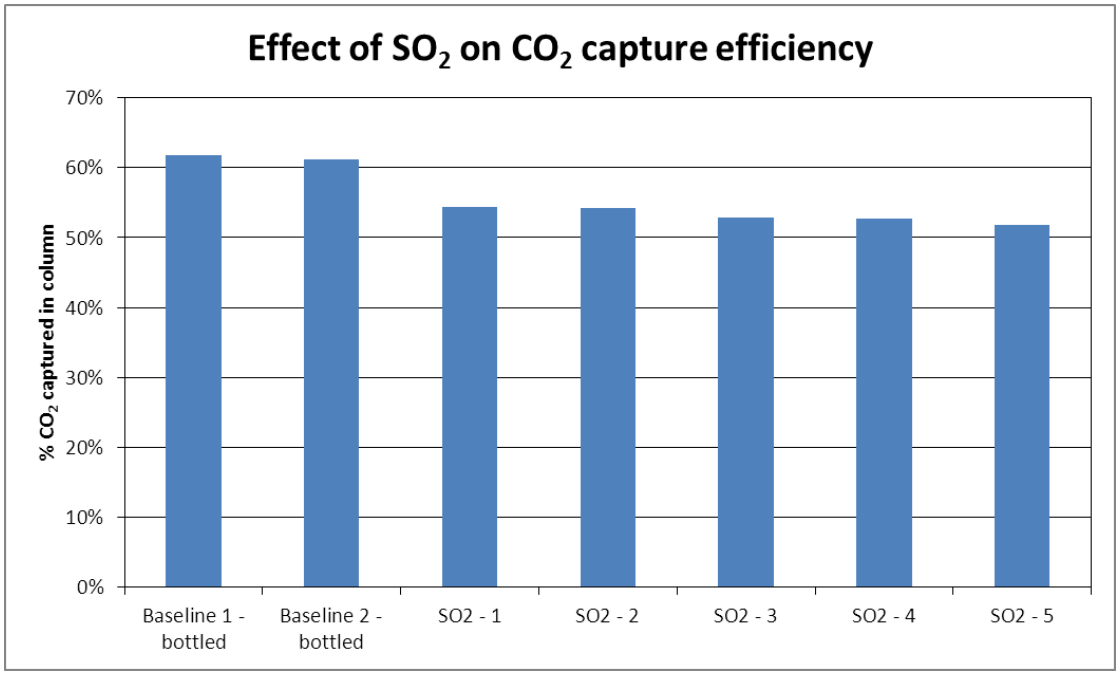

Figure 130. Effect of 45 ppm of SO_2 on CO_2 capture efficiency.

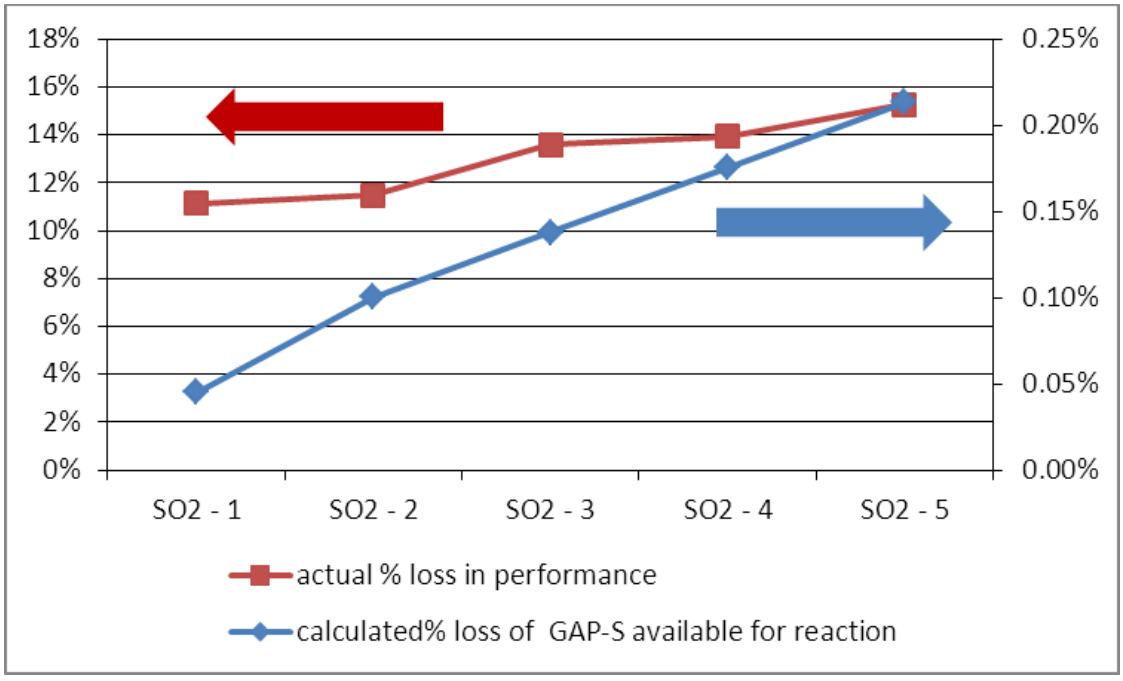

Figure 131. Comparison of actual loss of performance (calculated from % CO_2 captured from gas) and calculated % loss GAP-1m available for reaction assuming all SO_2 introduced to the system reacts irreversibly with GAP-1m.

The loss in performance was confirmed by measuring the equilibrium uptake of CO_2 in the GAP-1m/TEG before and after it was exposed to SO_2 in the system after all experiments with SO_2 were completed (there were three additional SO_2 experiments completed at a desorber temperature of 150 °C and at increased liquid flow rates). The equilibrium absorption was measured using the same experimental setup that was previously used for the absorption isotherms for GAP-1m diluted in TEG. These experiments were completed using a partial pressure of CO_2 of 2.41 psi and temperatures of both 30 °C and 45 °C were investigated. Table 48 summarizes the results. As expected, the equilibrium CO_2 uptake decreased significantly upon exposure to SO_2, between 25 and 30%.

Table 48. Equilibrium weight gain of 60/40 GAP-1m/TEG upon exposure to CO_2 before and after exposure to SO_2.

	% weight gain at 30 °C upon exposure to CO_2 (P_{CO2} = 2.41 psi)	% weight gain at 45 °C upon exposure to CO_2 (P_{CO2} = 2.41 psi)
Fresh sample	8.9%	6.6-7.4%
Aged sample not exposed to SO_2	7.7%	7.6%
Aged sample exposed to SO_2	5-5.8%	6-6.3%

The effect of SO_2 on the CO_2 capture efficiency of the aminosilicone solvent system was studied further. It was shown above that in the presence of SO_2, the CO_2 capture efficiency in the absorber first appears to decrease and then appears to level off, as shown in Figure 132 (data set #1). For the second set of data shown in Figure 132, six experiments were performed; four using bottled gases (red data points) and two using exhaust gas from the generator (green data points). For each experiment, the target inlet gas concentration of 16 vol% CO_2 and 45 ppm (by vol) SO_2 was achieved by mixing either bottled nitrogen (for the bottled gas experiments) or exhaust gas (for the generator experiments) with enough CO_2 and SO_2 added to create a gas stream with the desired composition. The results of these experiments were compared to a set of baseline experiments having the same total liquid and gas flow rates, CO_2 inlet gas concentration, absorber inlet temperatures, and desorber temperature, pressure, and mixing conditions. Figure 132 shows that exposure to SO_2 significantly decreases the CO_2 capture efficiency of the solvent. Data set #2 appears to show a continued decrease upon exposure to SO_2. Both bottled gas and exhaust gas were studied for data set #2 to determine if the presence of water played a significant role in how the SO_2 affected the performance of the system. From this limited data set, it does not appear that the performance of the system is different with

SO_2 and water together in the inlet gas compared to SO_2 alone. However, the water concentration in the inlet gas for the higher water experiments (using the generator exhaust gas), were around 1.2 – 1.3 mol%, and so the effect of higher water concentrations in the presence of SO_2 remains unknown.

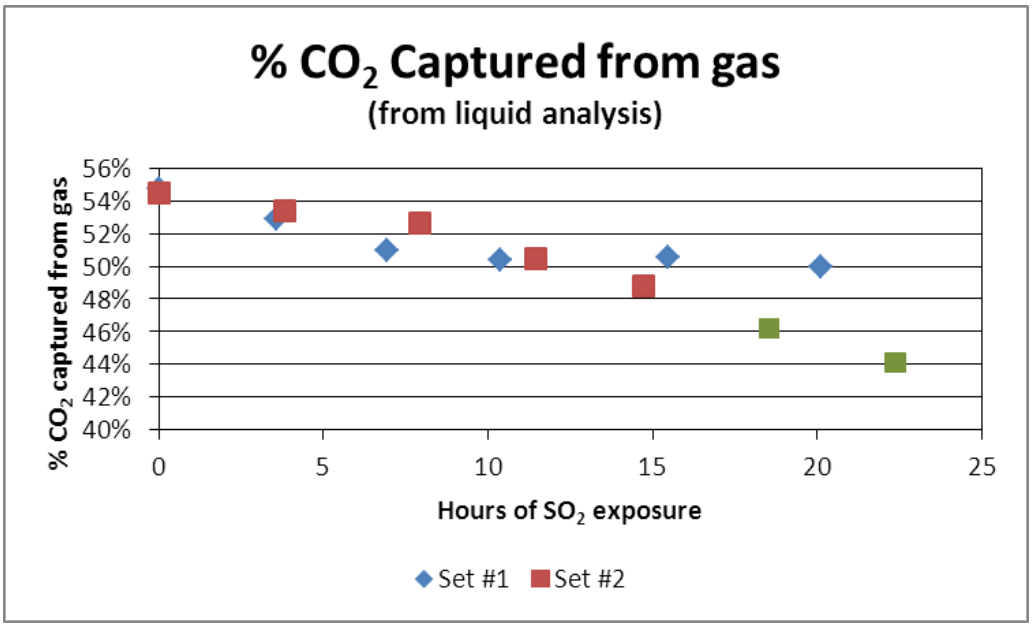

Figure 132. Effect of 45 ppm of SO_2 on CO_2 capture efficiency. For Set #2, the red points correspond to experiments using bottled gas, while the green points correspond to experiments using the exhaust from the diesel generator.

It should be noted that the CO_2 capture efficiencies reported in Figure 132 were calculated using the concentrations of GAP-1m carbamate in the liquid phase as determined by the height of the FTIR peak at approximately 1450 cm^{-1}. Previously reported CO_2 capture efficiencies were calculated using gas phase data from the CO_2 analyzer, and as a result, there may be small differences between the two sets of reported data due to errors associated with each analysis technique.

<u>Exposure of GAP-1m/TEG to NO and SO_2</u>

Further analysis of GAP-1m/TEG samples that were exposed to NO and SO_2 was undertaken with the 2D GCxGC MS method. Figure 133 shows the chromatogram of a freshly prepared sample of GAP-1m/TEG. As before, the TEG was a large peak smeared over a large area due to

its adherence to the chromatography medium. The GAP-1m homologues manifest themselves as a series of peaks that represent the GAP-0, GAP-1, GAP-2, etc. series which also, in some cases show the β vs γ isomer content.

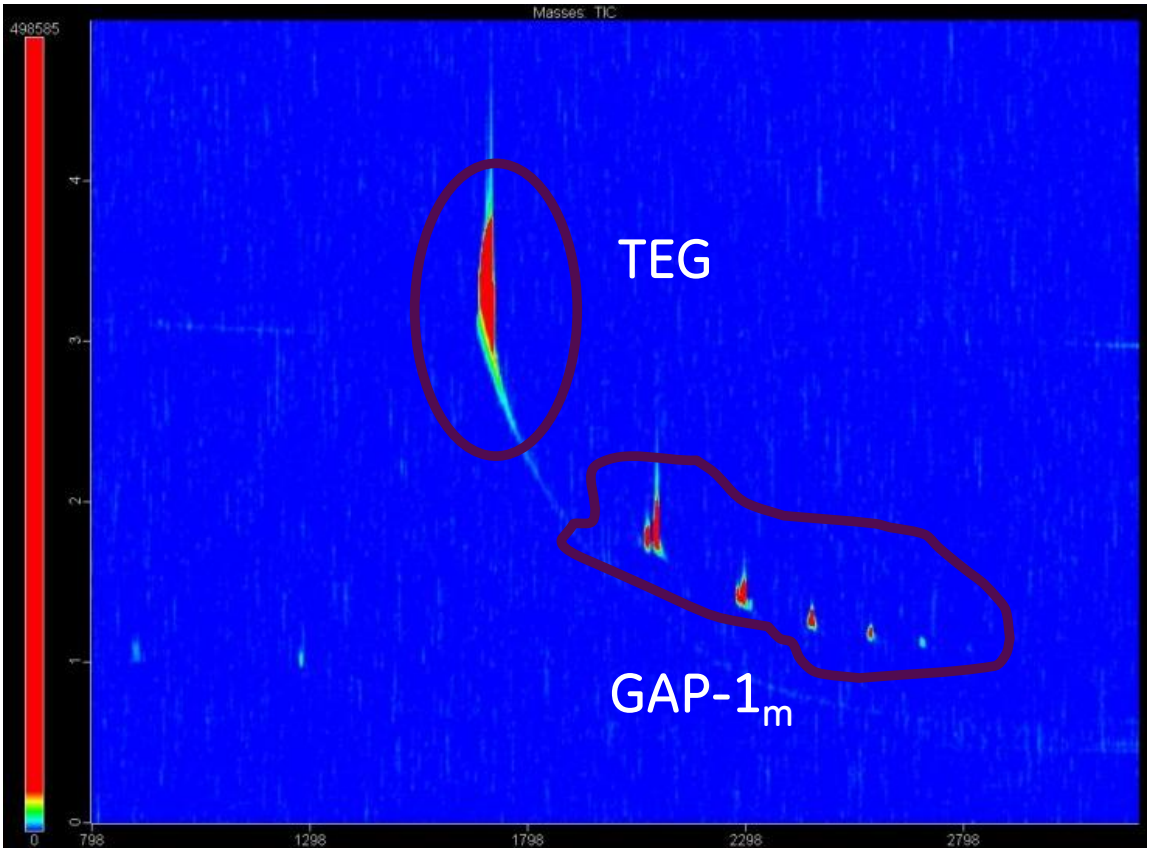

Figure 133. GCxGC chromatogram of GAP-1m/TEG mixture.

Analysis of the GAP-1m/TEG mixture exposed to NO for 18 hours shows very little change in the composition as seen by this technique (Figure 134). This is consistent with CO_2 uptake results discussed earlier. However, exposure of GAP-1m/TEG to SO_2 for 32 hours resulted in a mixture that contained a number of small, but observable by-products as seen in Figure 135. Figure 136 is the expanded version of Figure 135, with selected ions of 30 and 73 mass units indicative of siloxane-containing fragments. While a large number of small peaks appear, comparison with a chromatogram of aged GAP-1m/TEG shows that all but 2 peaks are present in the non-SO_2 treated GAP-1m/TEG material. These peaks are circled in Figure 135. The identity of these new peaks is unknown at this time.

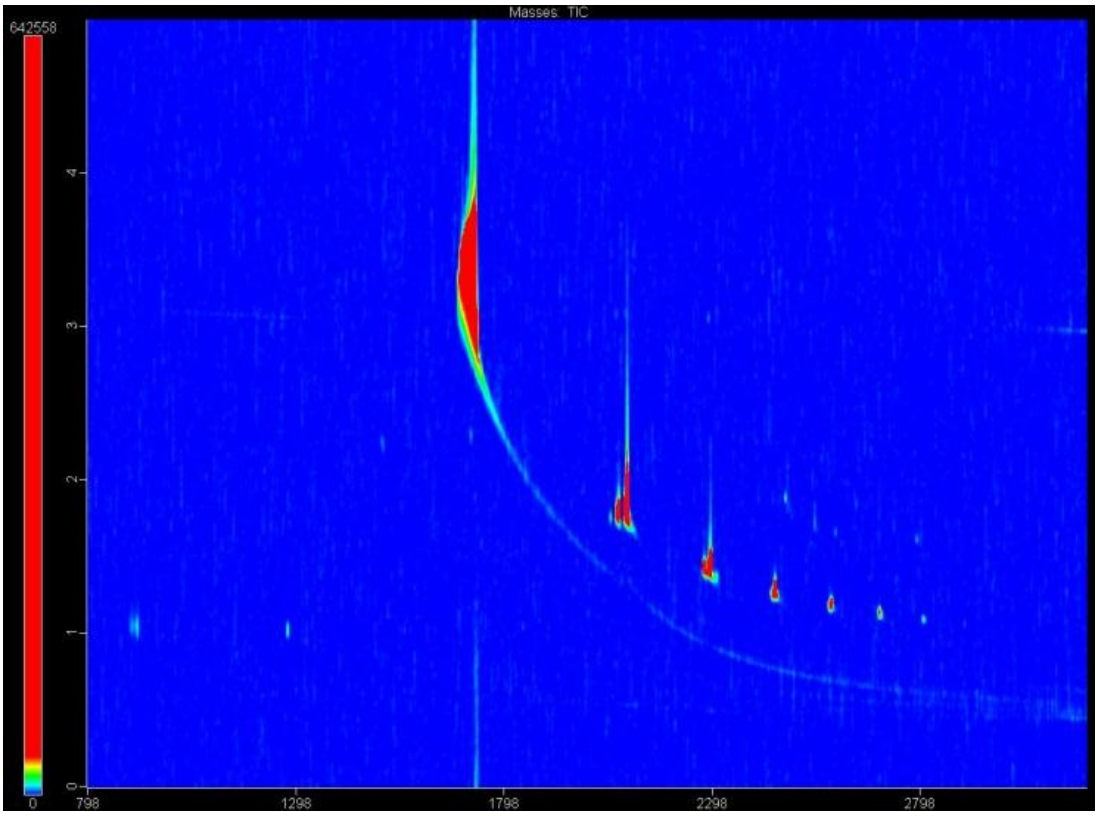

Figure 134. GCxGC chromatogram of GAP-1m/TEG mixture after NO exposure.

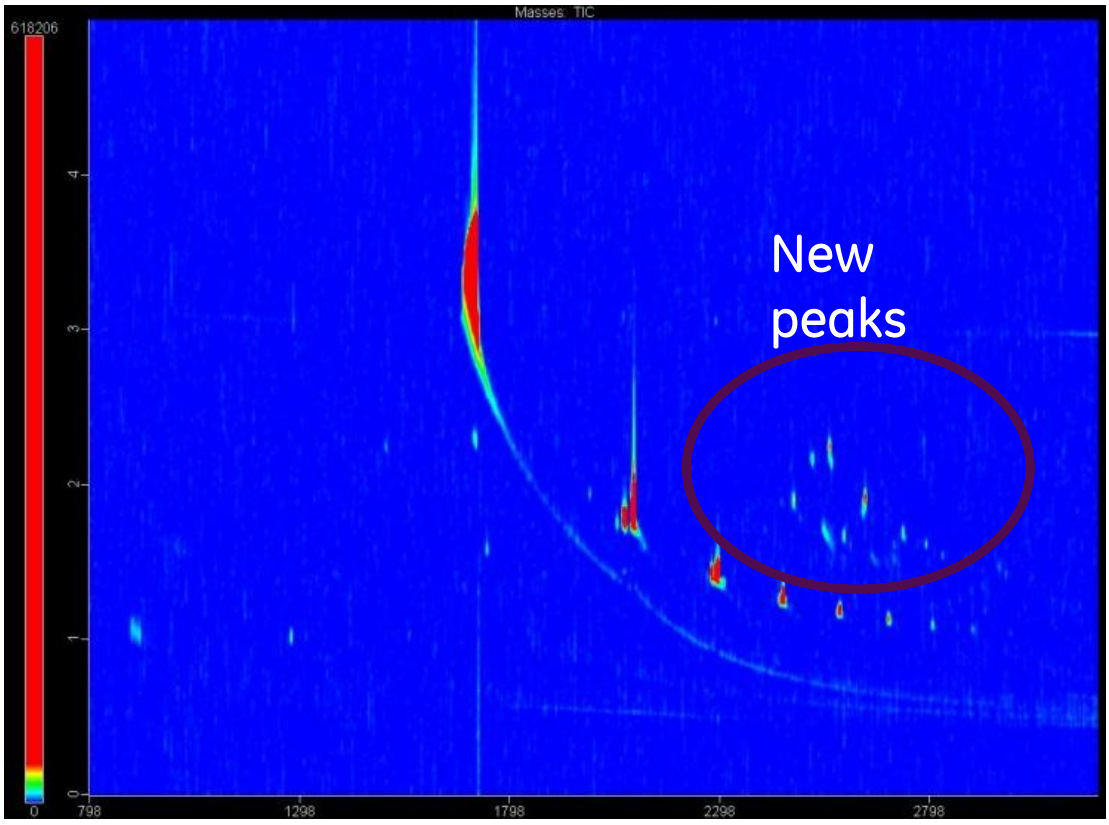

Figure 135. GCxGC chromatogram of GAP-1m/TEG mixture after SO_2 exposure.

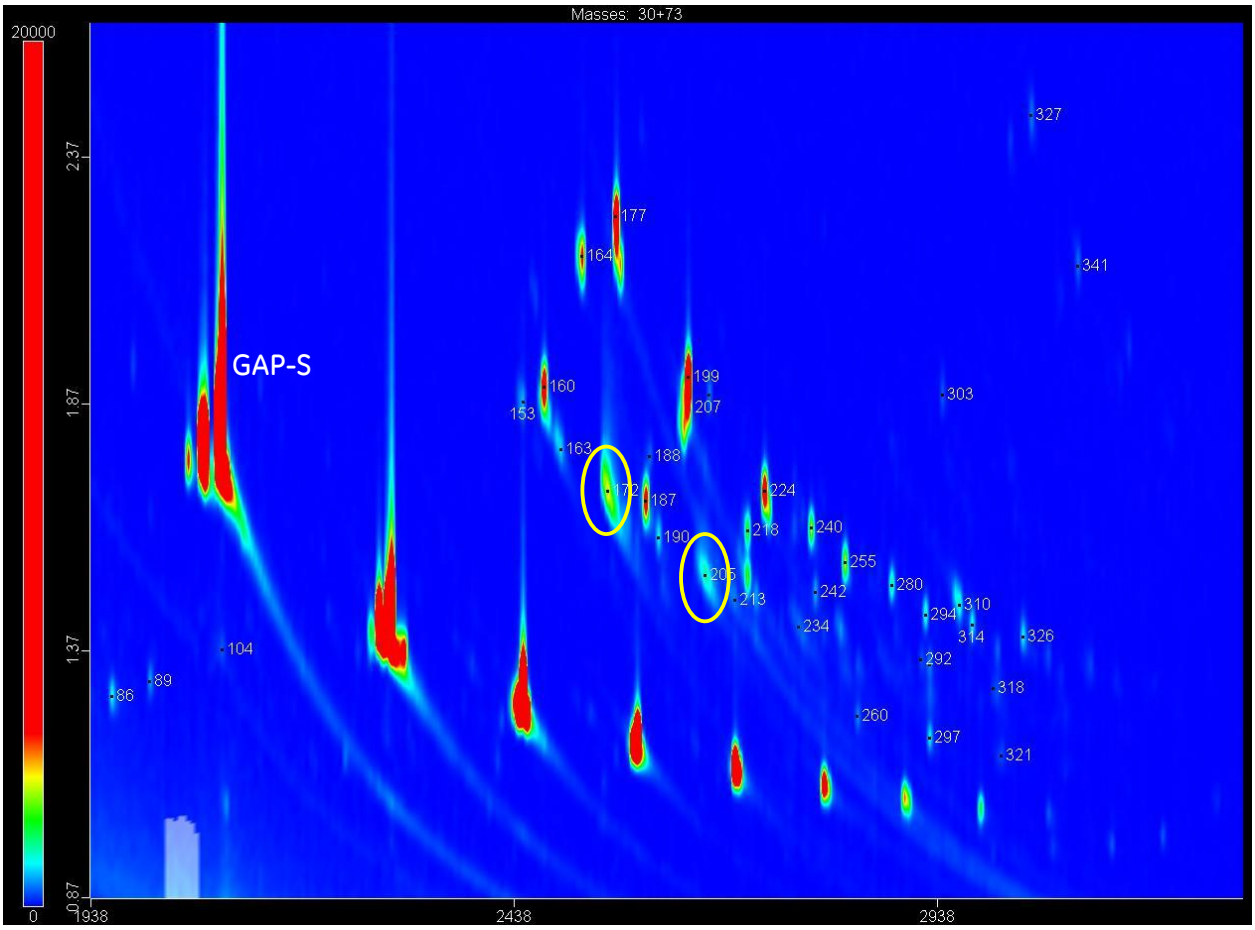

Figure 136. Expanded chromatogram of GAP-1m/TEG mixture after SO_2 exposure.

The same samples analyzed by NMR were not as informative. Figures 137 and 138 are the ^{1}H and ^{13}C NMR spectra of the unaged GAP-1m/TEG mixture and those treated with NO and SO_2. The ^{1}H NMR showed little discernible difference between the unaged mixture and the NO treated sample, the same result seen from the 2D GCxGC data. The SO_2 treated sample also showed little difference. The ^{13}C NMR data did show extra peaks emerging after treatment but were unable to be assigned.

Figure 139 shows the ^{29}Si NMR spectra associated with these samples. The only noticeable differences were the increase in TEG-reacted side-products and some amine backbiting as discussed in previous reports.

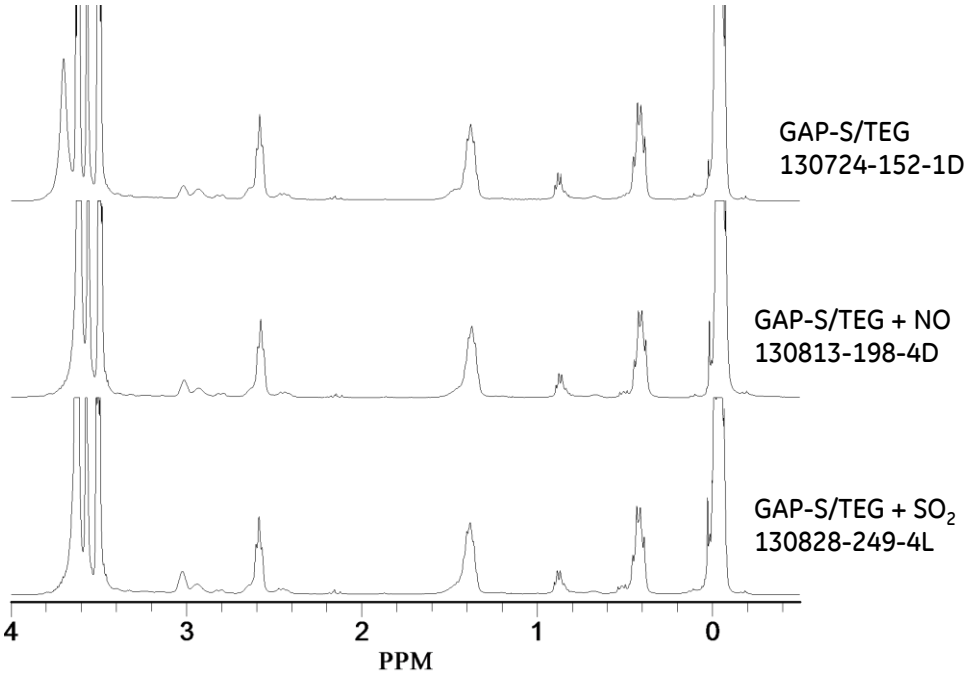

Figure 137. ^{1}H NMR of GAP-1m/TEG mixtures exposed to NO and SO_2.

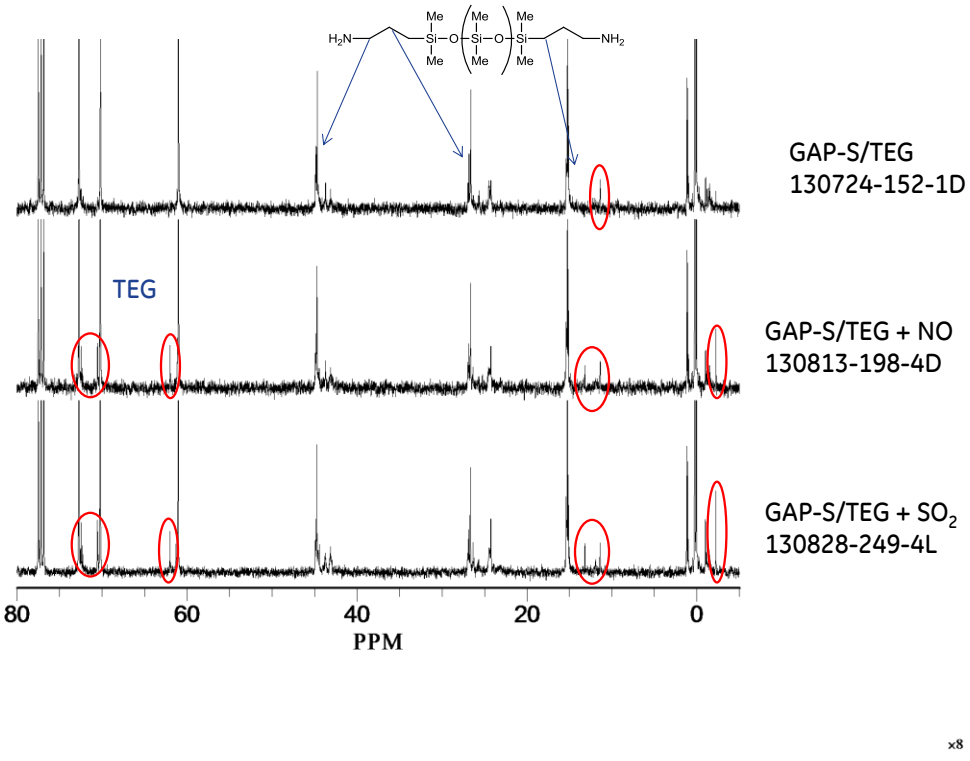

Figure 138. ^{13}C NMR of GAP-1m/TEG mixtures exposed to NO and SO_2.

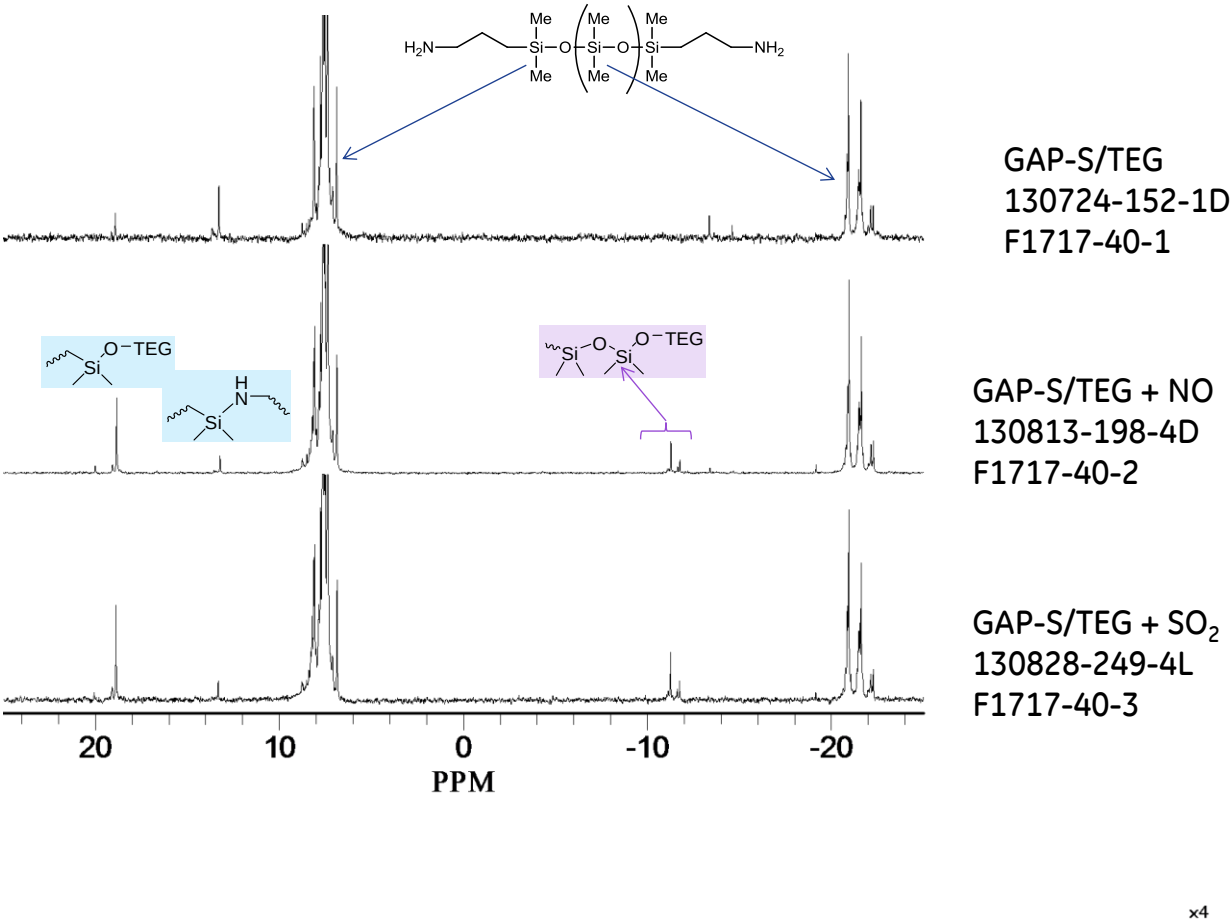

Figure 139. ^{29}Si NMR of GAP-1m/TEG mixtures exposed to NO and SO_2.

Determine Effect of Water on the System Performance

Several experiments were performed with the bench-scale system to study the effect of water on the CO_2 capture efficiency. These experiments were all performed using a liquid flow rate of 0.5 LPM, a gas flow rate of 112 SLPM, a desorber temperature of 140 °C, a desorber pressure of 45 psig, an absorber temperature of 40 °C, and an inlet CO_2 gas concentration of ~16 mol% (on a dry basis). Three levels of water were studied. The low water concentration was achieved using bottled gases and the ~1 mol% and ~5.5 mol% concentrations were achieved using exhaust gas from the gasoline generator and cooling the exhaust gas to the appropriate temperature to achieve the desired equilibrium level of water. Several experiments were performed at ~1 mol% water concentration. However, only one experiment was successful using ~5.5 mol% water in the gas, due to issues with water condensing in both the blower and flow meter before the absorption column.

Figure 140 shows the effect of water concentration on CO_2 capture efficiency. From this chart, it appears that increasing the water in the gas stream improves the CO_2 capture efficiency significantly. However, when the liquid mass balance is performed, this improvement in CO_2 capture efficiency is not observed. In Figure 141, the %GAP-S reacted as a function of water concentration in the inlet gas stream increases when calculated from the gas mass balance, but remains flat when calculated from the liquid mass balance. The data for the liquid mass balance comes from analyzing the samples using FTIR and the data for the gas mass balance comes from the CO_2 analyzer. Typically there is good agreement between the two methods. Potentially, water present in either the gas or liquid phases is interfering with one or both of the analysis techniques. For the gas stream, the water concentration in the gas analysis stream, after the condenser, ranges from ~0.02% (for the low water sample) to ~1.4% for the high water sample. It is possible that those levels of water in the gas stream could cause such a large change in the measured CO_2 levels. For the liquid phase, exact concentrations are unknown at this point, however, water can easily be seen by IR, and an examination of the IR spectra for these samples did not show any new peaks that may be interfering with the peak calibrated for carbamate concentration or any shift in the calibrated peak that correlated with inlet water concentration in the gas. Therefore, the cause of the differences observed between the two mass balances may be due to water impacting the readings from the gas analyzer. There is currently no evidence that water in the flue gas results in decreased CO_2 capture efficiency, and may have a beneficial effect.

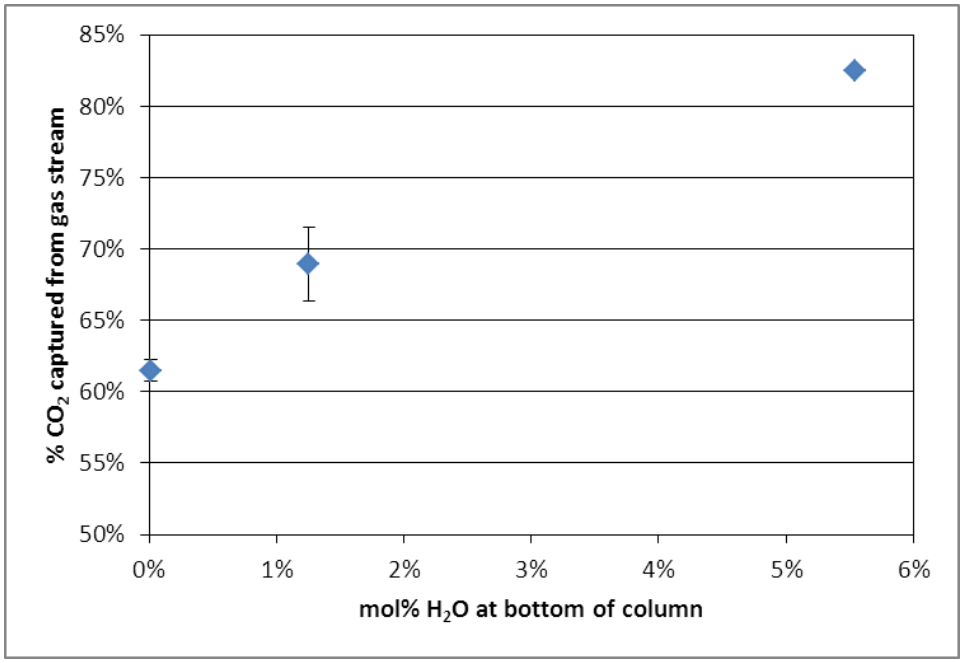

Figure 140. Effect of water concentration in the inlet gas on CO_2 capture efficiency.

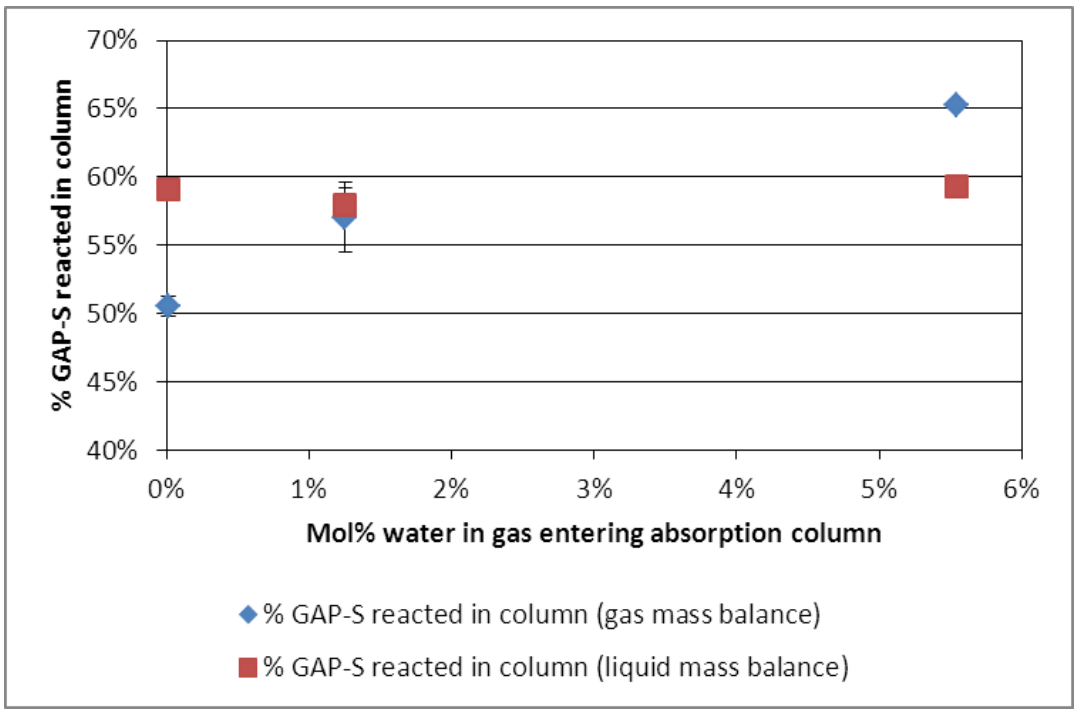

Figure 141. Effect of water concentration in the inlet gas on % GAP-1m reacted in the column.

Comparison of Titration/CO_2 Analyzer/IR Results

In analyzing the data from the bench-scale system, deviations between the results calculated based on the CO_2 analyzer (gas phase) and the FTIR results (liquid phase) were observed for some experiments. A titration method was developed as a third method to determine which analysis technique was giving the more accurate results. The method is described below.

Experimental – Determination of CO_2 Concentration in the Liquid by Titration

Glacial acetic acid (AcOH) was used as received and the silicone oil was less than 200 cstk for rapid response times. Greater accuracy can be achieved in a temperature controlled environment and if a barometer is available to determine the true atmospheric pressure at the time of the experiment.

The carbamate sample (appropriately sized for the burette used) was weighed in the reaction vessel which was equipped with a stir bar, a pressure equalizing dropping funnel, and an adapter to connect to the gas burette. AcOH was added to the dropping funnel and the silicone oil reservoir was raised to the upper most position and then the T-stopcock was turned to isolate the system. The level of the silicone oil was recorded and then the acid was added in

one dose from the dropping funnel to the sample. Immediate gas evolution occurred and stirring continued for approximately 30-60 seconds. After this time, no more gas evolution was observed. The reservoir was moved to make the level in both the reservoir and burette equal. The level on the burette was recorded and the appropriate calculations made.

Titrations were performed on the steady state bench-scale samples from the absorber and desorber for three separate experiments. These experiments were performed under identical conditions, except for the concentration of water in the inlet gas stream to the absorber (desorber temperature = 140 °C, desorber pressure = 45psig, Lm/Gm = ~0.45, L = 0.5 LPM, G = 112 SLPM). In Figure 142, the titration results are compared to the two different FTIR peaks that have been calibrated to carbamate concentration, 1450 cm^{-1}, and 1600 cm^{-1}. The titration results agree most closely with the 1450 cm^{-1} FTIR results for the two experiments having lower levels of water in the inlet gas stream to the absorber. Larger differences between the IR results and the titration results are observed for the experiment with the highest water concentration in the inlet gas stream.

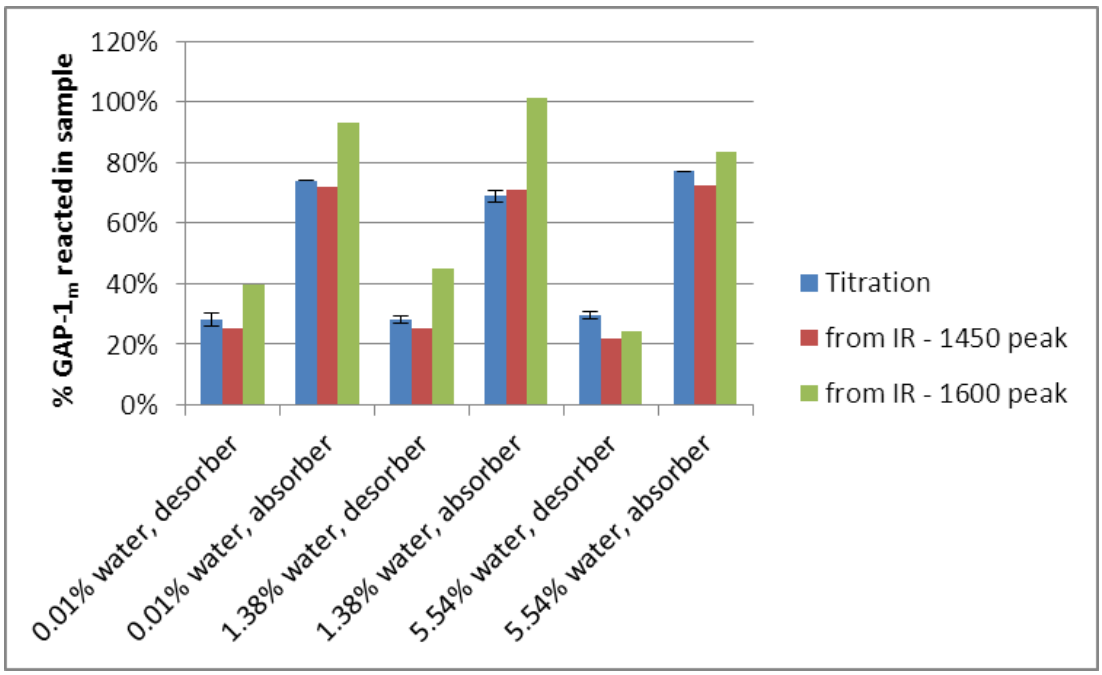

Figure 142. Comparison of titration and FTIR results.

From the liquid data shown in Figure 142, the % GAP-1m reacted in the column can be calculated and compared to the results from the CO_2 analyzer gas phase results, as shown in

Figure 143. From this analysis, it is shown that the FTIR results from the 1450cm^{-1} peak most closely match the titration results, with the best match being for the experiment with the lowest water concentration in the inlet gas stream to the absorber.

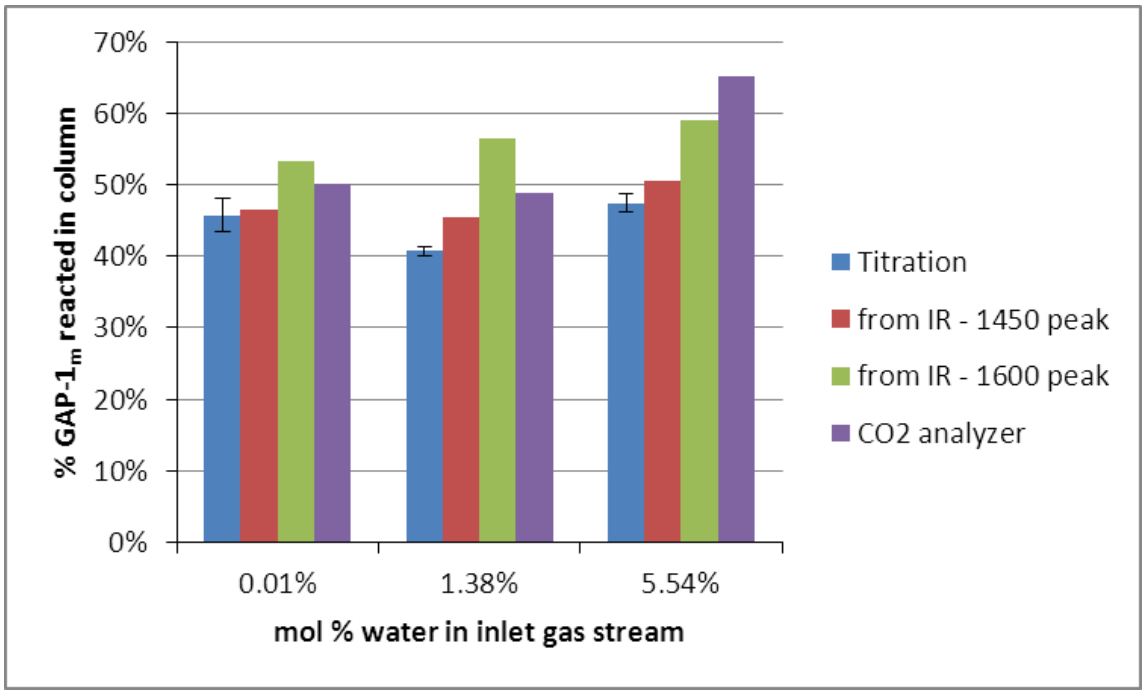

Figure 143. Comparison of titration, FTIR, and CO_2 analyzer results.

Task 7.2: Determine Scale-Up Effects

The original column sizing for the bench-scale CO_2 capture skid was determined using data from the 50 mm lab-scale column filled with ~5mm Rachig rings. The overall gas-phase mass transfer coefficients (K_Ga) for the absorption of CO_2 into a 60/40 (by weight) mixture of GAP-1m and triethylene glycol (TEG) were determined in that column for that packing as a function of column height and molar liquid to gas ratio (Lm/Gm). Due to ceiling height constraints, the height of the bench-scale column was capped at 3 meters, and the K_Ga values calculated from the lab-scale column data were used to determine if 90% CO_2 capture was achievable with the bench-scale column. The number of equilibrium stages used for this calculation, 2.3, was determined numerically using the lab-scale data and experimentally determined equilibrium curves. Figure 144 shows the results of this analysis. It was determined through this analysis that 90% capture was likely achievable at higher Lm/Gm ratios for a 1 LPM liquid flow rate. And

by either doubling the overall gas-phase mass transfer coefficient or halving the liquid flow rate, a 12 inch column 3 m high would be able to demonstrate 90% CO_2 capture.

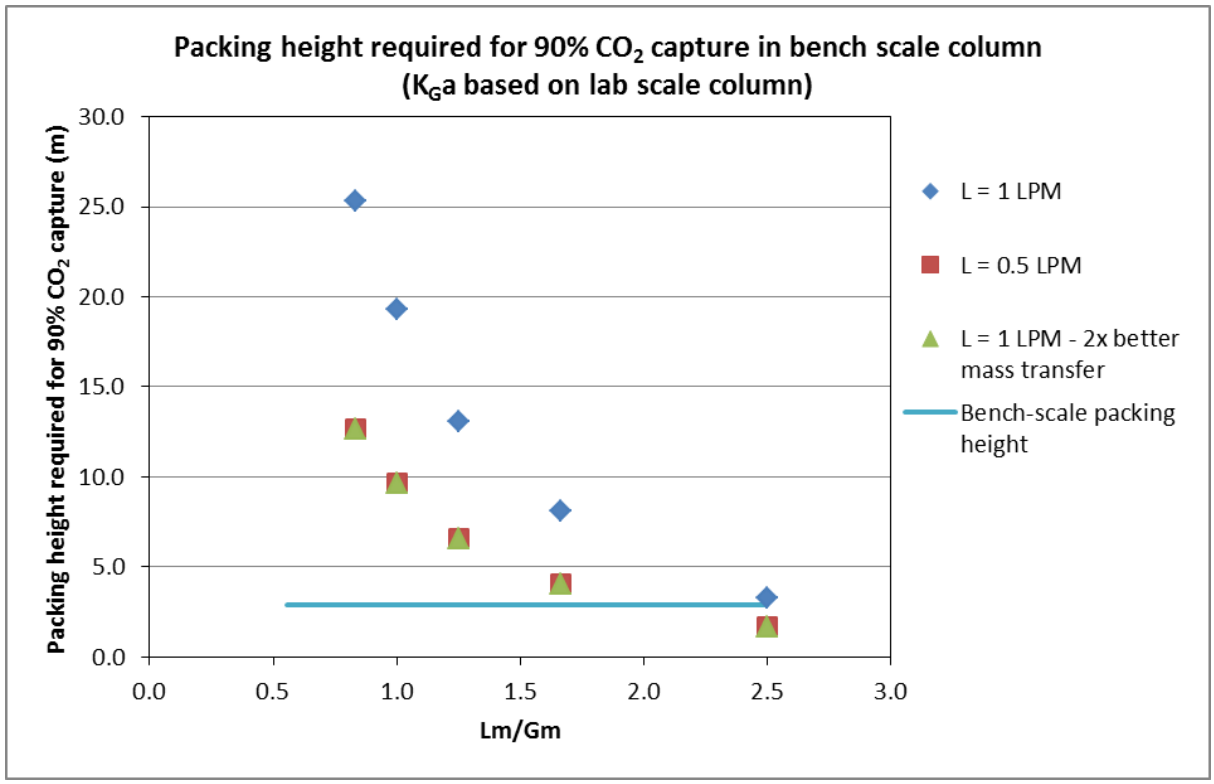

Figure 144. Predicted packing height required to achieve 90% CO_2 capture in bench-scale column based on lab scale K_Ga results.

It is likely that the K_Ga values calculated from the lab-scale data underestimate the achievable mass transfer coefficients on the bench scale for several reasons. The packing used in the laboratory scale column was essentially 5mm glass tubing cut into small cylinders of approximately 5 mm in length. The overall diameter of the lab column was 50 mm, so at most, 10 pieces of packing could fit across the column. This could result in edge effects affecting the overall mass transfer coefficient. There was no liquid distribution system in this column, so distribution at the top of the packing was uneven, and uneven wetting of the packing was observed. Since not all of the packing was used in the mass transfer, the actual effective height of the packing was unknown, and an underestimated overall mass transfer coefficient could have been calculated.

While the overall gas phase mass transfer coefficient was likely underestimated, it could not be determined what the actual achievable mass transfer coefficients would be with the bench scale packing (Intalox Ultra – T) and the GAP-1m/TEG solvent system until the bench scale system was actually built and tested. However, the bench-scale system could easily be designed for a wide range of liquid and gas flow rates to ensure that 90% CO_2 capture could be achieved. Ultimately the bench-scale system was designed to operate with liquid flow rates of 0.5 – 2 LPM and gas flow rates of 20 – 200 SLPM. The actual achievable maximum liquid flow rate was 1.8 LPM due to cooling constraints on the heat exchanger on the liquid exit of the desorber. The maximum achievable gas flow rate was ~185 SLPM using generator exhaust due to constraints on the gas blower in the system, and 120 SLPM for bottled gases.

To determine the overall gas-phase mass transfer coefficients for the bench scale system, a series of experiments were performed that varied the liquid flow rate from 0.5 to 1.5 LPM and the gas flow rate from 50 to 119 SLPM. The desorber conditions for all of these experiments were 160 °C and 0 psig. The CO_2 capture efficiency results for these experiments are shown in Figure 145.

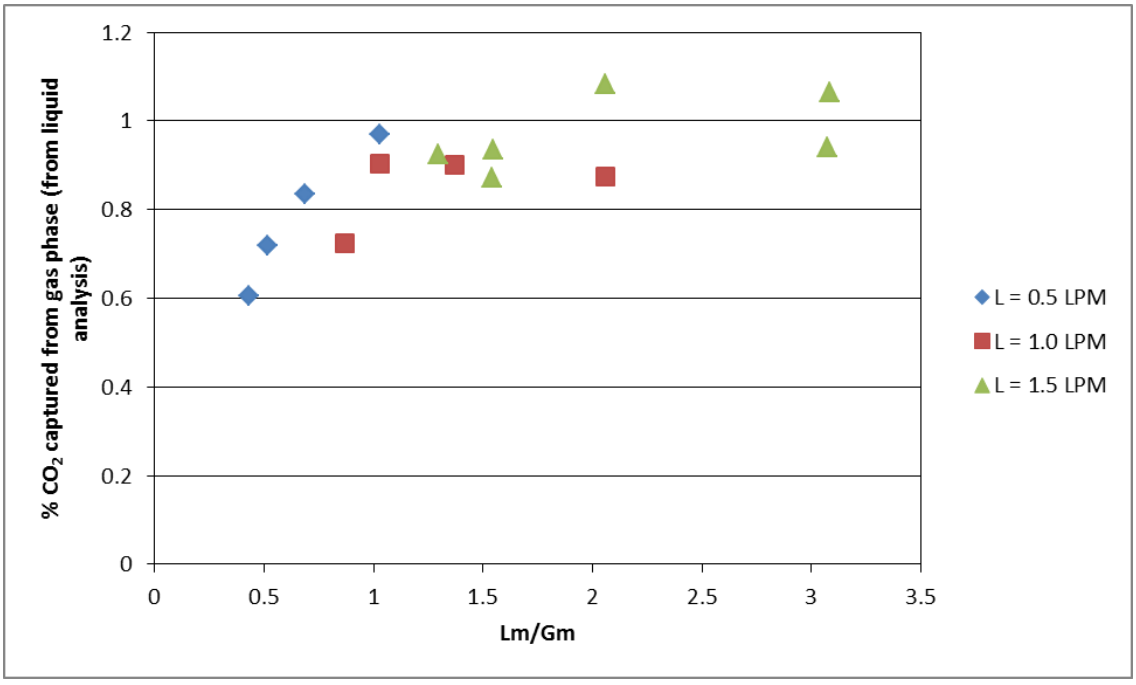

Figure 145. CO_2 capture efficiency results for bench scale system experiments.

The K_Ga values for these experiments were determined by regressing the mole ratio (Y) verses column height data (z) to determine the best fit curve, and then the maximum slope of that curve (dY/dz) was used to calculate K_Ga. For some experiments, it was difficult to determine accurate mass transfer coefficients, because either most, if not all, of the CO_2 was absorbed right at the bottom of the column and there were not enough data points available along the height of the column to fit a good curve or the shape of the curve did not allow for a maximum slope to be determined. The data from those experiments were removed from the analysis.

Figure 146 shows the K_Ga values calculated from the bench-scale experiments described above and in Figure 145. As expected, as the gas flow rate increases, the mass transfer coefficients also increase, and at a given Lm/Gm ratio, higher overall liquid and gas flow rates result in higher mass transfer coefficients. Only one experiment at the liquid flow rate of 1.5 LPM gave data that could be analyzed.

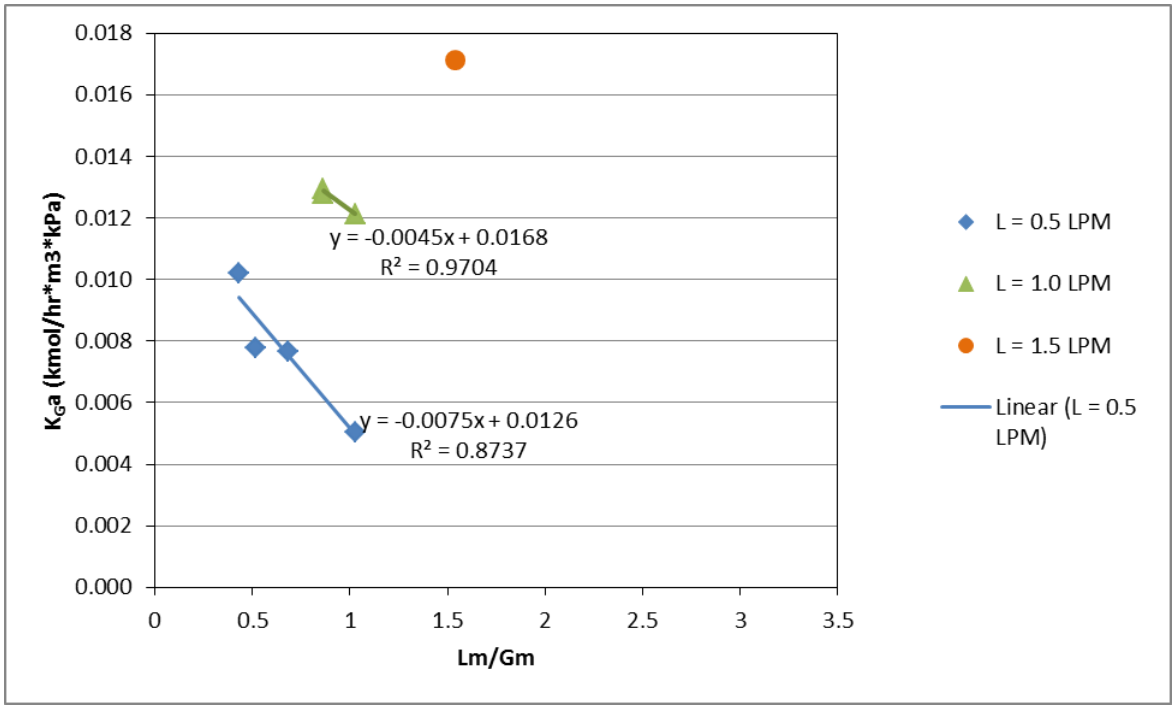

Figure 146. K_Ga values calculated from bench scale system experimental data.

When compared to the K_Ga values calculated using the laboratory scale data, the bench scale values for the lowest liquid flow rate are approximately the same as the lab scale values, and at

the high liquid flow rates are approximately double or more. Potential causes of this increase are:

- better wetting of the packing increasing the wetted surface area (more surface area available for absorption)
- better liquid distribution at the top of the column
- larger volume to circumference ratio minimizing the edge effects
- increased column temperature resulting in lower liquid viscosity and therefore thinner films

There is potential for more improvement in the $K_G a$ values under more optimized conditions. As shown in Figure 146, higher gas flow rates (and therefore higher gas velocities), could result in greater $K_G a$ values by increasing gas turbulence in the column.

The $K_G a$ values calculated from the bench scale data can then be used to determine the actual packing height required to achieve 90% CO_2 capture in the bench scale system, and the predicted packing heights based on the laboratory-scale data can be compared to the packing heights predicted from the bench-scale data and the actual packing heights as used experimentally. These results are shown in Figure 147. The packing height required for 90% CO_2 capture in the column was only calculated for the range of Lm/Gm values for which $K_G a$ values were determined. In general, higher Lm/Gm ratios require a shorter column height to achieve 90% capture. Overall, the packing heights shown in Figure 147 agree with the experimental CO_2 capture efficiency data in Figure 145. Comparing Figure 144 and Figure 147, a shorter column than originally predicted is required to achieve 90% CO_2 capture in the bench-scale system and lower than predicted Lm/Gm ratios could be used to achieve the desired capture efficiency. While the $K_G a$ values based on the bench scale data for the liquid flow rate of 0.5 LPM are similar to the values calculated from the lab-scale data, the calculated number of equilibrium stages is much lower for the bench-scale data, resulting in a lower required packing height.

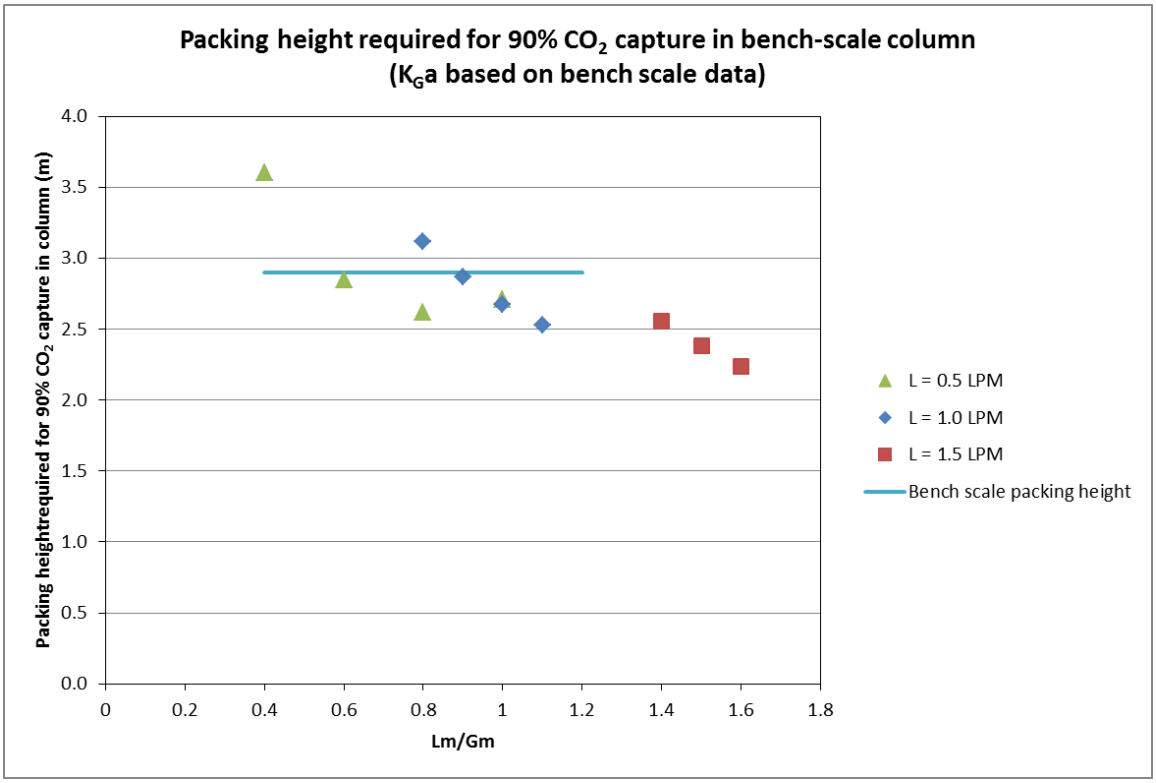

Figure 147. Packing heights predicted to achieve 90% CO_2 capture in the bench-scale column using K_Ga values calculated from bench scale experimental data.

Task 7.3: Determine Necessary Physical Properties of Capture Materials

Table 49 reports the updated state-point data table for the aminosilicone solvent and process.

Table 49. State-point data table.

	Units	Measured/Estimated Performance
Pure Solvent		
Molecular Weight	mol^{-1}	322.67 (GAP-1_m) / 150.17 (TEG)
Normal Boiling Point	°C	310 (GAP-1_m) / 287 (TEG)
Normal Freezing Point	°C	-85 (GAP-1_m) / -7 °C (TEG)
Vapor Pressure @ 15°C	bar	0.005 bar @ 140 °C (TEG) 0.037 bar @ 140 °C (GAP-1_m)
Working Solution		
Concentration	kg/kg	60/40 GAP-1_m/TEG
Specific Gravity (22 °C/20 °C)	-	0.913 (GAP-1_m) / 1.124 (TEG)
Specific Heat Capacity @ 40 °C and 1 bar	kJ/kg-K	2.319 (60/40 GAP-1_m/TEG)
Viscosity @ STP	cP	4.37 (GAP-1_m) / 49 (TEG)
Surface Tension @ STP	dyn/cm	Undetermined (GAP-1_m)/ 45.5 (TEG)
Absorption		
Pressure	bar	0 (gauge)
Temperature	°C	40-60 °C
Equilibrium CO_2 Loading	mol/mol	0.78 (CO_2) / 1 (GAP-1_m)
Heat of Absorption	kJ/mol CO_2	99.7 (60/40 GAP-1_m in TEG)
Solution Viscosity (@40 °C)	cP	431 (60/40 GAP-1_m in TEG)
Desorption		
Pressure	bar	2 (gauge)
Temperature	°C	140 °C
Equilibrium CO_2 Loading	mol/mol	0.25 (CO_2) / 1 (GAP-1)
Heat of Desorption	kJ/mol CO_2	99.7 (60/40 GAP-1_m in TEG)

Molecular Weight

The molecular weights were calculated based on the structures of the molecules.

Normal Boiling Point

The boiling point of GAP-1m was measured in the laboratories at GE GRC. The normal boiling point of TEG was found on the DOW website.[83]

Normal Freezing Point

The normal freezing point for TEG was found on the DOW website.[83] The normal freezing point for GAP-1m was measured by slowly lowering the temperature of the material until solidification occurred, and then raising the temperature until melting occurred to confirm the results.

Vapor Pressure

Vapor pressure measurements for GAP-1m were completed in the laboratories at GE GRC. The system consisted of a high temperature 0-15 psia pressure transducer, an oil bath with the capability of reaching 180 °C, a sample holder and valve. The sample holder and valve were designed to be submersible in the oil bath, as to maintain a consistent system temperature. Prior to completing the temperature ramps, nitrogen was bubbled through the material for 2-3 hours. The material was then loaded into the apparatus, placed with only the sample holder in the oil bath and hooked up to vacuum at elevated temperature for approximately one hour before starting the temperature ramp. Each temperature ramp ranged from room temperature to 180 °C. The temperature and pressure were continuously monitored throughout the experiment. The vapor pressure of TEG is 0.005 bar at 140 °C.[84]

Specific Gravity

The specific gravity for GAP-1m was determined by measuring out a specific volume in a tared volumetric flask and then weighing the flask, and calculating the density of the GAP-1m. The specific gravity of TEG was obtained from the DOW website.[83]

---

[83] http://msdssearch.dow.com/PublishedLiteratureDOWCOM/dh_004d/0901b8038004d042.pdf?filepath=ethyleneglycol/pdfs/noreg/612-00004.pdf&fromPage=GetDoc (accessed on 03/14/2011).

[84] Yaws, Carl L. (2003). Yaws' Handbook of Thermodynamic and Physical Properties of Chemical Compounds. Knovel. Online version available at: http://app.knovel.com/hotlink/toc/id:kpYHTPPCC4/yaws-handbook-thermodynamic.

Specific Heat Capacity

The specific heat capacity was measured using a Perkin-Elmer DSC7 differential scanning calorimeter following ASTM E1269.[85]

Heat of Absorption/Desorption

The heat of absorption of CO_2 was measured using an OmniCal ReactMax–Z3-UL Reaction Calorimeter. A Sierra Instruments Smart-Trak 2 Model# C100L mass flow controller was used to measure the amount of CO_2 added to the reactor. The reactor containing the sample was filled with ~20 SCC of CO_2. The reaction was allowed to proceed for 2 hours. This procedure was repeated 13 more times, for a total CO_2 addition of ~280 SCC of CO_2. The total amount of CO_2 added to the system, heat flow, and pressure were recorded throughout the experiment and used to calculate the heat of absorption for the sample.

Solution Viscosity

60/40 GAP-1m/TEG solution was reacted completely with CO_2 (as determined gravimetrically) and the viscosity of the solution was measured at 40 °C using a Paar Physica UDS 200 viscometer. The viscosity of pure GAP-1m was measured using Brookfield DV-II + Pro Programmable viscometer.

Equilibrium CO_2 Loading

A 25mL 3-neck round bottom flask was loaded with approximately 2g of a 60/40 wt/wt GAP-1m/TEG mixture. The flask was fitted in one neck with a glass stirrer bearing, a ground glass stir shaft, and a Teflon stirrer paddle. In the other two necks were a gas inlet port and a gas outlet port. The gas outlet port was then connected with Tygon tubing to a silicone bubbler containing less than 1" of silicone oil. The gas inlet port was connected to two mass flow controllers, one of which was connected to a bottle of 16.44 vol% CO_2 in N_2 and the other of which was connected to a bottle of 100% N_2. The set-points for the mass flow controllers were varied for each experiment to adjust the partial pressure of CO_2 to the desired value. The total flow sent to the round bottom flask was fixed at 45 SCC. The flask loaded with the GAP-1m/TEG mixture was immersed in a silicone oil bath set at the desired temperature. The overhead stirrer was set at a fixed stir rate. The gas outlet and gas inlet were connected to the flask and the gas flow was started. The gas flow was stopped and the flask was removed from the oil bath and weighed every 5-10 minutes to track the uptake of CO_2 in the liquid. The experiment was

[85] ASTM Standard E1269, 1990 (2001), "Standard Test Method for Determining Specific Heat Capacity by Differential Scanning Calorimetry," ASTM International, West Conshohocken, PA, 2001, 10.1520/E1269-01, www.astm.org.

stopped when the reaction was determined to have reached equilibrium (the weight did not change significantly for at least 3 measurements).

Absorber/Desorber Temperature and Pressure

These values were set while running a 60/40 (wt/wt) GAP-1m/TEG mixture in the continuous bench-scale CO_2-capture system.

Heat of Absorption of CO_2 as a Function of CO_2 Loading

The heats of absorption of CO_2 with 60wt%/40wt% GAP-S/TEG was measured using an OmniCal ReactMax–Z3-UL Reaction Calorimeter. Hasteloy-C reactor vessels (25mL) supplied by the calorimeter manufacturer were used that can withstand pressures up to 34.5 bar. An additional stainless steel vessel was added adjacent to the calorimeter in order to supply heated CO_2 to the reactor vessel. This additional vessel was placed in a heated box fitted with a circulating fan. A Sierra Instruments Smart-Trak 2 Model# C100L mass flow controller was installed in-between the reactor vessel and the additional stainless steel CO_2 storage vessel to measure the amount of CO_2 added to the reactor. This mass flow controller has an integrated totalizer to measure the total flow of a gas over a user-defined time.

The reactor vessel was filled with ~1.5 grams of material, and a magnetic stir bar was added. The exact volume of the sample was calculated using the density of each sample. The reactor was sealed, placed inside the calorimeter, stirring set to ~530 RPM and the temperatures of the calorimeter and the CO_2 storage vessel were set to the desired temperature. The CO_2 storage vessel was filled with CO_2 from the supply tank. The system was then allowed to come to equilibrium for 1-2 hours. When both the heat flow and the calorimeter temperature achieved steady-state, the system was considered to be at equilibrium.

The totalizer on the mass flow controller was reset to zero and the reactor was filled with ~20 SCC of CO_2, unless otherwise noted. The value on the mass flow controller totalizer was recorded and the reaction was allowed to proceed for 2 hours. This procedure was repeated 13 more times, for a total CO_2 addition of ~280 SCC of CO_2. For each addition of CO_2, the baseline value for the heat flow was established and subtracted from the raw data. The baseline-subtracted heat flow was then integrated over the reaction time to determine the total reaction heat. The total amount of CO_2 remaining in the headspace of the reactor was calculated from the pressure, temperature, and headspace volume. The total amount of CO_2 absorbed by the sample was calculated by subtracting the CO_2 remaining in the headspace at the end of the reaction from the total CO_2 that was added plus the CO_2 remaining in the headspace after the previous reaction step. The heat of reaction for each step was then calculated by dividing the total reaction heat by the amount of CO_2 absorbed by the sample.

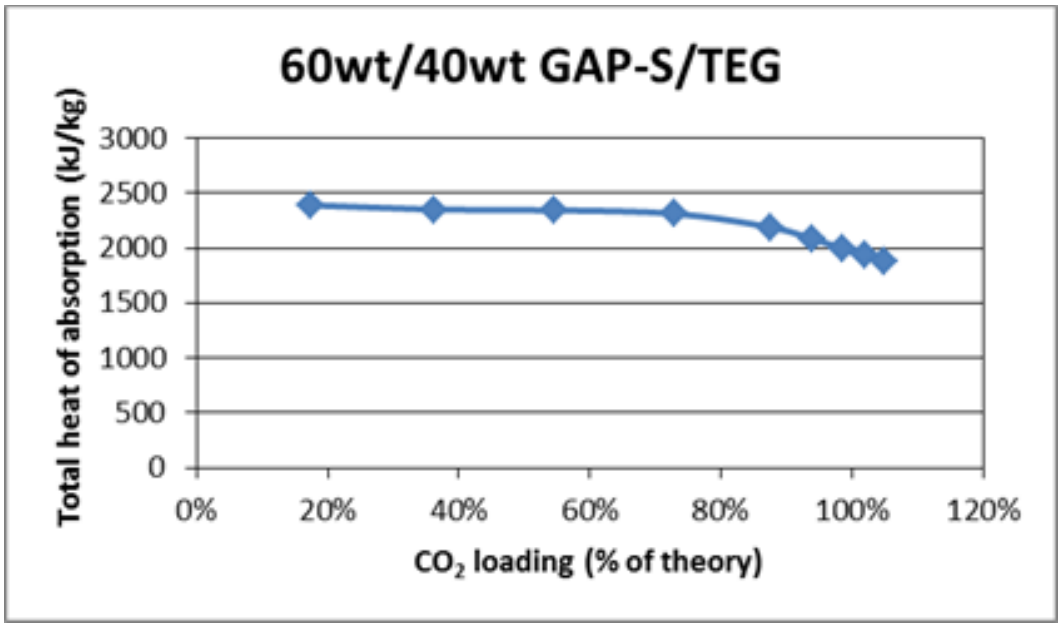

Figure 148. Heat of absorption of CO_2 in 60wt/40wt GAP-S/TEG as a function of CO_2 loading.

Task 7.4: Determine Suitable Materials of Construction

Three sets of corrosion coupons were installed in the bench-scale system during the first quarter of 2013. At three points during the testing schedule a set of coupons was removed from the bench-scale system, cleaned and measured for weight loss. The conditions to which all three sets of samples were exposed are shown in Table 50.

Table 50. Exposure conditions for corrosion coupons.

	First sampling			Second sampling			Third sampling		
	Desorber	Lean storage	Absorber sump	Desorber	Lean storage	Absorber sump	Desorber	Lean storage	Absorber sump
Time @ RT (hrs)	973	972	972	2398	2396	2397	6138	6138	6138
Time @ > RT (hrs)	64	65	65	169	170	170	388	380	389
Avg. temp > RT (°C)	154	34	51	153	34	52	145	34	52

The samples were cleaned according to the procedure listed in ASTM G1-03. The C1018 samples were cleaned using the solution in Table A1.1 of the ASTM with the designation C.3.5 (500 mL HCl, sp gr 1.19, 3.5 g hexamethylene tetramine, reagent water to make 1000 mL). The coupons were exposed to the solution for 10 minutes at room temperature, rinsed with deionized water, dried, weighed, and then returned to the cleaning solution bath until the slope of the weight loss verses time curve matched that of samples that had not been exposed to the test environment. Figure 149 shows the weight loss verses cleaning cycle results for the C1018 (carbon steel) samples. The curves are labeled with the location of the coupon in the bench-scale system and the number after the location refers to when the coupon was removed from the system (1 = ~65 hours of exposure, 2 = ~170 hours of exposure, 3 = ~388 hours of exposure). Figure 149 shows that after 2 cleaning cycles, the % weight loss for all C1018 samples matches that of the untreated sample.

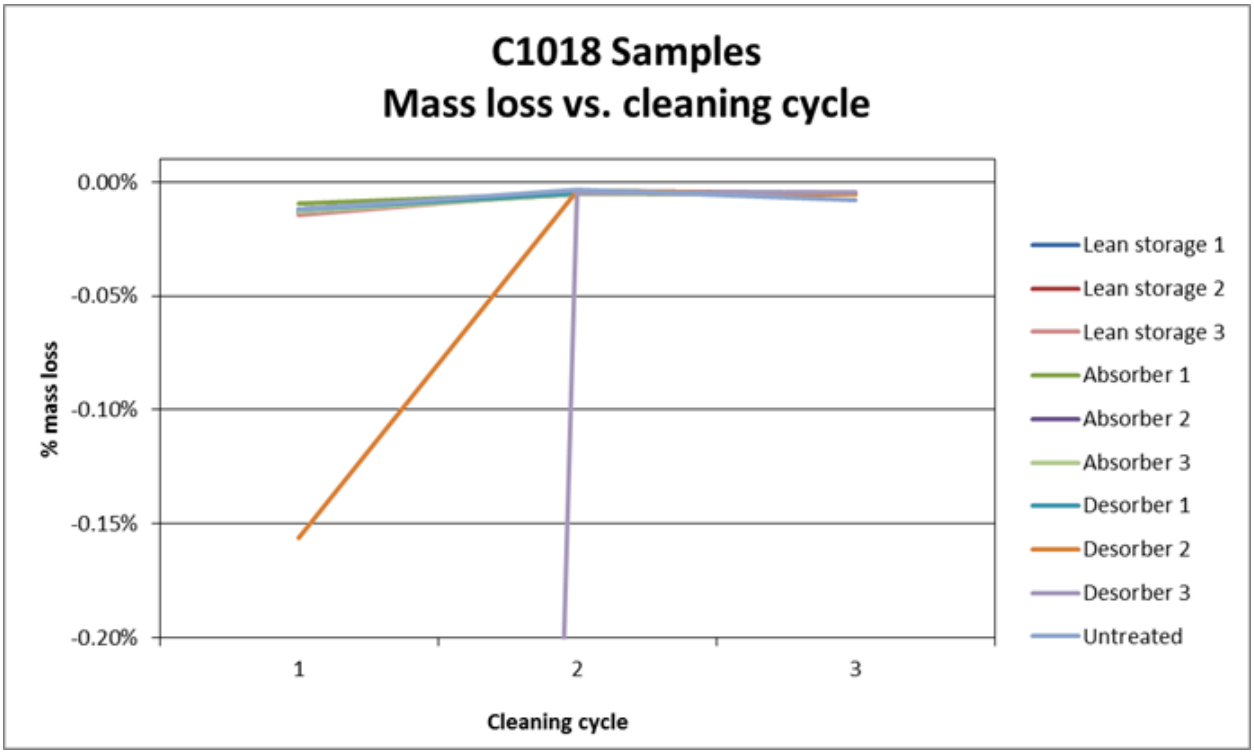

Figure 149. Weight loss of C1018 corrosion coupons as a function of cleaning cycle.

The 304L (stainless steel) samples were cleaned using the solution in Table A1.1 of the ASTM with the designation C.7.1 (100 mL nitric acid, reagent water to make 1000 mL). These samples were exposed to the solution for 20 minutes at 60 °C, rinsed with deionized water, dried, weighed, and then returned to the cleaning solution bath until the slope of the weight loss verses time curve matches that of samples that had not been exposed to the test environment. Figure 150 shows the weight loss verses cleaning cycle results for the 304L samples. The curves are labeled with the location of the coupon in the bench-scale system and the number after the location refers to when the coupon was removed from the system (1 = ~65 hours of exposure, 2 = ~170 hours of exposure, 3 = ~388 hours of exposure). Figure 150 shows that after 1 cleaning cycle, the % weight loss for all 304L samples matches that of the untreated sample.

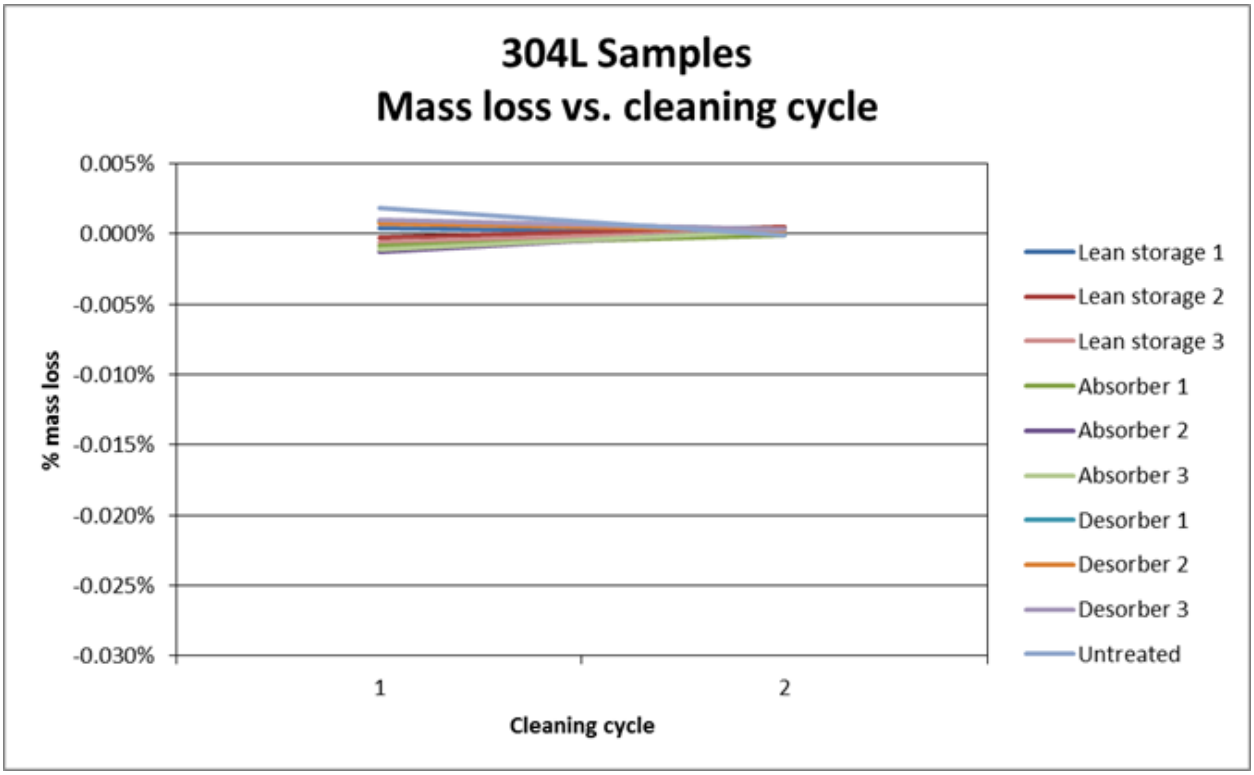

Figure 150. Weight loss of 304L corrosion coupons as a function of cleaning cycle.

Figure 151 shows the % mass loss for all corrosion coupons as a function of location of corrosion coupon in the bench-scale system and time of exposure. This figure shows that the only corrosion coupons showing appreciable corrosion are the C1018 samples that were located in the desorber.

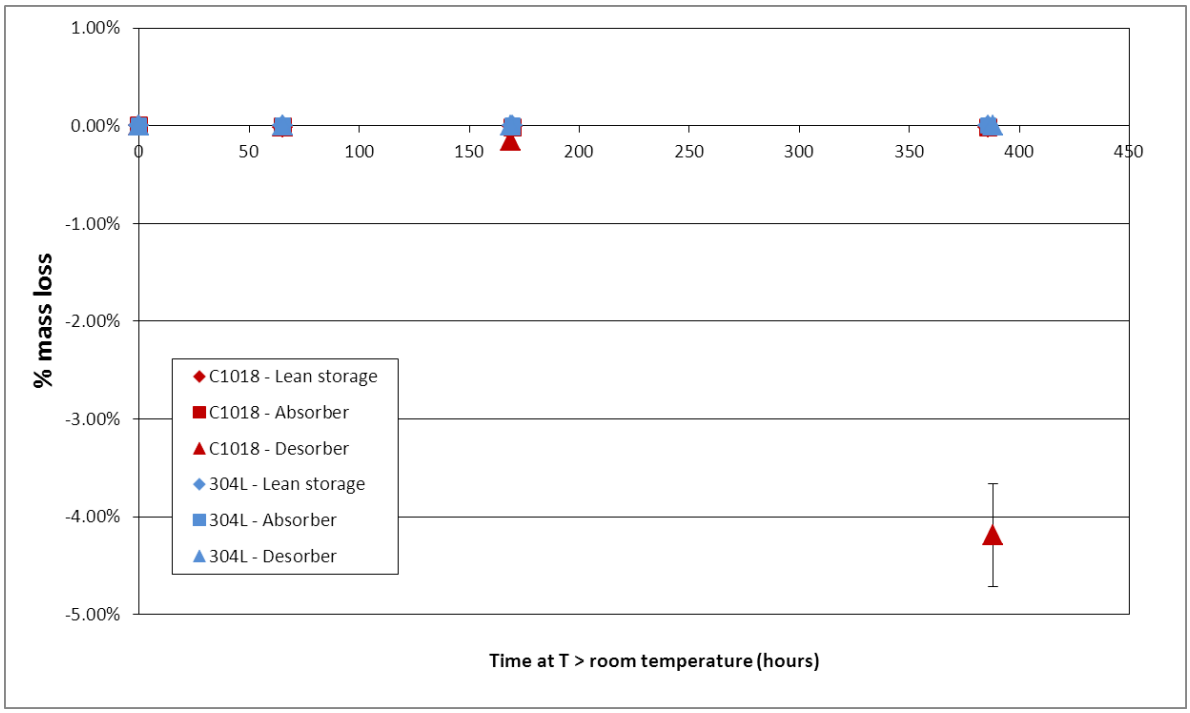

Figure 151. Corrosion coupon mass loss in bench scale system vs. time of exposure at T > RT.

SEM images of both the C1018 samples and the 304L samples are shown in Tables 51 and 52. For the C1018 samples, some small pitting is observed for the lean storage and absorber sump samples, while large scale pitting and erosion is observed for the desorber samples. For the 304L samples, it appears that for the exposed samples the surface topography is more well-defined than for the unexposed samples.

Table 51. SEM images of C1018 samples, before and after ~388 hours of exposure.

Location / Metal Type	Conditions	Unexposed samples	Exposed samples
Lean Storage / C1018	~380 hours at ~34 °C and ~6138 hours at ~25 °C	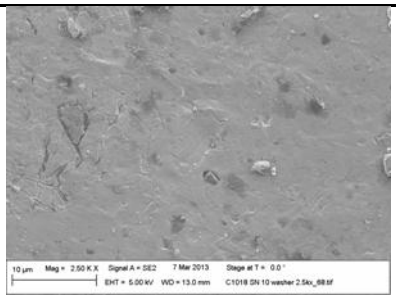	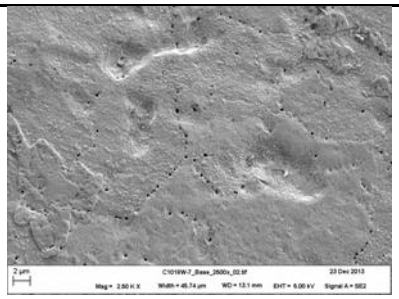
Absorber Sump/ C1018	~389 hours at ~52 °C and ~6138 hours at ~25 °C	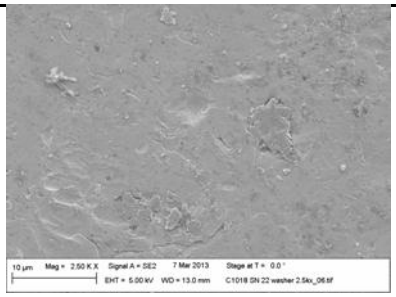	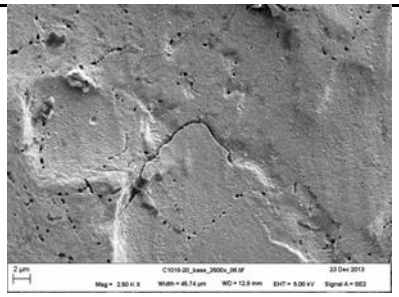
Desorber / C1018	~388 hours at ~145 °C and ~6138 hours at ~25 °C	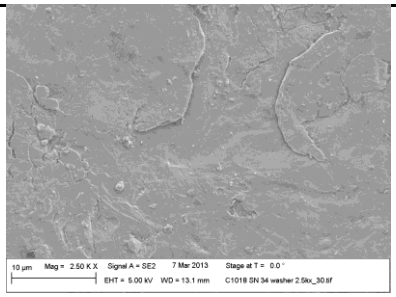	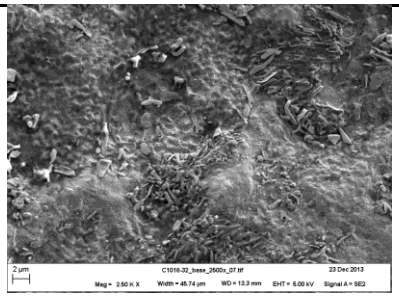

Table 52. SEM images of 304L samples, before and after ~388 hours of exposure.

Location / Metal Type	Conditions	Unexposed samples	Exposed samples
Lean Storage / 304L	~380 hours at ~34 °C and ~6138 hours at ~25 °C	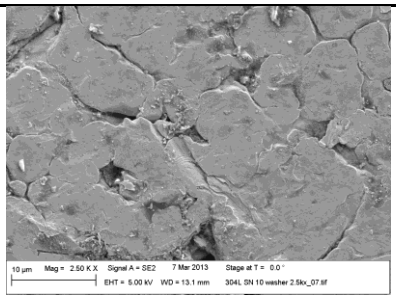	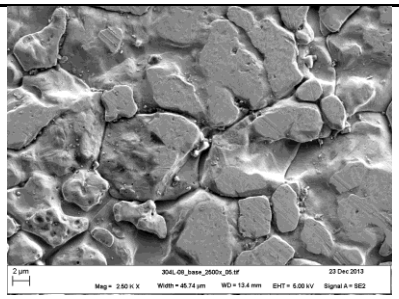
Absorber Sump/ 304L	~389 hours at ~52 °C and ~6138 hours at ~25 °C	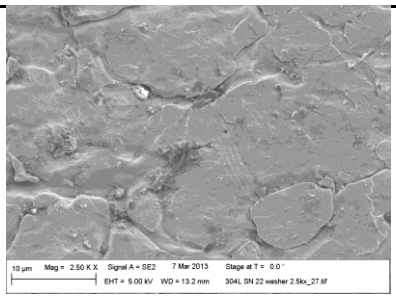	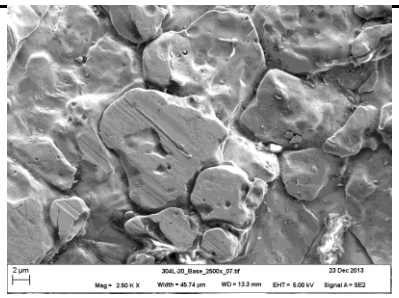
Desorber / 304L	~388hours at ~145 °C and ~6138 hours at ~25 °C	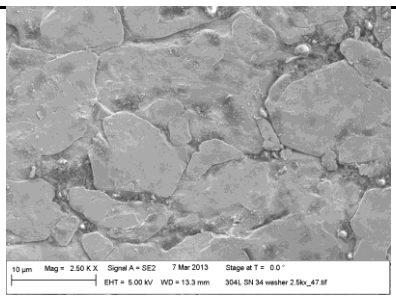	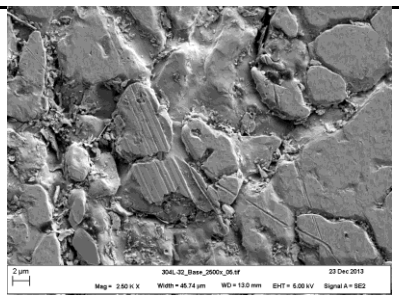

Welded, bent samples were also exposed to the test environment. These samples were stressed according to ASTM G30-97, installed in the lean storage tank, absorber sump, and desorber, and exposed to elevated temperatures for ~380-390 hours and to room temperature conditions for ~6138 hours. The samples were removed at the end of testing and imaged using SEM. The results are shown in Tables 53 and 54. For the C1018 samples, some large cracks were observed in the samples prior to exposure. The surface characteristics of the lean storage and absorber sump samples did not appear to change significantly. However, the surface of the desorber sample appeared to roughen, and a large number of small cracks appeared. A higher magnification image in Figure 152 shows the cracking in these samples more clearly. For the

304L samples, no cracking or significant change was observed upon exposure to the test environment.

Table 53. SEM images of C1018 welded samples, before and after ~388 hours of exposure.

Location / Metal Type	Conditions	Unexposed samples (interface images)	Exposed samples (interface images)
Lean Storage / C1018	~380 hours at ~34 °C and ~6138 hours at ~25 °C	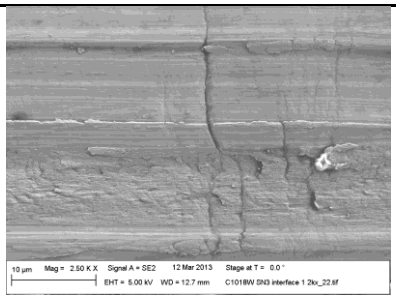	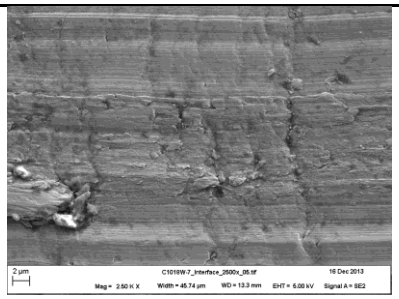
Absorber Sump / C1018	~389 hours at ~52 °C and ~6138 hours at ~25 °C	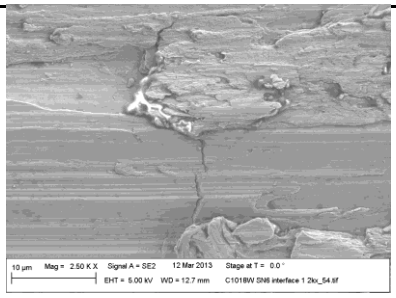	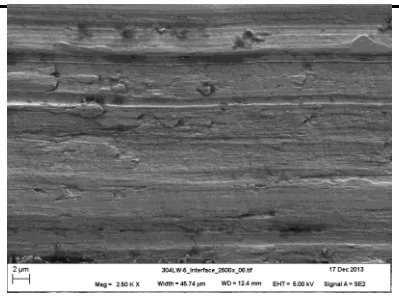
Desorber / C1018	~388hours at ~145 °C and ~6138 hours at ~25 °C	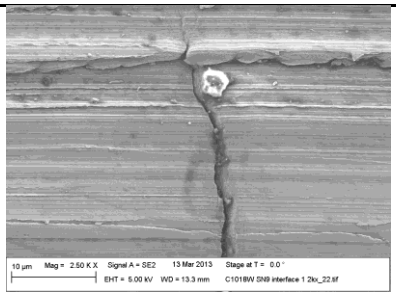	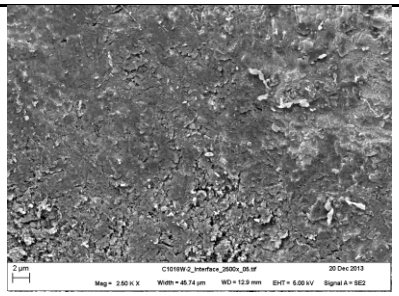

Table 54. SEM images of 304L samples, before and after ~388 hours of exposure.

Location / Metal Type	Conditions	Unexposed samples	Exposed samples
Lean Storage / 304L	~380 hours at ~34 °C and ~6138 hours at ~25 °C	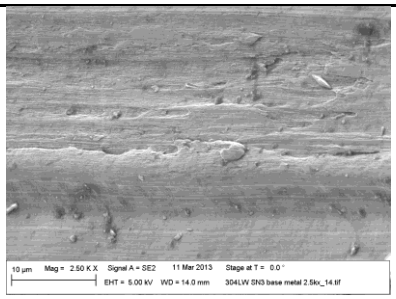	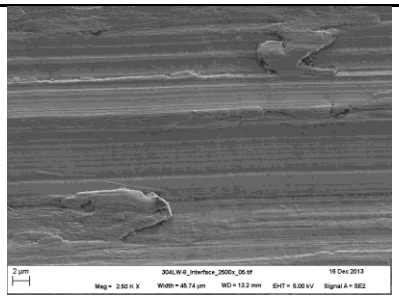
Absorber Sump/ 304L	~389 hours at ~52 °C and ~6138 hours at ~25 °C	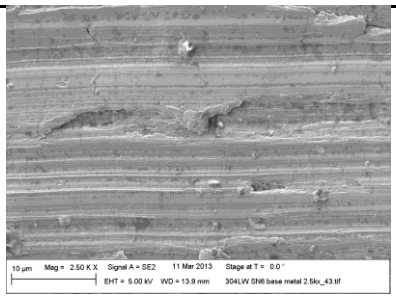	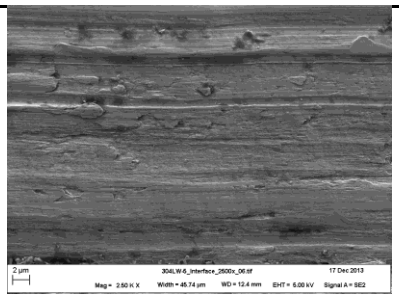
Desorber / 304L	~388hours at ~145 °C and ~6138 hours at ~25 °C	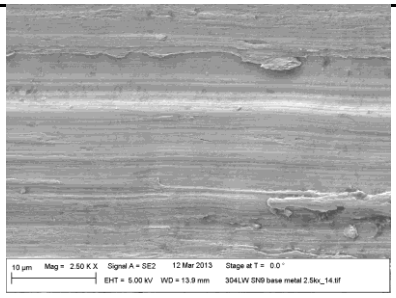	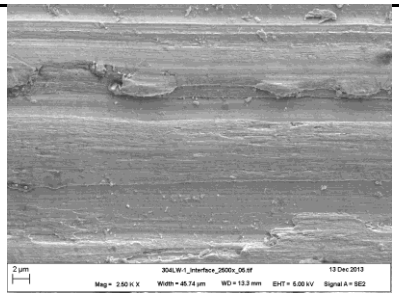

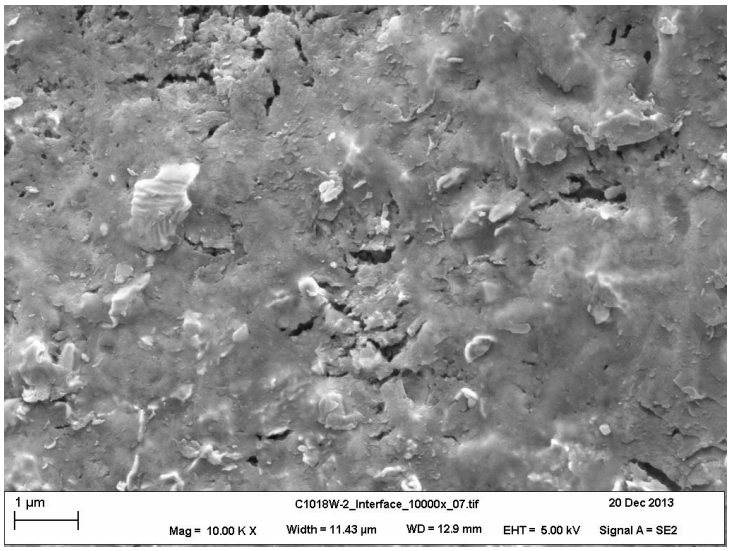

Figure 152. SEM image (10,000x magnification) of C1018 welded u-bend exposed to ~145 °C for ~388 hrs.

The corrosion rate in µm/year can be calculated from these results. The corrosion rates for samples in the system for 388 hours of exposure time are shown in Table 55. Negative values are interpreted as ~0.

Table 55. Corrosion rates for corrosion coupons in system at T>RT for 388 hours of exposure.

Sample	**Corrosion rate (µm/yr)**
C1018 – lean storage	1.27
C1018 - absorber	0.47
C1018 - desorber	2188
304L – lean storage	0.31
304L – absorber	0.53
304L – desorber	-0.50

Task 8: Economic and Scale-Up Analysis

A process model for the bench-scale system was developed and the data generated in Task 7 was used to calibrate it. The bench-scale model was used to update the plant model. The plant model was used to complete the final technology feasibility study. A sensitivity analysis was performed to identify design and operating points with minimal increase in COE. Finally, a strategy was developed for scaling up the aminosilicone-based solvent process.

Task 8.1: Develop Model of Bench-Scale System Performance

The absorber and desorber models developed in the first quarter of 2013 were combined to build an Aspen Plus™ process model of the bench-scale process. The combined model is shown in Figure 153 below.

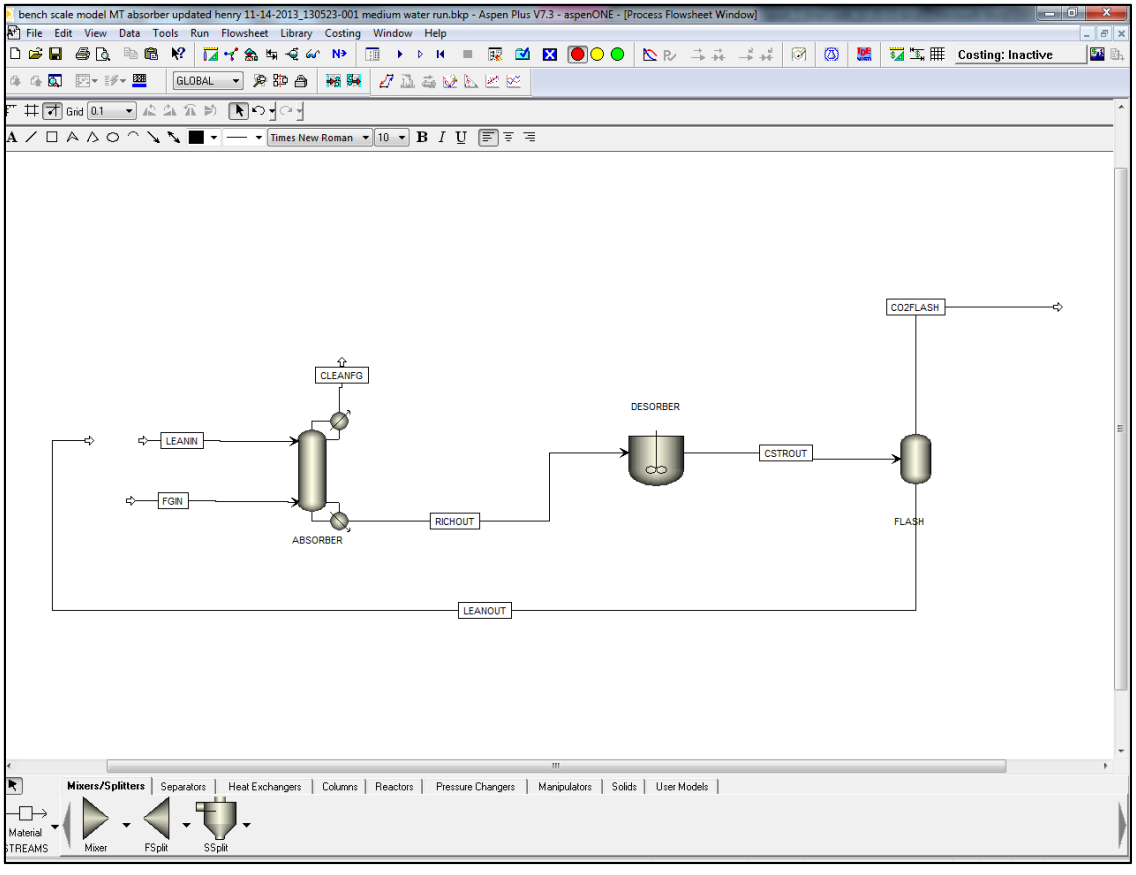

Figure 153. Bench-scale model of GAP-1m/TEG process.

One of the biggest challenges in model development was a proper physical properties set-up because GAP-1m is a novel compound. Aspen Plus™ does not have built-in properties for it. Molecular structure, molecular weight, and boiling point were manually input into the model. Also, some properties such as vapor pressure and viscosity were measured experimentally and then regressed in the model. Figure 154 compares experimental vapor pressure of GAP-1m with the model.

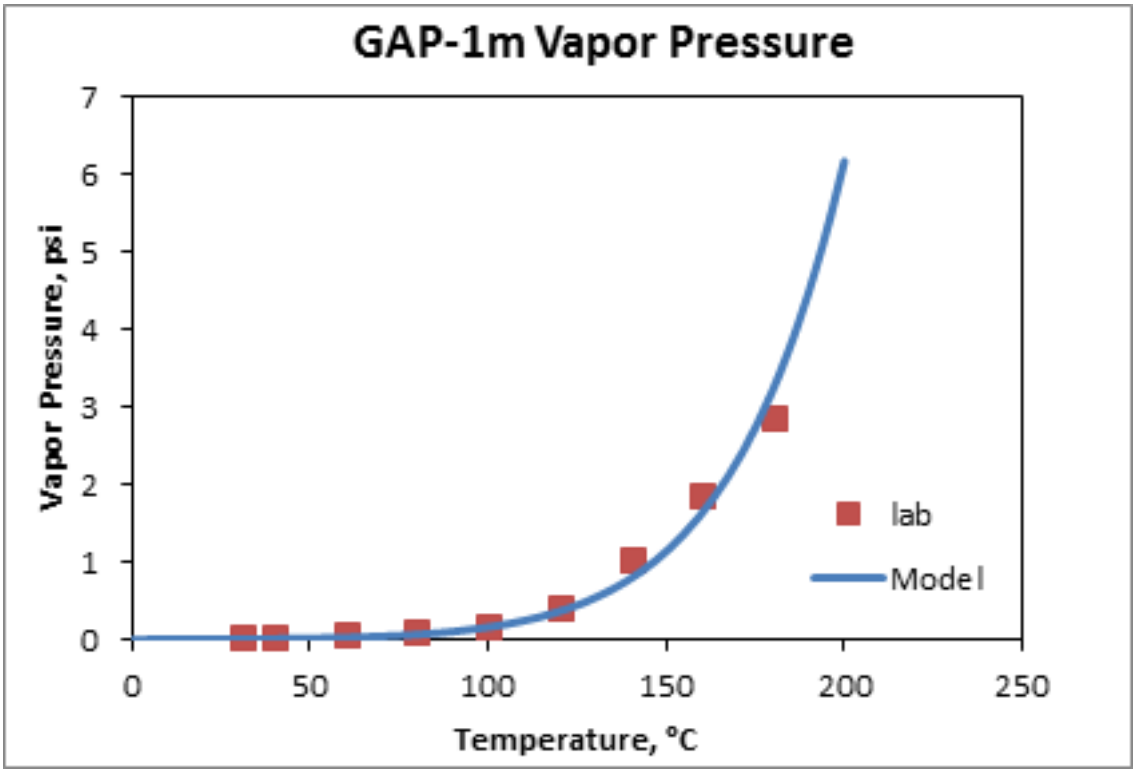

Figure 154. Comparison of experimental values of vapor pressure of GAP-1m with model values.

Henry's law constants for CO_2 in TEG, GAP-1m, and GAP-1m carbmate are important values, but the Aspen Plus™ Database does not have them built-in as well. For the values of Henry's law constants for CO_2 in TEG, ASPEN HYSYS software was used. It has a glycol properties package which is widely used in the oil and gas industries for modeling of the process to dry natural gas with TEG. The simple model, which was developed in HYSYS, is presented below in Figure 155.

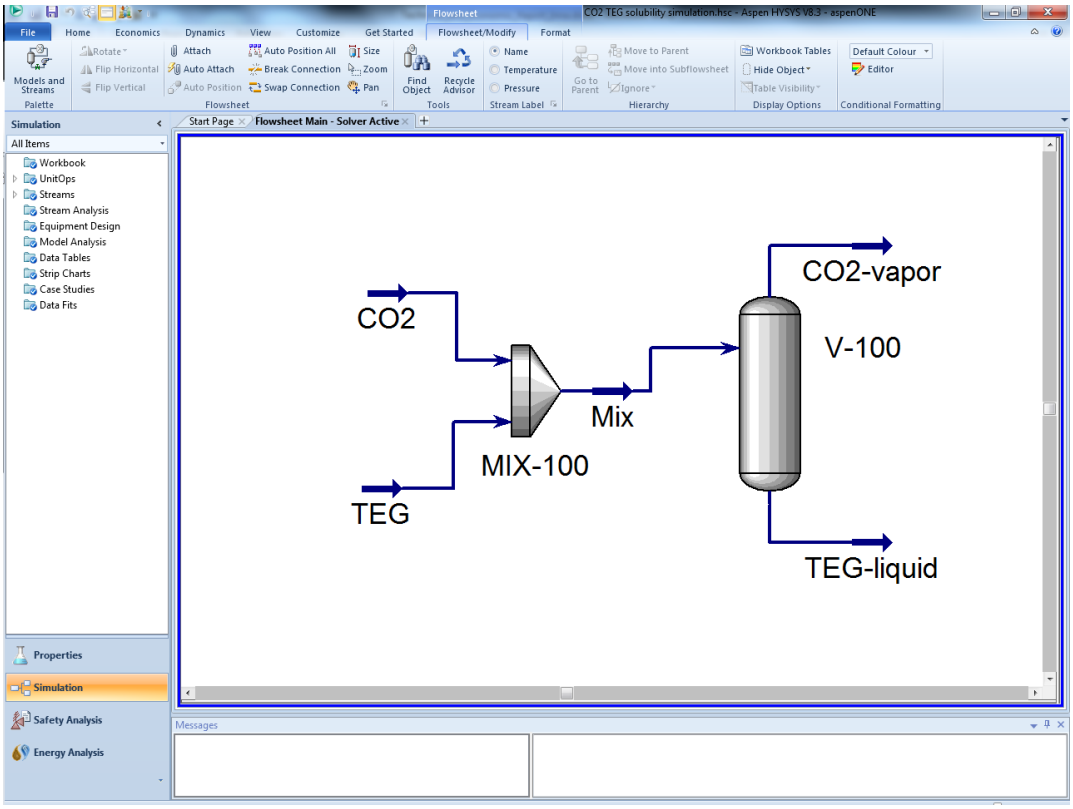

Figure 155. ASPEN HYSYS model to determine solubility of CO_2 in TEG.

An array of temperatures from 25 to 75 °C, and pressures from 200 to 500 kPa was selected to determine the solubility of CO_2 in TEG at equilibrium conditions, and the results are presented below in Figure 156.

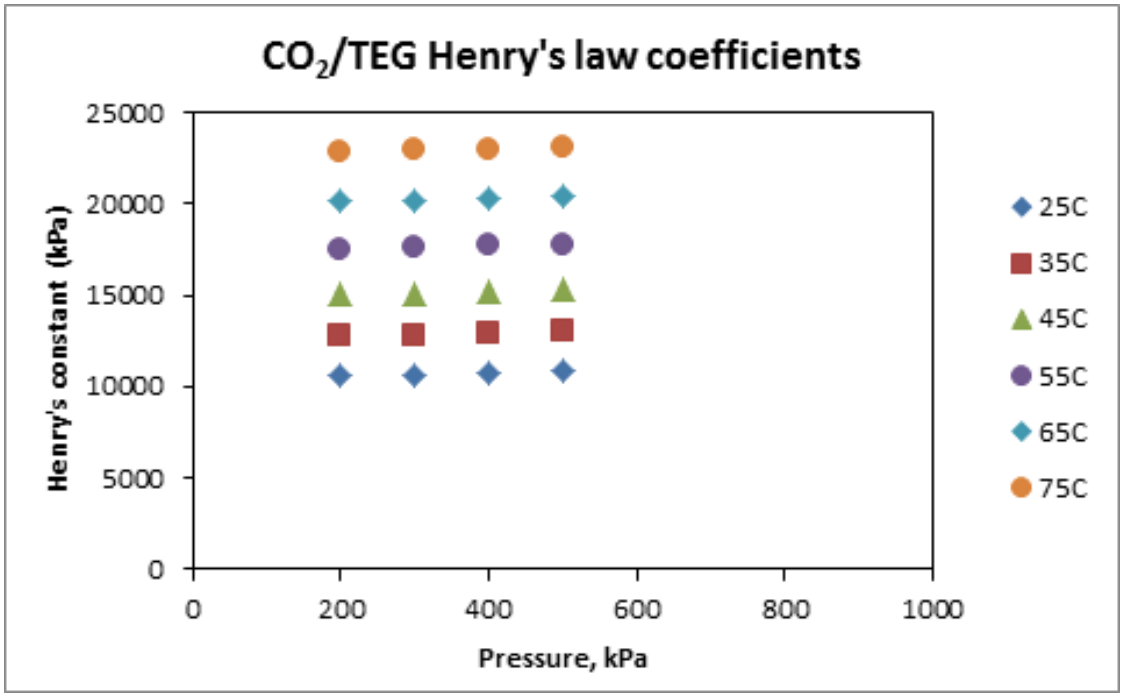

Figure 156. Henry's law constants of CO_2 in TEG based on ASPEN HYSYS modeling.

These values were used to calculate Henry's law constants and they were input into the DATA information of Aspen Plus™ for regression as it shows in Figure 157.

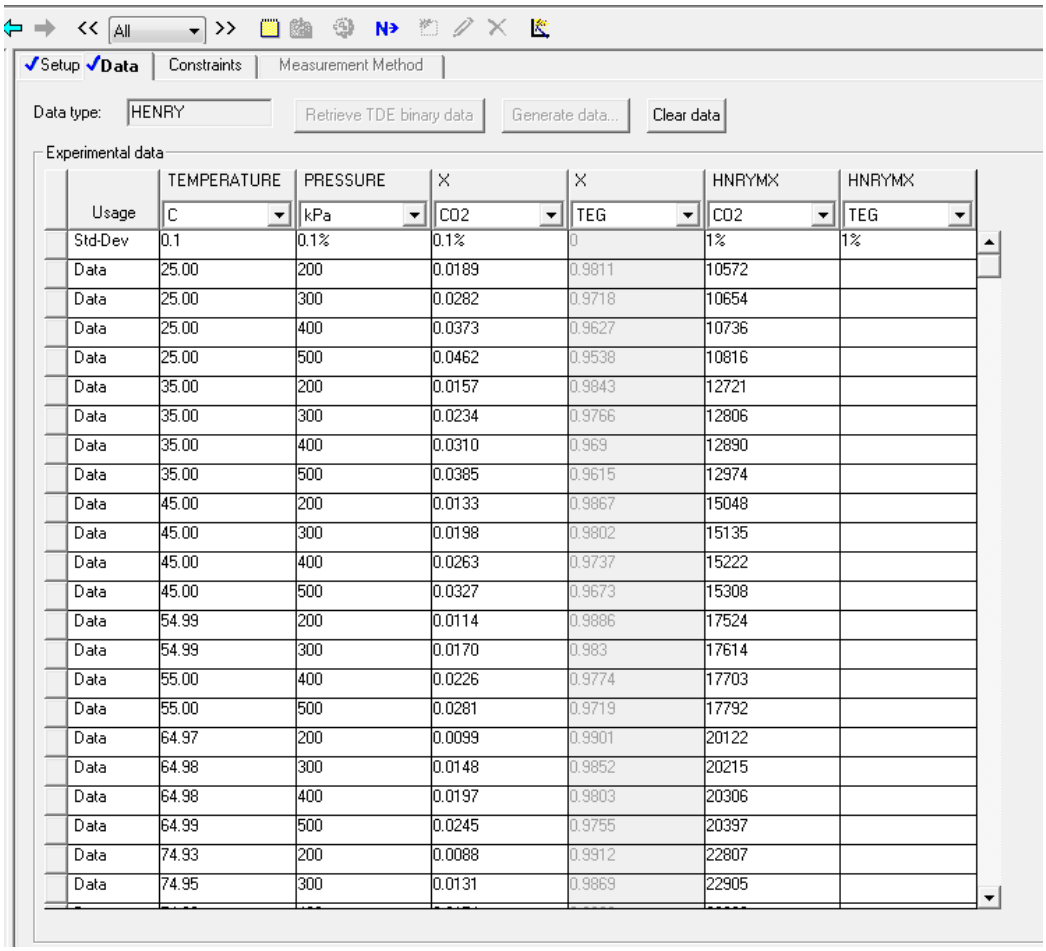

Usage	TEMPERATURE	PRESSURE	X	X	HNRYMX	HNRYMX
	C	kPa	CO2	TEG	CO2	TEG
Std-Dev	0.1	0.1%	0.1%	0	1%	1%
Data	25.00	200	0.0189	0.9811	10572	
Data	25.00	300	0.0282	0.9718	10654	
Data	25.00	400	0.0373	0.9627	10736	
Data	25.00	500	0.0462	0.9538	10816	
Data	35.00	200	0.0157	0.9843	12721	
Data	35.00	300	0.0234	0.9766	12806	
Data	35.00	400	0.0310	0.969	12890	
Data	35.00	500	0.0385	0.9615	12974	
Data	45.00	200	0.0133	0.9867	15048	
Data	45.00	300	0.0198	0.9802	15135	
Data	45.00	400	0.0263	0.9737	15222	
Data	45.00	500	0.0327	0.9673	15308	
Data	54.99	200	0.0114	0.9886	17524	
Data	54.99	300	0.0170	0.983	17614	
Data	55.00	400	0.0226	0.9774	17703	
Data	55.00	500	0.0281	0.9719	17792	
Data	64.97	200	0.0099	0.9901	20122	
Data	64.98	300	0.0148	0.9852	20215	
Data	64.98	400	0.0197	0.9803	20306	
Data	64.99	500	0.0245	0.9755	20397	
Data	74.93	200	0.0088	0.9912	22807	
Data	74.95	300	0.0131	0.9869	22905	

Figure 157. Henry's law constants of CO_2 in TEG in DATA tab in Aspen Plus™.

Regression fit of these data is shown on Figure 158.

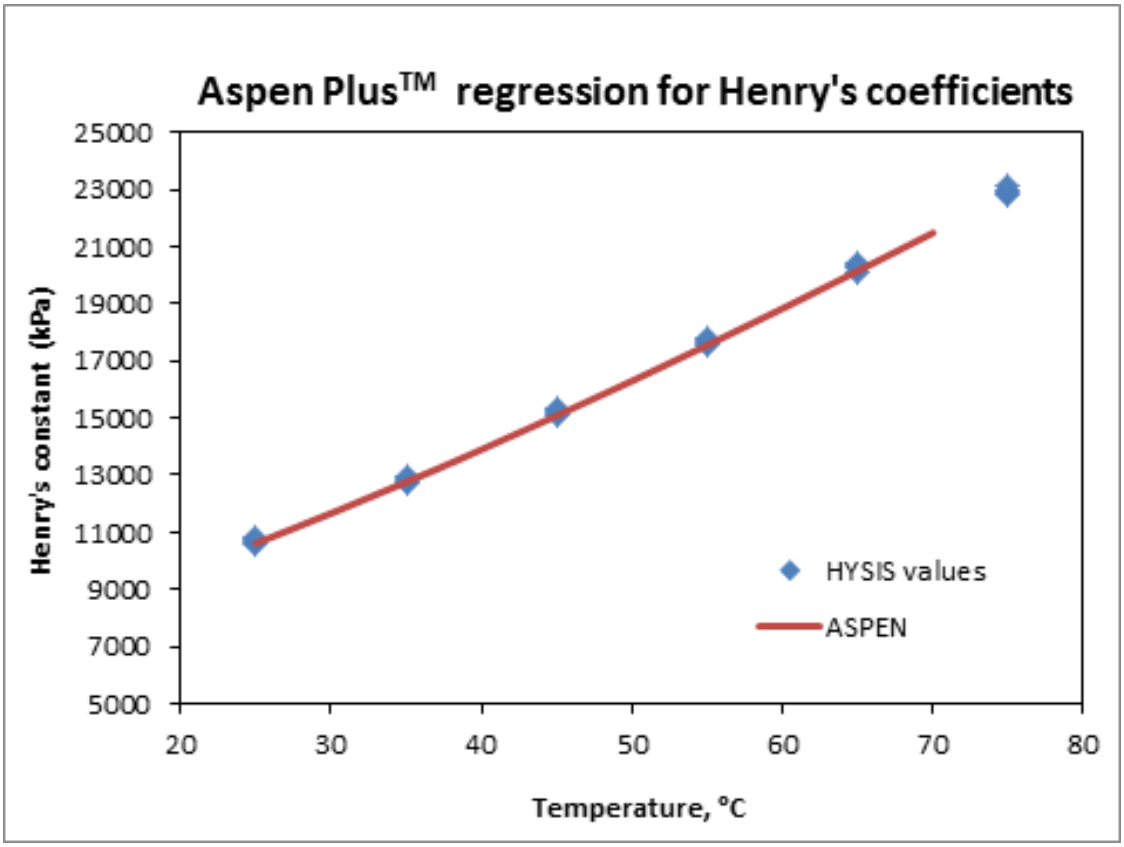

Figure 158 Regression of Henry's law constants of CO_2 in TEG in Aspen Plus™.

It was challenging to measure the solubility of CO_2 in GAP-1m experimentally, because of the chemical reaction of CO_2 with the GAP-1m and the inability to separate physical solubility and reaction. It was also challenging to experimentally measure solubility of CO_2 in GAP-1m carbamate. The Aspen Plus™ database has the properties for D4, octamethylcyclotetrasiloxane, and it was assumed that the solubility of CO_2 in GAP-1m and GAP-1m carbamate are similar to the solubility in D4.

A set of bench-scale steady-state experiments was selected using an experimental design of experiments that was completed during the second quarter of 2013. The experiments were selected such that they were representative of the overall design of experiment matrix for absorber and desorber conditions. Five experiments were selected to validate the desorber model predictions with experimental results. The process conditions for these five experiments are shown in Table 56. The main parameters that were changed were the temperature and the pressure of the desorber. The inlet gas-phase CO_2 concentration to the absorber was around 16% in all the experiments.

Table 56. Five experiments selected to confirm bench-scale model performance.

Case	Temperature (°C)	Pressure (psig)	Actual CO_2 % inlet to absorber
#1:130522-292	140	0	16.54%
#2:130523-001	140	45	15.99%
#3:130530-021	140	45	15.72%
#4:130606-058	150	45	15.92%
#5:130618-082	120	45	16.24%

The liquid solvent composition at the exit of the desorber (inlet of the absorber) is a critical parameter to observe for this set of experiments. The model predictions were compared with the experimental results. There was good agreement between the predicted and the measured values as shown in Figure 159. Also, the effect of increasing pressure and decreasing temperature is observed in both experimental results and model predictions. Comparison of case #1 with Case #2 and Case #3 shows the effect of increasing pressure. With increase in desorber pressure the GAP-1m concentration decreases and GAP-1m-carbamate concentration increases. Comparison of Case #2 and Case #3 with Case #4 and Case #5 shows the effect of desorber temperature. With increase in desorber temperature the GAP-1m concentration increases and GAP-1m-carbamate concentration decreases.

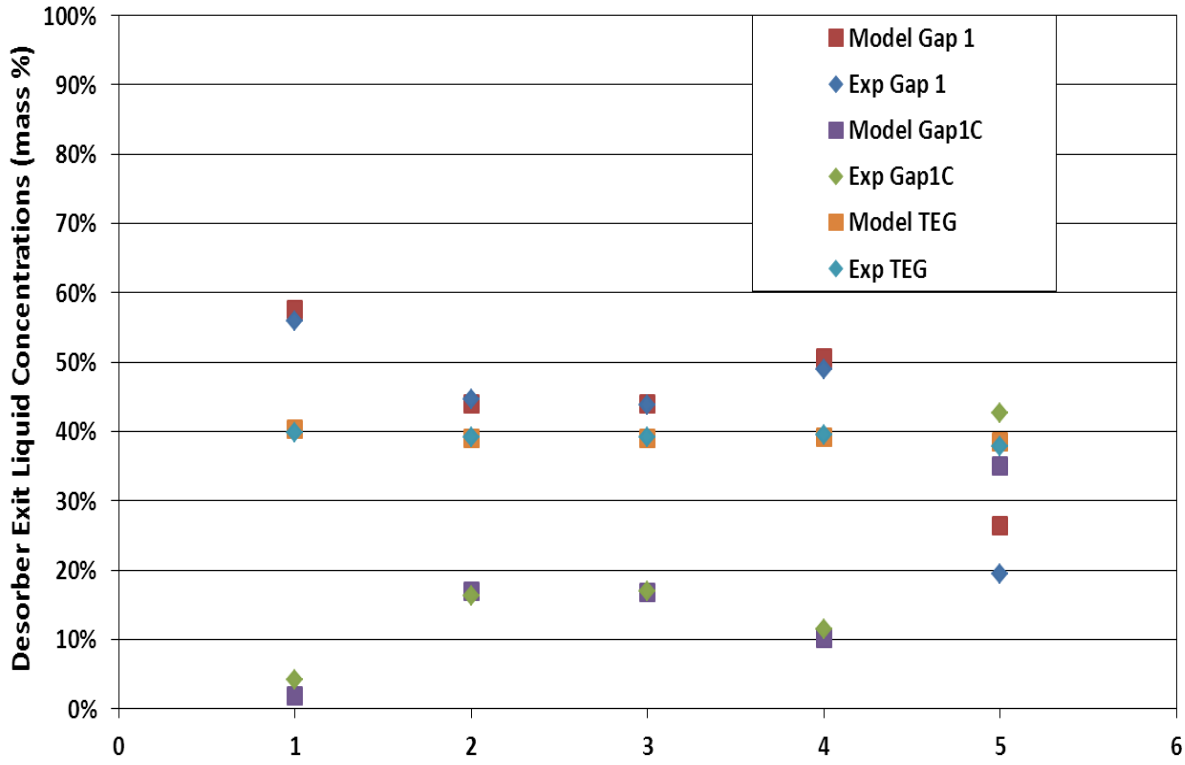

Figure 159. Comparison of experimental results and model predictions for desorber outlet concentrations of GAP-1m, TEG, and GAP-1m-carbamate.

The absorber response was also compared for these five experiments. The liquid and gas flow rates into the absorber were not varied between these five experiments. The desorber exit liquid was recycled back into the absorber after cooling the lean solvent.

The absorber was modeled by two separate methods. In the first method the mass transfer and the chemical reactions taking place were modeled as equilibrium (top two charts in Figures 160-164) whereas in the second method the mass transfer was modeled as rate and the reaction was modeled as equilibrium (bottom two charts in Figures 160-164).

The absorber response observed experimentally was compared with the model predictions. Two main parameters were selected for the comparison, the gas phase CO_2 concentration profile and temperature profile along the length of the absorber. The next set of figures show these comparisons (Figures 160-164). It is observed that the second method, using the rate/equilibrium model, gives very good predicted values when compared to the experimental

observations for both the CO_2 concentration as well as the temperature profile in the absorber. The equilibrium/equilibrium model is less consistent with experimental observation.

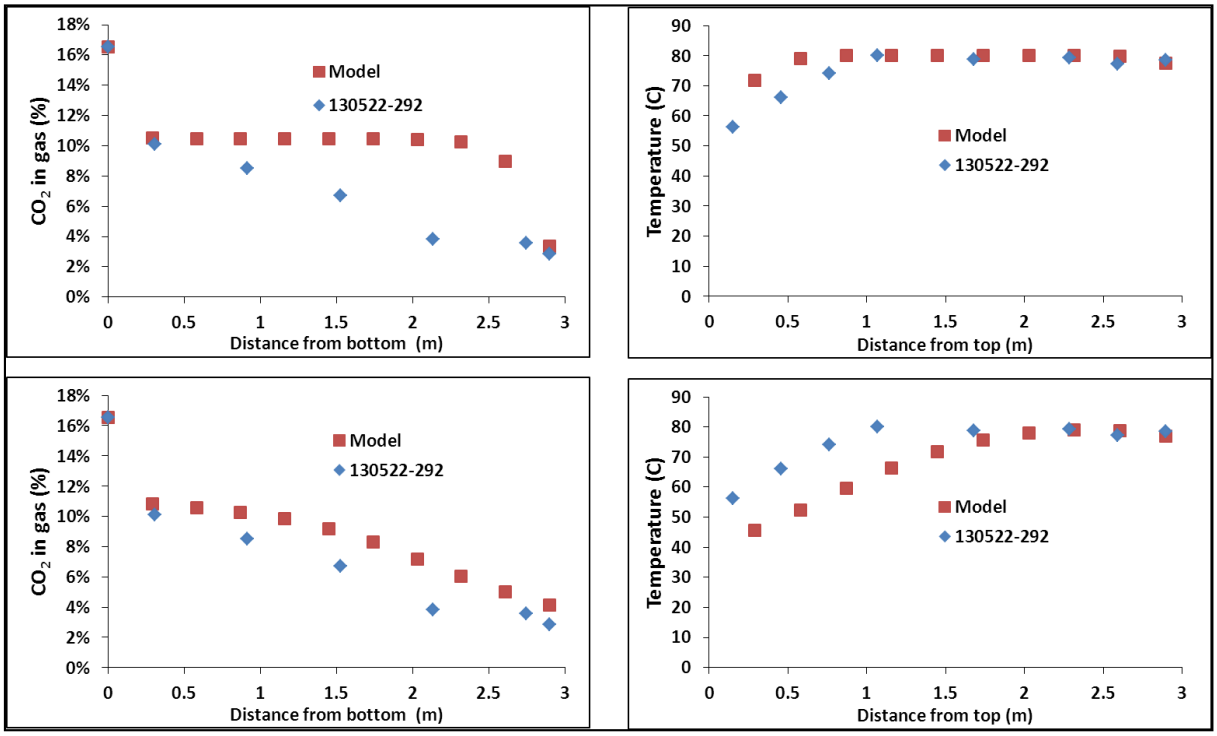

Figure 160. Absorber response for Case #1. The top two charts use the equilibrium/equilibrium model in Aspen Plus™. The bottom two charts use the rate/equilibrium model.

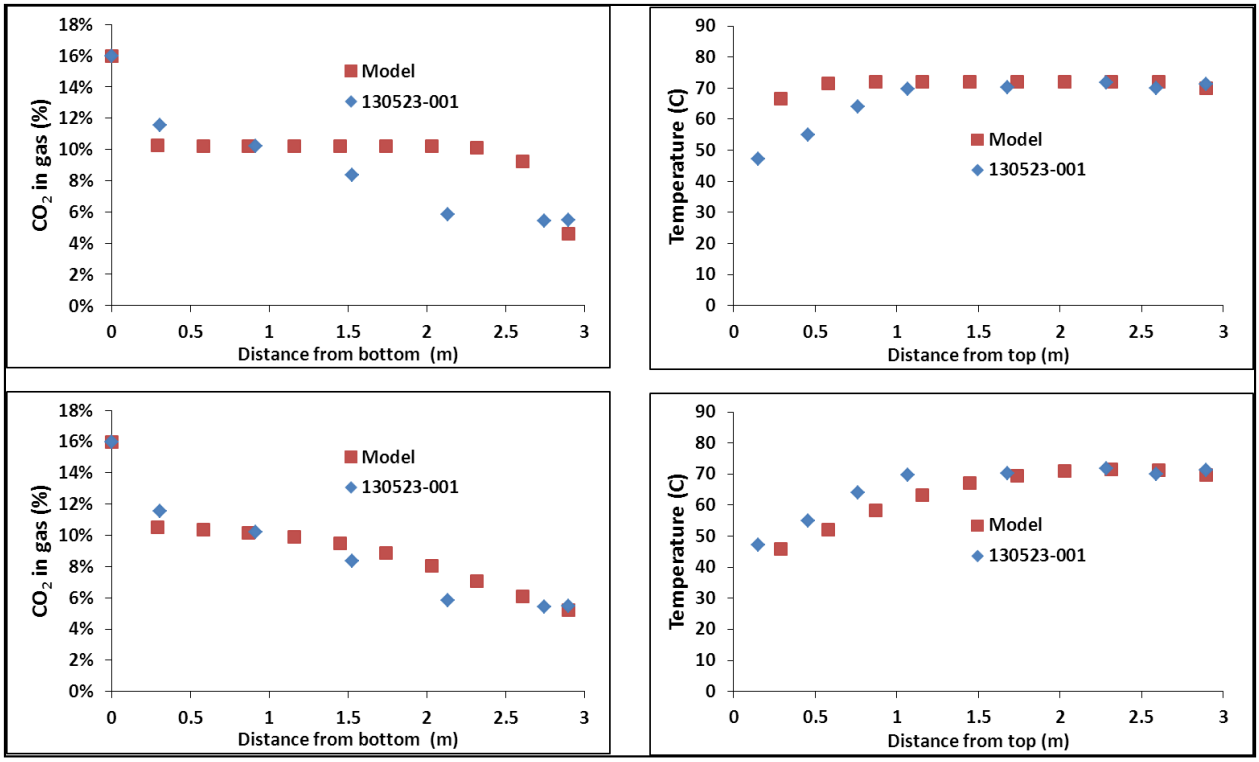

Figure 161. Absorber response for Case #2. The top two charts use the equilibrium/equilibrium model in Aspen Plus™. The bottom two charts use the rate/equilibrium model.

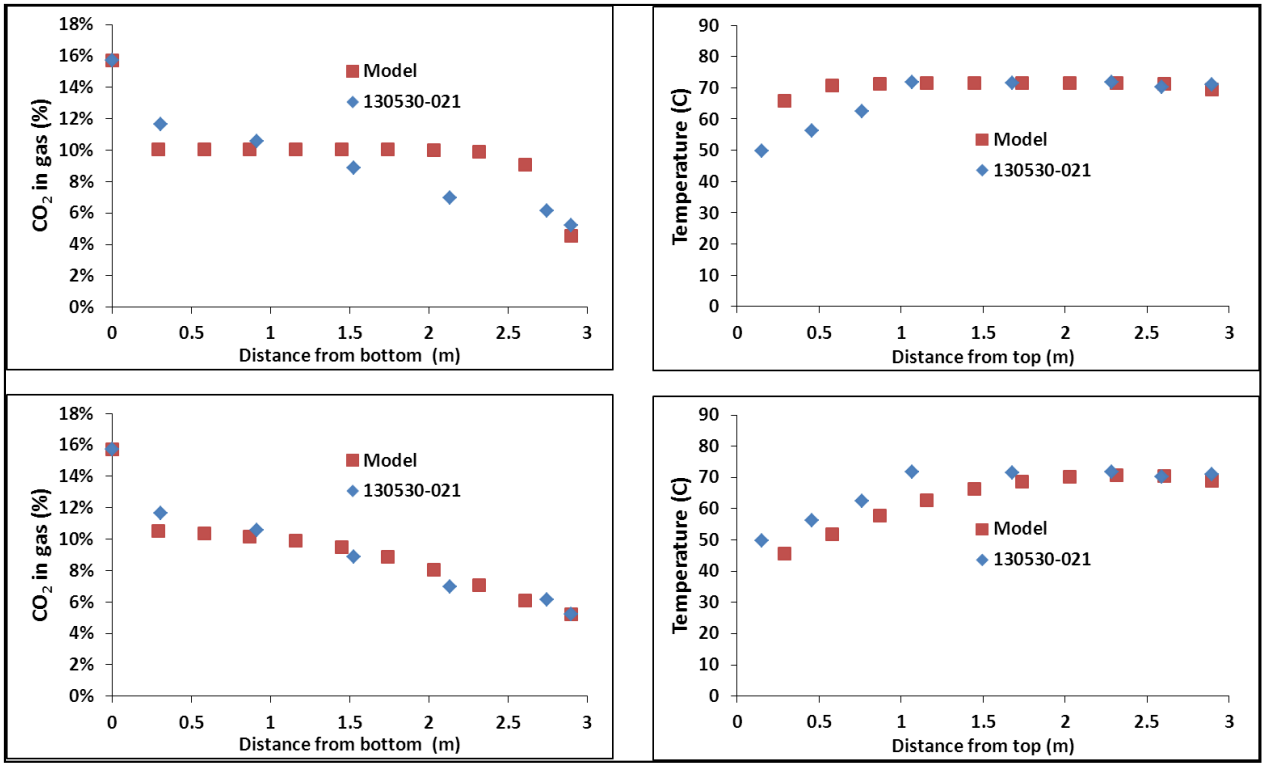

Figure 162. Absorber response for Case 3. The top two charts use the equilibrium/equilibrium model in Aspen Plus™. The bottom two charts use the rate/equilibrium model.

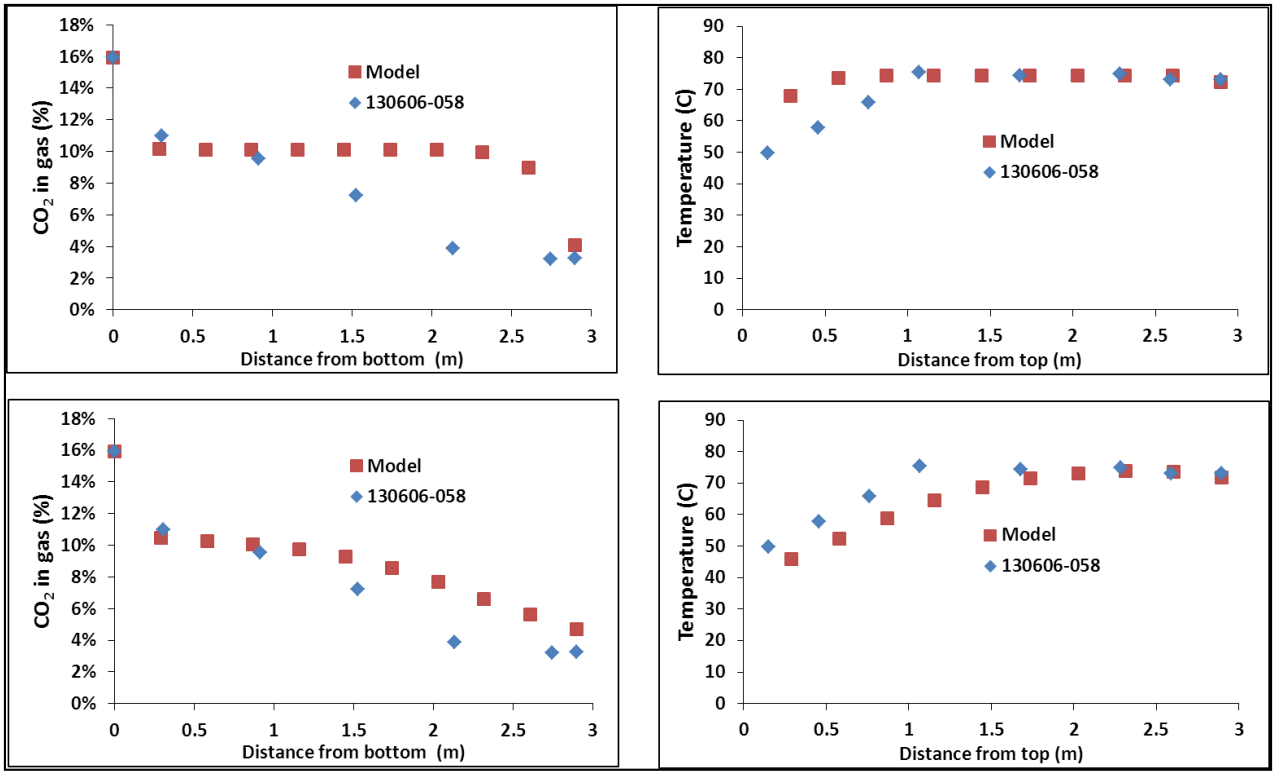

Figure 163. Absorber response for Case #4. The top two charts use the equilibrium/equilibrium model in Aspen Plus™. The bottom two charts use the rate/equilibrium model.

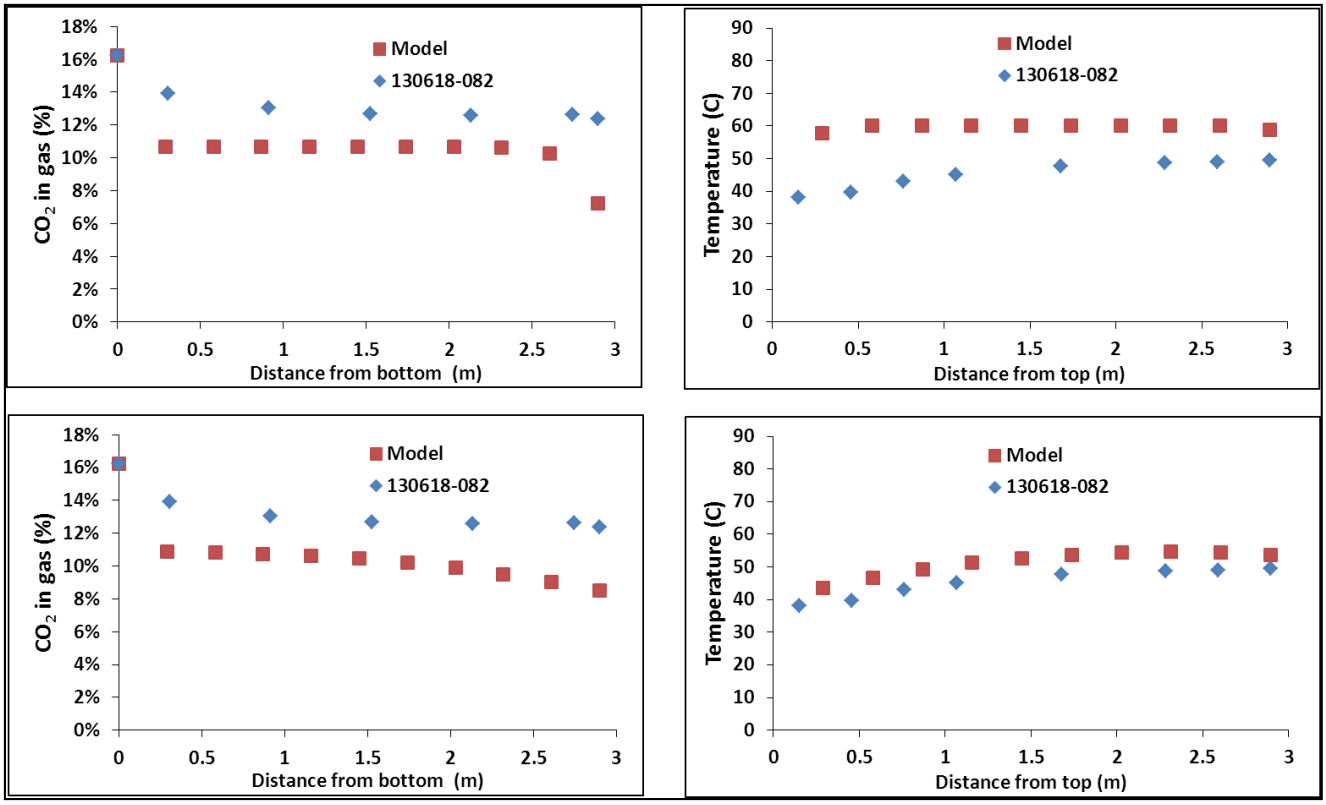

Figure 164. Absorber response for Case #5. The top two charts use the equilibrium/equilibrium model in Aspen Plus™. The bottom two charts use the rate/equilibrium model.

Four more experiments were selected to compare the absorber response with the model predictions. In these selected experiments the gas flow rate and the liquid (lean solvent) flow rate were varied as shown in the Table 57 below. The CO_2 concentration in the gas phase inlet to the absorber was fixed around 16%. Note that the temperature profile for Case #6 was not available experimentally. Good agreement was again observed between the experimental results and the model predictions via the second method, the rate/equilibrium model. Generally, excellent agreement was observed at the inlet and outlet conditions. The concentration and temperature profiles showed generally good agreement even though there were some differences between the rate/equilibrium model and the experimental observations in some of the selected cases. The comparisons are shown in Figures 165-168.

Table 57. Experiments selected for comparison of model predictions with experimental observations.

Case	Gas flow rate (slpm)	Liquid flow rate (lpm)	Actual CO_2 % inlet to absorber
#6:130411-152	75	0.5	16.10%
#7:130422-167	100	0.5	16.27%
#8:130423-177	119	0.5	16.29%
#9:130509-257	119	1	16.14%

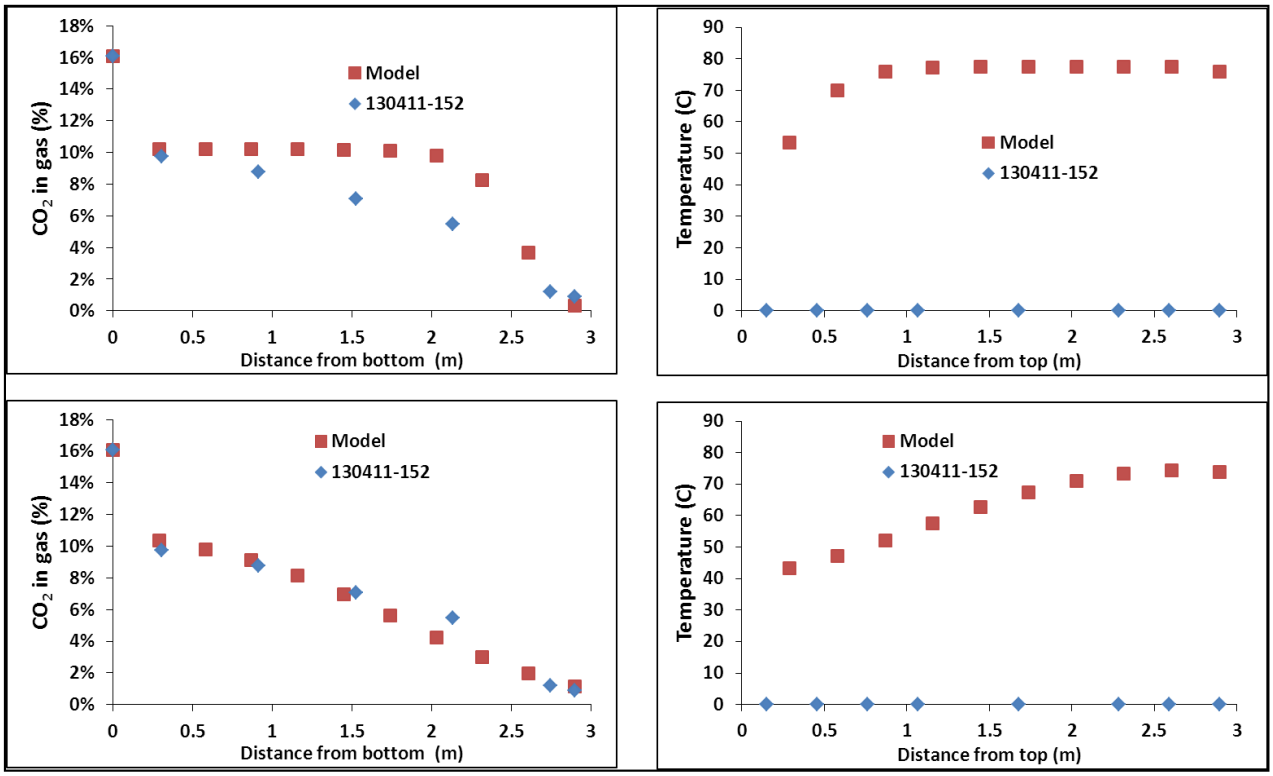

Figure 165. Absorber response for Case #6. The top two charts use the equilibrium/equilibrium model in Aspen Plus™. The bottom two charts use the rate/equilibrium model. The experimental temperature profile was not measured in this experiment.

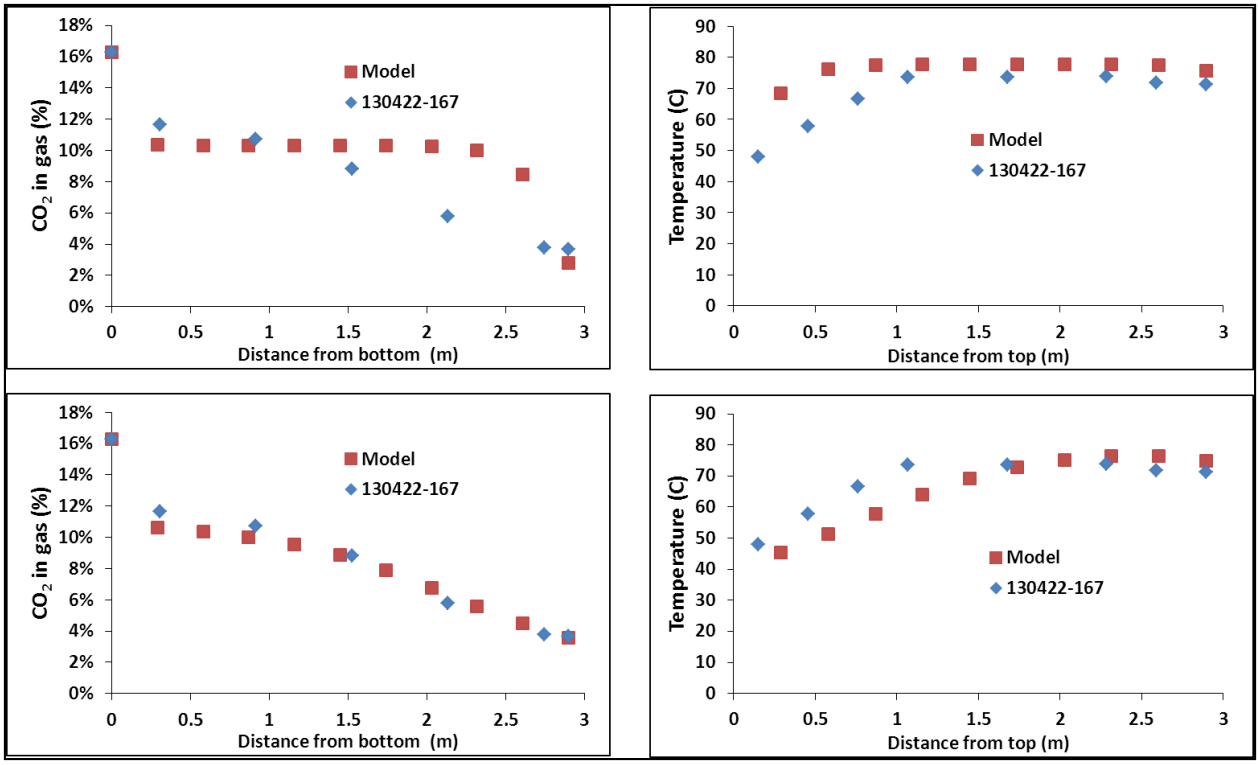

Figure 166. Absorber response for Case #7. The top two charts use the equilibrium/equilibrium model in Aspen Plus™. The bottom two charts use the rate/equilibrium model.

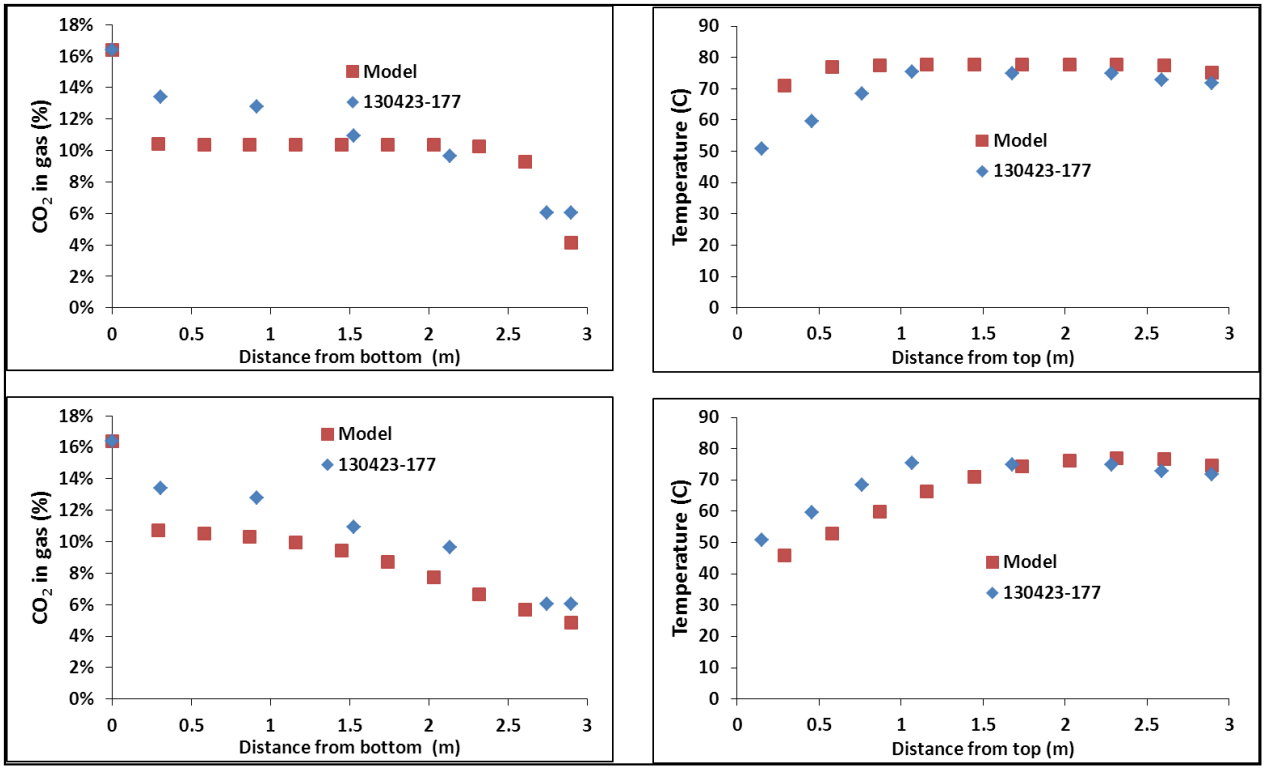

Figure 167. Absorber response for Case #8. The top two charts use the equilibrium/equilibrium model in Aspen Plus™. The bottom two charts use the rate/equilibrium model.

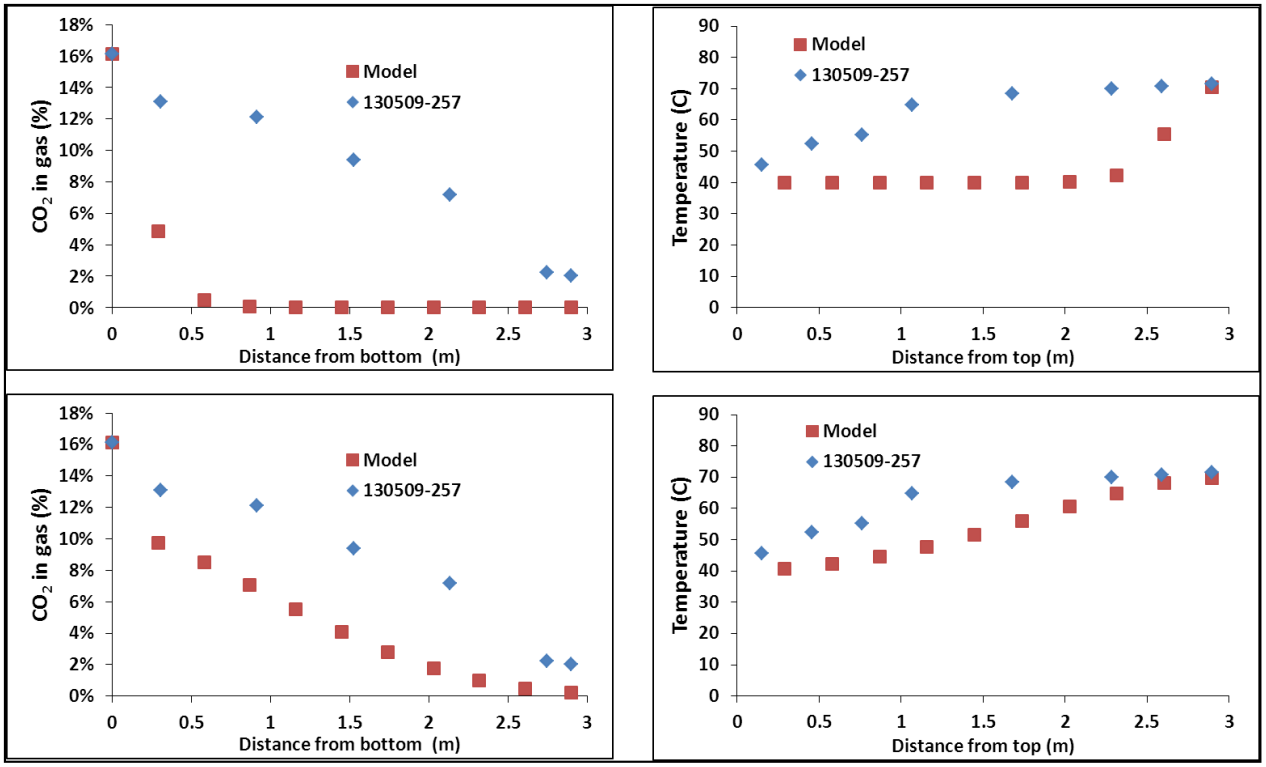

Figure 168. Absorber response for Case #9. The top two charts use the equilibrium/equilibrium model in Aspen Plus™. The bottom two charts use the rate/equilibrium model.

In one of the cases for economic evaluation, the temperature of the desorber was taken to be 130 °C, and therefore additional comparison of three bench-scale experiments and model predictions was conducted. These runs were at the following conditions.

Table 58. Operating conditions for runs compared with bench-scale model performance.

	Run 130605-047	**Run 130620-100**	**Run 131003-060**
Desorber T, °C	130.8	131.5	130
Desorber P, psig	45.3	45.3	45
%mol CO_2 in FG	16.01%	15.94%	16.80%
Gas flowrate, SLPM	112	112	119
Liquid flowrate, lpm	0.5	0.5	1.8

These input data were properly set up in the Aspen Plus™ bench-scale model, and for all analyses the absorber was modeled with Rate-based mass transfer since it demonstrated much better agreement with experiment. The results are presented below for each of the models. Error bars were determined through a Gage R analysis for the experimental data.

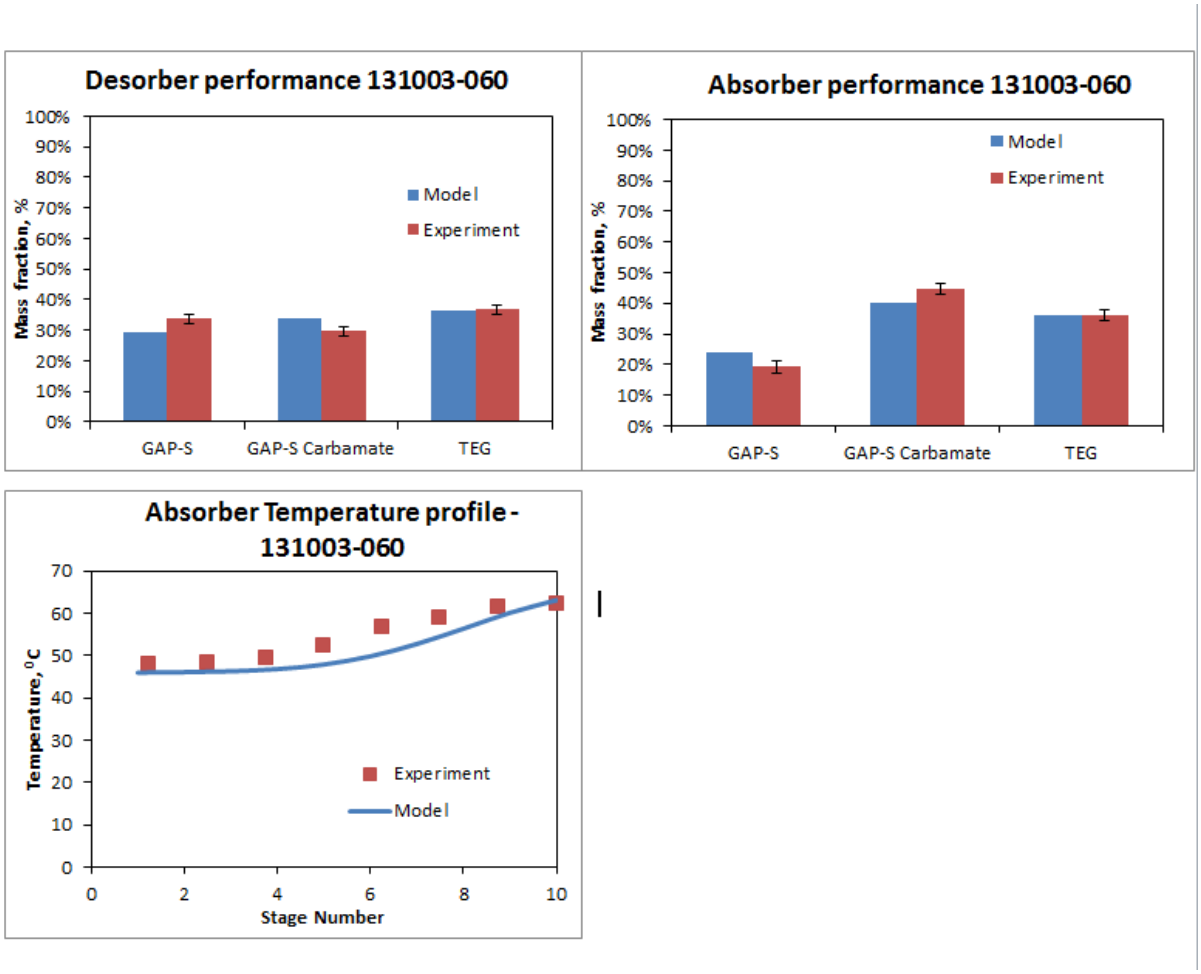

Figure 169. Comparison of bench-scale model with experimental data for Run 131003-060.

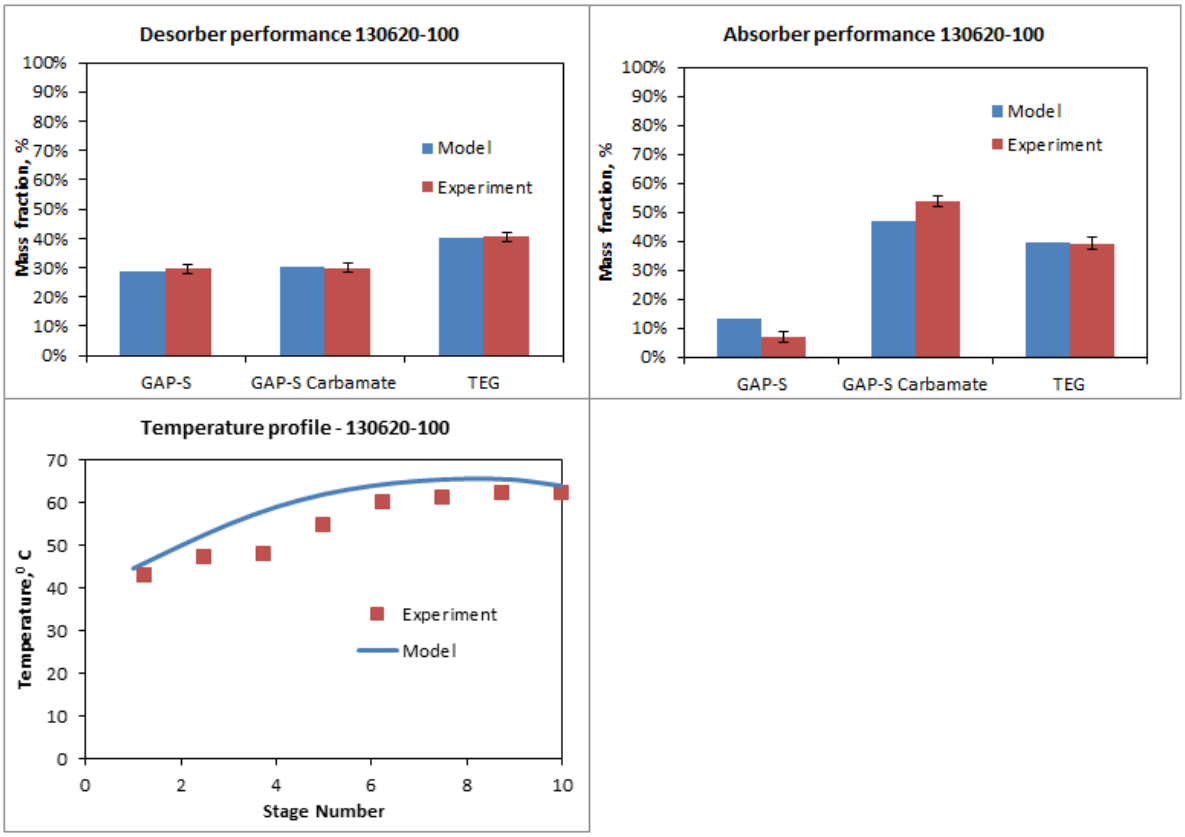

Figure 170. Comparison of bench-scale model with experimental data for Run 130620-100.

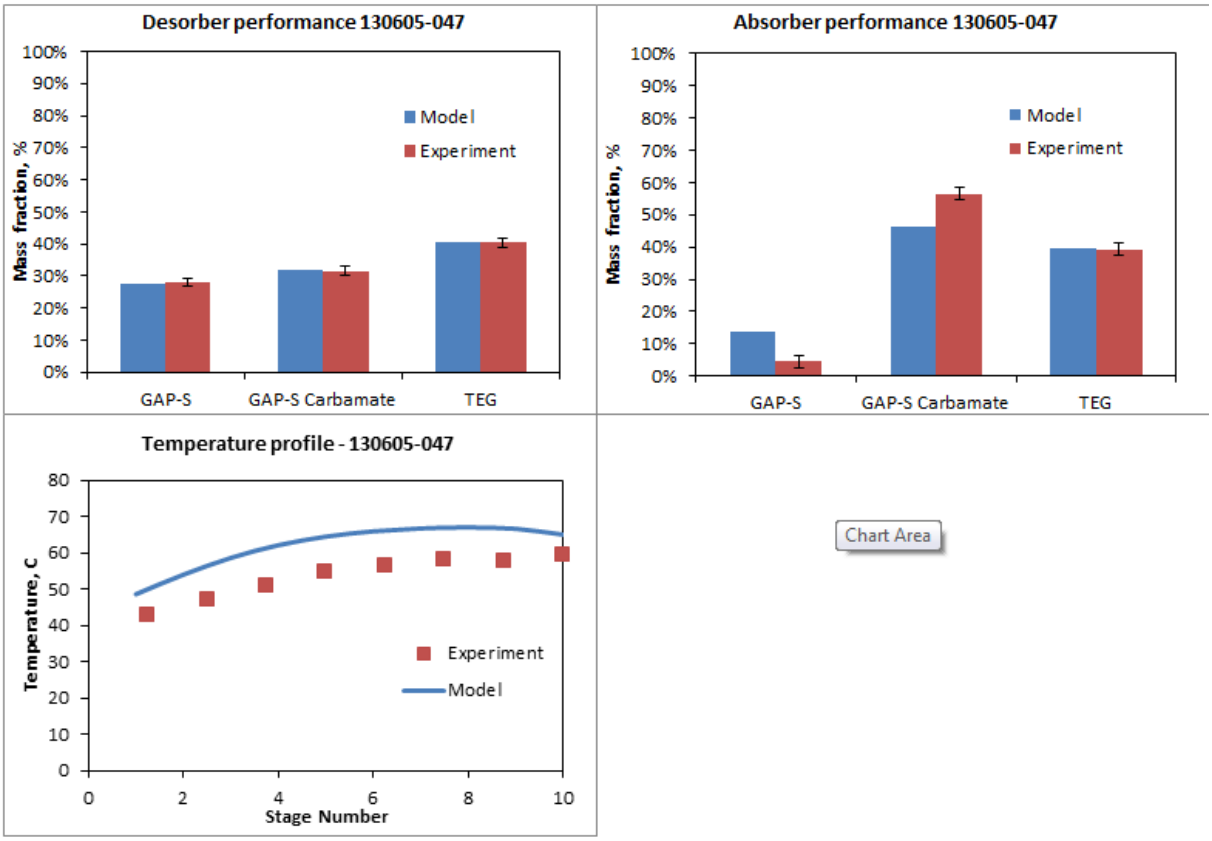

Figure 171. Comparison of bench-scale model with experimental data for Run 130605-047.

Task 8.2: Perform Final Technical and Economic Feasibility Study and Update COE Calculations

Process Description

The pulverized coal (PC) plant and CO_2 separation unit based on mono-ethanol amine (MEA) is described in Case 10 of the DOE report titled "Cost and Performance Baseline for Fossil Energy Plants, DOE/NETL-2007/1281, Volume 1: Bituminous Coal and Natural Gas to Electricity Final Report, May 2007".

A simplified block diagram of the power plant and CO_2 separation system is shown in Figure 172. The pulverized coal boiler generates steam, which is sent to the steam turbines. The flue gas is sent through a selective catalytic reduction (SCR) unit to reduce nitrogen oxides (NO_X), a

bag house to remove fly ash, and a flue gas desulfurizer (FGD) to remove sulfur dioxide. The flue gas is then sent through the carbon dioxide separation unit before venting the flue gas.

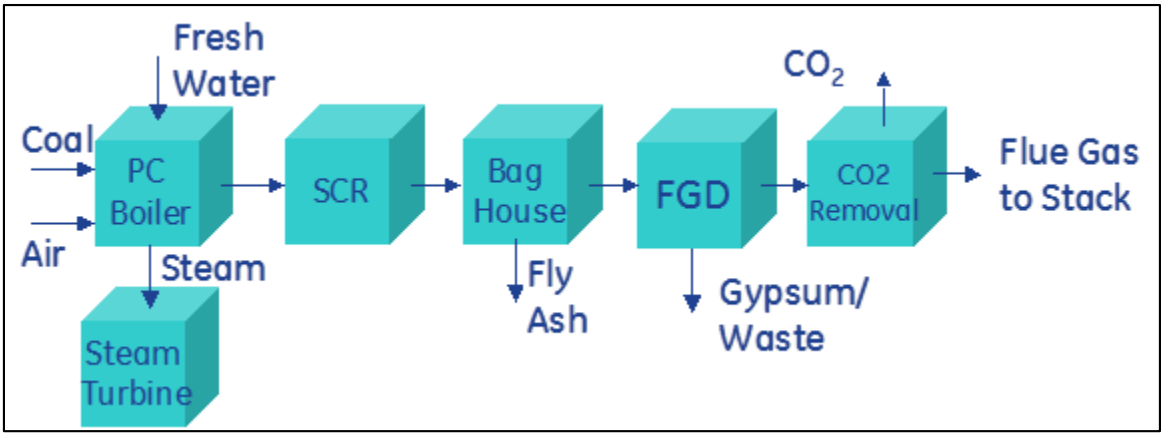

Figure 172. System block diagram.

The MEA and GAP-1m/TEG CO_2 separation units utilize four key processes, CO_2 absorption, CO_2 desorption, sorbent handling, and CO_2 compression.

The flue gas from the power plant is processed in a direct contact cooler to reduce the temperature to 40 °C (104 °F) and then enters the absorber, as shown in Figure 173. The lean sorbent enters the absorber at 40 °C (104 °F) and captures most of the CO_2 from the flue gas and the rich sorbent leaves the absorber. The CO_2 absorption increases the temperature of the sorbent. The absorber is operated at 66-82 °C (150-180 °F) and at atmospheric pressure.

The rich sorbent from the absorber is fed to the rich-lean heat exchanger and heated up before being fed to the desorber (stripper) for separation of the absorbed CO_2. A 5.6-11.7 °C (10-30 °F) approach is assumed for this rich-lean heat exchanger. This is defined as the hot fluid outlet temperature minus the cold fluid inlet temperature. The lean sorbent from the desorber is passed through the other side of the rich-lean heat exchanger.

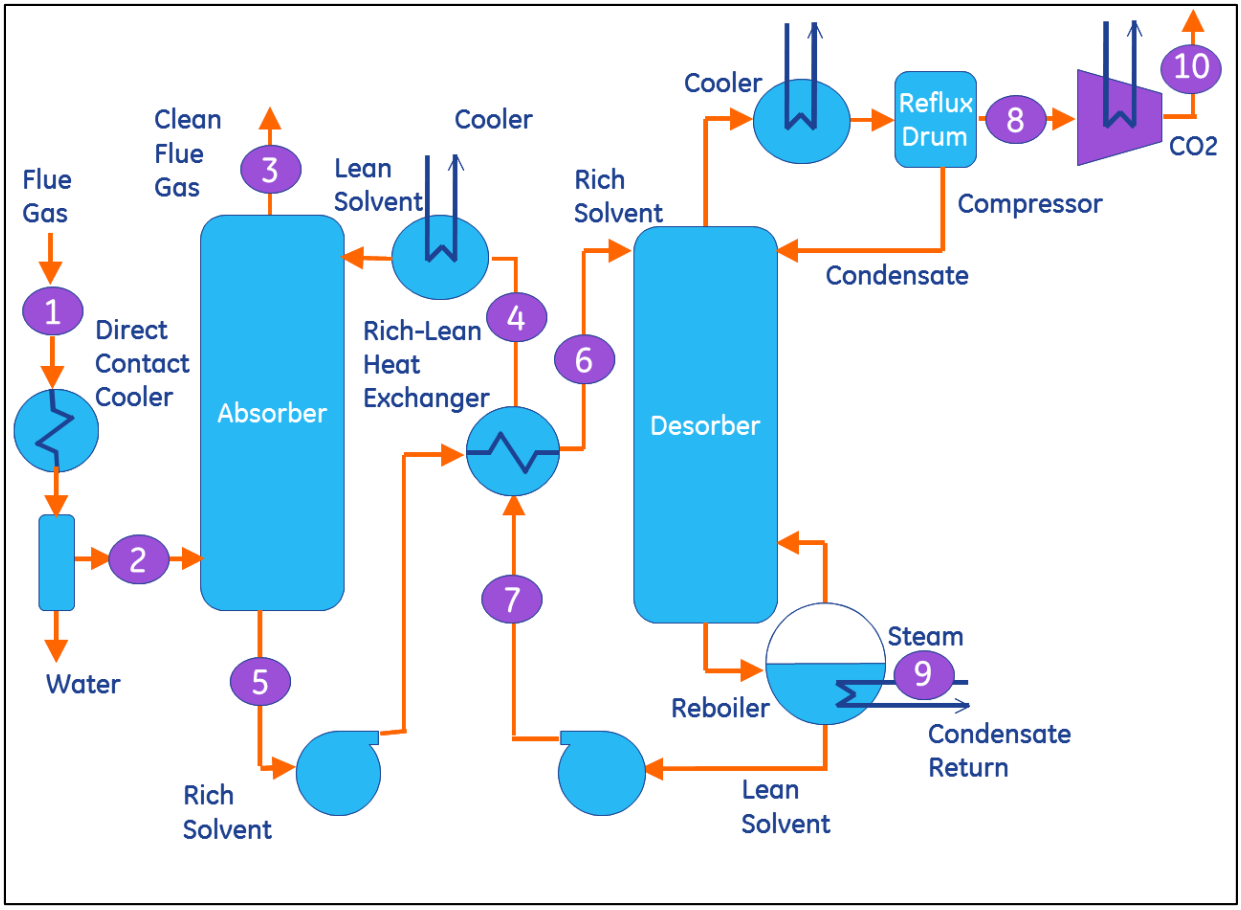

Figure 173. CO_2 separation sub-system.

For the aminosilicone solvent baseline case, the desorber operates at 140 °C (284 °F) and 4.3 atm (63 psia). For the sensitivity studies, the desorber conditions were varied from 130 to 140 °C (266 to 284 °F) and from 1.4 to 5.1 atm (20 to 63 psia) and these results are presented in subsequent sections. For the MEA Baseline Case, the desorber reboiler conditions are about 116 °C (240 °F) and 1.6 atm (23 psia). Steam is supplied to the desorber to provide heat, which releases CO_2 from the rich sorbent. Steam is supplied from the low pressure (LP) section of the steam turbine in the power plant sub-system. Steam conditions were given in the cooperative agreement. The hot vapor from the top of the desorber consisting primarily of CO_2 is cooled in a heat exchanger utilizing water. The stream then flows to a separator where the vapor and entrained liquid are separated. The CO_2 gas is removed from the separator and then delivered to the CO_2 product compressor. The liquid from the bottom of the separator is returned back to the desorber.

The lean sorbent from the desorber is pumped through the rich-lean heat exchanger to the absorber. The lean sorbent is cooled further before being fed to the absorber in order to increase the loading of CO_2 in the absorber.

GAP-1m/TEG Plant-Scale Model Development

Since the bench-scale model demonstrated good predictability of the experimental data, it was used to build a more detailed model for the plant-scale GAP-1m/TEG process, and it is presented in Figure 174.

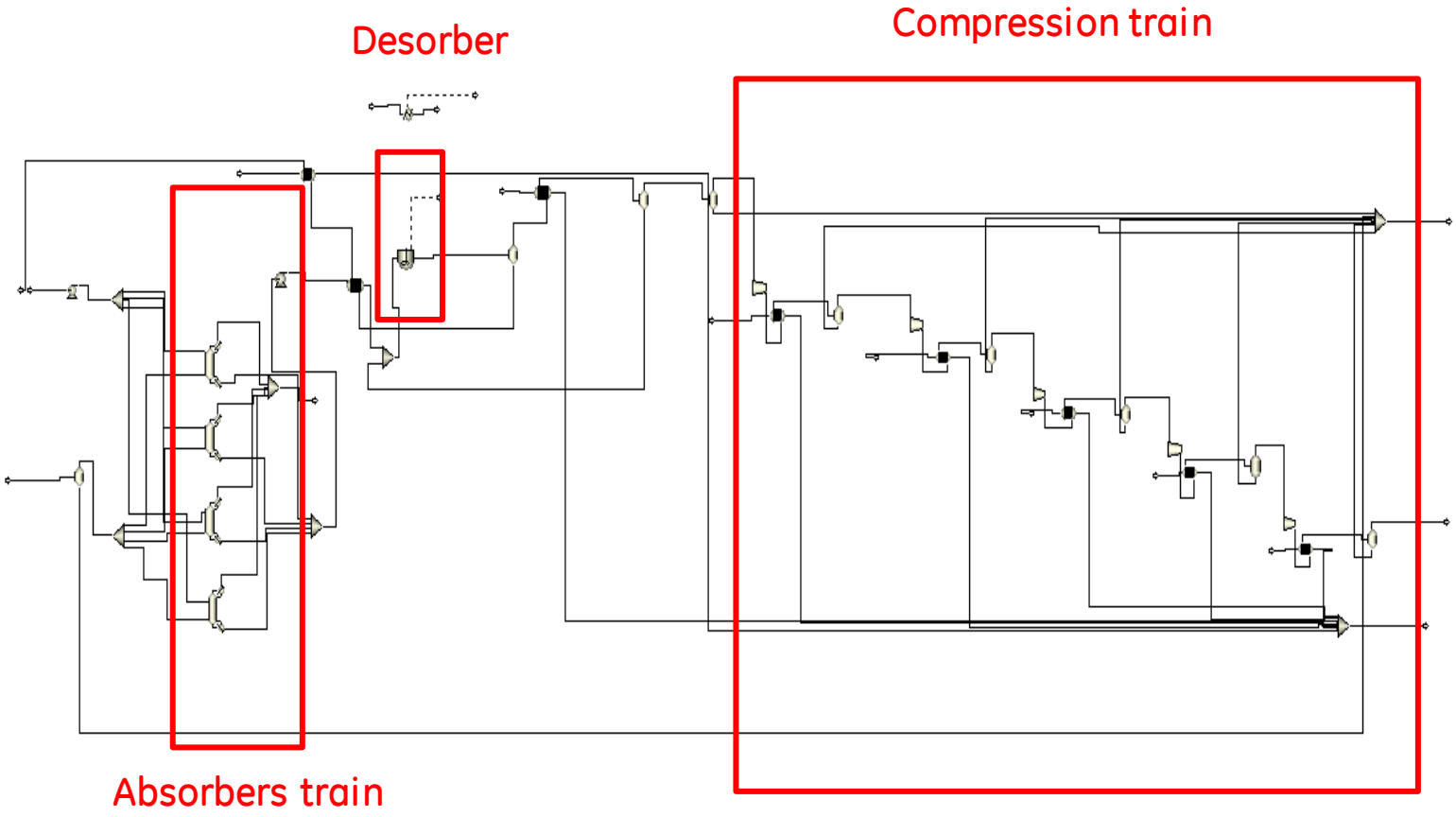

Figure 174. Plant-scale Aspen Plus™ model for 60/40 GAP-1m/TEG CO_2 capture process.

Each step of this model will be discussed in detail.

Absorber Design

Absorber train consists of 4 absorbers and the flow diagram is presented below.

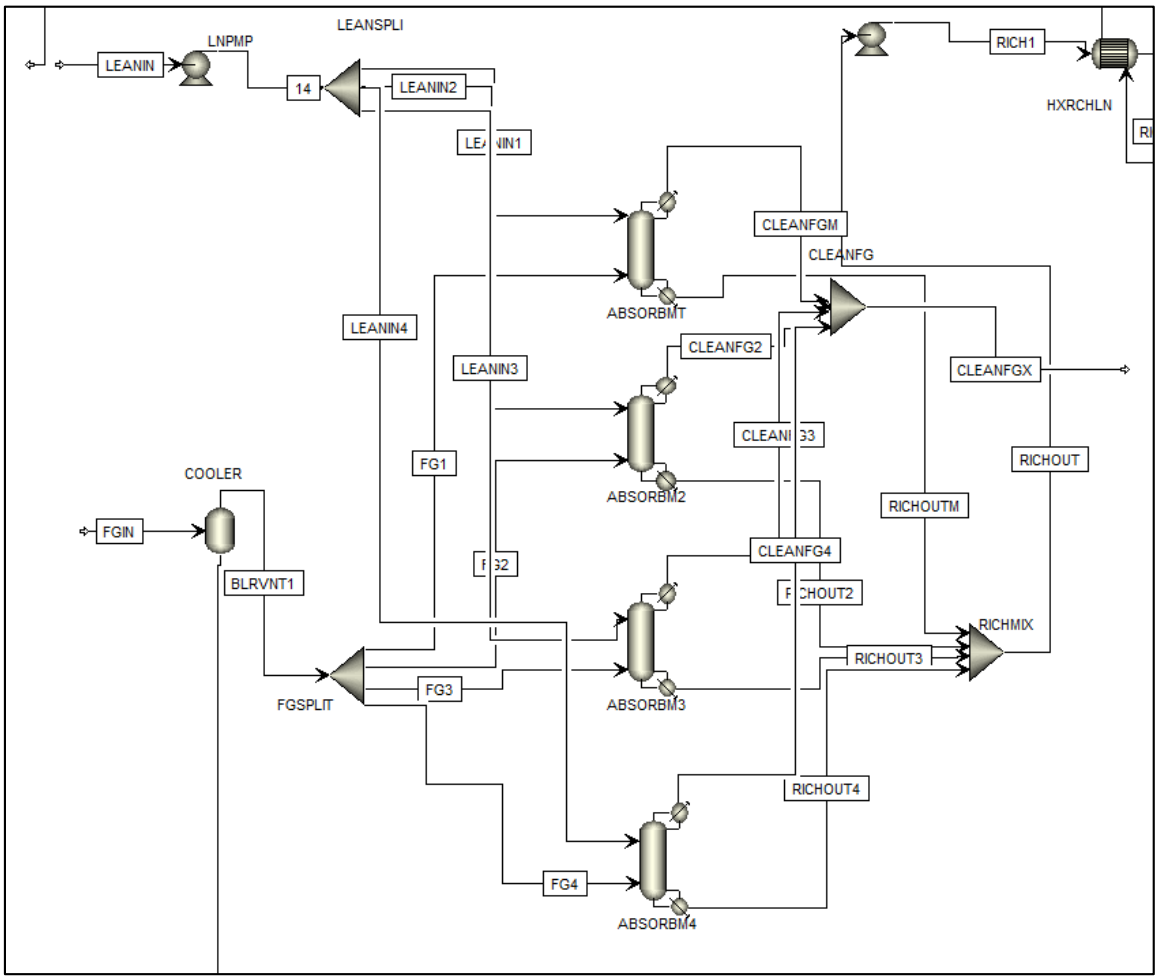

Figure 175. Absorber train of 4 absorbers for 60/40 GAP-1m/TEG CO_2 capture plant-scale process.

Significant improvements in the absorber model have been made. In the preliminary Technical and Economic Feasibility Study, the absorber was modeled as a yield reactor. In the current model each absorber is modeled using the RadFrac block which models packed towers with chemical reaction. The same set-up is used for the absorbers in the detailed model for the MEA processes.

Packing information is built into the Aspen Plus™ software for specific types of packing. The packing most similar to the packing in the bench-scale model was used. The diameter of the absorber column is determined mainly by the gas flow rate, and an iterative analysis was conducted to determine minimal diameter without flooding in the column (38 ft).

Height of the packing in the absorber is determined by 2 main factors, mole ratio of total liquid flow rate (Lm) to the total gas flow rate (Gm) and the required CO_2 capture by the absorber, which is 90%. Sensitivity analysis in the model was conducted to determine the minimal packing height required to obtain 90% of CO_2 capture at fixed Lm/Gm ratio. From the results of this sensitivity analysis, a packing height of 50 ft was selected, with a slight increase in lean solvent flow rate required to obtain the specified CO_2 capture.

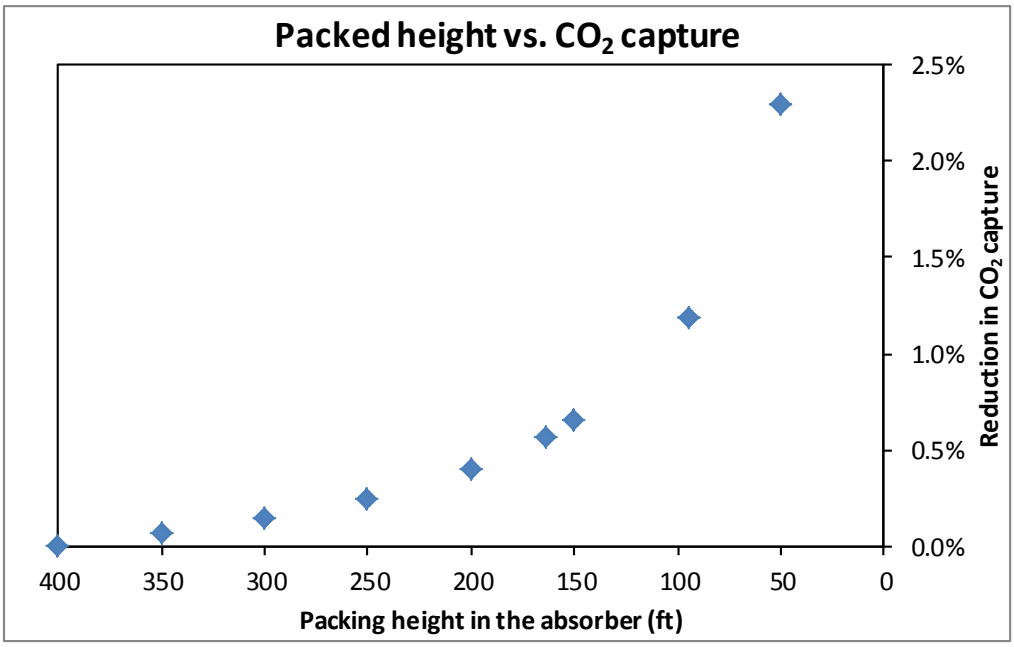

Figure 176. Reduction in CO_2 capture versus height of packing in absorber relative to 400 ft of packing.

Several cases were considered to determine the optimal economic option. The following cases were considered.

Table 59. Process conditions for cases considered for economic analysis and comparison.

	Lm/Gm	*Desorber T, °C*	*Desorber P, psia*	*Intercoolers*	*Material*
Case 1	1.12	140	63	No	CS/SS
Case 2	0.81	140	63	Yes	CS/SS
Case 3	0.66	140	20	Yes	CS/SS
Case 4	0.72	130	20	Yes	CS/SS
Case 6	0.99	130	63	Yes	CS/SS
Case 7	0.81	140	63	Yes	CS

In each case 90% CO_2 capture was obtained. Since the flue gas flow rate is fixed for all of the cases, the dimensions of the absorber units are the same. The diameter of the absorber is 38 ft, and the packed height is 50 ft.

Case 1 primarily uses carbon steel (CS) components with stainless steel (SS) used in the most corrosive portions of the process. Case 2 and higher have absorber stage intercoolers incorporated into the model. They reduce the temperature of the solvent in the absorber. By doing so, more CO_2 is captured per lean solvent amount, therefore reducing the Lm/Gm ratio. There are several ways to set up intercoolers in Aspen Plus™ software. It can be set up as a total heat load removed or amount removed per stage from the vapor and liquid phases. Case 7 uses carbon steel for all components.

During bench scale experiments some heat was lost into the environment, although the bench-scale model doesn't incorporate this and considers the absorber to perform adiabatically. Some iterative work was conducted to determine how temperature profile in the model is affected by heat loss from the solvent. One experimental run was selected, and the temperature profile was analyzed at different levels of heat removal.

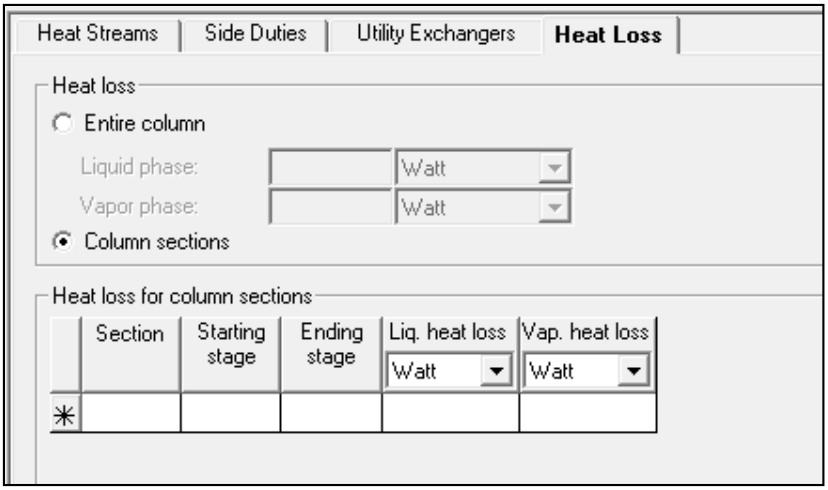

Figure 177. Heat loss set-up for the absorber in Aspen Plus™.

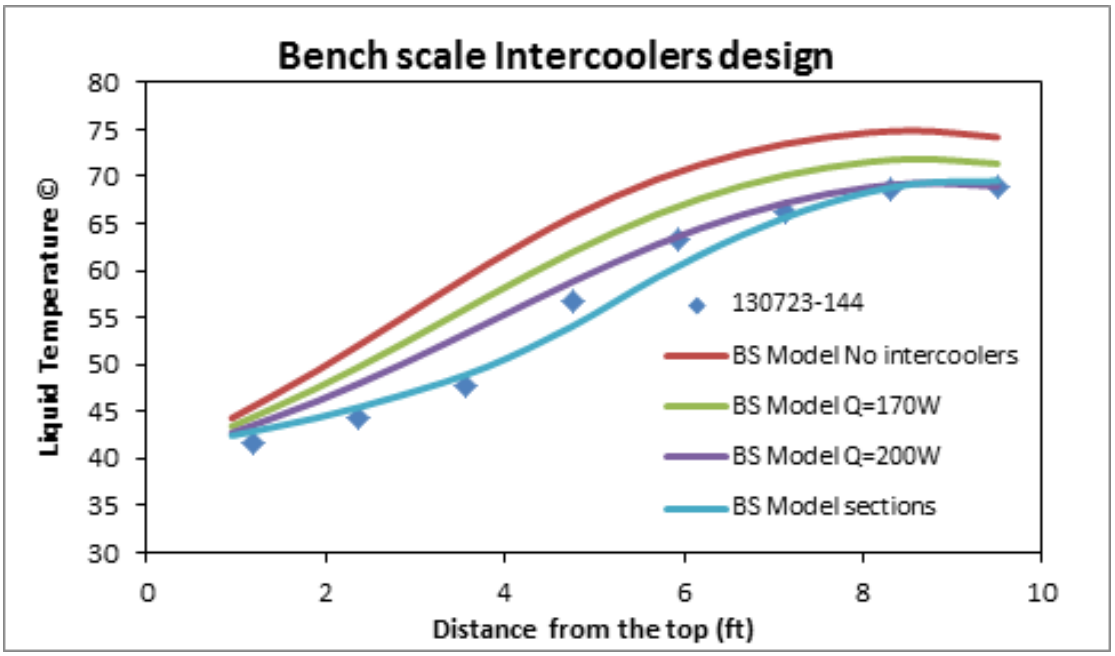

Figure 178. Effect of different heat removal amounts on temperature profile in the absorber.

It can be see that by addition of the intercoolers into the model the model temperature profile better matches the experimental bench-scale data. During the following pilot-scale program the

absorber will be equipped with intercoolers. Therefore, the amount of heat removed from the column will be known and will be incorporated in the process model.

Desorber Design

The desorber was designed as a CSTR for the bench-scale system, and it will be scaled up as a CSTR as well. The plant scale model for the desorber unit is presented below in Figure 179.

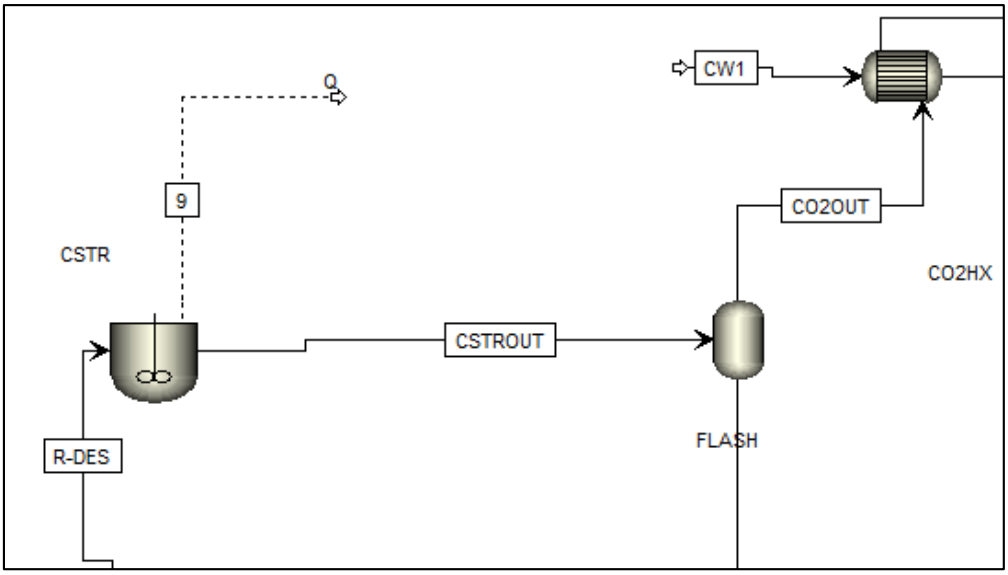

Figure 179. Desorber unit of plant-scale model.

The main design parameters for the CSTR are temperature, pressure, and residence time. Temperature and pressure were varied for different cases (see above). Residence time was selected to be 11 minutes because a sensitivity analysis determined that to be the minimum time at which the process reaches equilibrium.

Since the desorber unit is a critical unit operation in this process, redundacy will be required at the commercial scale to ensure safe process operation. Therefore, the desorber system consists of two CSTR reactors, each with a recirculation loop. The recirculation loops include shell-tube heat exchangers and pumps. The recirculation loops server two functions. First, they will transfer required heat to the solvent, and second they will increase mixing, thus reducing the mass transfer limitations. Since solvent flow rate varies in each considered case, the size of the desorber and recirculation loop heat exchanger will vary in each case.

The values of the overall heat-transfer coefficicents for desorber jacket and shell and tube heat exchangers was found in the literature, and the following values were used as shown in Table 60.

Table 60. Values for overall heat transfer coefficients for jacketed vessel and shell and tube heat exchanger.

Type of heat transfer unit	*Overall heat transfer coefficient U (BTU/hr·ft^2·F)*
Jacketed vessels: steam to organics, SS wall, average	100
Shell and Tube heat exchanger: steam to light organics, average	185

Based on a specified residence time of 11 minutes, the volume of the reactor can be determined. The amount of heat which can be transfered through the jacket of the reactor can be determined through the following equation.

$$Q_{reactor} = U * A * LMTD$$

And the heat required to be transferred through the recirculation loop is calculated by the difference of the total heat load and $Q_{reactor}$. Based on the obtained value, the size of the heat exchanger and number of cycles is determined. Below is the summary table (Table 61) for the desorber design for different cases.

Table 61. Conditions for cases considered for economic analysis.

	Desorber diameter, m	*Desorber height, m (includes 5 m V-L disengagement volume)*	*Area of Recirculation loop heat exchanger, m^2*	*Number of cycles/min*
CASE 1	10	20	519	0.34
CASE 2	10	16	534	0.43
CASE 3	10	15.4	572	0.50
CASE 4	10	15.9	553	0.45
CASE 6	10	18.2	503	0.36

These dimensions were used in the economic calculations.

CO_2 Separation Unit Key System Assumptions

The model used the following process design assumptions given in cooperative agreement DE-FE0007502.

1) Composition of flue gas leaving FGD (wet basis):

	Volume %
CO_2	13.17
H_2O	17.25
N_2	66.44
O_2	2.34
Ar	0.8
	ppmv
SOx	42
NOx	74

2) Flow rate of flue gas leaving FGD (based on 550 MW net PC plant): 5,118,399 lb/hr

3) Pressure and temperature of flue gas leaving FGD: 14.7 psia and 135 °F

4) Conditions for LP steam available from power plant: 167.7 psia and 743.3 °F

5) Conditions for cooling water: feed = 60 °F, return = 80 °F with a minimum approach of 30 °F

6) CO_2 removal from flue gas: greater than 90%

7) CO_2 purity: greater than 95 vol%

8) CO_2 delivery pressure and temperature: 2,215 psia and 124 °F

The MEA and aminosilicone solvent baseline models are based on the typical temperature-swing sorbent separation process. The systems have four process variables that dominate the performance with a given sorbent and they are absorber temperature, desorber temperature, desorber pressure, and rich/lean heat exchanger approach temperature. The system models account for the major energy penalties for CO_2 separation, and they include the energy required:

(1) for vaporization of water

(2) to desorb the carbon dioxide (i.e., reaction energy)

(3) for sensible heating of the sorbent

The energy is supplied by feeding steam to the desorber unit. The models also account for CO_2 compression energy and auxiliary loads.

The sorbent rich loading is defined as the weight % of CO_2 in the rich sorbent leaving the absorber column. The sorbent lean loading is defined as the weight % of CO_2 in the lean sorbent leaving the desorber column. The sorbent net loading is defined as the difference between the rich loading and the lean loading and was obtained from bench-scale experiments for the GAP-1m/TEG system.

A detailed MEA Aspen Plus™ model that was built under this project was used for comparison.

The main features of the MEA model include an absorber, rich-lean heat exchanger, and a desorber. The same unit operations are important for the GAP-1m/TEG system. The baseline MEA case is built from the description given in the Volume 1: Bituminous Coal and Natural Gas to Electricity" report by National Energy Technology Laboratory.

Heat and material balances for the MEA and aminosilicone solvent (Case 1) baseline cases are provided in Exhibits 1-1 and 1-2 respectively.

Exhibit 1-1 Case 1 Stream Table, MEA Base Case									
	Lean solvent to absorber	*FG to ABSORBER*	*Clean FG*	*HP CO_2 final stream*	*Rich solvent from absorber*	*Rich solvent to desorber*	*Lean solvent from desorber*	*CO_2 stream to compressor*	*Lean solvent to cooler*
	LEANIN	FLUEGAS	CLEANFGX	HPCO2					
Mole Frac									
MEA	0.0541	0.0000	0.0001	0.0000	0.0020	0.0020	0.0578	0.0000	0.0570
H_2O	0.8746	0.0736	0.2482	0.0030	0.8581	0.8581	0.8680	0.0470	0.8683
CO_2	0.0000	0.1474	0.0140	0.9968	0.0001	0.0001	0.0000	0.9528	0.0000
H_3O^+	0.0000	0.0000	0.0000	0.0000	0.0000	0.0000	0.0000	0.0000	0.0000
OH^-	0.0000	0.0000	0.0000	0.0000	0.0000	0.0000	0.0000	0.0000	0.0000
HCO_3^-	0.0003	0.0000	0.0000	0.0000	0.0103	0.0103	0.0012	0.0000	0.0004
CO_3^{-2}	0.0010	0.0000	0.0000	0.0000	0.0017	0.0017	0.0001	0.0000	0.0006
$MEAH^+$	0.0362	0.0000	0.0000	0.0000	0.0708	0.0708	0.0371	0.0000	0.0376
$MEACOO^-$	0.0340	0.0000	0.0000	0.0000	0.0571	0.0571	0.0358	0.0000	0.0361
N_2	0.0000	0.7527	0.7129	0.0001	0.0000	0.0000	0.0000	0.0001	0.0000
O_2	0.0000	0.0262	0.0248	0.0000	0.0000	0.0000	0.0000	0.0000	0.0000
CO	0.0000	0.0000	0.0000	0.0000	0.0000	0.0000	0.0000	0.0000	0.0000
H_2	0.0000	0.0000	0.0000	0.0000	0.0000	0.0000	0.0000	0.0000	0.0000
H_2S	0.0000	0.0000	0.0000	0.0000	0.0000	0.0000	0.0000	0.0000	0.0000
HS^-	0.0000	0.0000	0.0000	0.0000	0.0000	0.0000	0.0000	0.0000	0.0000
S^{-2}	0.0000	0.0000	0.0000	0.0000	0.0000	0.0000	0.0000	0.0000	0.0000
Total	1.00	1.00	1.00	1.00	1.00	1.00	1.00	1.00	1.00
Total Flow lbmol/hr	688821	160486	169459	21348	658595	658595	654269	22336	654260
Total Flow lb/hr	17161570	4772875	4381883	937772	17552562	17552562	16538436	955661	16538436
Total Flow cuft/hr	256399	65960274	75697370	44422	247067	247055	260654	5780069	249264
Temperature F	104	104.0	153.1	104	115	115	240	104	135
Pressure psia	14.70	14.7	14.70	2220	15	100	23	23	93
Vapor Frac	0	1	1.000	0.999	0	0	0	1	0
Enthalpy Btu/lb	-5181	-1090	-1069	-3893	-5095	-5095	-5013	-3877	-5096.1515
Density lb/cuft	66.93	0.07	0.06	21.11	71	71	63	0.165	66.349
Average MW	24.91	29.74	25.86	43.93	27	27	25	43	25.278

Exhibit 1-2 Stream Table, GAP-1/TEG Base Case									
	Lean solvent into absorber	*FG to absorber*	*Clean FG*	*HP CO_2 final stream*	*Rich solvent from absorber*	*Rich Solvent to desorber*	*Lean solvent from desorber*	*Lean solvent to cooler*	*CO_2 to compressor*
Mole Frac									
H_2O	0.2407	0.0731	0.0659	0.0008	0.2583	0.2669	0.2350	0.2350	0.0170
CO_2	0.0082	0.1475	0.0165	0.9919	0.0005	0.0005	0.0084	0.0084	0.9759
N_2	0.0001	0.7532	0.8861	0.0072	0.0012	0.0012	0.0001	0.0001	0.0071
O_2	0.0000	0.0262	0.0309	0.0000	0.0000	0.0000	0.0000	0.0000	0.0000
GAP-S	0.2653	0.0000	0.0004	0.0000	0.0912	0.0906	0.2632	0.2632	0.0000
GAP-S CARB	0.0339	0.0000	0.0003	0.0000	0.2032	0.2007	0.0377	0.0377	0.0000
D4	0.0000	0.0000	0.0000	0.0000	0.0000	0.0000	0.0000	0.0000	0.0000
TEG	0.4519	0.0000	0.0000	0.0000	0.4456	0.4400	0.4556	0.4556	0.0000
Total	1.00	1.00	1.00	1.00	1.00	1.00	1.00	1.00	1.00
Total Flow lbmol/hr	130000	160395	136160	21065	131821	133536	128942	128942	21415
Total Flow lb/hr	22148650	4771236	3803405	924170	23116261	23179467	22124069	22124069	930560
Total Flow cuft/hr	302858	66001755	59958986	59567	309581	333217	339703	315827	2056175
Temperature F	104	104	143	124	158	260	285	179	104
Pressure psia	15	14.7	14.6959488	2215	15	63	63	63	63
Vapor Frac	0	1	1	1	0	0	0	0	1
Enthalpy Btu/lb	-2241.92	-1087.77	-343.17	-3817.30	-2334	-2288	-2153	-2206	-3834
Density lb/cuft	73.13	0.07	0.06	15.51	75	70	65	70	0.45
Average MW	170	30	28	44	175	174	172	172	43

The MEA equipment list is summarized in Table 62.

Table 62. MEA equipment list.

Equipment Number	*Description*	*Type*	*Design Conditions*	*Quanitity*
NA	Desorber recirculation heater	Not used	NA	NA
E002	CO_2 Cooler	Shell and tube; CS Shell; CS Tubes	Heat duty = 424 MMBTU/hr (1)	4
E003	Rich/Lean heat Exchanger	Shell and tube; CS shell; SS Tubes	Heat duty = 1,413 MMBTU/hr	1
E004	Lean Solvent cooler	Shell and tube; CS Shell; CS Tubes	Heat duty = 691 MMBTU/hr	1
NA	Absorber intercoolers	Not used	NA	NA
P001	Rich Solvent Pump	Centrifugal, CS	9,140 gpm at 85 psi pressure change	4
P002	Lean Solvent Pump	Centrifugal, CS	9,593gpm at 69.7 psi pressure change	4
	Desorber Recirculation pump	Not used	NA	NA
T001	Absorber	Packed Tower	39ft ID x 65.6 ft packed height	4
TK001	Direct contact Feed cooler	Heat Exchanger Tower, CS	66 ft ID x 10 ft height	1
TK002	Solvent feed holding tank	Vertical Cylindrical, CS	319675 gallon capacity	1
T002	Desorber	Packed Tower	25ft ID x 65.6 ft packed height	4
CPP001	CO_2 compression package	Integrally geared, multistage centrifugal	937,000 lb/hr at 2215 psia	1 train

The GAP-1m/TEG equipment table is summarized below in Table 63.

Table 63. GAP-1m/TEG equipment list.

Equipment Number	Description	Type	Design Conditions				
			Case 1	Case 2	Case 3	Case 4	Case 6
E001	Desorber Recirculation Heater	Shell and tube SS shell; SS tubes	Duty = 947 MMBtu/hr (1)	Duty = 974 MMBtu/hr (1)	Duty = 1045 MMBtu/hr (1)	Duty = 1052 MMBtu/hr (1)	Duty = 958 MMBtu/hr (1)
E002	CO2 Cooler	Shell and tube CS shell; CS tubes	Duty = 150 MMBtu/hr (1)	Duty = 139 MMBtu/hr (1)	Duty = 200 MMBtu/hr (1)	Duty = 162 MMBtu/hr (1)	Duty = 109 MMBtu/hr (1)
E003	Lean/Rich Heat Exchanger	Shell and tube CS shell; SS tubes	Duty = 1380 MMBtu/hr (1)	Duty = 1160 MMBtu/hr (1)	Duty = 991 MMBtu/hr (1)	Duty = 891 MMBtu/hr (1)	Duty = 1250 MMBtu/hr (1)
E004	Lean Solvent Cooler	Shell and tube CS shell; CS tubes	Duty = 1220 MMBtu/hr (1)	Duty = 769 MMBtu/hr (1)	Duty = 798 MMBtu/hr (1)	Duty = 829 MMBtu/hr (1)	Duty = 879 MMBtu/hr (1)
E005	Absorber Intercoolers	Shell and tube CS shell; CS tubes	Not Used	Duty = 408 MMBtu/hr (1)	Duty = 408 MMBtu/hr (1)	Duty = 408 MMBtu/hr (1)	Duty = 408 MMBtu/hr (1)
P001	Rich Solvent Pump	Centrifugal, CS	4 op/4 sp @ 13,160 GPM	4 op/4 sp @ 9,650 GPM	4 op/4 sp @ 9,110 GPM	4 op/4 sp @ 9,720 GPM	4 op/4 sp @ 11,700 GPM
P002	Lean Solvent Pump	Centrifugal, CS	4 op/4 sp @ 12,800 GPM	4 op/4 sp @ 9,440 GPM	4 op/4 sp @ 8,770 GPM	4 op/4 sp @ 9,370 GPM	4 op/4 sp @ 11,420 GPM
P003	Desorber Recirculation Pump	Centrifugal, CS	2 op/2 sp @ 96,300 GPM	2 op/2 sp @ 99,100 GPM	2 op/2 sp @ 106,300 GPM	2 op/2 sp @ 102,800 GPM	2 op/2 sp @ 97,500 GPM
T001	Absorber	Packed tower: CS shell; SS internals	4 @ 38 ft ID x 68 ft T/T	4 @ 38 ft ID x 66 ft T/T	4 @ 38 ft ID x 66 ft T/T	4 @ 38 ft ID x 66 ft T/T	4 @ 38 ft ID x 67 ft T/T
TK001	Direct Contact Feed Cooler	Heat Exchanger Tower, CS	1 @ 66 ft ID x 10 ft ht	1 @ 66 ft ID x 10 ft ht	1 @ 66 ft ID x 10 ft ht	1 @ 66 ft ID x 10 ft ht	1 @ 66 ft ID x 10 ft ht
TK002	Solvent Feed Holding Tank	Vertical cylindrical, CS	510,700 gallon capacity	377,600 gallon capacity	350,800 gallon capacity	374,800 gallon capacity	456,600 gallon capacity
TK003	Desorber CSTR	CSTR, CS w/SS cladding	2 @ 33 ft ID x 66 ft T/T	2 @ 33 ft ID x 53 ft T/T	2 @ 33 ft ID x 51 ft T/T	2 @ 33 ft ID x 52 ft T/T	2 @ 33 ft ID x 60 ft T/T
CPP001	CO2 Compressor Package	Integrally geared, multi-stage centrifugal	937,000 lb/hr @ 2215 psia	931,000 lb/hr @ 2215 psia	969,000 lb/hr @ 2215 psia	969,000 lb/hr @ 2215 psia	951,000 lb/hr @ 2215 psia
Note 1:	Total duty for all trains.						
Note 2:	Case 7 is based on Case 2 sizing but with all carbon steel metallurgy.						

Cost Estimates

In Phase 1 of the project in 2012, cost estimates were conducted using the Aspen™ Cost Estimator using the results from the revised Aspen Plus™ models. The same Aspen software was used for the current study with some minor refinements made to the 2012 model. The 2012 model had used the default plot plan which was much too small. For 2013, the plot plan area was estimated using sized equipment dimensions when available. The final plot plan area was 72,600 ft^2.

In the 2012 report, the importance of the lean/rich heat exchanger heat transfer coefficient was pointed out due to the significant of the lean/rich solvent heat exchanger area on the overall costs. Refer to the 2012 report for the detailed discussion. The same heat-transfer coefficients used in the 2012 report were used for this phase, namely, 75 Btu/hr/ft^2/°F for the GAP-1m/TEG aminosilicone solvent and 120 Btu/hr/ft^2/°F for the MEA solvent.

For the MEA model, a six stage compressor using the same inter-stage pressures as the one described in Section 4.1.7 of the DOE/NETL-2007/1281 report was used. Inter-stage coolers and knockout drums for the compressor were also sized. Carbon steel metallurgy was assumed.

For GAP-1m/TEG, the absorber was still sized as a packed tower but the desorber is now modeled and sized as a CSTR reactor. For MEA, the DOE/NETL-2007/1281 report had used packed towers so packed towers were used for both of these vessels in the MEA cost estimate.

For MEA, the rich solvent is corrosive so the absorber towers were assumed to use carbon steel shells with stainless steel packing. Also, stainless steel tubes were used for the lean/rich solvent heat exchanger and the steam reboiler in the desorber column.

In the first half of 2013, bench-scale experimental work on the aminosilicone system was conducted. Consequently, more accurate aminosilicone solvent circulation rates were used to re-size the equipment. For example, compared to the conditions for Case 1 (used in 2012 report), the solvent circulation mass rate was increased by a factor of 1.5.

For the aminosilicone (GAP-1m/TEG) solvent, six cases are considered (Cases 1-4, 6 and 7). For Cases 1-4 and 6, the metallurgy for the carbon separation unit was assumed to be carbon steel with the exception of heat exchanger tubes in the hot, rich solvent service and column internals (packing), which were made of stainless steel. In Case 7, all parts are assumed to be carbon steel to check the sensitivity of the cost of the metallurgy requirement. It is expected that the aminosilicone system is less corrosive than the MEA system and further studies will need to be done to evaluate if all components can be made from carbon steel.

The features of the six cases are shown in Table 64.

Table 64. Aminosilicone case features.

	Case 1	Case 2	Case 3	Case 4	Case 6	Case 7
Absorber Intercooler	No	Yes	Yes	Yes	Yes	Yes
Desorber Pressure, psia	63	63	20	20	63	63
Desorber Temp, deg C	140	140	140	130	130	140
Material	CS/SS	CS/SS	CS/SS	CS/SS	CS/SS	CS

Aminosilicone (GAP-1m/TEG) System

The capital cost for the MEA unit for Case 10 in the DOE/NETL-2007/1281 report is $484 Million and this is based on flue gas flow of 7,578,830 lbs/hr. In this project, DOE specified a flue gas flow of 5,118,399 lbs/hr. The correction factor for capital cost based on capacity differences between the DOE report and this project is:

CAPEX Capacity Correction Factor= (5,118,399 lbs per hour/ 7,578,830 lbs per hour)$^{0.6}$ = 0.79

Therefore, the capacity adjusted capital cost for the MEA unit based on DOE NETL Report is:

= 0.79 x $484.5 Million ~ $383 Million

GE also did an estimate of an MEA unit as an independent check and the resulting project cost was in relatively good agreement.

The relative capital costs of the various aminosilicone solvent cases versus the conventional MEA case (based on modeling performed by GE in this project, using commercially available Aspen^{TM} cost estimation software) are given in the Table 65.

Table 65. Relative CAPEX case summary.

	Case 1	Case 2	Case 3	Case 4	Case 6	Case 7
Relative Cost to MEA	0.93	0.86	0.87	0.82	0.89	0.61

Case 1 is operated at the same absorber/desorber conditions as reported in the 2012 report. Overall project cost rose by approximately 10%. The chief driver for the cost increase is the increased solvent circulation rate (about 50% higher) which results in higher heat exchange costs. Another cost adder was the switch to a CSTR type reactor system. On the other hand, costs were mitigated downward by optimizing the absorber system (reduced packed bed and overall absorber height).

Case 2 clearly demonstrates the favorable impact of absorber intercooling. Absorber intercooling is kept for the rest of the cases.

Cases 3 and 4 operate at a lower desorber pressure of 20 psia. This results in a reduced solvent circulation requirement which is off-set by the increasing product CO_2 compression cost (another compression stage is needed).

Case 6 is similar to Case 2 with the exception of a lower desorber temperature. Higher CO_2 concentration in the lean solvent to the absorber (reduced solvent capacity) results in a higher solvent circulation rate. The overall impact is a CAPEX increase.

Case 7 assumes all carbon steel metallurgy to check the sensitivity of the cost of metallurgy requirement. The cost of aminosilicone solvent Case 2 was repeated assuming a lower metallurgy for the tower internals and heat exchanger tubes (substituting carbon steel for stainless steel). It is expected that the aminosilicone system is less corrosive than the MEA system and further studies will need to be done to evaluate if all components can be made from carbon steel. If only carbon steel is required, the overall unit costs for the aminosilicone system would fall to ~70% of the aminosolvent case and to ~60% of the MEA case.

Power Plant Efficiency and Energy Penalty

The system utilities for the MEA system are summarized in the following table:

POWER SUMMARY	
AUXILIARY LOAD SUMMARY, kWe	
Feed Gas Blower	9,254
CO_2 Separation Auxiliaries	2,896
CO_2 Compression	39,712
Cooling Water Fans/Pumps	7,242
TOTAL AUXILIARIES, kWe	59,104
COOLING WATER, ton/hr	19,051
STEAM, ton/hr	688.3

The system utilities for a typical GAP-1m/TEG system are summarized in the following table:

POWER SUMMARY	
AUXILIARY LOAD SUMMARY, kWe	
Feed Gas Blower	9,254
CO_2 Separation Auxiliaries	2,087
CO_2 Compression	35,208
Cooling Water Fans/Pumps	14,332
TOTAL AUXILIARIES, kWe	60,881
COOLING WATER, ton/hr	37,704
STEAM, ton/hr	594.1

The water falls for power plant net efficiency due to CCS are shown in Figure 180 and Figure 181 at steam temperatures of 743 °F and 400 °F, respectively. The water falls for power plant energy penalty due to CCS are shown in Figure 182 and Figure 183 at steam temperatures of

743 °F and 400 °F, respectively. The 1st column is for the MEA solvent. The remaining columns are for aminosilicone solvent cases. The aminosilicone cases have significantly lower energy penalties when compared with MEA.

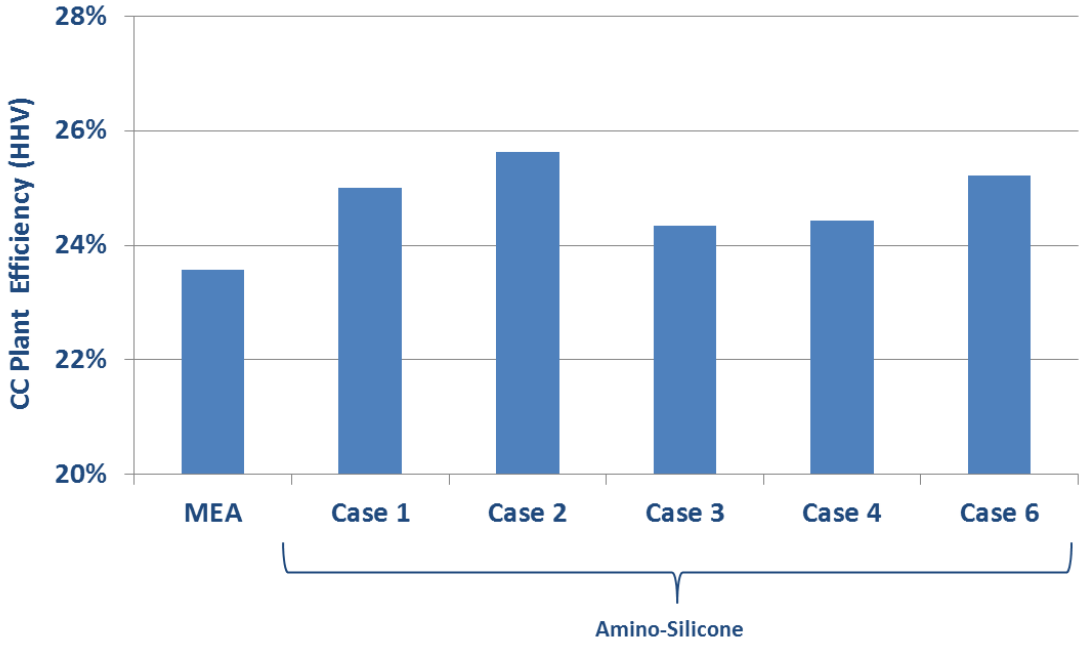

Figure 180. Plant efficiency based on HHV at steam temperatures of 743 °F.

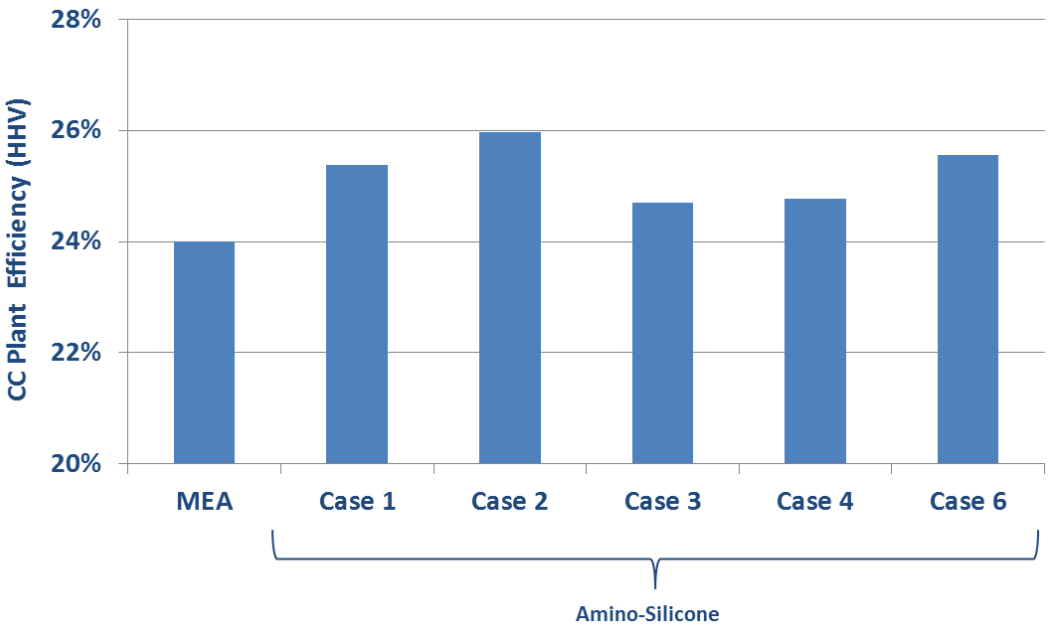

Figure 181. Plant efficiency based on HHV at steam temperatures of 400 °F.

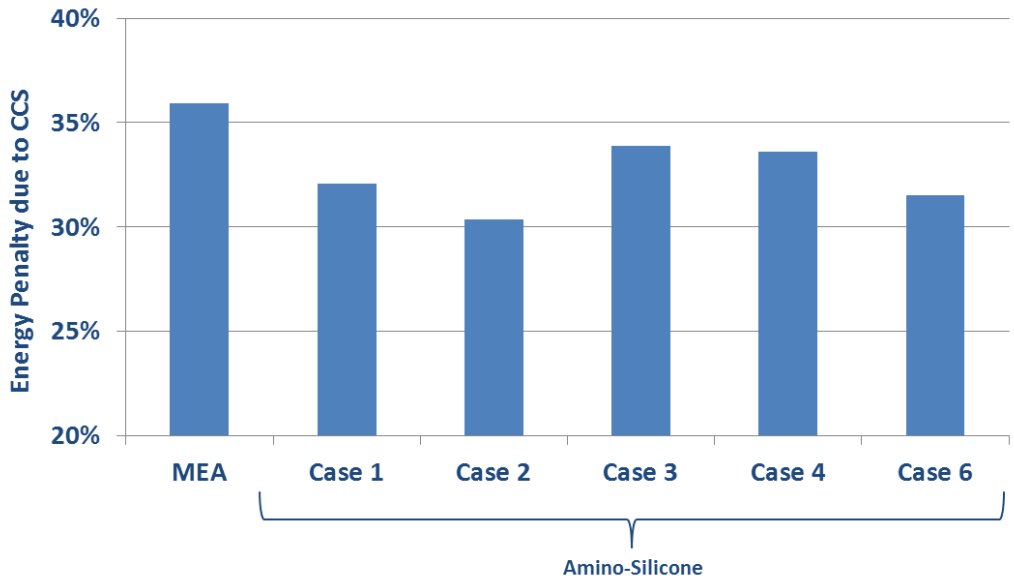

Figure 182. Energy penalty due to CCS at steam temperatures of 743 °F

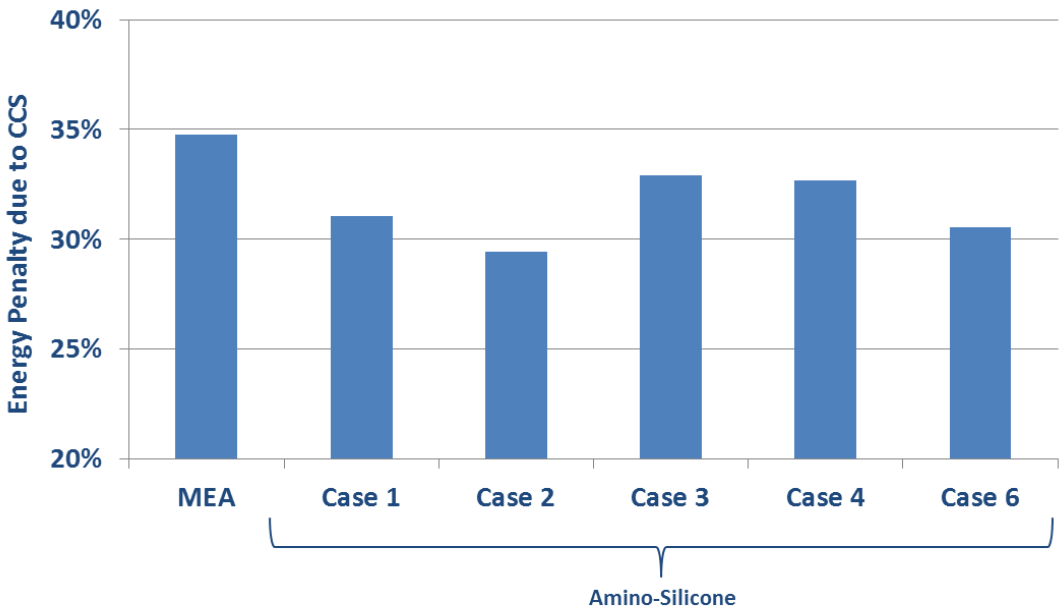

Figure 183. Energy penalty due to CCS at steam temperatures of 400 °F.

Cost of Electricity

Economic Analysis Assumptions:

As per the cooperative agreement the following economic assumptions were used:

1) Levelized-Cost of Electricity without CO_2 capture: 64 mills/kWh
2) Levelized-Cost of Steam without CO_2 capture: $5.83 / 1,000 lbs
3) Levelized-Cost of Cooling Water: $0.12 / 1,000 gal
4) Levelized-Cost of Process Make-Up Water: $0.07 / 1,000 lb
5) Levelized-Cost of Wastewater Treatment: $0.21 / lb
6) Levelized-Cost of Solid-Waste Disposal: $17.87 / ton
7) Levelized-Cost of Toxic-Waste Disposal: $89.36 / ton
8) Levelized-Cost of CO_2 Transport, Storage & Monitoring: $4.05 / ton CO_2
9) Plant On-Stream Factor: 310.25 days/yr
10) Retrofit Factor: 1.0
11) Plant Location: generic plant site, U.S. Midwest
12) Dollar-Year Reporting Basis: 2007
13) Total Fixed O&M Levelized-Costs $995 / calendar day

14) Levelized Maintenance-Material Costs 2% (as percentage of initial equipment and materials costs)
15) Capital Charge Factor: 17.5%/yr (based on 20-year levelized cost of electricity, LCOE)

The solvent usage per year was calculated assuming that one mole of SO_2 degrades one mole of solvent. This resulted in a GAP-1m loss of 122 lbs/hr.

The water fall chart for increase in cost of electricity (COE) over a non-capture case is shown in Figure 184 for a steam temperature of 743 °F, using the following equation which is specified in the contract and is marked "simple" in the chart.

$$\{\text{cost of electric power in mills/kWh}\} = 0.3073 \times \{\text{total power loss in MWe}\} + 64.00$$

The water fall chart for increase in COE using the "simple" calculation is shown in Figure 185 for a steam temperature of 400 °F. The best aminosilicone case has significantly lower COE when compared with MEA.

As outlined earlier, a range for the solvent cost was estimated by SiVance. Using the DOE assumptions listed above, the increase in COE, at steam temperatures of 743 °F and the higher solvent cost, over a plant without CO_2 capture is shown in Figure 186. This figure is marked "detailed" since more detailed calculations were performed. The increase in COE, at steam temperatures of 743 °F and the lower solvent cost, over a plant without CO_2 capture at the low solvent cost is shown in Figure 187. The increase in COE at steam temperatures of 400 °F and different solvent costs is shown in Figure 188 and Figure 189.

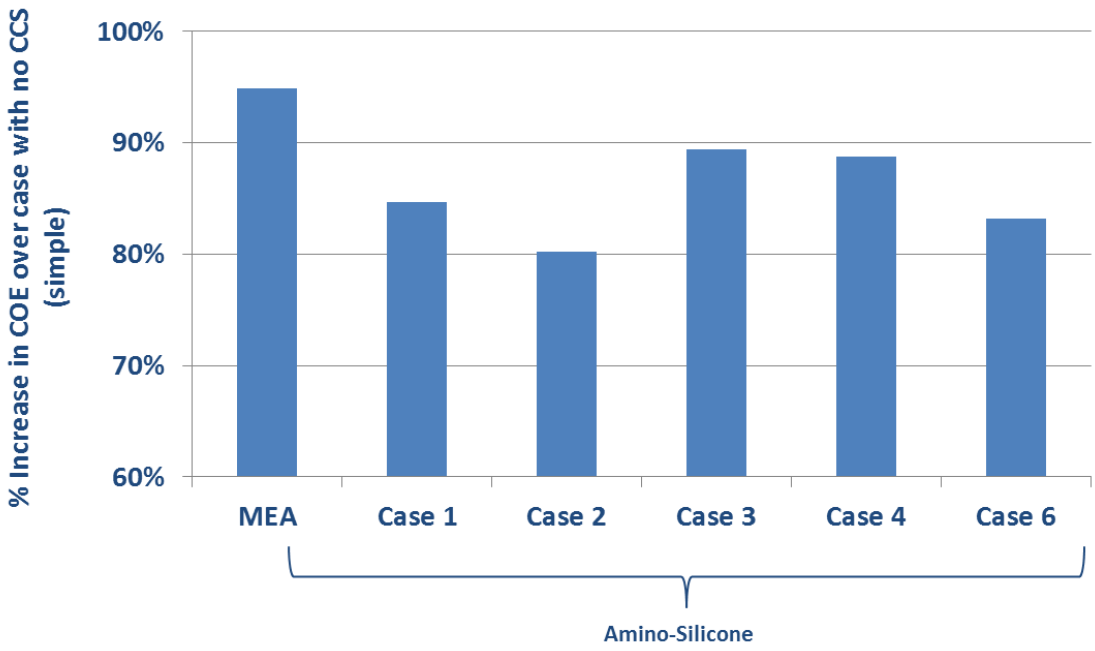

Figure 184. Increase in COE using simplified calculation as set in the award at a steam temperature of 743 °F.

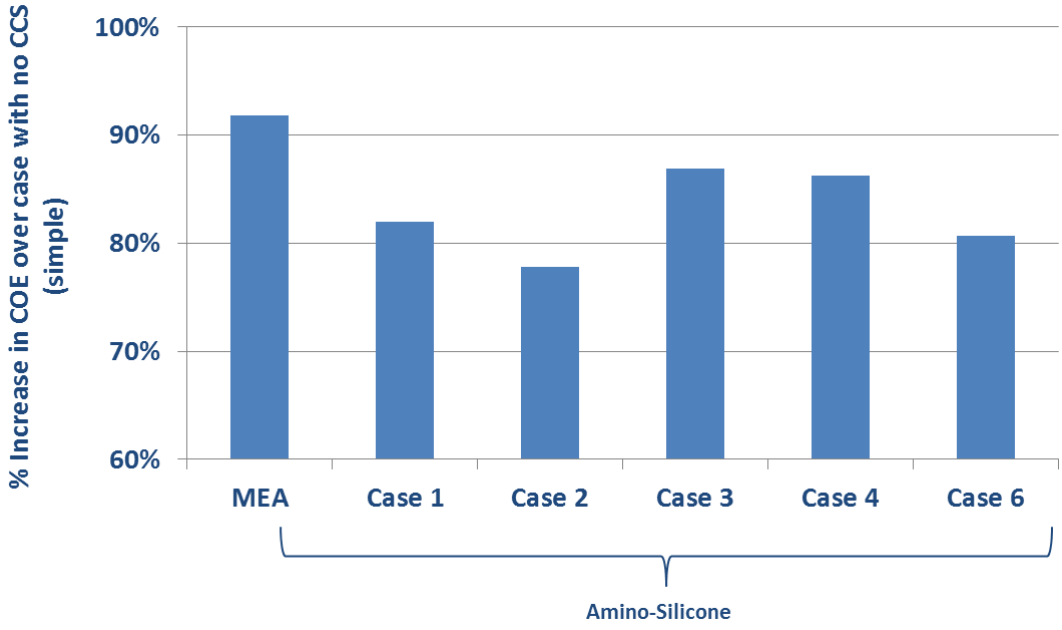

Figure 185. Increase in COE using simplified calculation as set in the award at a steam temperature of 400 °F.

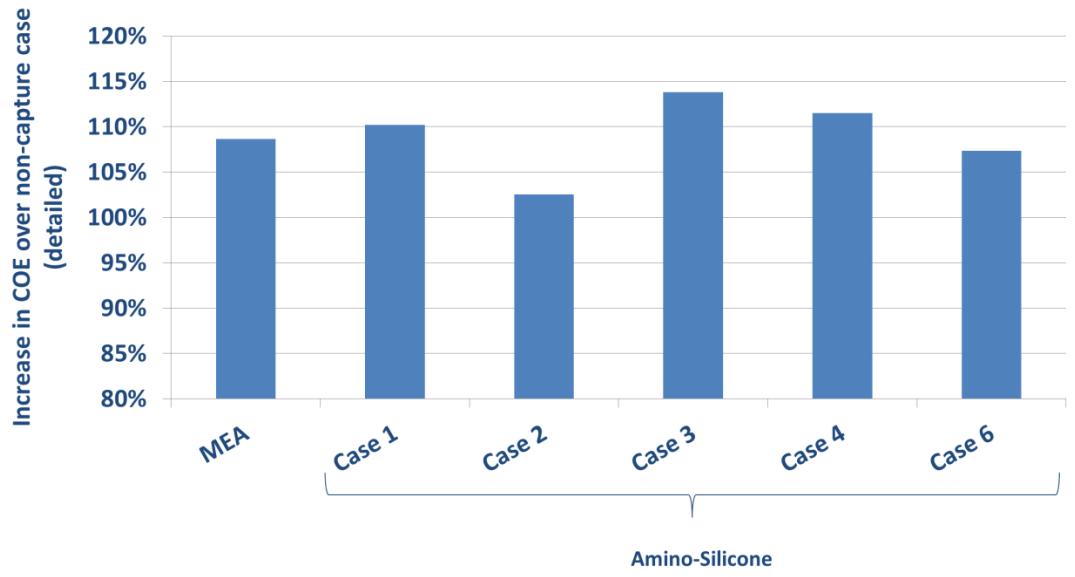

Figure 186. Increase in COE as calculated from detailed analysis using energy penalty and Capex estimates at a steam temperature of 743 °F and the high solvent cost.

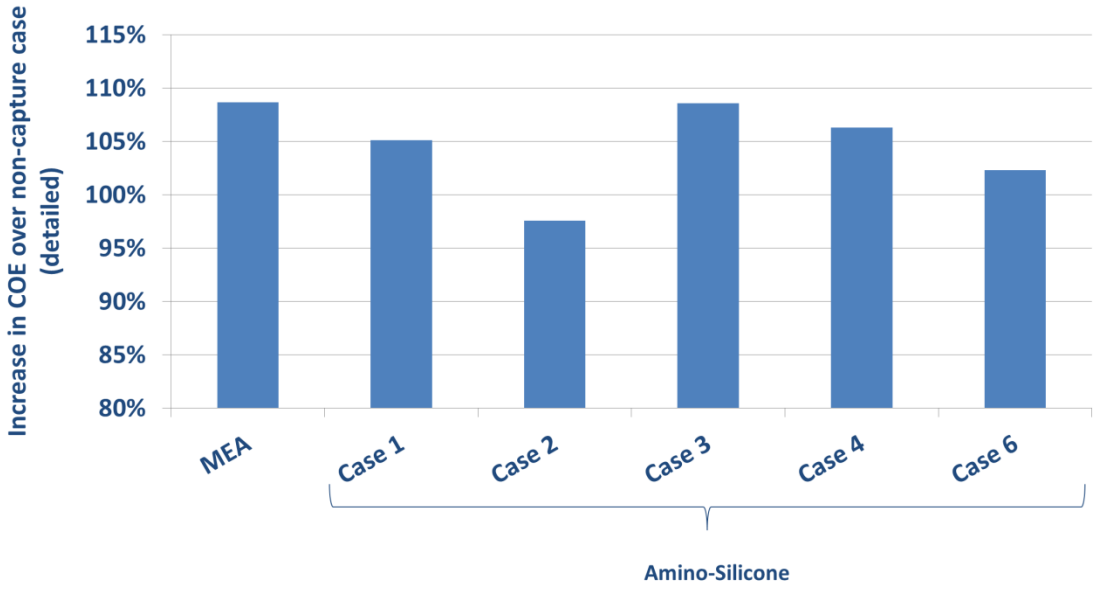

Figure 187. Increase in COE as calculated from detailed analysis using energy penalty and Capex estimates at a steam temperature of 743 °F and the low solvent cost.

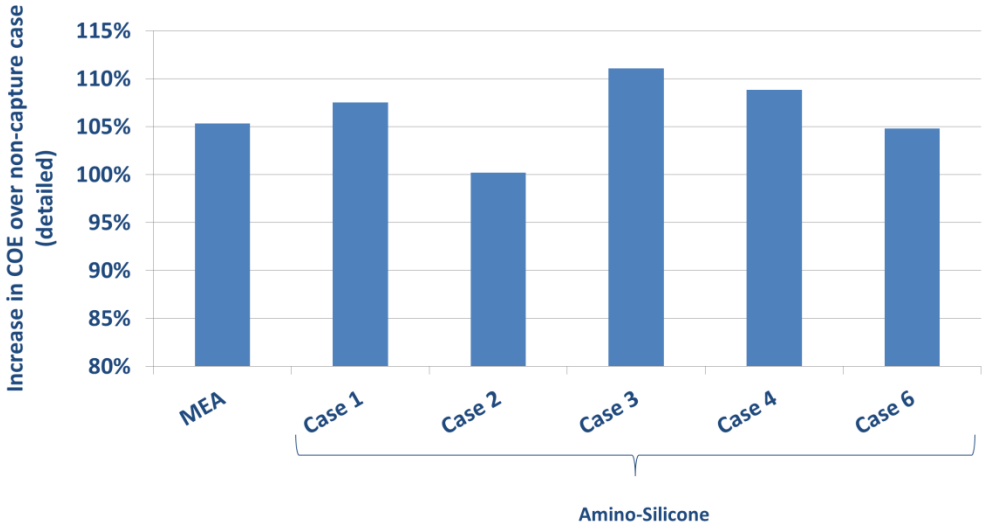

Figure 188. Increase in COE as calculated from detailed analysis using energy penalty and Capex estimates at a steam temperature of 400 °F and the high solvent cost.

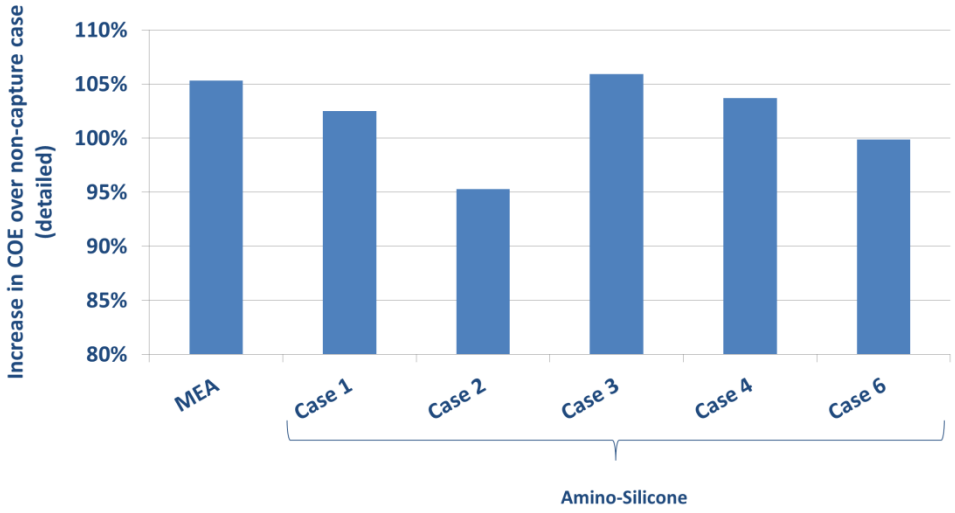

Figure 189. Increase in COE as calculated from detailed analysis using energy penalty and Capex estimates at a steam temperature of 400 °F and the low solvent cost.

As seen in the economic analysis above, Case 2 consistently outperforms the MEA case.

The cost of steam is shown in the following tables using the following equation, specified by DOE.

Cost of steam in $/1000 lb = 0.028 * {Total power loss in MWe} + 5.83

The cost of CO_2 is shown in the following tables using 3 different methodologies, specified by DOE.

1. Cost of CO_2 method specified in the cooperative agreement, which is

   Total cost of capturing CO_2 =
   {cost of all materials and utilities consumed in the CO_2 system}
   + {cost of treating or disposing of any effluent streams from the system, including transport, storage and monitoring of CO_2}
   + {cost of maintenance and materials}
   + {fixed O&M Costs}
   + {capital charge for CO_2 capture system}

   The cost per ton of CO_2 is obtained by dividing this cost by the tons of CO_2 captured by the process.

2. Removal cost of CO_2, specified in bituminous baseline report

$$Removal\ Cost = \frac{\{LCOE_{with\ removal} - LCOE_{w/o\ removal}\}\$/MWh}{\{CO_2\ removed\}tons/MWh}$$

3. Avoided cost of CO_2, specified in bituminous baseline report

$$Avoided\ Cost = \frac{\{LCOE_{with\ removal} - LCOE_{w/o\ removal}\}\$/MWh}{\{Emissions_{w/o\ removal} - Emissions_{with\ removal}\}tons/MWh}$$

A summary of key parameters specified by DOE are shown in the following table for GAP-1m/TEG Case 2 with the higher solvent cost.

	MEA	GAP1-TEG
Cost of Steam - $/1000 lbs	$ 11.36	$ 10.51
Cost of CO2 - $/ton	$ 25.42	$ 30.95
Removal cost for CO2 - $/ton	$ 52.53	$ 53.87
Avoided Cost for CO2 - $/ton	$ 87.31	$ 69.55
% decrease in PC Plant Efficiency	13.2%	11.2%

A summary of key parameters specified by DOE are shown in the following table for GAP-1m/TEG Case 2 with the lower solvent cost.

	MEA	GAP1-TEG
Cost of Steam - $/1000 lbs	$ 11.36	$ 10.51
Cost of CO2 - $/ton	$ 25.42	$ 28.34
Removal cost for CO2 - $/ton	$ 52.53	$ 51.26
Avoided Cost for CO2 - $/ton	$ 87.31	$ 66.18
% decrease in PC Plant Efficiency	13.2%	11.2%

Task 8.3: Develop Scale-Up Strategy

The data from Task 7 and Subtasks 8.1 and 8.2 was used to develop a strategy for moving the aminosilicone-based CO_2-capture process toward commercialization. One outcome of this strategy has been the identification of the next stage for process evaluation and validation. The objective of this stage would be to gain deeper understanding of the operational aspects of individual equipment and the overall CO_2-capture process in order to (a) optimize equipment-sizes and process layout, and (b) improve prediction of performance and costs for the commercial scale system. This strategy was delineated in the proposal AOI-1S1 for a pilot-scale CO_2-capture system that was submitted and granted in response to DE-FOA-0000785[86]. The scale-up strategy is summarized below in Table 66.

[86] Project: "AOI-1S1—PILOT-SCALE SILICONE PROCESS FOR LOW-COST CO2 CAPTURE", Benjamin Wood, PI, submitted in response to DE-FOA-0000785, May 1, 2013.

Table 66. Summary of commercialization scale-up strategy for CO2-capture using aminosilicones.

Scale	Bench-scale	Pilot-scale	Commercial-scale
Time Frame	10/1/2010-12/31/2013	1/1/2014-12/31/2015	
Location	GE GRC, Niskayuna, NY	NCCC, Alabama	
Flue Gas	Diesel Generator + bottled CO_2, SO_2, N_2, NO	Slip-stream from a coal-fired boiler	Pulverized coal burners
Equivalent Power	0.003MWe	0.5 MWe	550MWe
Gas flow rate	3 - 12 kg/hr	1,410–2,290 kg/hr	~ 2,300,000 kg/hr
% CO_2 in flue gas	2% - 16% (dry basis)	11.4 - 12.9% (wet basis)	11 - 13% (wet basis)
SOx	45 ppmv	1 ppmv	

The main objective of the proposed pilot-stage will be to evaluate the performance of the aminosilicones system to capture CO_2 from an actual flue gas stream from a coal-fired utility. As noted previously, the current bench-scale system has used an exhaust from a gasoline-powered engine with additional bottled-CO_2 to simulate the high-CO_2 content from a coal-fired utility. The pilot-stage test will operate using a slipstream from a coal fired power plant at the National Carbon Capture Center (NCCC), in Alabama. The system will be designed to nominally operate at the gas flow rate range of 1410–2290 kg/hr, which is approximately equivalent to 0.5 MWe for a coal-fired power plant. Data obtained from operating this pilot-scale system will be used to perform a technology EH&S study and a techno-economic assessment of the CO_2 capture technology as integrated into a 550 MWe (net) power plant.

The CO_2-recovery process that will be executed at the pilot-stage is illustrated in Figure 190. The flue gas is fed to the absorber column. The operating conditions are chosen to enable 90% capture of the CO_2 in the flue gas into the solvent. The CO_2-lean gas exiting the absorber is sent to the wash column to cool the gas and recover any solvent before the gas is vented to the atmosphere. The recirculated wash liquid is cooled via the wash cooler. Periodically a portion of the wash liquid is sent to the desorber to recover any built-up aminosilicones solvent; this is replenished by fresh lean solvent.

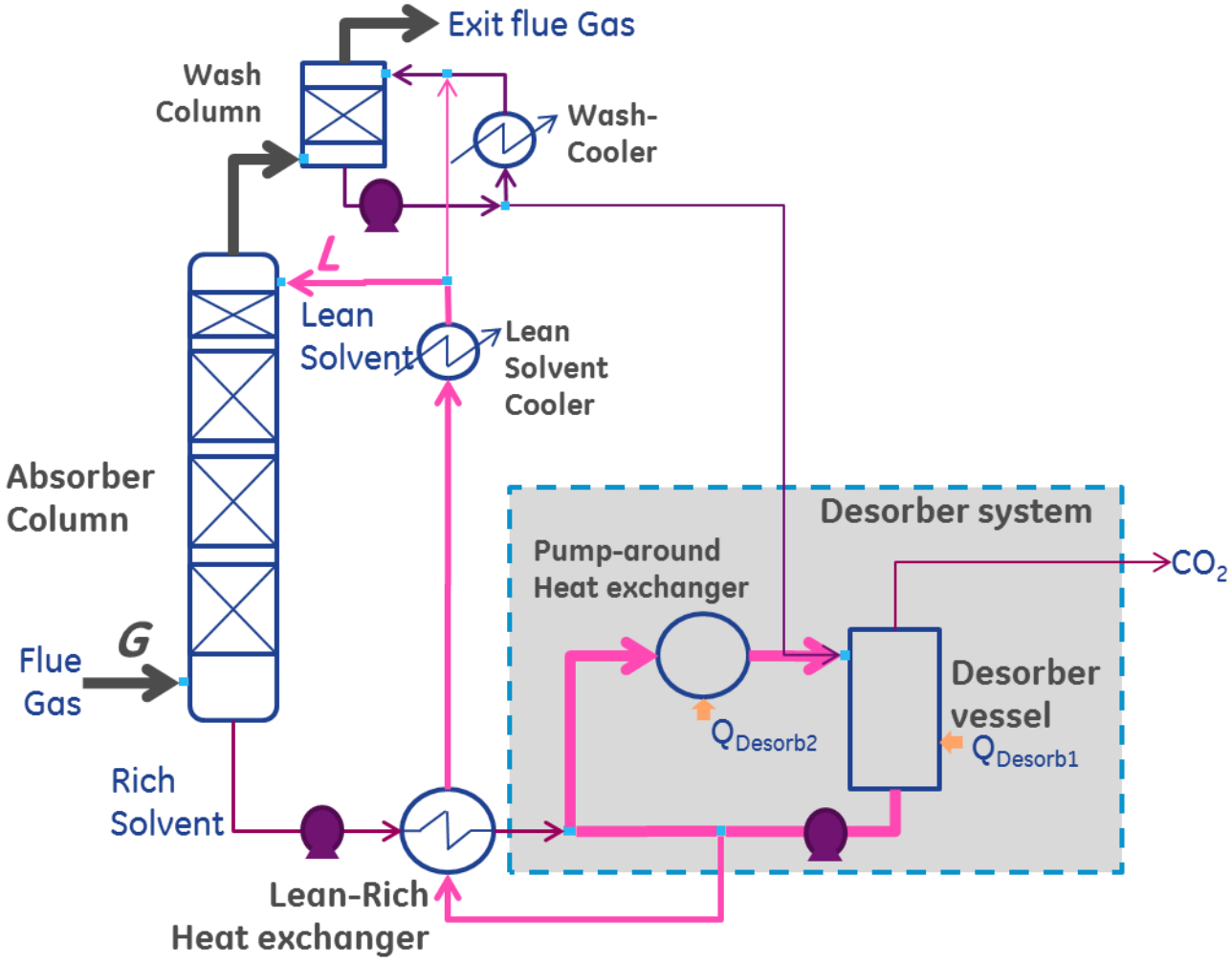

Figure 190. CO_2-capture process envisioned for pilot-scale evaluation.

The rich solvent leaving the absorber is passed via the lean-rich heat exchanger to the desorber system. In the desorber system the CO_2 is stripped from the solvent, and the lean solvent is returned via the lean-rich heat exchanger to the absorber. The desorption system is configured to consist of: (a) a CSTR vessel (referred to as the desorber in Figure 190) and (b) a recirculation loop with a heat exchanger that is connected to the desorber vessel. The heat required for stripping the CO_2 in the desorber system is thus provided via two means: (a) steam condensing in the jacket of the desorber vessel, i.e. $Q_{Desorb1}$ and (b) steam condensing in the pump-around heat exchanger, $Q_{Desorb2}$. Thus, the overall desorption heat load is $Q_{Desorb} = Q_{Desorb1} + Q_{Desorb2}$.

It was determined that key operating process parameters that affects the sizes (costs) of the equipment and overall performance are:

(a) Circulation rate of the aminosilicone solvent in the process: Reducing the flow rate will entail lower sizes for the desorber system and the lean-rich heat exchanger. However, lowering solvent flow rates in the absorber would reduce the rate of CO_2-capture due to (a) reduced driving force for CO_2 absorption when the CO_2 concentration in solvent increases, and (b) increased temperature, which decreases the CO_2 solubility in the solvent. Hence, to achieve the desired 90% CO_2-capture target, lowering solvent flow rate may result in the need for employing a taller absorber column (that entails higher equipment-related costs).

(b) Desorber system operating parameters, mainly residence time of the solvent, pressure, and temperature: Reducing the residence time will lower the volume of the desorber but may limit the extent of CO_2-stripping from the solvent, more specifically the conversion of GAP-1m/carbamate to GAP-1m and CO_2. Reducing the pressure will increase the CO_2-stripping rate but entail higher CO_2-compression costs. Increasing the temperature will increase CO_2-stripping rate but increase the desorber heat load and the need for higher steam quality, both of which will have energy penalty implications. Also, high temperatures may affect the solvent stability.

Absorber System Optimization

The pilot-stage provides an excellent opportunity for validation of the reaction and mass-transfer correlations for CO_2-capture with aminosilicones, which will enable greater confidence in the design and performance prediction for commercial-scale operation. The pilot-stage also provides an opportunity to investigate concepts for optimizing the absorber system performance while reducing the size of the column.

The available absorber column at the NCCC that will be used for the pilot-stage is illustrated in Figure 191. The column has an OD of 26 ft and an overall height of 115 ft. The overall packed section is 70 ft that is split into zones as shown in Figure 191. The height of Zone 1 at the top of the column is 10 ft while the height of Zones 2-4 are 20 ft each.

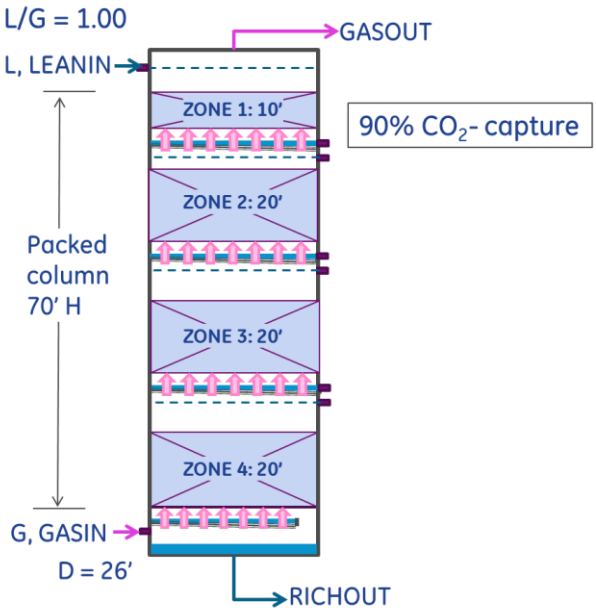

Figure 191. Schematic of the absorber column at the NCCC. This also represents the absorber configuration in Case 8.3-a, namely adiabatic operation.

The operation of the absorber column was simulated in ASPEN using the same model mass-transfer and reaction parameters as in the bench-scale model, but using the dimensions for the NCCC column and the anticipated flow rates and compositions at the pilot-stage. The ASPEN flowchart is shown in Figure 192.

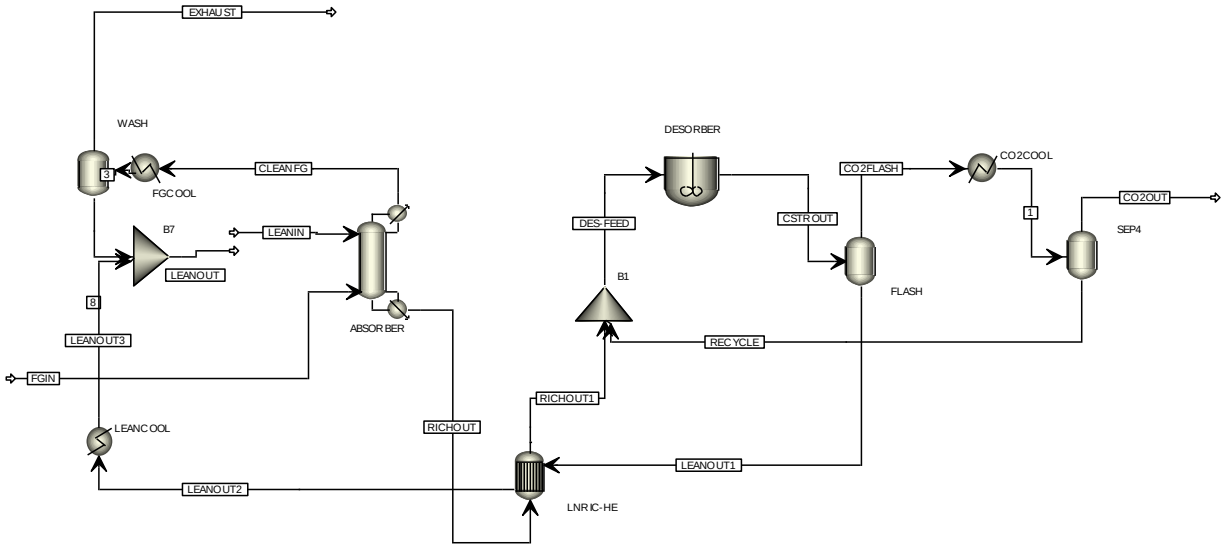

Figure 192. Diagram of the ASPEN simulation of the CO_2-capture process using aminosilicones for the pilot-stage evaluation

The conditions for the adiabatic operation of the absorber column are shown in Table 67 for 90% CO_2-capture in the column. The L/G ratio = 66.42/66.13 ~ 1.

Table 67. Compositions and flow rates of the flue gas and lean solvent for the pilot-scale study for the Case 8.3-a, namely adiabatic operating conditions for 90% CO_2-capture in the absorber column (Figure 191).

Component	Flue Gas	Lean Solvent	Rich Solvent	Clean Flue Gas
H2O	7.3099%	16.6374%	19.2602%	5.0127%
CO2	14.7514%	0.7200%	0.0567%	1.7659%
N2	75.3176%	0.0073%	0.1527%	90.0007%
O2	2.6211%	0.0000%	0.0000%	3.1383%
GAP1	0.0000%	29.2482%	14.9475%	0.0503%
GAP1CARB	0.0000%	3.1242%	16.5610%	0.0305%
D4	0.0000%	0.0000%	0.0000%	0.0000%
TEG	0.0000%	50.2627%	49.0218%	0.0016%
Total Flow kmol/hr	66.13	66.42	68.10	55.23
Total Flow kg/hr	1,967	12,249	12,660	1,556
Total Flow cum/hr	1,699	10	11	1,525
Temperature F	104.0	104.0	175.8	145.9

The profiles of the temperature and CO_2-concentration in the vapor are plotted in Figure 193. The liquid temperature is observed to reach a maximum of 180 °F (82 °C) along the column and is flat for a large section of the column between 15 ft and 55 ft. More interestingly, the CO_2-vapor concentration shows sharp changes near the top of the column where lean solvent is introduced and near the bottom of the column where the CO_2-concentration in the vapor is highest, but the profile is flat for a significant section near the middle of the column between ~25 ft to ~40 ft, which indicates very little mass transfer in this section. This profile provides an opportunity to investigate alternatives for optimizing the operating conditions to provide a uniform mass-transfer rate along the column and thus possibly reduce the packed section height and the overall absorber column dimensions.

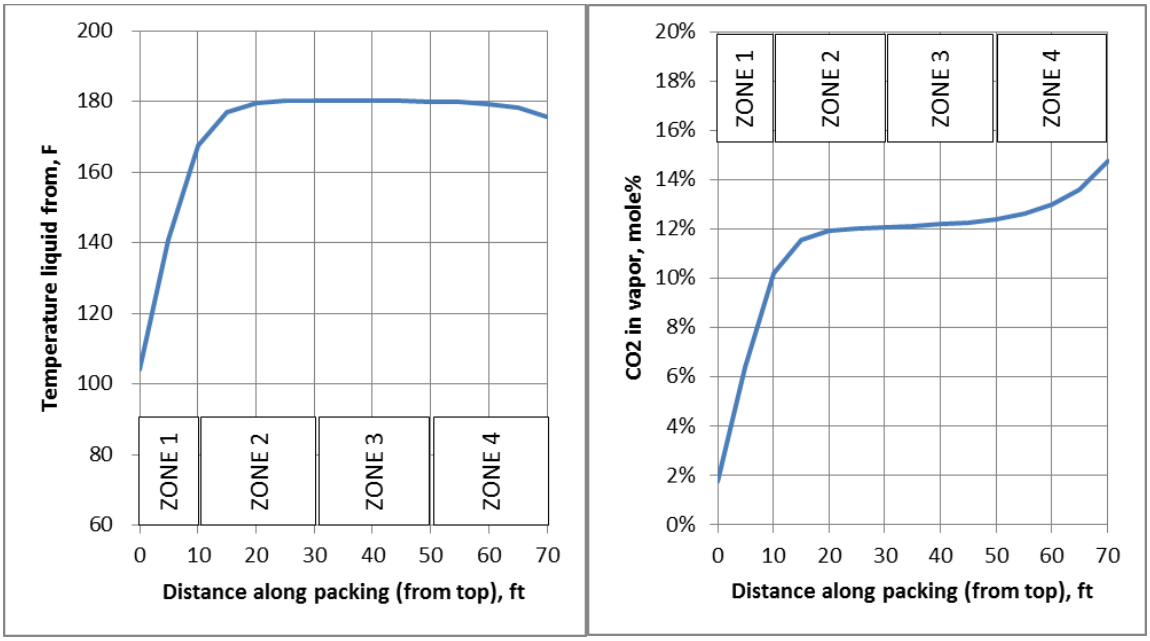

Figure 193. Profiles of the liquid temperature and the CO_2 concentration in the vapor along the absorber column height for Case 8.3-a (Figure 191 and Table 67).

In Task 8.2, the concept of inter-stage cooling as the solvent flows down the absorber was considered at the 550 MW scale. For the Case 2 simulation (see Table 64) that considered uniform heat removal from the solvent along the absorber column height, a significantly lower L/G value of 0.82 was sufficient for 90% CO_2 capture compared to a value of 1.21 required for the adiabatic operation (Case 1 in Table 64). As shown in Section 8.2, this lower solvent rate for Case 2 had significant impact on the overall process costs.

In the pilot-stage this concept of inter-stage absorbent cooling will be investigated. Since it is not possible to provide and control uniform heat removal along the length of the absorber column, a practical solution is to extract the liquid at convenient locations in the column, cool the liquid in an external heat exchanger, and re-introduce the cooled liquid at the same column location. This is depicted in Figure 194 for case 8.3-b where the liquid is extracted after Zone 1 and cooled before returning to the column prior to Zone 2. Similarly, Figures 195 and 196 correspond to liquid being drawn after Zones 2 and 3, respectively. These cases are referred to as 8.3-c and 8.3-d, respectively. In each of these cases the inter-stage cooling load is 100 kW, which corresponds to approximately 9.5% of the heat of absorption in the column for the adiabatic case (Case 8.3-a). This corresponds to a liquid stream temperature decrease of about 15 °F. Heat removal was limited to 100 kW due to available cooling water temperatures at the NCCC.

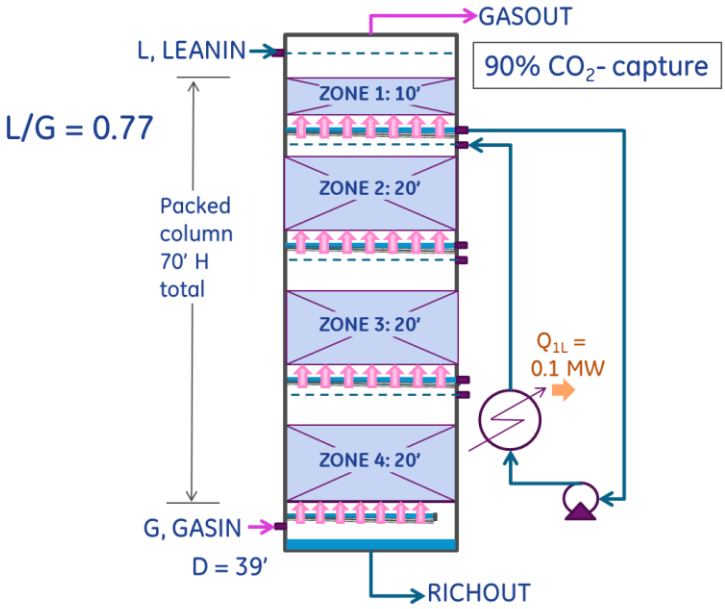

Figure 194. Schematic of Case 8.3-b where inter-stage liquid cooling has been used after Zone 1.

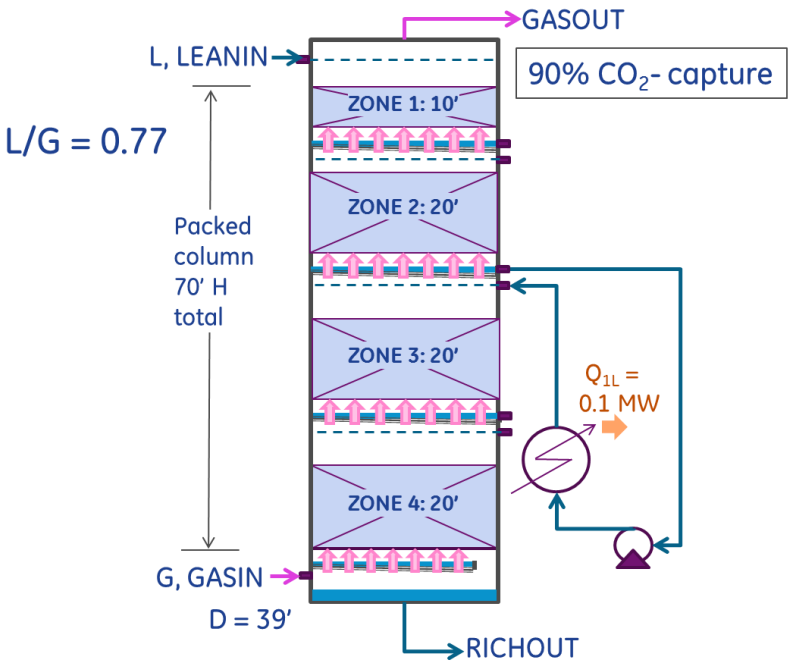

Figure 195. Schematic of Case 8.3-c where inter-stage liquid cooling has been used after Zone 2.

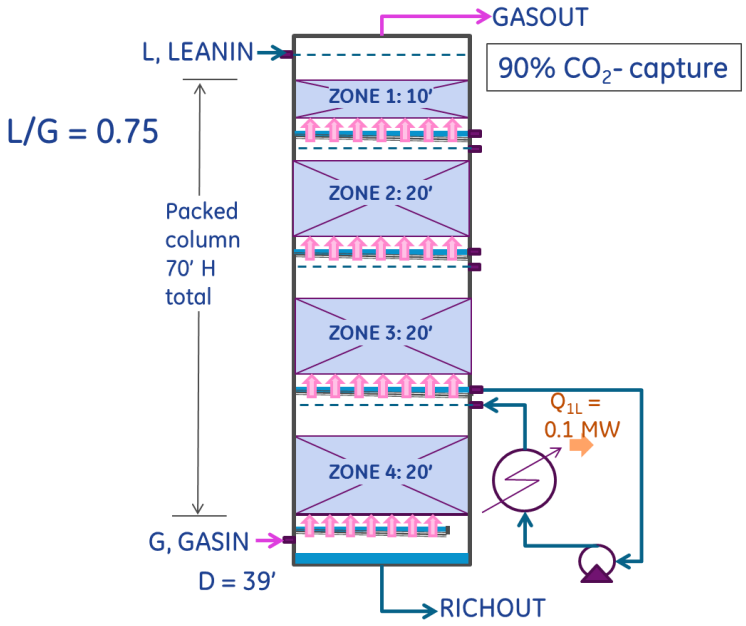

Figure 196. Schematic of Case 8.3-d where inter-stage liquid cooling has been used after Zone 3.

The key operating and performance parameters for these cases are shown in Table 68.

Table 68. Key operating and performance parameters for the absorber inter-stage cooling cases.

Height along Column Packing, ft	Cases	Units	Case8.3-a: Adiabatic, Q=0	Case 8.3-b: After Zone 1 (10ft), Q=-100kW	Case 8.3-c: After Zone 2 (30ft); Q=-100kW	Case 8.3-d: After Zone3 (50ft), Q = -100kW
5	Heat removal	kW	-	-	-	-
10	Heat removal	kW	-	(100.00)	-	-
15	Heat removal	kW	-	-	-	-
20	Heat removal	kW	-	-	-	-
25	Heat removal	kW	-	-	-	-
30	Heat removal	kW	-	-	(100)	-
35	Heat removal	kW	-	-	-	-
40	Heat removal	kW	-	-	-	-
45	Heat removal	kW	-	-	-	-
50	Heat removal	kW	-	-	-	(100)
55	Heat removal	kW	-	-	-	-
60	Heat removal	kW	-	-	-	-
65	Heat removal	kW	-	-	-	-
70	Heat removal	kW	-	-	-	-
	Total Heat Removal	kW	-	(100)	(100)	(100)
	Performance parameters					
	CO2 capture	%	90.0%	90.0%	90.0%	90.0%
	L/G (=LEANIN1/FG1)	mole/mole	1.004	0.775	0.752	0.749
	Flue Gas Temperature	°F	104.00	104.00	104.00	104.00
	Clean Gas Temperature	°F	145.90	143.05	147.64	148.14
	Lean Solvent Temperature	°F	104.00	104.00	104.00	104.00
	Rich Solvent Temperature	°F	175.79	164.13	163.29	163.07

The circulation rate of the liquid to achieve 90% CO_2-capture in the absorber column, as represented by the L/G ratio is shown in Figure 197. It was observed that the removal of only ~ 9.5% of the heat of absorption has a significant (~ 25%) decrease in the amount of lean solvent required compared to the adiabatic operation case.

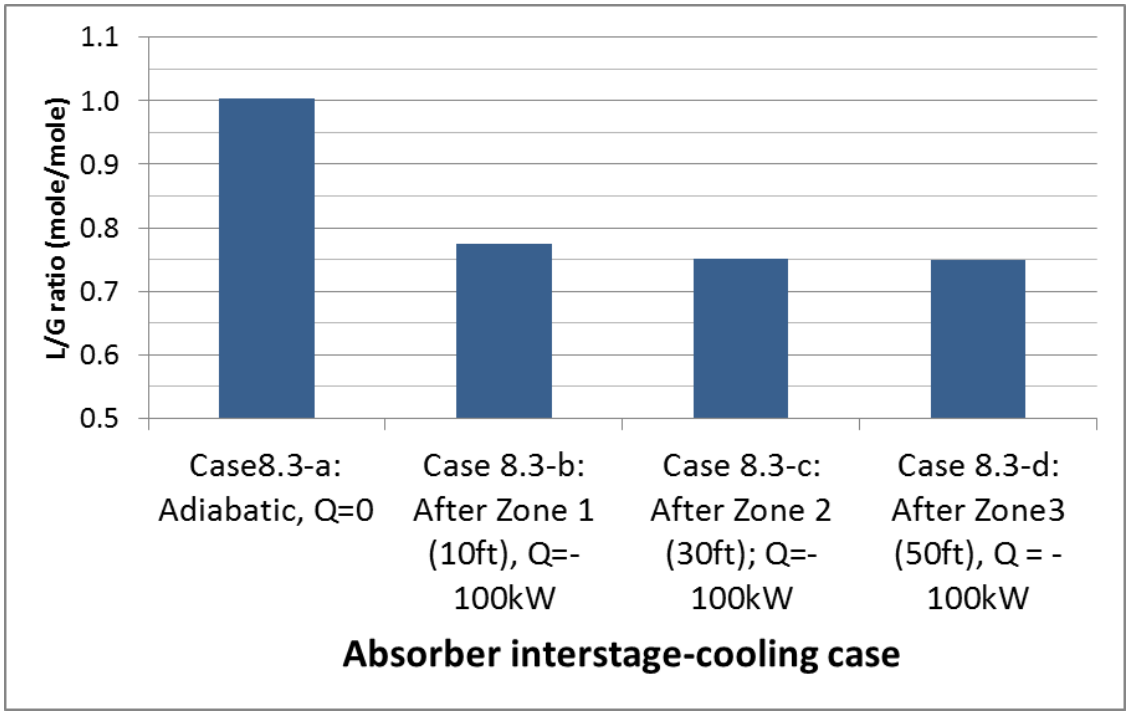

Figure 197. Effect of absorber inter-stage cooling location on L/G required for 90% CO_2-capture.

The profiles for the liquid temperature in the absorber column for Cases 8.3-a through 8.3-d are shown in Figure 198. There was a significant impact of ~ 15 – 20°F on the liquid temperature profile due to inter-stage cooling vs. the adiabatic operation (8.3-a) profile. The effect on the vapor-temperature profiles due to inter-stage cooling is shown in Figure 199. There is a similar effect of ~ 15-20 °F on the vapor temperatures, although the minimum in the vapor temperature occurs about 5 ft away from the location of the inter-stage cooling.

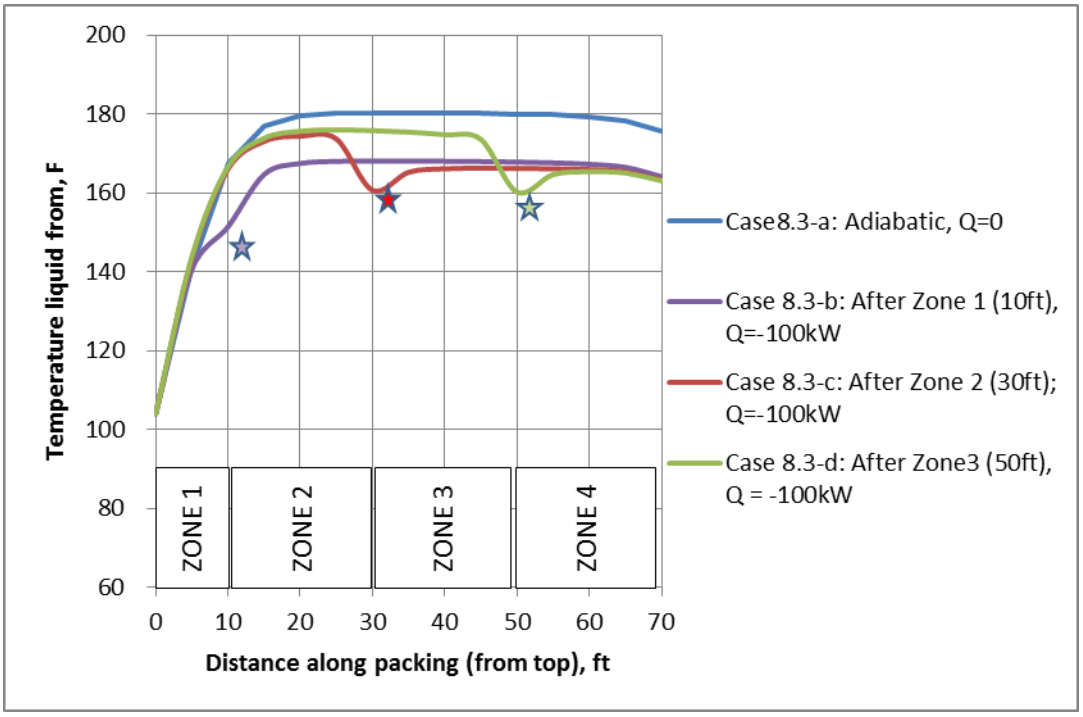

Figure 198. Liquid-temperature profiles along the absorber column for Cases 8.3 –a through –d. The stars represent the locations of the inter-stage-coolers for the respective cases.

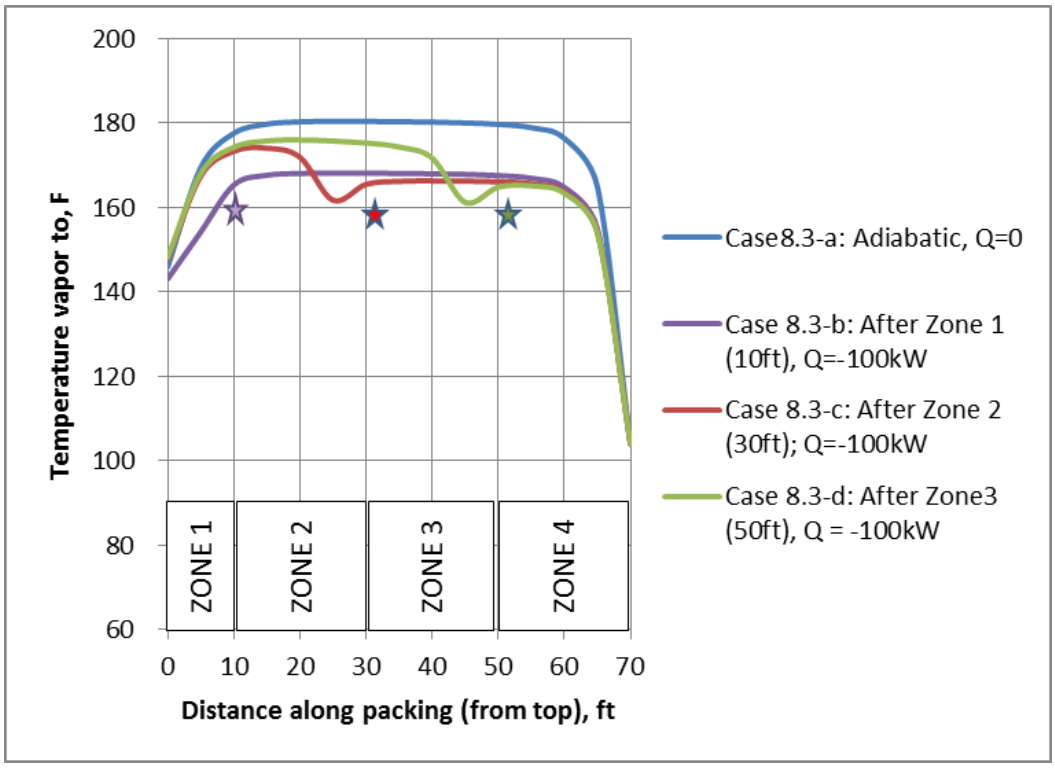

Figure 199. Vapor-temperature profiles along the absorber column for Cases 8.3 –a through –d. The stars represent the locations of the inter-stage-coolers for the respective cases.

The profiles for the CO_2-concentration in the vapor are plotted as a function of the packed bed height for Cases 8.3-a through 8.3-d are shown Figure 200. The inclusion of the inter-stage cooling has a significant impact on the CO_2-concentration profiles. Interestingly, there is very little change in the vapor concentration a few feet below the location of the inter-stage cooling. Moreover, the flat region observed in the profile for the adiabatic case (8.3-a) between about 20 ft through 40 ft has been altered for Cases 8.3-c and –d. Thus, it may be possible by means of appropriately located inter-stage cooling to reduce the solvent flow rate as well as reduce the column height.

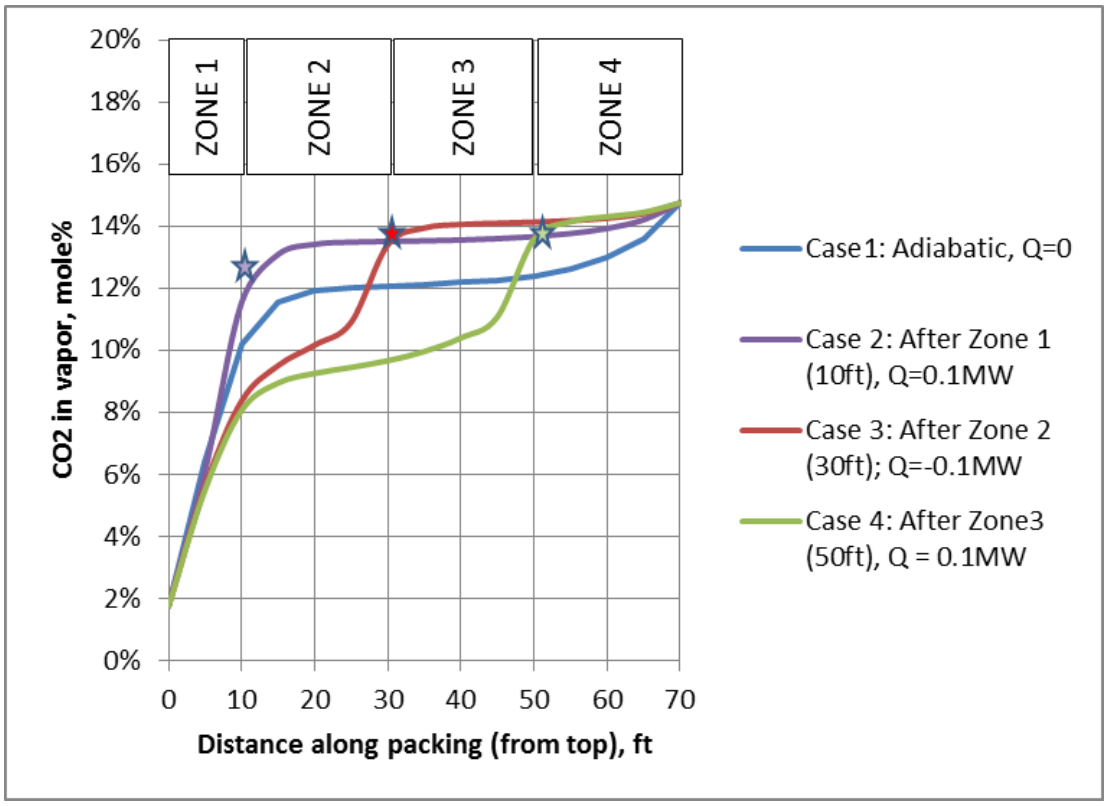

Figure 200. Profiles of the CO_2 concentration in the vapor along the absorber column for Cases 8.3 –a through –d. The stars represent the locations of the inter-stage coolers for the respective cases. Interestingly, there is negligible CO_2-capture for points in the absorber column located below the inter-stage cooler location.

The above analysis provides a basis for investigating strategies and designing experimental protocols at the pilot scale that will enable optimization of the absorber column conditions for commercial-scale operation.

Desorber System Optimization

The key desorber system operating parameters of interest are (a) the residence time of the solvent in the desorber and (b) desorber pressure. The other key desorber parameter, namely the desorber temperature is assumed to be 140 °C (284 °F) for all cases. The effect of residence time in the desorber system on the solvent regeneration or conversion of GAP-1m/carbamate to CO_2 and GAP-1m is shown in Figure 201. The conversion is a strong function of desorber pressure, increasing nearly 15% when the pressure is decreased from 4.3 bar (63 psia) to 1.2

bar (17 psia). The conversion also increases with increasing residence time; however, this increase is not so significant for residence time greater than 15 minutes.

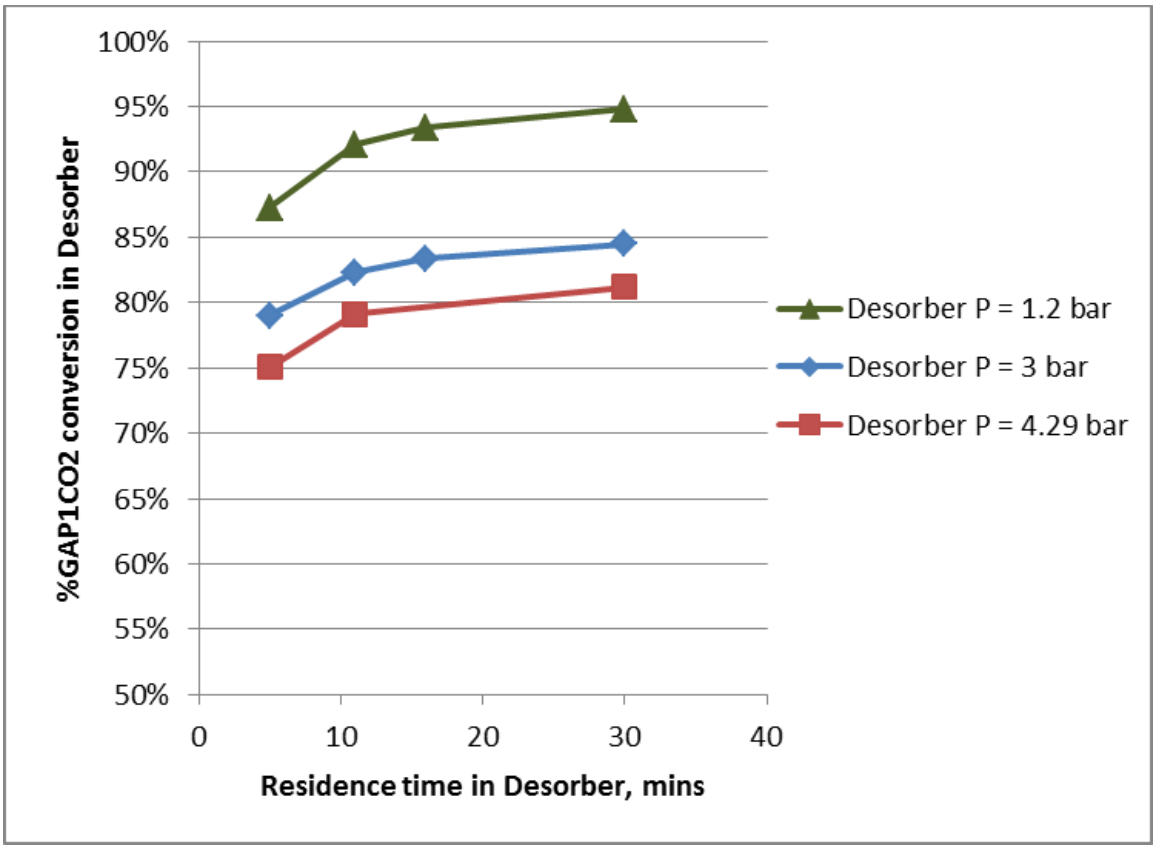

Figure 201. Effect of liquid residence time in the desorber on the conversion of GAP-1m/carbamate to GAP-1m and CO_2 for varying desorber pressures.

The L/G ratios required to achieve 90% CO_2-capture in the absorber are shown as a function of desorber operating conditions in Figure 202. For higher desorber pressures, higher L/G ratios are required in the absorber. This is a consequence of lower conversion of GAP-1m/carbamate in the desorber (Figure 201) which lowers the working capacity of the solvent. This dependence is illustrated in the second graph in Figure 202 where the L/G ratio is plotted as a function of the conversion of GAP-1m/carbamate accomplished at the desorber operating conditions.

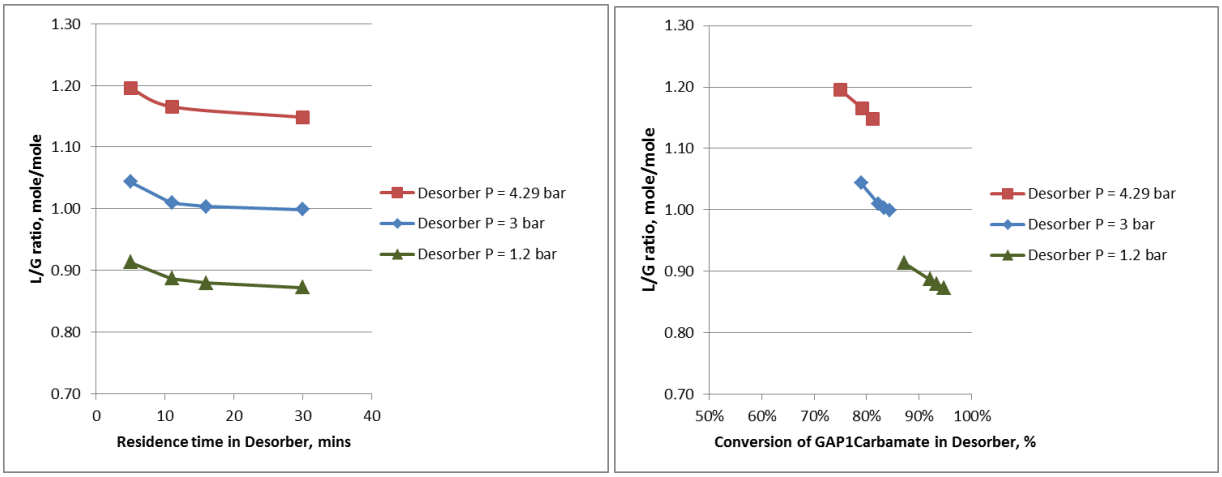

Figure 202. Effect of liquid residence time in the desorber on the L/G ratio required to achieve 90% CO_2 capture in the absorber for varying desorber pressures.

As described earlier, the desorption system is configured to consist of: (a) a CSTR vessel (referred to as the desorber vessel in Figure 190) and (b) a recirculation loop with a heat exchanger that is connected to the desorber vessel.

The design conditions for the desorber vessel are chosen as follows:

Desorber Liquid Volume, V_{Liquid} = Residence Time x Rich Solvent flow rate

Liquid Height/Diameter ratio, H_{Liquid}/D ratio = 1

Thus, Desorber Diameter, $D = (4 * V_{Liquid} / \pi * (H_{Liquid}/D \text{ ratio} = 1))^{(1/3)}$

Vapor Residence time, t_{Vapor} = 30 seconds

Vapor velocity, v_{Vapor} = Vapor flow rate/($\pi D^2/4$), where Vapor flow rate is the desorbed CO_2-product vapor flow rate from the desorber vessel

Height of Desorber Vapor space, $H_{Vapor} = t_{Vapor} * v_{Vapor}$

Assuming that the Desorber is an almost flat-bottom and flat-top vessel:

$$\text{Desorber Volume} = \pi/4 * D^2 * (H_{Liquid} + H_{Vapor})$$

The estimated desorber diameter and desorber vessel volume for the desorber vessel operating conditions are shown in Figure 203. While the desorber diameter is a strong function of the residence time, it is not significantly affected by the choice of the operating pressure. The desorber vessel volume is, as expected, a linear function of the residence time. However, interestingly, although the desorber volume decreases by about 1 to 1.5 m^3 as the pressure is increased from 1.3 bar to 3 bar, there is negligible impact of further increase in operating pressure on the desorber volume.

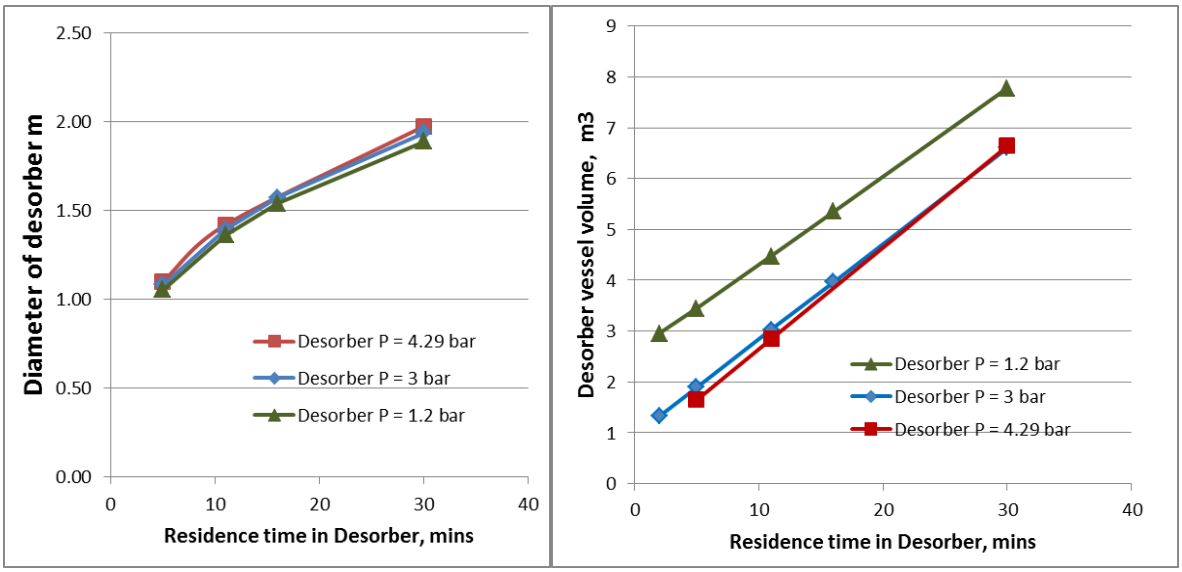

Figure 203. Effect of residence time in desorber on the diameter and volume of the desorber vessel as a function of operating pressure in the desorber.

The desorber heat duty is plotted as a function of residence time in Figure 204. There is negligible effect of the desorber operating conditions since the value is dominated by the heat of desorption for the CO_2, which is the same for all cases since all cases correspond to 90% CO_2-capture from the flue gas in the absorber.

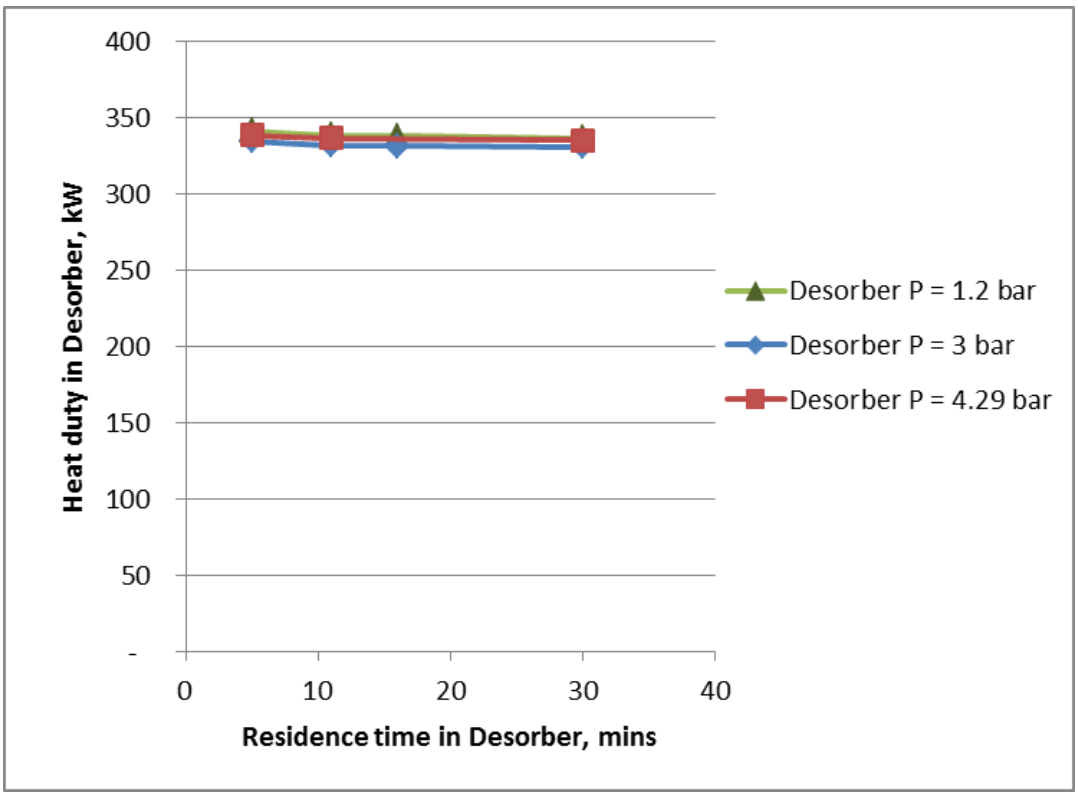

Figure 204. Effect of liquid residence time in desorber on the heat duty of the desorber as a function of desorber pressure.

The heat required for stripping the CO_2 in the desorber is expressed as:

$$Q_{Desorb} = Q_{Desorb1} + Q_{Desorb2}$$

where $Q_{Desorb1}$ is the heat provided by steam condensing in the jacket of the desorber vessel and $Q_{Desorb2}$ is provided by steam condensing in the pump-around loop heat exchanger.

The heat provided by steam condensing in the jacket of the desorber vessel, $Q_{Desorb1}$ is estimated as follows:

Jacket height, $H_{Jacket} = H_{Liquid,}$ i.e. Liquid height in the Desorber

Heat transfer surface area, $A_{Desorb1} = \pi * D_{Desorber} * H_{Jacket}$

Steam conditions: 167.7 psia & 743 °F, but since this does not correspond to saturated steam conditions it is prudent to consider the saturated steam temperature at 167.7

psia, namely 367 °F (186 °C) to be the condensing temperature for heat transfer area estimations.

Desorber liquid is chosen to be at 140 °C

Overall heat transfer coefficient for steam condensing in a jacket, U_{jacket} = 100 $W/m^2/K$

Hence, $Q_{Desorb1} = U_{jacket} * A_{Desorb1} * (186 – 140)$

The heat duty for the pump-around loop heat exchanger is thus:

$$Q_{Desorb2} = Q_{Desorb} - Q_{Desorb1}$$

The estimated values for $Q_{Desorb1}$ and $Q_{Desorb2}$ are plotted as a function of the residence time and desorber pressure in Figure 205. Increasing residence time entails larger vessel diameter and consequently larger vessel height (since it is assumed that H/D = 1), and thus higher jacket heat transfer area. Consequently, there are higher jacket heat transfer rates with increasing residence time in Figure 205. Nevertheless, the extent of heat transferred via the jacket is fairly limited and the bulk of the heat required for the desorption will have to be supplied by the pump-around heat exchanger, as shown in Figure 205.

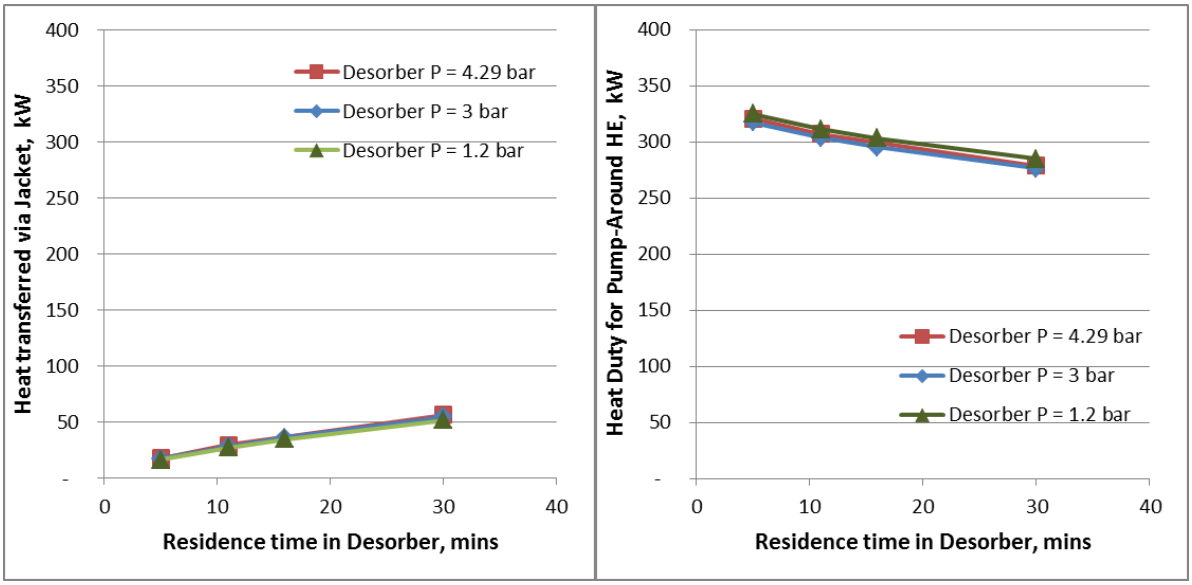

Figure 205. Heat transferred via steam condensing in desorber jacket and the heat duty for the pump-around heat exchanger as a function of desorber operating conditions, namely liquid residence time and pressure in desorber for 90% CO_2-capture from the flue gas.

The heat-transfer area for the pump-around heat exchanger is obtained as follows:

Steam temperature (condensing), T_{steam} = 186 °C

Liquid temperature in, T_{in} = 140 °C

Temperature rise in the heat exchanger, ΔT = 15 °C

Temperature out, $T_{out} = T_{in} + \Delta T$ = 155 °C

LMTD = 38 °C

Overall heat transfer coefficient for condensing steam/light organics, U_{ht} = 185 W/m^2/K

Hence, $A_{PumpAroundHE} = Q_{Desorb2}/(U_{ht} * LMTD)$

The heat exchanger area required for the pump-around heat exchanger is shown in Figure 206.

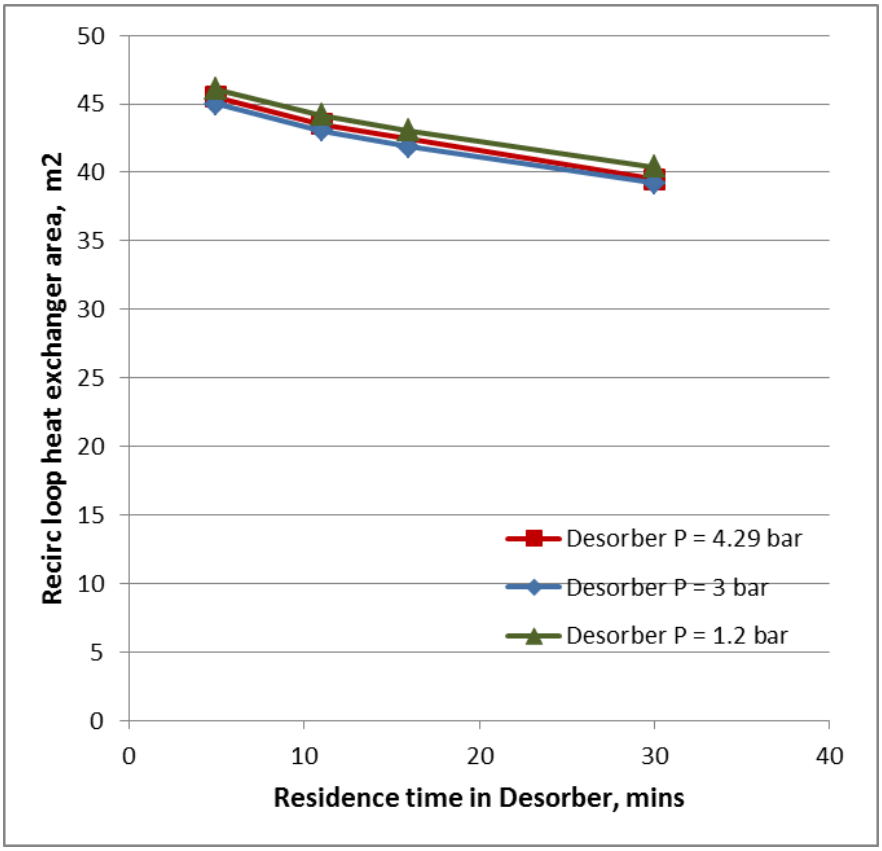

Figure 206. Effect of liquid residence time in desorber on the recirculated-loop heat exchanger area, as a function of desorber operating pressure.

The heat duty in the lean/rich heat exchanger and the heat-transfer area are shown as a function of the desorber operating conditions in Figure 207.

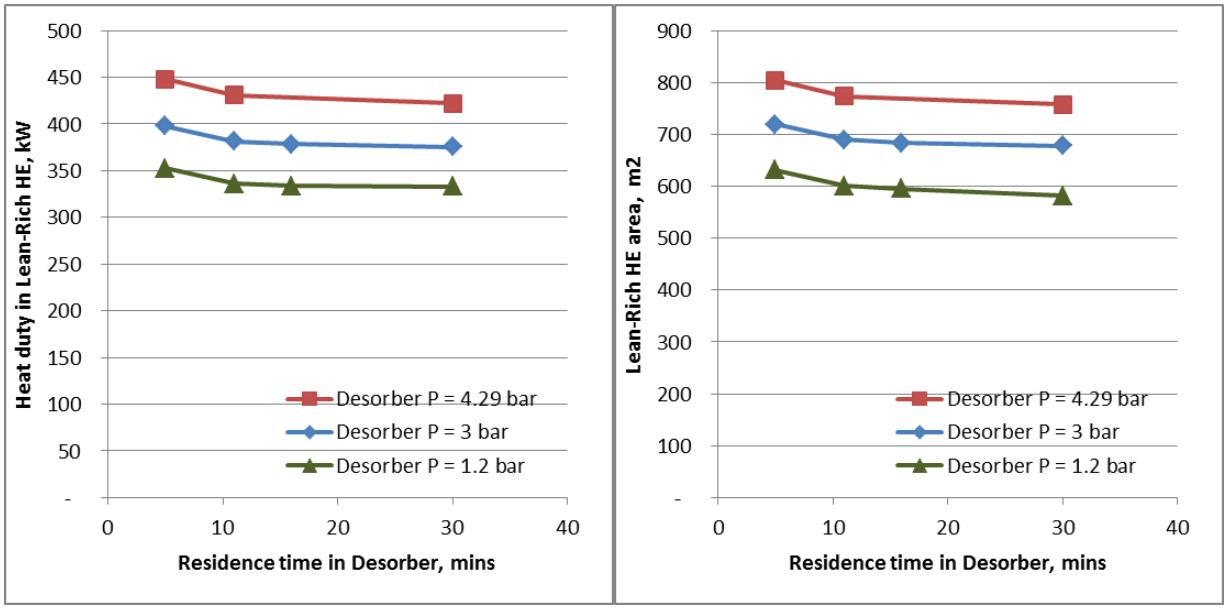

Figure 207. Effect of liquid residence time in the desorber on the heat duty in the lean-rich heat exchanger and the heat-transfer area, as a function of desorber pressure.

The above analysis provides a basis for investigating strategies and designing experimental protocols in the pilot-stage that will enable optimization of the desorber system conditions for commercial-scale operation.

Conclusions:

A bench-scale system was designed and built to test an aminosilicone-based solvent. This process has a number of advantages relative to a traditional MEA CO_2 capture process, including significantly lower solvent volatility, which decreases the amount of energy wasted vaporizing solvent during desorption. The low volatility of the solvent also simplifies the separation of CO_2 from the solvent in the desorption process, allowing the separation to be affected in a simple CSTR rather than a distillation column, which is typical of processes using more volatile solvents. The low volatility also decreases issues with airborne release of solvent. The aminosilicone-based solvent demonstrates a significantly higher thermal stability than MEA. This allows the desorption of CO_2 to be conducted at higher temperatures, resulting in greater working capacity and/or higher desorption pressures. Also, because the solvent is a non-aqueous material, there is much less energy used in vaporizing water than is typical in a 30 wt% aqueous MEA process.

A model was built of the bench-scale system and this model was scaled up to model the performance of a carbon capture unit, using aminosilicones, for CO_2 capture and sequestration (CCS) for a pulverized coal (PC) boiler at 550 MW. System and economic analysis for the carbon capture unit demonstrates that the aminosilicone solvent has significant advantages relative to an MEA-based system. The CCS energy penalty for MEA is 35.9% and the energy penalty for aminosilicone solvent is 30.4% using a steam temperature of 395 °C (743 °F). If the steam temperature is lowered to 204 °C (400 °F), the energy penalty for the aminosilicone solvent is reduced to 29%. The increase in COE over the non-capture case for MEA is ~109% and increase in COE for aminosilicone solvent is ~98 to 103% depending on the solvent cost at a steam temperature of 395 °C (743 °F). If the steam temperature is lowered to 204 °C (400 °F), the increase in COE for the aminosilicone solvent is reduced to ~95-100%.

There are a number of areas where the performance of the aminosilicone-based CO_2 capture process may be optimized in the future. As was shown, inter-stage cooling in the absorber can significantly improve process performance and economics. However, a complete investigation of the optimal amount of inter-stage cooling has not been conducted. Although the aminosilicone demonstrates high thermal stability, several stabilizers have been identified that further increase the solvents thermal stability. An economic analysis is required to determine the amount of solvent-loss cost savings that can be achieved through the use of stabilizers. As with other amines, the aminosilicone solvent reacts with sulfur compounds in the flue gas, resulting in costs associated with solvent loss. Improved pre-scrubbing of the flue gas to remove sulfur compounds may result in additional cost savings. Although the solvent demonstrated low corrosivity in most of the process, the corrosivity in the desorber requires that the desorber be made of stainless steel. Corrosion inhibitors may allow the desorber to be fabricated from less expensive materials, such as carbon steel, which will decrease capital costs. Finally, the CO_2 capture system has not been optimized with respect to the power plant. Through heat integration between the CO_2 capture system and power plant, the steam required by the desorber can be decreased.